



HAL
open science

Structure and variability of the subtropical gyre

Guillaume Maze

► **To cite this version:**

Guillaume Maze. Structure and variability of the subtropical gyre. Ocean, Atmosphere. Université de Bretagne Occidentale, Brest, 2020. tel-03344568

HAL Id: tel-03344568

<https://hal.science/tel-03344568v1>

Submitted on 15 Sep 2021

HAL is a multi-disciplinary open access archive for the deposit and dissemination of scientific research documents, whether they are published or not. The documents may come from teaching and research institutions in France or abroad, or from public or private research centers.

L'archive ouverte pluridisciplinaire **HAL**, est destinée au dépôt et à la diffusion de documents scientifiques de niveau recherche, publiés ou non, émanant des établissements d'enseignement et de recherche français ou étrangers, des laboratoires publics ou privés.

HABILITATION A DIRIGER DES RECHERCHES DE

L'UNIVERSITE
DE BRETAGNE OCCIDENTALE
COMUE UNIVERSITE BRETAGNE LOIRE

ECOLE DOCTORALE N° 598

Par

Guillaume MAZE

Structure and variability of the subtropical gyre

Thèse présentée et soutenue à Brest, le 27 novembre 2020

Unité de recherche : Laboratoire d'Océanographie Physique et Spatiale

Rapporteurs avant soutenance :

Fabien Durand Chargé de recherche HdR IRD, LEGOS
Juliette Mignot Directrice de recherche IRD, LOCEAN
Gilles Reverdin Directeur de recherche CNRS, LOCEAN

Composition du Jury :

Guillaume Rouillet Professeur UBO, LOPS
Président
Xavier Carton Professeur UBO, LOPS
Fabien Durand Chargé de recherche HdR IRD, LEGOS
Juliette Mignot Directrice de recherche IRD, LOCEAN
Gilles Reverdin Directeur de recherche CNRS, LOCEAN
Sabrina Speich Professeur ENS, LMD
Toshio Suga Professeur Tohoku Univ., Japan



Structure and variability of the subtropical gyre

Habilitation à Diriger des Recherches

Guillaume Maze

A Gabriel et Marianne

J'ai soutenu ma thèse il y a 14 ans, tu étais âgé de quelques mois au fond de la salle. Tu es née quand, revenant des États-Unis il y a 11 ans, j'ai entamé un long marathon de concours. Cette tranche de carrière professionnelle c'est donc surtout le début de ma vie avec vous.

HABILITATION À DIRIGER DES RECHERCHES, UNIVERSITÉ DE BRETAGNE OCCIDENTALE

Ifremer, UMR 6523, Laboratoire d'Océanographie Physique et Spatiale, F-29280 Plouzané, France

Contact: gmaze@ifremer.fr

Version released to the jury, 2020/03/12

Structure et variabilité du gyre subtropical

Résumé: Le gyre subtropical est un grand système de courants océaniques et de masses d'eau qui s'étendent sur chacun des océans aux moyennes latitudes. Principalement entraînée par les vents, la circulation océanique proche de la surface a tendance à accumuler des masses d'eau au centre du gyre. Cette accumulation entraîne : une stratification spécifique, une circulation de grande échelle dirigée vers l'équateur dans la partie supérieure de l'océan et un courant compensateur très étroit dirigé vers le pôle, circulant le long du bord ouest de l'océan (ex: le Gulf Stream dans l'Atlantique Nord ou le Kuroshio dans le Pacifique Nord). La circulation du gyre est responsable du transfert de la chaleur absorbée par l'océan aux basses latitudes vers les hautes latitudes et l'atmosphère, ainsi que d'un stockage important de chaleur et de carbone anthropique dans les masses d'eau aux moyennes latitudes. La dynamique du gyre entraîne également une ventilation peu profonde de l'océan (1000m) sur des échelles de temps allant de 1 à 20 ans, ce qui joue un rôle dans le climat en modérant les flux océan-atmosphère à ces échelles de temps intermédiaires.

Pendant 14 ans, mes travaux se sont concentrés sur ces gyres subtropicaux, en particulier celui de l'océan Atlantique Nord et ses masses d'eau. Je décris mes contributions de recherche aux problématiques de caractérisation et de compréhension de la stratification océanique dans le gyre: vis à vis de sa structure méso-grande échelle et de sa variabilité saisonnière à décennale. Je réponds à ces problématiques appliquées à la plus importante masse d'eau du gyre subtropical de l'océan Atlantique Nord, l'eau dite "à dix-huit degrés". Pour ce faire, je montre comment j'ai utilisé les principes de dynamique des fluides géophysiques liés à la ventilation de l'océan. L'accent est clairement mis sur le processus de transformation de masse d'eau. Je présente en outre de nouvelles techniques d'analyse et de diagnostic que j'ai développées pour étudier objectivement la stratification de l'océan à partir de simulations numériques de la circulation océanique, d'estimations de l'état de l'océan basées sur l'assimilation de données et de mesures directes de l'océan. Enfin, je conclus par les principaux axes de recherche que je me propose d'étudier dans les années à venir : la variabilité passée et future des courants de bord ouest.

Mots clés: Dynamique océanique aux moyennes latitudes, cycle de vie des masses d'eau, processus océaniques et d'interactions océan-atmosphère de méso à grande échelle, variabilité saisonnière à interannuelle.

Structure and variability of the subtropical gyre

Abstract: The subtropical gyre is a large system of ocean currents and water masses stretching across each of the oceans at mid-latitudes. Primarily driven by winds, the upper ocean circulation tends to accumulate water masses in the center of the gyre. This accumulation drives: a specific stratification, a large scale equatorward circulation in the upper ocean and a compensating intense and narrow current flowing poleward along the western boundary of the ocean (eg: the Gulf Stream in the North Atlantic or the Kuroshio in the North Pacific). The gyre circulation is responsible for redistributing heat taken up by the ocean at low-latitudes to the higher latitudes and to the atmosphere, as well as for storing heat and anthropogenic carbon in its water masses at mid-latitudes. The gyre dynamic furthermore leads to a shallow (1000m) ventilation of the ocean on time scale ranging from 1 to 20 years that plays a role in climate by moderating ocean-atmosphere fluxes on these intermediate timescales.

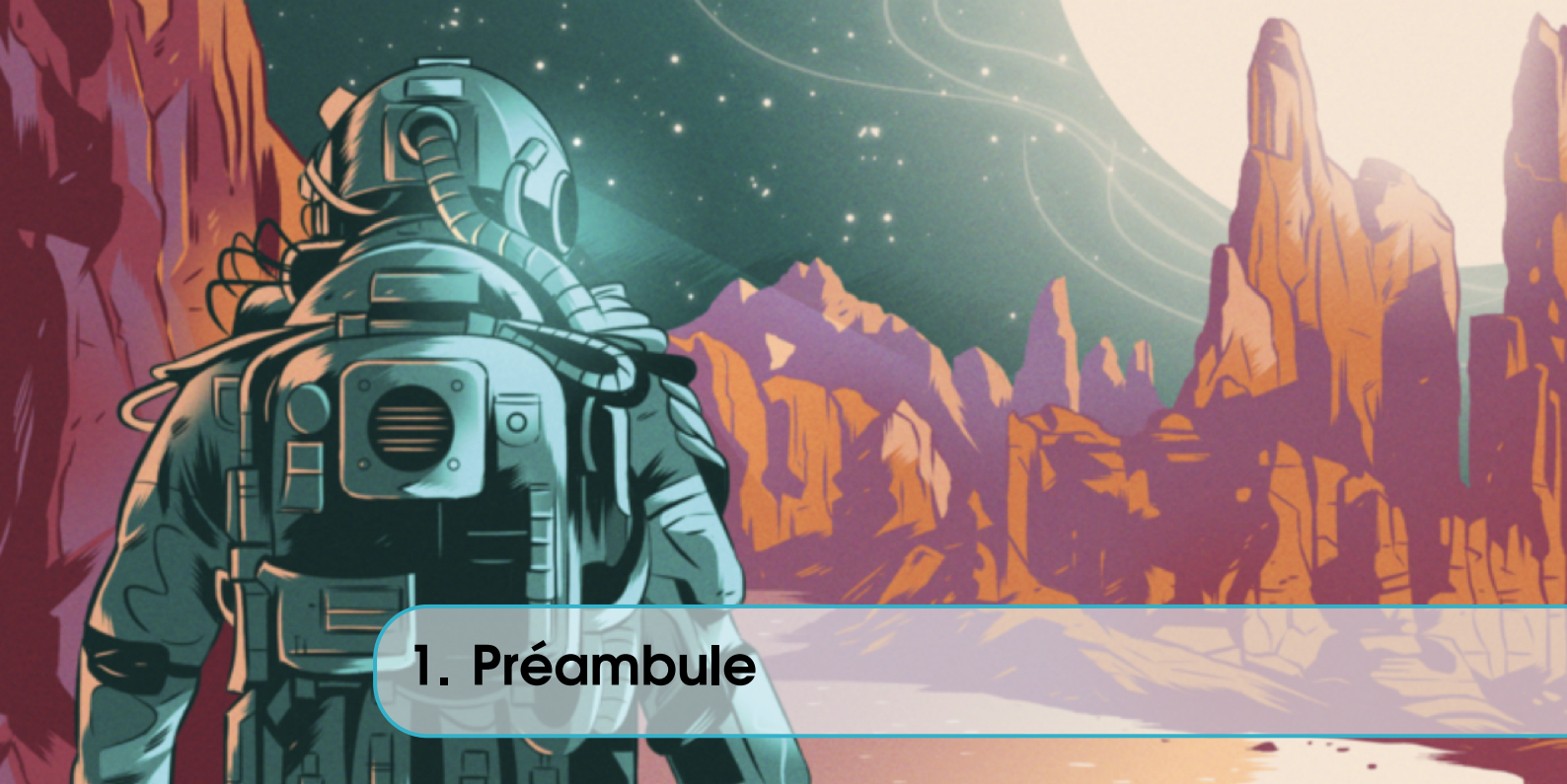
Over 14 years, my work has been centered on subtropical gyres with a focus on the North Atlantic gyre and its water masses. I provide a description of my research contributions to key physical oceanographic questions: what is, and what controls, the ocean stratification structure and variability on seasonal to decadal time-scales ? I answer these questions applied to the most important subtropical gyre water mass of the North Atlantic, the "Eighteen Degree water". I show how I used geophysical fluid dynamic principles of the ocean ventilation. A clear emphasis is made on the water-mass transformation process. I will furthermore present new analysis and diagnostic techniques I developed to objectively study the ocean stratification from ocean circulation numerical simulations, ocean state estimates based on data assimilation and direct ocean measurements. Last, I conclude with the main research axes I propose to investigate in the upcoming years: the past and future variability of western boundary currents.

Keywords: Mid-latitude ocean dynamic, water mass life cycle, oceanic processes and air-sea interactions from meso to large scale, seasonal to interannual variability.



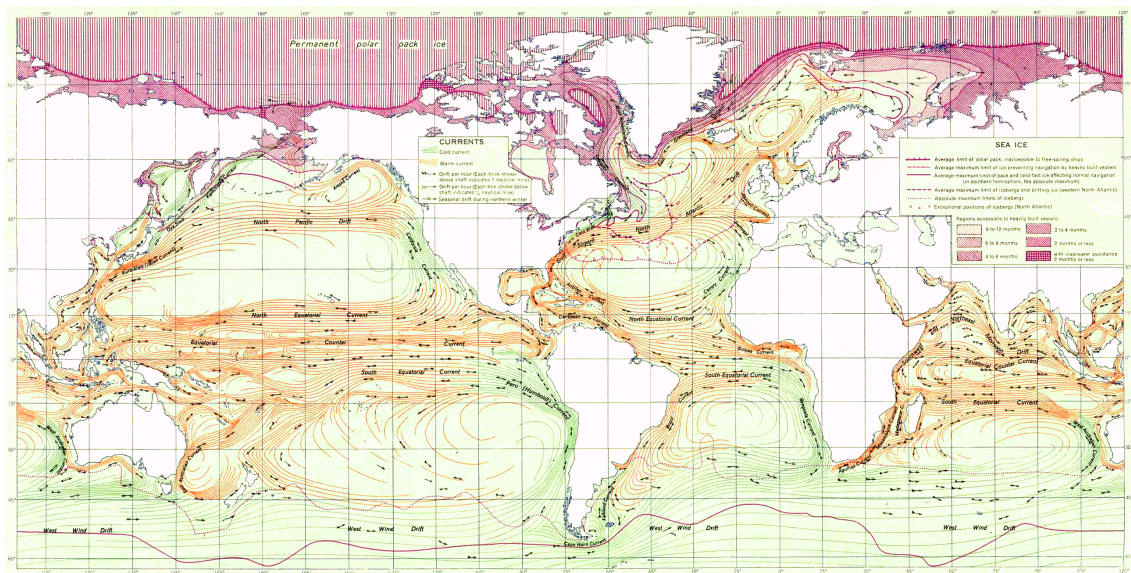
Contents

1	Préambule	7
2	Historical perspectives on the EDW	13
3	Seasonal EDW volume fluctuations	31
4	Water-mass transformation processes	39
5	Low-frequency variability of the EDW	57
6	Ventilation of the subtropical Gyre	65
7	Coherence of the gyre stratification	75
8	Observing the ocean with Argo	85
9	Future work	97
10	Appendix	103



1. Préambule

Ma spécialité de recherche est la physique de l'océan subtropical. La carte ci-dessous représente la vision que l'on avait des grands courants océaniques de surface à la fin de la 2nd guerre mondiale ([Atlas of World Maps, 1943](#)): l'océan subtropical correspond aux zones où de grands tourbillons, ou "gyre" s'étendent au travers de chacun des bassins océaniques entre 15 et 45 degrés de latitude.



Dans ce manuscrit, je décris mes contributions de recherche à une meilleure compréhension de ces gyres. J'y aborde plus particulièrement les problématiques suivantes: le cycle de vie saisonnier des masses d'eau, la variabilité basse fréquence et sa phénoménologie extreme, la ventilation océanique et comment elle structure l'océan subtropical et enfin, la turbulence de méso-échelle et son impact sur la grande échelle. J'ai jusqu'ici dérivé ces problématiques principalement pour l'océan Atlantique Nord. Je décris également dans le dernier chapitre ma contribution au réseau d'observation global de l'océan Argo.

Mon parcours scientifique

D'avril 2006 à décembre 2008, j'ai travaillé au département des Sciences de la Terre, des Atmosphères et Planétaires du MIT (Massachusetts Institute of Technology) dans l'équipe du Pr. J. Marshall et au sein du projet CLIMODE (CLIVar MOde Water Dynamic Experiment). Ce premier projet postdoctoral a consisté à étudier à partir des **observations** et de simulations numériques réalistes contraintes par l'**assimilation de données** le cycle de vie des eaux modales subtropicales de l'Atlantique Nord. J'ai développé de **nouvelles méthodes de caractérisation** du processus de ventilation des masses d'eau afin de pouvoir déterminer dans le temps et l'espace où les eaux modales sont formées/détruites et par quel processus (Maze et al., 2009; Marshall et al., 2009; Forget et al., 2011; Maze and Marshall, 2011; Cerovečki et al., 2013; Maze et al., 2013).

De janvier 2009 à décembre 2010, j'ai travaillé au sein du GIS Europole Mer, au LPO et au LEMAR (UMR 6539) en tant que postdoc. J'ai étudié de quelle manière la ventilation des masses d'eau pouvait être caractérisée par la concentration océanique en oxygène (Maze et al., 2012). Ce traceur non-conservatif (c'est à dire qui dépend des processus biogéochimiques) est utilisé qualitativement depuis les débuts historiques de l'océanographie. Il s'agissait dans ce projet exploratoire de déterminer les utilisations quantitatives que pourra permettre l'afflux massif de nouvelles mesures issues des **capteurs innovants** du réseau d'**observation expérimental** BIO-Argo. J'ai également étudié de manière plus théorique les paramètres contrôlant les propriétés de la couche de minimum d'oxygène que l'on observe dans tous les océans.

De janvier 2011 à juin 2012, j'ai conduit un dernier postdoctorat à l'Ifremer au LPO au sein de l'équipe du projet "Observatoire de la variabilité interannuelle et décennale en Atlantique Nord" (OVIDE). J'ai continué mon analyse de la structure océanique en oxygène en la rapprochant de celle de la stratification, ces deux propriétés étant liées par les processus de ventilation océanique. J'ai ainsi étudié comment caractériser et comprendre de manière plus fondamentale le processus de ventilation des masses d'eau grâce à l'analyse dans les **observations** de la structure et variabilité de la thermocline principale aux moyennes latitudes de l'Atlantique Nord.

En juillet 2012, j'ai intégré l'Ifremer en tant que chercheur permanent avec pour projet de documenter la structure et la variabilité des gyres subtropicaux grâce aux observations Argo, et d'identifier et comprendre les mécanismes fondamentaux qui les contrôlent. Ma mission incluait également de contribuer au développement du réseau d'observation global Argo.

Mes activités se sont alors organisées autour de 4 thèmes: les observations in-situ, les approches méthodologiques, la structure globale de la stratification subtropicale et la phénoménologie des extrêmes de variabilité basse fréquence des masses d'eau.

- *les observations in-situ*. En 2013 j'ai pris en charge la coordination scientifique des activités liée à Argo en France et à partir de 2015 je me suis également impliqué dans les évolutions du réseau Argo, notamment sa composante profonde qui lui permettra d'observer l'océan jusqu'au fond (contrairement à la profondeur d'observation actuelle qui est de 2000m). Ces travaux m'ont permis de contribuer à une plus forte structuration et représentation des activités Argo en France (Maze et al., 2014c, 2015b, 2016b, 2017d; Riser et al., 2016; POULIQUEN et al., 2017) mais aussi de participer au développement de nouvelles technologies qui permettront au réseau Argo de répondre à de nouvelles questions scientifiques (Zilberman and Maze, 2015; Le Reste et al., 2016; de Lavergne et al., 2016).
- *les approches méthodologiques*. Une fois les observations acquises, il faut les traiter et les analyser. Dès 2011 j'avais débuté le développement d'un nouvel algorithme de caractérisation objective de la stratification subtropicale basé sur une reconnaissance des formes associées aux eaux modales et à la pycnocline permanente (par opposition à une identification non-objective basée sur leurs propriétés). C'est Charlène Feucher qui, pendant sa thèse (que j'ai co-encadré avec Herlé Mercier de septembre 2013 à novembre 2016 Feucher et al., 2016a), a achevé ce développement avec succès. En parallèle des travaux de Charlène, j'ai commencé d'explorer en 2014 de nouvelles méthodes statistiques avancées, ou pour le moins innovantes dans notre domaine, qui permettent le traitement et l'analyse des bases de données massives (Maze et al., 2014b,a). Ces travaux ont conduit à plusieurs résultats portant sur l'identification objectives de structures océaniques remarquables (Maze et al., 2017c; Rosso et al., acc,

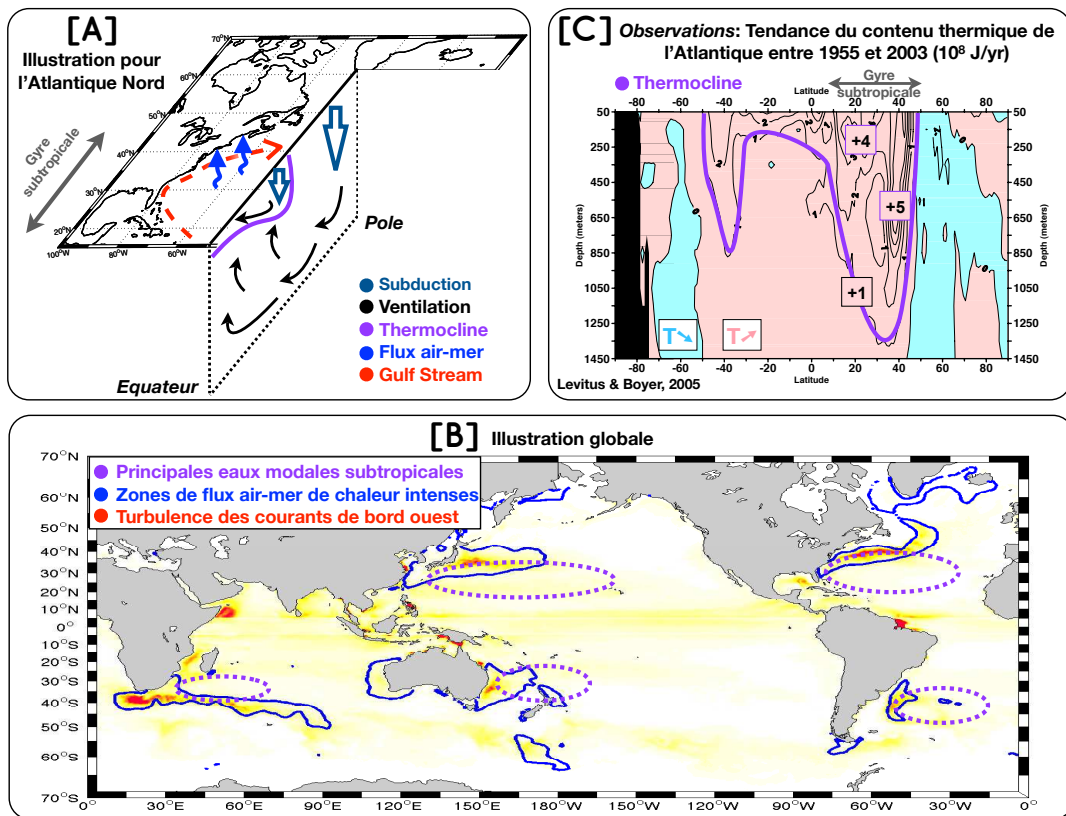


Figure 1.1: A: Illustration schématique du processus de ventilation dans le gyre subtropical Nord Atlantique. B: Distribution verticale/nord-sud de la tendance 1995-2003 de contenu de chaleur en Atlantique Nord. C: Illustration globale des éléments clés des gyres subtropicaux: eaux modales et courants de bord ouest, sièges des plus intenses échanges de chaleur entre l'océan et l'atmosphère.

2020) et le traitement des données Argo (Perez, 2017).

- *la structure globale de la stratification subtropicale.* Lors de la thèse de Charlène Feucher que j'ai co-encadré avec Herlé Mercier, nous avons étudié la stratification subtropicale Nord Atlantique dans son ensemble (Feucher et al., 2016b). Cette approche vise à considérer conjointement les eaux modales et la pycnocline principale dans une description continue horizontalement et verticalement de la structure du gyre subtropical. Nous avons ainsi pu mettre en évidence des gradients de densité important le long des pycnostades et pycnoclines qui contrastent avec une vision classique en "bol" des surfaces isopycnales dans les gyres forcées par le vent. Nous avons ensuite mis en évidence les mêmes structures dans les autres gyres (Feucher et al., 2019).
- *la phénoménologie des extrêmes de variabilité basse fréquence des masses d'eau.* Dans la thèse de Kenneth Lee que j'ai co-encadré à nouveau avec Herlé Mercier, nous avons caractérisé les extrêmes de variabilité interannuelle d'une eau modale particulière et en avons exploré les mécanismes. Nous avons pu montrer que c'est l'amplitude de la divergence des transports latéraux de chaleur dus aux transports d'Ekman qui principalement contrôle les occurrences de ventilation extreme de la masse d'eau (Lee, 2020). J'ai également pu diagnostiquer qu'en 2018, cette masse d'eau avait atteint un minimum d'épaisseur encore jamais observé depuis 1950, des suite d'une forte réduction engagée depuis 2014 (Stevens et al., acc., 2020; Maze et al., 2019a,b).

Le gyre subtropical

Les observations montrent une tendance climatique au réchauffement des couches de surface de l'océan et à une hausse du niveau de la mer (Levitus et al., 2005; Church and White, 2006). Les projections climatiques montrent que ces tendances se renforceront à l'avenir sous l'effet de la constante augmentation de la concentration atmosphérique en CO₂ d'origine anthropique (IPCC, 2007; Stocker et al., 2013). Le cycle global du carbone s'en trouvera profondément altéré (à cause des changements induits dans les flux air-mer, la solubilité, le mélange vertical) et avec lui le climat terrestre. Ces évolutions climatiques, passées et à venir, de la structure de l'océan traduisent une évolution de la stratification océanique et du processus de ventilation des masses d'eau. Il est donc nécessaire de mieux documenter et de comprendre les processus fondamentaux qui contrôlent la variabilité de ces éléments.

Les signaux climatiques pénètrent dans l'océan à la faveur du processus de ventilation des masses d'eau. La ventilation est l'ensemble des mécanismes par lesquels l'information d'une interaction avec l'atmosphère est intégrée dans l'océan (voir l'illustration régionale pour l'océan Atlantique Nord figure 1.1-A):

$$\text{Ventilation} = \text{subduction} + \text{circulation/mélange} + \text{re-émergence}$$

La variabilité du climat est en grande partie contrôlée par les échelles de temps liées à ce cycle. La dynamique grande échelle de l'océan fait que les signaux climatiques pénètrent lentement l'océan profond par les hautes latitudes et ne peuvent en re-émerger qu'après un laps de temps relativement long (»20 ans). Par contre, les signaux climatiques pénètrent, circulent et re-émergent plus rapidement aux basses et moyennes latitudes (1-20 ans). Cette ventilation plus rapide des masses d'eau, au coeur de mon expertise de recherche, prend place dans les gyres subtropicaux présents dans tous les bassins océaniques.

Le gyre subtropical est un grand système de courants océaniques et de masses d'eau qui s'étendent sur chacun des océans aux moyennes latitudes. Principalement entraînée par les vents, la circulation océanique proche de la surface a tendance à accumuler des masses d'eau au centre du gyre. Cette accumulation entraîne : une stratification spécifique, une circulation de grande échelle dirigée vers l'équateur dans la partie supérieure de l'océan et un courant compensateur très étroit dirigé vers le pôle, circulant le long du bord ouest de l'océan (ex: le Gulf Stream dans l'Atlantique Nord ou le Kuroshio dans le Pacifique Nord). La circulation du gyre est responsable du transfert de la chaleur absorbée par l'océan aux basses latitudes vers les hautes latitudes et l'atmosphère, ainsi que d'un stockage important de chaleur et de carbone anthropique dans les masses d'eau aux moyennes latitudes. La dynamique du gyre entraîne également une ventilation peu profonde de l'océan (1000m) sur des échelles de temps allant de 1 à 20 ans, ce qui joue un rôle dans le climat en modérant les flux océan-atmosphère à ces échelles de temps intermédiaires.

Ces gyres sont caractérisés par trois éléments clés:

1. Dans leur coeur: les eaux modales subtropicales, des masses d'eau très volumineuses aux propriétés homogènes (Hanawa and Talley, 2001). Elles sont un réservoir, renouvelé localement, qui peut stocker sur des échelles de temps interannuelles à décennales des quantités très importantes de chaleur. Elles portent donc en elles une inertie thermique capable de faire re-émerger des anomalies climatiques dans le système couplé océan-atmosphère (Kwon and Riser, 2004; Sugimoto and Hanawa, 2007). C'est aussi vrai pour le carbone anthropique (Bates et al., 2002). J'ai contribué à une meilleure caractérisation et compréhension du cycle de vie des eaux modales subtropicales (Marshall et al., 2009; Forget et al., 2011). Mais les mécanismes connectant la formation et la circulation à ces réservoirs de chaleur sont encore peu étudiés (Maze and Marshall, 2011).
2. Sur leur flanc: les courants de bord ouest. Ils sont responsables de la majeure partie du transport de chaleur océanique de l'équateur vers les pôles. Ce transport de chaleur est un régulateur essentiel du climat, en particulier parce que la plus grande partie de cette chaleur est transférée à l'atmosphère lorsque les courants de bord ouest se détachent des continents, dans leur "extension". J'ai contribué à mieux comprendre la variabilité grande échelle des interactions océan-atmosphère aux moyennes latitudes (Maze et al., 2006; Maze, 2006). Du point de vue atmosphérique, ces flux air-mer de chaleur participent au forçage des grandes circulations d'ouest et influencent leurs modes de variabilité (Maze

et al., 2011). Du point de vue océanique, cette perte de chaleur est intimement liée au processus de formation des eaux modales (Maze et al., 2009). Cependant, les courants de bord ouest génèrent une intense activité turbulente à petite échelle (voir illustration pour l'océan globale figure 1.1-B) dont j'ai contribué à mieux déterminer les impacts sur les flux air-mer et le cycle de vie des eaux modales (Shuckburgh et al., 2011; Maze et al., 2013).

3. A leur base: une zone de forte stratification que je désignerai - abusivement - par thermocline principale. Elle est la limite entre les masses d'eau de surface ventilées rapidement localement et les masses d'eau profondes ventilées lentement à distance (hautes latitudes). Elle pourrait donc participer au contrôle de la re-émergence des signaux climatiques profonds vers la surface. La circulation océanique qui maintient la structure de la thermocline a deux composantes principales : une circulation peu profonde contrôlée par le vent et une circulation profonde thermohaline. Les différents modèles théoriques de la thermocline accordent plus ou moins d'importance à chacune de ces circulations (Luyten et al., 1983; Salmon, 1990, de la théorie de la thermocline adiabatique ventilée à la thermocline interne advective/diffusive). La réalité est un continuum complexe de ces deux régimes dans lequel s'insèrent les eaux modales (Samelson and Vallis, 1997) et où les mécanismes contrôlant la stratification sont encore mal identifiés (Marshall et al., 2002; Radko and Marshall, 2004a; Henning and Vallis, 2004; Cessi, 2007). Un pré-requis à cette compréhension est une meilleure caractérisation des propriétés de la thermocline principale, ce que j'ai réussi à déterminer grâce aux données du réseau Argo (Feucher et al., 2016b, 2019).

La Figure 1.1-C représente l'évolution typique du contenu thermique dans l'océan Atlantique au cours des 50 à 70 dernières années (Levitus et al., 2005). Elle illustre une caractéristique majeure du réchauffement climatique: il se concentre dans les zones de ventilation rapide des océans. Ainsi, les observations montrent que l'augmentation climatique du contenu thermique océanique se concentre aux couches localisées entre la surface et la thermocline principale sur les flancs équatoriaux des courants de bord ouest Wu et al. (2012) et que les eaux modales se réchauffent deux fois plus rapidement que la surface (Sugimoto et al., 2017). Les propriétés des eaux modales subtropicales portent donc en elles les propriétés de ce signal climatique tandis que la thermocline et son prolongement vers la surface au niveau du courant de bord ouest exercent clairement des contraintes sur la pénétration du signal dans l'océan. Voici donc les raisons fondamentales pour lesquelles je m'intéresse à mieux caractériser et comprendre le processus de ventilation dans les gyres subtropicaux.

Ce manuscrit de HdR portera sur mes travaux liés principalement à 2 de ces trois éléments: l'eau modale et la thermocline. Mon projet pour les années à venir se concentrera sur le troisième: le courant de bord ouest.

Dans le premier chapitre 2 j'offre une perspective historique sur l'eau modale subtropicale de l'Atlantique Nord, de 1877 à 2016. Dans le chapitre 3 je décris le cycle saisonnier de cette masse d'eau, puis dans le chapitre 4 j'explique les mécanismes physiques qui en sont responsables. Dans le chapitre 6 j'explique le processus de ventilation du gyre subtropical et dans le suivant je décris les phénomènes extrêmes qui caractérisent la variabilité basse fréquence de l'eau modale et en fournis une explication. Enfin dans le chapitre 7 je reviens à une approche globale et synthétique de la stratification subtropicale. Dans le dernier chapitre 8 je décris ma contribution au réseau d'observation global Argo avant de terminer par une brève description des projets que je compte mener dans les années qui viennent.

Le lecteur uniquement francophone me pardonnera le fait que le reste de ce manuscrit soit rédigé en anglais.



2. Historical perspectives on the EDW

The Eighteen Degree Water (EDW) is one of the oldest known features of the ocean. A full review of the literature with regard to the EDW is beyond the scope of this manuscript. In the introduction below, I will highlight the key results from a couple of historical papers ([Worthington, 1959](#); [Talley and Raymer, 1982](#); [Kwon and Riser, 2004](#)) and close this brief overview by my contributions to the most modern perspective on this water mass.

Contribution highlight My contributions to the scientific question: "What is the mean EDW structure ?" can be summarized as follows:

- a better localization of the EDW layer in the horizontal and vertical plans using Argo data ([Marshall et al., 2009](#); [Maze et al., 2009](#); [Lee, 2018](#)),
- an objective description of the unstratified EDW layer, as part of the subtropical gyre warm water sphere stratification ([Feucher et al., 2015, 2016a,b](#)).

Content of this chapter:

Introduction	14
History	16
The EDW within the global ocean	16
A pre-Argo perspective	17
The CLIMODE project	19
A modern perspective of the EDW layer	21
Data and methods	21
Defining the EDW layer	24
Results	25
The North Atlantic Mode Water continuum	26
Final remarks	27

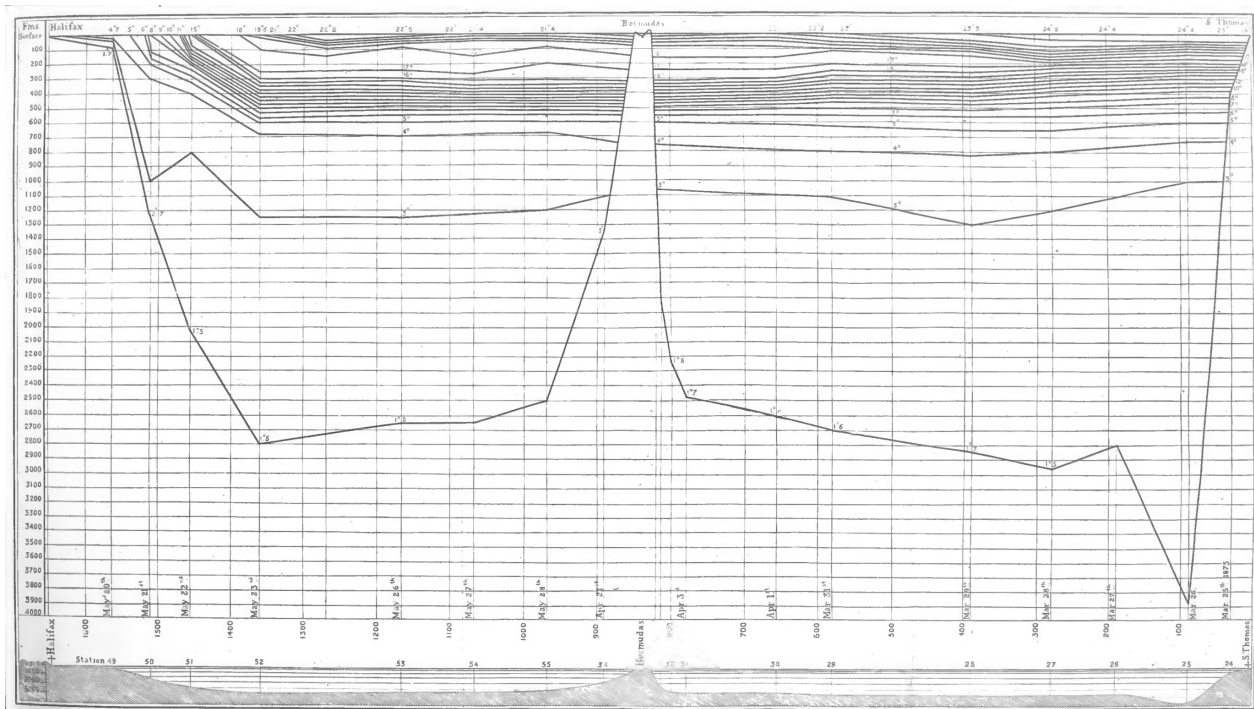


Figure 2.1: Plate IX from [Wyville Thomson \(1877\)](#). Diagram of the vertical distribution of temperature between St Thomas and Halifax. The Eighteen Degree Mode Water is clearly seen in the upper 500m as a thick thermocline. This is the first historical depiction of the EDW. Bottom: Figure 33 from [Worthington \(1976\)](#). Salinity at 300m. Black squares: 36.40 – 36.60‰ only. Numbered squares: 36.00 – 36.39‰ and 36.61 – 36.99‰. The symbol < represents values below 36.00. The black squares capture the salinity range of the EDW and provide indication of its geographical location.

Introduction

The EDW was first observed nearly 145 years ago during the circumnavigation of the Challenger expedition ([Wyville Thomson, 1877](#)). Considered as the first modern physical oceanographic cruise, the Challenger expedition sampled 17 stations of the water column temperature during its 1873 transect from St Thomas (Antilles, March 25th), to Bermuda (April 4th), Halifax (May 9th) and back to Bermuda (May 28th, 105 years before my exact birthday). [Figure 2.1](#) shows the resulting temperature section. This diagram is outstanding. As pointed out by [Wyville Thomson \(1877\)](#), it shows the key feature of the subtropical gyre stratification that this chapter is talking about: between 100 and 300m depths, the ocean temperature is nearly homogeneous from station 52 to station 25, i.e. over 1000km centered near Bermuda. This water mass with a temperature near 18°C (hence its name) is remarkable because it extends through a particularly large region and thickness, which is totally unusual for the upper surface layer of the ocean where it is found and that is typically much more stratified.

The first modern and specific study of the EDW was conducted by [Worthington \(1959\)](#). He provided a reasonable estimate of the EDW property ranges: $\theta = 17.9 \pm 0.3^\circ\text{C}$, $36.50\text{‰} \pm 0.10\text{‰}$. He also pointed out that the EDW observed by [Wyville Thomson \(1877\)](#) was penetrating the southern part of the Sargasso Sea where the winter time sea surface temperature is far warmer than 18°C, so that this local EDW must originate from elsewhere. Linking to [Iselin \(1936\)](#) analysis of the 1931-1934 "Atlantis" observations of the Western North Atlantic, [Worthington \(1959\)](#) noted that the winter mixed layer depth is particularly deep south of the Gulf Stream, reaching depths of about 400m and having a temperature around that of the EDW. In summer, the 18°C layer is found to remain thick, trapped below the seasonal pycnocline. The long lasting working hypothesis of the EDW formation mechanism was thus that the EDW was formed in the deep mixed layers

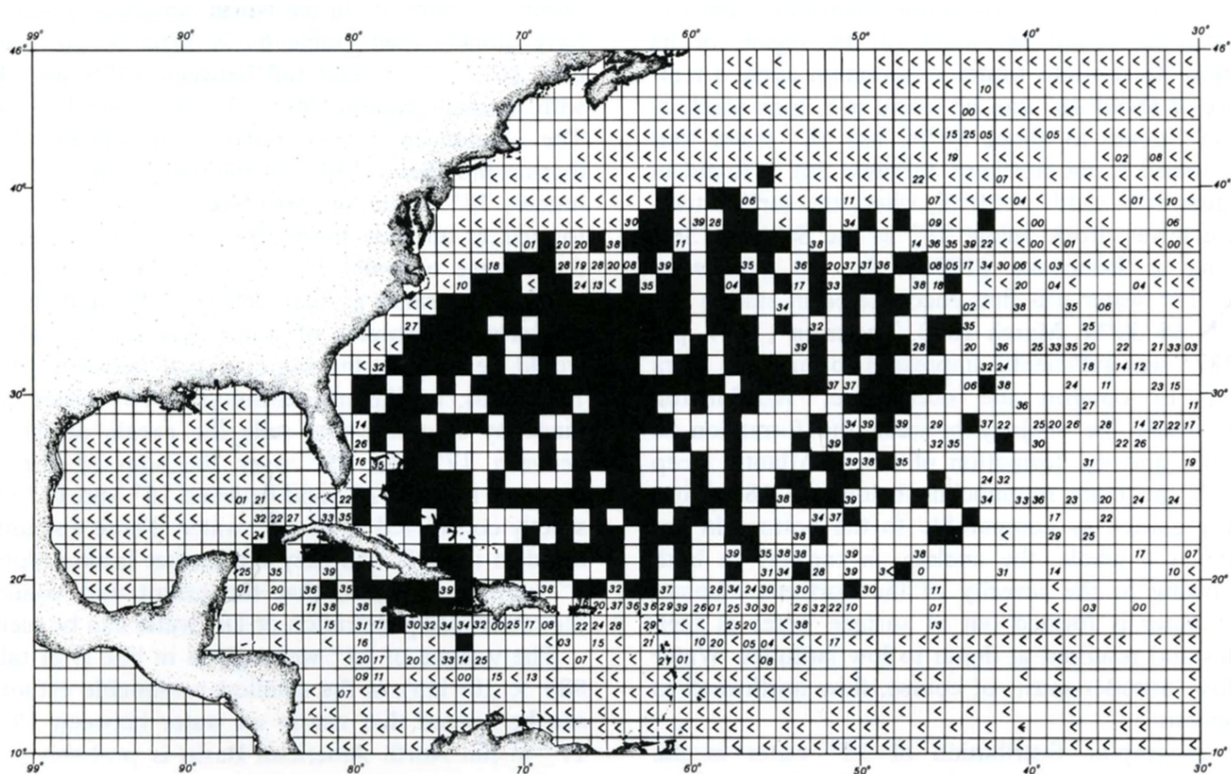


Figure 2.2: Figure 33 from [Worthington \(1976\)](#). Salinity at 300m. Black squares: 36.40 – 36.60‰ only. Numbered squares: 36.00 – 36.39‰ and 36.61 – 36.99‰. The symbol < represents values below 36.00. The black squares capture the salinity range of the EDW and provide indication of its geographical location.

south of the Gulf Stream and was then transported southward, down to 20°N. We note in passing that one had to wait 20 years for [Stommel \(1979\)](#) to recognize that only water parcels subducted at the end of the winter, in the deepest mixed layers, would irreversibly enter the ocean interior, (the so-called 'Stommel demon', a process later demonstrated many times, e.g. [Williams et al., 1995](#)).

[Worthington \(1959\)](#) has shown the EDW distribution using salinity data at 300m. This description was later updated by [Worthington \(1976\)](#). The results are reproduced here [Figure 2.2](#). It clearly shows that in the 1970s, it was already known that the mean geographical limits of the EDW could be defined to the North and to West by the Gulf Stream. However, the southern and eastern limits were much more fuzzier. To the South, the Antilles appear as a 20N limit; but one can note some EDW salinity penetrating in the Caribbean Sea, of which the origin was not clear. To the East, someone would basically say that no EDW could be found to the East of 40W. One had to wait for a more routinely used objective description of the EDW based on potential vorticity ([McCartney, 1982](#); [Talley and Raymer, 1982](#); [Ebbesmeyer and Lindstrom, 1986](#)) and for more data ([Levitus, 1982](#)) to draw a reasonably detailed and robust distribution map of the EDW layer.

[Talley and Raymer \(1982\)](#) analyzed the EDW temporal variability (see below) and noted that it encompasses, at several time scales, the same order of magnitude than the spatial range of EDW properties. This provides an additional difficulty to determine meaningful distribution maps from any non synoptic data without excessive averaging. This key issue was also raised by ([McCartney, 1982](#)) and won't be clearly addressed before the advance of the Argo observational array (see later).

With regard to the EDW variability, [Schroeder et al. \(1959\)](#) noted the remarkably constant temperature and salinity of the EDW off Bermuda, using data from the Atlantis surveys in the 30s, and more robustly, using the first years of measurements from the Bermuda Biological Station which was established in 1954. Later on, [Talley and Raymer \(1982\)](#) revisited the Bermuda station data and showed that the EDW core potential density

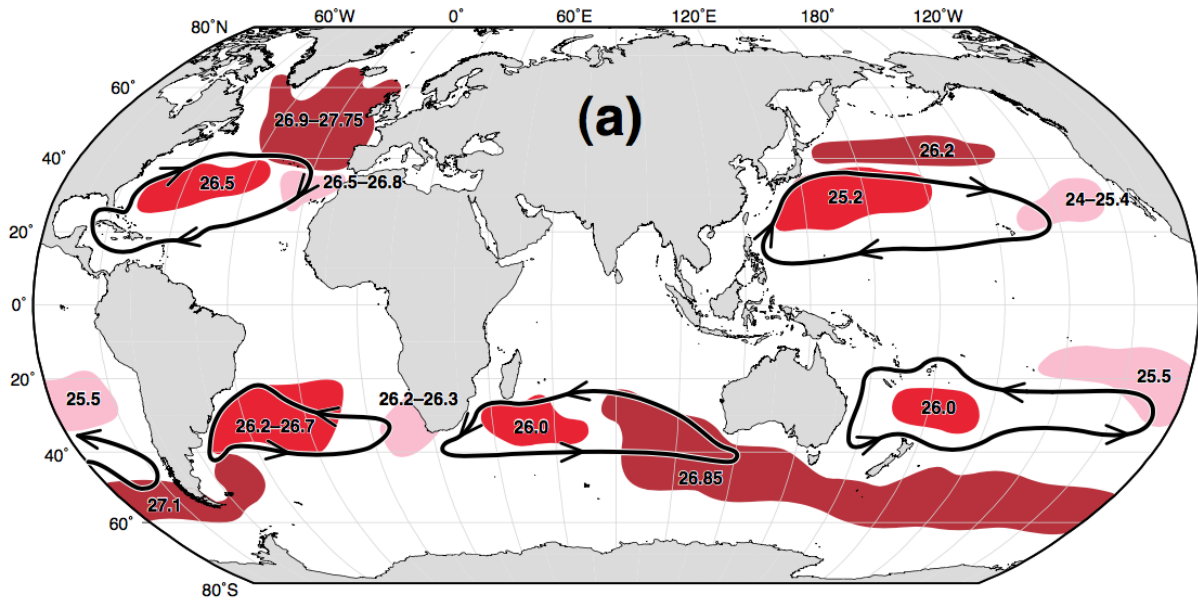


Figure 2.3: Early 2000s schematic view of the warm mode water distributions in the world's oceans from [Hanawa and Talley \(2001\)](#), a minor update to [Talley \(1999\)](#). Red colored areas show the subtropical mode waters (STMWs) associated with the subtropical western boundary currents in each ocean (STMW-I). Purple colored areas show the eastern type of subtropical mode waters (STMW-II), including Madeira Mode Water, North Pacific Eastern STMW and South Pacific Eastern STMW. Brown colored areas show the third type of subtropical and subpolar mode waters, including North Atlantic Subpolar Mode Water, Subantarctic Mode Water and North Pacific Central Mode Water. Approximate potential densities σ_0 are indicated. Black arrows roughly represent the subtropical gyre circulation.

and temperature could remain relatively constant for about 10 years (from 1953 to 1964) and then show some decreasing temperature and increasing salinity raising the EDW density for about 5 years (from 1964 to 1971). The month-to-month variability of the EDW properties at Bermuda over these first 15 years of data was found to be quite large: of about the same order of magnitude than the interannual signal: about 0.1 kg m^{-3} , 0.5°C and 0.1‰ .

[Talley and Raymer \(1982\)](#) also found that the EDW at Bermuda could be linked to water properties convected several months before, South of the Gulf Stream. So they furthermore tried, but without success, to positively correlate the EDW temperature variability at Bermuda to that of air-sea heat fluxes South of the Gulf Stream. The working hypothesis was that negative heat fluxes, cooling the ocean, would lead to cooler EDW variety and greater renewal. Surprisingly, they found little direct correlation and even an out of phase relation, pretty much like previous work from [Jenkins \(1982\)](#) and [Worthington \(1972\)](#). In fact, these early studies failed at finding such correlations because they suffered from the poor knowledge of air-sea heat fluxes in the region. Heat budgets of the EDW layer could not be conducted reliably in order to determine how much of the heat advected into the region by the warm core of the Gulf Stream was impacting the EDW layer vs how much heat was flux out toward the atmosphere (a key mechanism driving the atmospheric baroclinicity that is still studied to day, e.g. [Kelly et al., 2010](#)).

History

The EDW within the global ocean

Mode waters resembling the EDW have been discovered elsewhere. Indeed, as the other subtropical gyres have been explored, it was found over the years that in all warm recirculation regions of Western Boundary Currents (WBC) a specific mode water, resembling the EDW, is observed. [Talley \(1999\)](#) first introduced a

global schematic for the distribution of these mode waters. This schematic was later updated by [Hanawa and Talley \(2001\)](#). It is that later reference that is the most widely cited, and their schematic, reproduced here [Figure 2.3](#), is clearly state-of-the-art. Later in this manuscript, I will present an update to this schematic based on an objective identification of the mode water layers from modern Argo data ([chapter 7](#)).

It is worth noting that the "warm" mode waters described by [Talley \(1999\)](#) and [Hanawa and Talley \(2001\)](#) are most often referred to as "Subtropical Mode Waters" (STMW), a term introduced by [Masuzawa \(1969\)](#) by reference to the North Pacific counter part of the EDW. From [Figure 2.3](#), one can clearly see five STMWs of the same type as the North Atlantic EDW (the red water mass) in each of the subtropical gyres. More precisely, [Hanawa and Talley \(2001\)](#) introduced a nomenclature for the different flavors of STMWs:

- Type I (STMW-I): associated with western boundary currents (WBC) and their extensions. The EDW is of this type. There is a STMW-I on the warm flank of each WBC extensions. They are characterized by nearly the same temperature of $17 - 18^{\circ}\text{C}$ and their clear signature below the seasonal thermocline.
- Type II (STMW-II): found in the eastern part of the subtropical gyres. They are characterized by temperature/salinity gradients, density compensated and by the fact that they tend to not persist over a seasonal cycle.
- Type III (STMW-III): associated with the warm flank of the subpolar fronts. They are the densest flavor of the STMWs.
- Type IV (STMW-IV): associated with the maximum salinity region in the high evaporation regions of the subtropical gyres.

[Hanawa and Talley \(2001\)](#) (re)introduces the notion of mode water as a water mass having uniform properties over a significant fraction of the water column and relatively large geographical domains. The term "mode" arises from the idea that a regular temperature/salinity (T/S) sampling of a domain encompassing a mode water will exhibit a "mode", i.e. a maximum in volume inventory, centered on the T/S properties of that mode water. However, it is also worth noting that the term EDW is sometimes referring to the entire bulk of water with temperature around 18°C , and sometimes referring to the subset of that water mass with a poor stratification. That later definition is similar to the STMW-I. This confusion in the terminology and the mode water definitions lead to difficulties in the comparison of the various estimates of mode water volume and its variability. This will be explained in details in the next [chapter 3](#).

[Hanawa and Talley \(2001\)](#) furthermore contains an exhaustive review of all mode waters properties and their variability driving mechanisms. At the seasonal time scale, they noted that the EDW variability has been mostly studied through the Bermuda Station time series. Unfortunately, the station is located well downstream of the formation region near the Gulf Stream, which precludes any serious study of the EDW formation seasonal cycle. So, this let us with the rough description from [Kwon and Riser \(2004\)](#): a larger volume in late winter and a smaller volume in the late fall (see next section). [Hanawa and Talley \(2001\)](#) also noted that the EDW low-frequency variability was small at the inter-annual time scale, and was dominated by decadal variations linked to the NAO. This is not so clear from [Kwon and Riser \(2004\)](#) analysis that revealed an interannual signal correlated with the NAO at 2 years, but also, indeed, a 10-to-14 year cycle for the 1961-1981 period (see [Figure 2.4](#)).

A pre-Argo perspective

At the time of the [Hanawa and Talley \(2001\)](#) review writing, the PhD work from Young-Oh Kwon was still in progress. However, it is his work, published in [Kwon \(2003\)](#); [Kwon and Riser \(2004, 2005\)](#) that really sets the state of the art of our knowledge with regard to the EDW dynamic in the early 2000s. His work is a first attempt to address the two key points that drove all the improvements and dedicated work conducted after the historical studies before the 90s:

1. the lack of synoptic observations to fully characterized the bulk of EDW layer,
2. the large uncertainties on air-sea fluxes, especially in the region of the Gulf Stream.

These key points could be generalized to many more regions of the World Ocean, and in fact, were fundamental drivers in the set-up of the WOCE in the late 80s and 90s. They would also be ultimately addressed by the

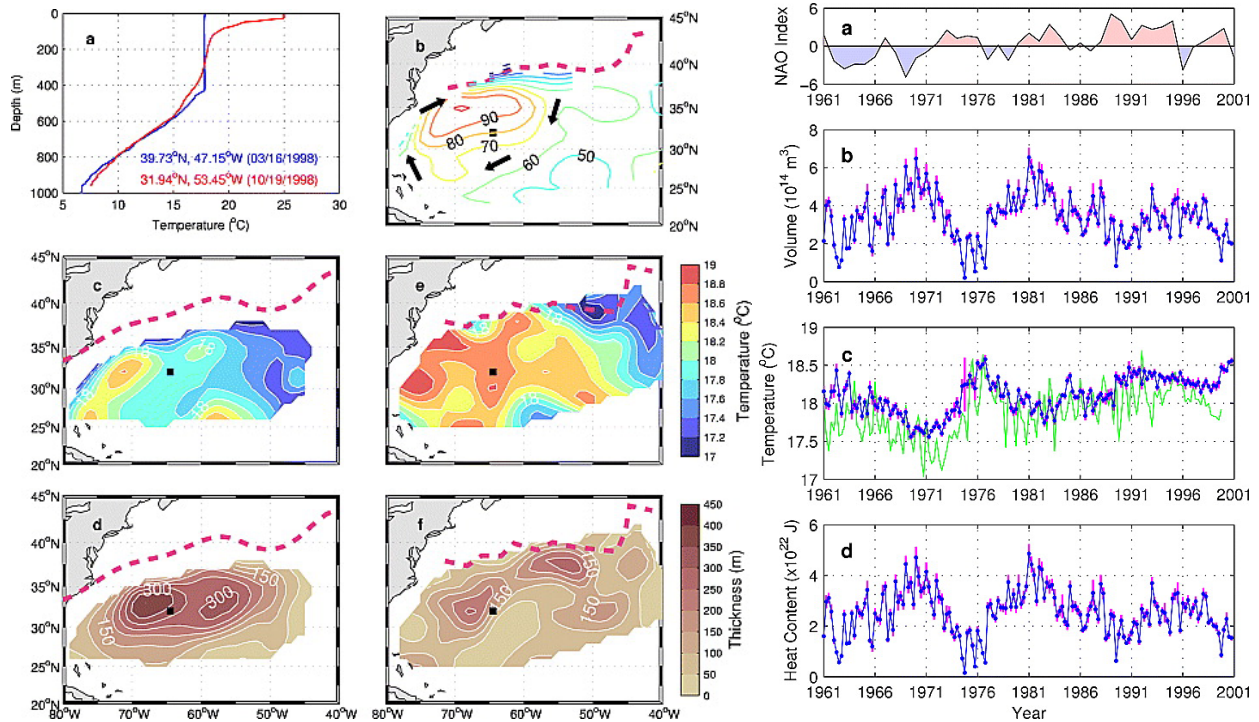


Figure 2.4: From [Kwon and Riser \(2004\)](#): Left a: typical temperature profiles, b: geostrophic pressure on the EDW isopycnal surface, c/d: EDW temperature/thickness for Jun. 1981, e/f: EDW temperature/thickness for Jun. 2000. Right: 1961-2001 NAO index (a) and EDW volume (b), temperature (c) and heat content (d) time series.

Argo array (which was set-up during the 1st Ocean's Obs. conference in 1999, [Roemmich et al., 1998](#)) that will provide enough synoptic observations to be used to constrain air-sea heat flux estimates and to monitor the EDW layer structure.

[Kwon and Riser \(2004\)](#) summarized the understanding of the EDW dynamic at the end of the WOCE. Their description of the EDW distribution and variability was based on all historical data and from the late 1990s deployments of the new PALACE profiling floats, as part of the WOCE. Their key results are summarized [Figure 2.4](#). Using objective mapping they could determine the first accurate EDW volume estimate and time series. They identified the EDW layer as the portion of profiles with temperature within $17 - 19^{\circ}\text{C}$ and vertical temperature gradient smaller than $0.006^{\circ}\text{C}/\text{m}$. The thickness and mean temperature for that portion of profiles was then calculated and mapped over 3-months windows from 1961 to 2001. [Fig.\(2.4\)](#)-left shows the temperature distribution within the EDW layer: it is warmer than 18°C in the northwest corner of the Sargasso Sea and colder in the northeast corner. The mean circulation map shows the warmer than 18°C water to spread eastward and the colder variety to spread southwestward. This was in line with the first EDW circulation inferences from [Worthington \(1976\)](#), later reproduced by [McCartney \(1982\)](#) and [Talley and Raymer \(1982\)](#), but was computed by [Kwon and Riser \(2004\)](#) with unprecedented precision. The EDW being spread along the Gulf Stream is furthermore reflected in the EDW thickness distribution of a thick layer, greater than 300m, in the formation area on the southern flank of the Gulf Stream and a thinner EDW layer further South in the Sargasso Sea.

[Kwon and Riser \(2004\)](#) also have shown that over a seasonal cycle, the EDW volume is the largest in winter, because of the active ventilation in the deep mixed layers South of the Gulf Stream, and that it is minimum in the fall. The winter time (from late fall, NDJ, to later winter, FMA) volume increase determined using only the PALACE floats data went from 2.4 to $4.7 \times 10^{14} \text{m}^3$ with about 10% uncertainty. Using all historical data, they get a smaller seasonal cycle from 2.8 to $3.9 \times 10^{14} \text{m}^3$. This could be translated into annual EDW production rates of 3.5Sv and 7.4Sv , respectively. As shown [Figure 2.4](#)-right, this seasonal cycle

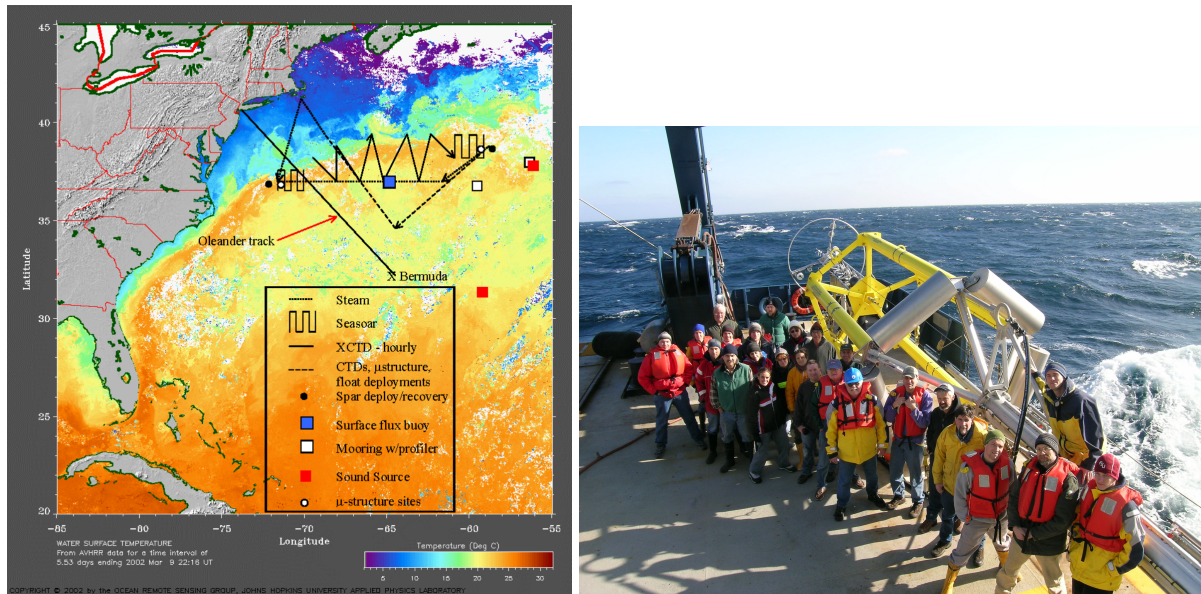


Figure 2.5: Left: Design of the CLIMODE in-situ observation experiments. 6 winter-time cruises were conducted from Nov. 2005 to Nov. 2007. Right: The scientific crew onboard the R/V Atlantis for the 2nd CLIMODE cruise in Jan. 2006. Behind the group seats the huge ASIS buoy used to measure air-sea fluxes.

amplitude is about the same order of magnitude as the lower frequency variability of the EDW volume, even smaller in fact.

The EDW heat content was primarily correlated with its volume and was found maximum in the later winter, despite the fact that the winter-time EDW was found to be colder than its annual mean. They also estimated that about $7.43 \pm 0.14 \times 10^{20} J$ were necessary to erode the seasonal thermocline in the formation region (using a typical fall temperature profile down to a mean Mixed Layer Depth). This estimate represents around 70% of the total winter-time surface heat loss in the region, as inferred from the best air-sea flux estimate at that time.

Last, [Kwon and Riser \(2004\)](#) have found a time lagged anti-correlation between the North Atlantic Oscillation (NAO, the dominant mode of atmospheric variability over the North Atlantic [Hurrell, 1995](#)) and the EDW temperature. Such a correlation had already been suggested based on Bermuda station data ([Joyce and Robbins, 1996](#)) and numerical modeling ([Paiva and Chassignet, 2002](#)). [Kwon and Riser \(2004\)](#) found a positive NAO to lead a positive EDW temperature anomaly by 1 to 6 years (maximum at 2 years). The broad peak indicates that the EDW has a memory of the atmospheric forcing that is consistent with its renewal time scale of about 3.5 years¹.

The CLIMODE project

The take-home message from the previous sections is that, as surprising as it could be, not much was known about the EDW in the early 2000s, even if it has been discovered more than 100 years ago. Therefore, in 2004, a multi-million dollars NSF-funded project was proposed by a group of American experts: CLIMODE, for CLIVar MOde water Dynamics Experiment (<http://www.climode.org>, [Figure 2.5](#)). This project proposed to study the formation, evolution, storage, dispersal and large-scale consequences of the EDW with a combination of observation and numerical modeling. In the previous sections, I've talked mainly from a rather descriptive point of view of the EDW structure and variability. The methodology of CLIMODE was to conduct a process study with a combination of theoretical, numerical and observational approaches in order to provide quantitative and satisfactory answers to some of the remaining key questions with regard to the EDW

¹Dividing the EDW volume by its annual production rate yields the turnover time, or renewal time scale

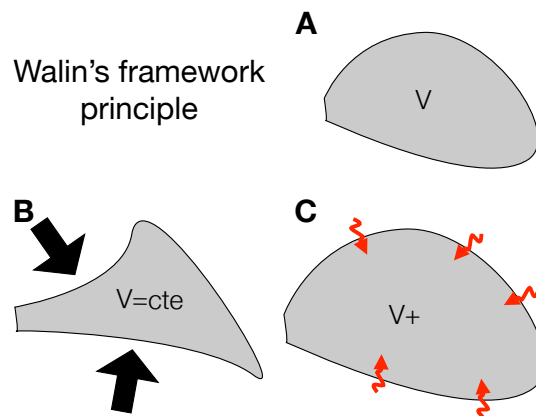


Figure 2.6: Highly schematic representation of the [Walın \(1982\)](#) framework of water-mass transformation. Let's consider a region bounded by isopycnal surfaces (A). Currents, or adiabatic processes, can only redistribute the mass within that region, i.e. deform it without changing its volume (B). Only diabatic processes, i.e. irreversible water mass transformations, can modify the total volume of the region (C). This is an "integral" or Lagrangian statement, from a "local" or Eulerian point of view, both diabatic and adiabatic process can create isopycnal movements.

life cycle. These were, for instance:

- How much of EDW is formed every winter ? an open question because independent estimates of formation rates did not match.
- How EDW is formed ? Beyond the 1-dimensional convective process, what is the role of lateral processes and the Gulf Stream ?
- Where EDW is lost to other density classes ? Where, how and how much mixing is eroding the EDW ?
- What is the effect of wind-driven processes in the EDW life-cycle ?
- What is the large-scale impact of EDW on the dynamics of the gyre ?

In fact, in the earlier 2000s, when each of the processes thought to be involved in the EDW volume or buoyancy budget were independently estimated (eg: air-sea heat flux driven formation, interior mixing rates): they could not be reconciled and the budget could not be closed within the error bars. For instance, the EDW in-situ volume estimates from [Kwon and Riser \(2004\)](#) yield a annual formation rate of about 3-7Sv. However, the formation rate estimated from air-sea flux and EDW outcropping was much larger, up to 15-20Sv ([Speer and Tziperman, 1992](#); [Marshall et al., 1999](#)).

I will describe in details in the next chapter 3 the theoretical framework used by CLIMODE to reach its objectives and will fully narrate my contributions to it. But let's introduce the reader with this simple, and yet so powerful, framework that was introduced by [Walın \(1982\)](#). [Figure 2.6](#) schematically represents this principle. It states that a given water body bounded by isopycnal surfaces can only see its volume to change by the effect of diabatic processes through its envelop. This statement is valid in the integral sense, not locally. If one draw an , imperfect, analogy with a plastic balloon, one can understand that even if the balloon is deformed by pressure forces (these would be adiabatic processes), it is only by air transfer through its "porous" surface that its volume could change. For a water mass, this means that only irreversible transformations of water parcels can modify its volume while currents will simply redistribute it in space. The CLIMODE project fully embraced this approach and provided a thorough quantitative estimate of all the terms responsible for the change of volume of the EDW layer.

In order to nail down a quantitative estimate of these processes, CLIMODE proposed a complete suite of in-situ observation experiments. The observational program is shown [Figure 2.5](#). It combines 6 winter-time cruises for upper ocean hydrography and currents sampling and direct air-sea flux measurements, as well as the release of both RAFOS and ARGO floats. A couple of moorings were also deployed. The idea was to observe the EDW formation along and South of the Gulf Stream, to track its circulation (floats were

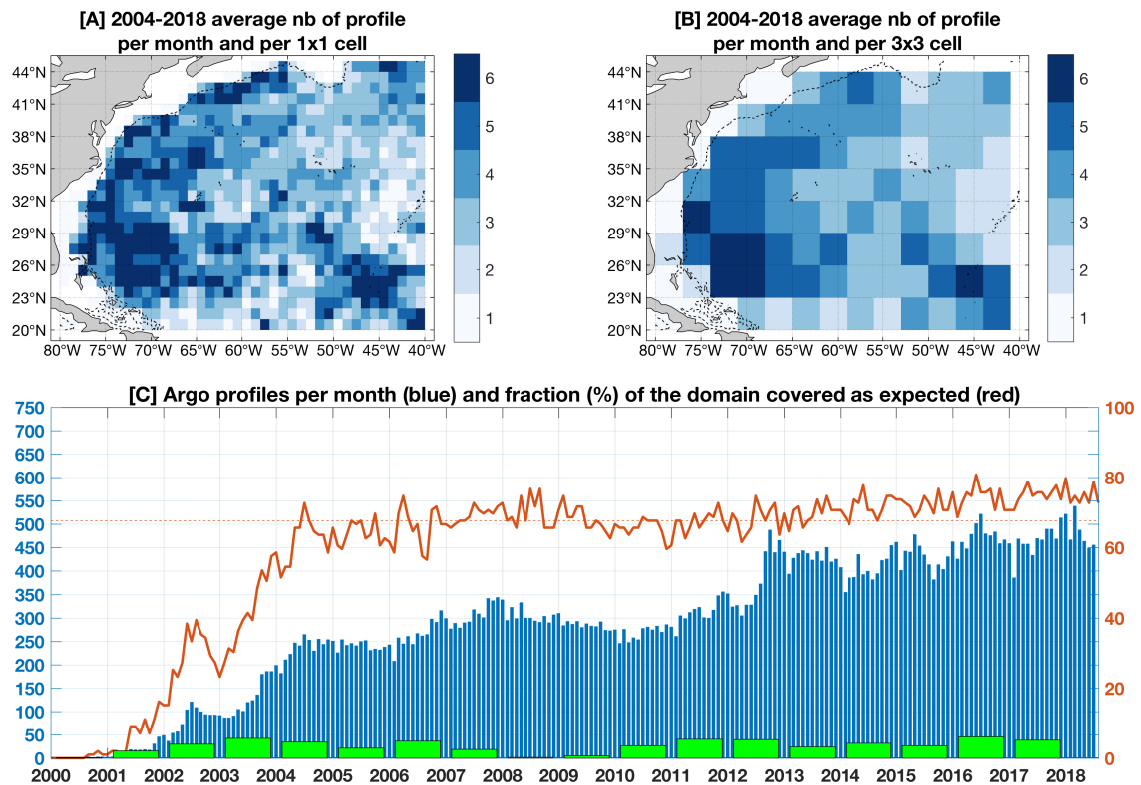


Figure 2.7: Plot A/B: Historical Argo data coverage of the Western North Atlantic per 3x3 (Plot B) and 1x1 (Plot C) cells. Plot C: Time series of the number of profiles per month (blue histogram), number of float deployments per year (green histogram) and the fraction of the domain – the Western North Atlantic – covered as expected (i.e. 1 profile per month per 3x3 cell). The dashed line indicates the median coverage of 68%.

set-up to drift along the EDW core isopycnal surface) and to improve the estimate of air-sea fluxes. I did not participate in any of the cruises. My postdoc studies at MIT was focusing on the formation processes due to air-sea fluxes with a more numerical approach.

I will simply conclude this EDW introduction by stating that EDW is the archetype of subtropical mode waters and that its life cycle is driven by a series of complex mechanisms encompassing a wide range of fundamental ocean processes. Therefore, to understand the EDW life cycle and be able to represent it correctly in realistic numerical simulations is a valuable target to improve ocean and climate modelling. This has been the core motivation of my contributions so far. So let's now review these contributions.

A modern perspective of the EDW layer

In order to understand the EDW seasonal cycle that will be the focus of the next chapters, it is of primary importance to be able to characterize accurately this water body distribution in space, starting by its climatology. This is not a trivial task because, as was pointed out in the previous chapter, the EDW is so large that it requires synoptic observations of the upper 1000m of the ocean; and these were not available before the advent of the Argo array.

Data and methods

Argo

Argo is a global network of profiling floats that will be described in details in [chapter 8](#). The Argo network is the primary source of in situ data observation for research in physical oceanography. It has global coverage and is not seasonally biased.

Contribution highlight France and Ifremer plays a key role in the Argo array sustainability and management. I contributed to the array as France representative into international Argo governance bodies and as national coordinator of the Management Board since 2013. This detailed in [chapter 8](#).

I furthermore contributed to the array through deployment of floats in the North Atlantic subtropical gyre.

With regard to the Western North Atlantic where the EDW is located, the Argo specific sampling is good. [Figure 2.7](#) shows (plots A and B) the 2004-2018 time mean number of profiles for 2 cell sizes: 3x3 and 1x1 (the 3x3 cell is the Argo *unit*). I computed the mean profile density only after 2004 because it is the year the network significantly reached its coverage target. The network coverage is clearly not uniform, with regions with a much higher sampling rate than others. For instance, the Sargasso Sea in the Bermuda Triangle is very well covered, and the Gulf Stream path as well. However, to the east and to the north of Bermuda, and along the eastern and southern regions of this domain, the coverage is no more than the reference target. Time series in [Figure 2.7](#) furthermore shows the number of profiles per month in the Western North Atlantic (blue bars). The network is clearly built until 2004 when it levels out to around 250/300 profiles per month. This also corresponds to the end of the yearly increase of new float deployments. In 2012, the coverage reaches another plateau and since then, Argo provides around 400/450 profiles per month in the region. This metric is impressive but should be analyzed with regard to the time evolution of the fraction of domain covered as expected (red curve). Indeed, the domain coverage reached nearly 70% at the end of 2004 after a rapid increase period corresponding the build up phase of the network. And then, the coverage does not significantly evolve and remain stable around 70%, despite the significant increase of profiles reported monthly after 2012. From the point of view of the network management, this means that despite a significant effort of float deployments (see the green bars) the initial target of the array is not improved. One can note that this could be due to different float mission parameters (for instance floats profiling more frequently).

Ocean Analysis

All along my mode water studies, I used ocean *analysis* along ocean state estimates. An ocean analysis is also an interpolation of observations but one that is not constrained by a GCM. It very often relies on the optimal interpolation (OI) technic introduced by [Bretherton et al. \(1976\)](#). At Ifremer/LOPS, such a technic is used to produce a global monthly mean time series of ocean temperature and salinity over the Argo period ([Kolodziejczyk et al., 2017](#)). Named "ISAS" it was developed by my former colleague Fabienne Gaillard ([Gaillard et al., 2009, 2016](#)). Using the OI technic, the interpolated data (namely the *analysis*) is computed as the sum of a background climatology (or reference) and an anomaly (or innovation):

$$\mathbf{x} = \mathbf{x}_{reference} + \mathbf{x}_{innovation} \quad (2.1)$$

where the anomaly is a weighting of the observations distance to the reference by the famous Kalman gain matrix \mathbf{K} , namely:

$$\mathbf{x}_{innovation} = \mathbf{K}(\mathbf{y} - \mathbf{H}\mathbf{x}_{ref}) \quad (2.2)$$

This formulation makes an implicit use of the observation operator \mathbf{H} , which, for instance, can simply be a linear interpolation operator from the analysis to the observation grid.

The weighting matrix \mathbf{K} basically controls the transfer of information from the observation to the analysis space. The formulation of this Kalman Gain matrix can be obtained through different approaches:

- by minimization of the analysis variance, i.e. the minimum sum of the diagonal elements of the analysis error covariance matrix: the Best Linear Unbiased Estimator (BLUE),
- using the Bayes theorem, update the prior knowledge of the reference state, $P(\mathbf{x})$, with observations, $P(\mathbf{y})$, and observations knowing the reference state, $P(\mathbf{y}|\mathbf{x})$, i.e. compute the posterior pdf of the state when observations are given, $P(\mathbf{x}|\mathbf{y})$: the most likely state (MAP),

- or following a least-squares approach where a cost function (linearly combining the background error weighted distance of the analysis with the background, with the observation error weighted distance of observations with the background) is minimized: this is the 3DVAR approach. It is a special case of the 4DVAR method briefly explained in the previous section, where the use of the model trajectory in time is relaxed to focus on a single timeframe, i.e. there's no time dependence taken into account in 3DVAR.

Whatever the chosen approach, under the assumption of Gaussian errors and with a linear observation operator \mathbf{H} , the Kalman gain formulae is given by:

$$\mathbf{K} = \mathbf{B}\mathbf{H}^{\top}(\mathbf{H}\mathbf{B}\mathbf{H}^{\top} + \mathbf{R})^{-1} \quad (2.3)$$

otherwise noted:

$$\mathbf{K} = \mathbf{C}_{ao}(\mathbf{C}_{oo} + \mathbf{R})^{-1} \quad (2.4)$$

where one can make explicit the covariance matrices $\mathbf{C}_{ao} = \mathbf{B}\mathbf{H}^{\top}$ between the analysis and observation points and $\mathbf{C}_{oo} = \mathbf{H}\mathbf{B}\mathbf{H}^{\top}$ between observation points. The matrix \mathbf{R} is the observations noise covariance matrix. In practice, these covariance matrices are partially known or simply way too large to be treated explicitly. It is thus made use of covariance modelling approach to run the method. The covariance model takes into account two sets of specific time and space scales: one for large scale oceanic structures, targeted by Argo (typically 300 km and 3 weeks) and one for the meso-scale (4 times the Rossby radius and 1 week). Last, we note that the covariance model relies on climatological estimates of the ocean variance at these different scales and takes into account the noise variance (un-resolved scales) and instrumental errors.

It is interesting to note that running this ocean analysis on Argo data provides a very clever way to perform an objective quality control of the data (Gaillard et al., 2009). By estimating the misfit between one float observations and the analysis (the residual, δ):

$$\delta = \mathbf{y} - \mathbf{H}\mathbf{x} \quad (2.5)$$

$$\delta = \mathbf{R}(\mathbf{C}_{oo} + \mathbf{R})^{-1}(\mathbf{y} - \mathbf{H}\mathbf{x}_{ref}) \quad (2.6)$$

one can assess if the float measurements are biased and, or drifting.

Using the method and software ISAS, the LOPS produces every two years an ocean state estimate based on carefully controlled data (Gaillard, 2015; Kolodziejczyk et al., 2017). It can be used to monitor ocean heat content (Gaillard et al., 2016) and water masses. Another version of the software is used in real-time at the Coriolis data center to quality control Argo data and to produce a real-time monthly mean analysis that is distributed by the Copernicus Marine Service².

ISAS is one of many ocean analysis produced throughout the world. The Argo website references about 13 such products. It has become a necessity to inter-compare the results of one diagnostic among several products in order to assess the reliability of a signal (eg Häkkinen et al., 2015; Xue et al., 2017). It has even become an international initiative for some specific variables and diagnostics important for climate change monitoring (Balmaseda et al., 2015). Note that in these inter-comparison exercises, ocean-only products, mostly based on Optimal Interpolation, are included along with ocean state estimates and re-analysis using an ocean model for the interpolation.

Contribution highlight For an ocean analysis to be performed, a collection of good Argo profiles interpolated onto Standard Depth Levels (SDL) has to be assembled. Because of their simplicity and quality (only Argo-qualified good data are retained and an additional quality control is generally performed), such products are very nice intermediate dataset to work with for non-expert users. As a member of the Argo Steering Team I argued for the extension of the list of Argo-based ocean analysis products listed on the AST website to include SDL Argo profiles generated by groups producing ocean (re)-analysis. [This](#)

²[Access product INSITU_GLO_TS_OA_NRT_OBSERVATIONS_013_002_a here](#)

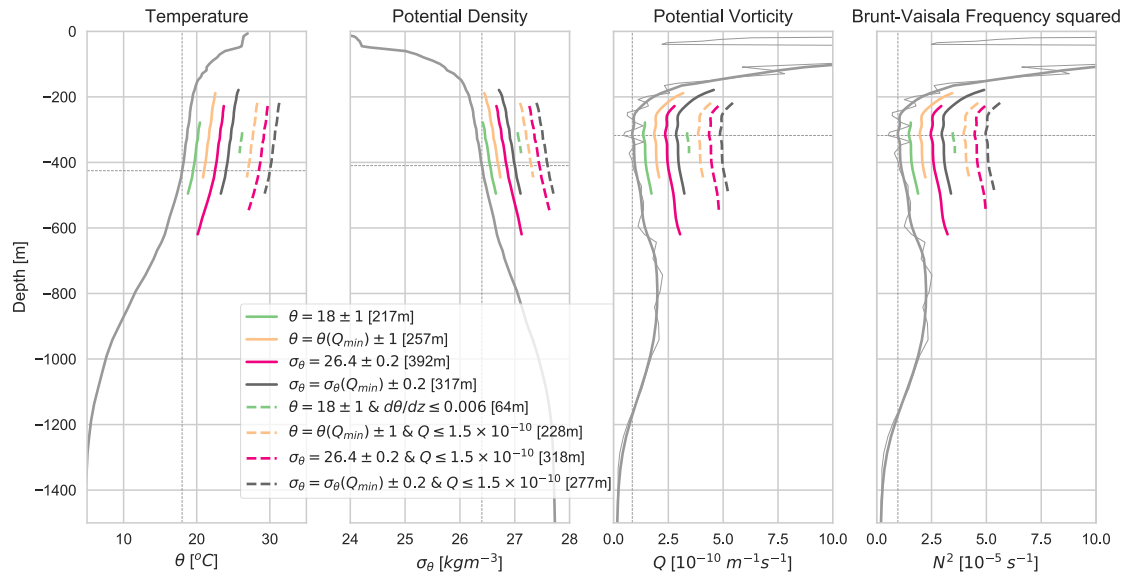


Figure 2.8: A typical Argo profile south of the Gulf Stream (WMO 6902564, 2017-26-09, 38N/61W) for which several EDW identification methods are shown.

[new product is available online here.](#)

Defining the EDW layer

Using its thermohaline properties

The historical and most simple method to identify the EDW layer is by the water column fraction with temperature centered at 18°C . Classically, a simple 1°C range is used so that all water parcels with temperature $18 \pm 1^{\circ}\text{C}$ is accounted for the EDW layer (e.g. [Worthington, 1976](#)).

This simple method relies on the idea that the mode water core temperature is indeed 18°C exactly. In practice, this is obviously not necessarily the case. This is illustrated [Figure 2.8](#) where typical temperature, potential density, potential vorticity and Brunt-Vaissalla frequency squared profiles from an Argo float profile in the Sargasso Sea are shown. Slightly shifted to each of these variables are the mode water layers as identified using several criteria.

Using the $18 \pm 1^{\circ}\text{C}$ criteria (green layer), one can clearly see in the PV and N^2 profiles that the identified mode water layer does not account for the full range of the stratification minimum, and more precisely, it falls short in the upper part. This is because the temperature at the depth of the stratification minimum (Q_{min}), also called the "core layer temperature" (CLT), is in this case warmer ($\theta(Q_{min}) = 18.7^{\circ}\text{C}$) than the expected 18°C .

So one could naturally adapt the simple temperature range criteria to account for local variations of the CLT. This $\theta(Q_{min}) \pm 1^{\circ}\text{C}$ criteria is shown by the orange layer. It is clearly more satisfactory than the previous one, although one could argue that it has the opposite effect of including too much of the seasonal thermocline to the EDW layer. Using a variable CLT in this case, increase the EDW layer by about 40m.

Using density instead of temperature leads to the same biases. The $26.4 \pm 0.2 \text{ kg.m}^{-3}$ criteria (magenta layer) is again not properly selecting the mode water layer because it reaches too deep toward the permanent pycnocline. Again, using the core layer potential density criteria, $\sigma_{\theta}(Q_{min}) = 26.3 \pm 0.2 \text{ kg.m}^{-3}$, improves the identification.

The previous 4 criteria identify the EDW layer using a property range without any restriction on the stratification amplitude. However, the EDW layer can furthermore be restricted to the water body with the lowest stratification level, a signature of recent overturning near the surface or subduction of a ventilated layer. Oxygen measurements can be very useful to identify water masses that were in recent contact with the atmosphere. But the lack of systematic oxygen observations prevents its generalization. CLIMODE

experiments did make a wide use of oxygen measurements for the process study though (e.g. [Thomas and Joyce, 2010](#)).

The subset of EDW with a poor stratification level is referred to as the North Atlantic Subtropical Mode Water (NASTMW).

In [Figure 2.8](#) are also shown the previous property ranges to which I added a stratification threshold (dashed lines). The stratification criteria on the vertical temperature gradient is clearly the most restrictive. I illustrate this criteria using a value of $\partial_z \theta < 0.006 \text{ } ^\circ\text{C m}^{-1}$ because it was used by [Kwon and Riser \(2004\)](#) who was discussed at length in the previous [section 2](#). We see here how restrictive was their definition and hence how such a parameter can dramatically influence the result of an EDW diagnostic.

From [Figure 2.8](#) we see that it is easy to get differences of more than 50m in thickness estimates. This may not seem important at first sight. However, considering that the typical thickness of the EDW layer is 200m (see also [Figure 2.4](#)), that's a non-negligible 25% relative error ! The complex seasonal cycle structure of the mixed layer makes this error non-systematic. In [Forget et al. \(2011\)](#) we discussed at length the influence of the EDW definition criteria on its seasonal cycle estimate, an important result detailed in the next chapter.

Using its stratification signature

It was of primary interest to the CLIMODE project to reconcile the different estimates of EDW seasonal cycle amplitude that were strongly diverging in the early 2000s. The core reason explaining why these amplitudes were different was simply that the EDW layer was not defined with the same method (see previous section) and that the synoptic Argo data were not yet available.

After my series of EDW papers ([Maze et al., 2009](#); [Marshall et al., 2009](#); [Maze and Marshall, 2011](#); [Forget et al., 2011](#); [Maze et al., 2013](#)), I started to look at the subtropical stratification with a much wider perspective, replacing the EDW within the pycnocline framework and what someone would call *the warm water sphere*. As a result, I started the development of a more objective approach, based on stratification patterns, to identify the EDW, and more generally any subtropical mode water. These developments were finalized and implemented on Argo data by my first PhD student Charlène Feucher. We coined the method **OAC-P** for "Objective Algorithm for the Characterisation of the Pycnocline" because it aims to identify the mode water layer together with the underlying permanent pycnocline, as one cannot go without the other in the subtropics. OAC-P is described at length in Charlène's PhD manuscript [Feucher \(2016\)](#).

Briefly, OAC-P works as follows:

- As a first guess, localize the N2 minimum between the Mixed Layer Depth and the maximum expected depth of the regional mode water (e.g. 600m),
- Then, localize the N2 maximum between that N2 minimum and the depth of the *abyssal* ocean below the permanent pycnocline (e.g. 1000m),
- Finally, update the 1st guess of N2 minimum by localizing the N2 minimum between the Mixed Layer Depth and the N2 maximum depth.

The depth of the N2 maximum is that of the permanent pycnocline underlying the mode water, localized by the N2 minimum. Additional robustness tests are automatically performed in order to remove the dependance to the fixed parameters (the maximum expected depth of the regional mode water and the abyssal depth of the ocean below the permanent pycnocline) and to take into account the case where the mode water is being ventilated and located within the mixed layer.

Contribution highlight The OAC-P method we developed is able to track the mode-water/permanent-pycnocline structure very well. We applied it to Argo data in the North Atlantic ([Feucher et al., 2016b](#)) and globally ([Feucher et al., 2019](#), see [chapter 7](#) for more details).

Results

By *modern*, here I mean an Argo based description of the EDW layer. Kenneth Lee, my 2nd PhD student (2017-2019), is currently working on the interannual variability of the EDW. To start his analysis, he has

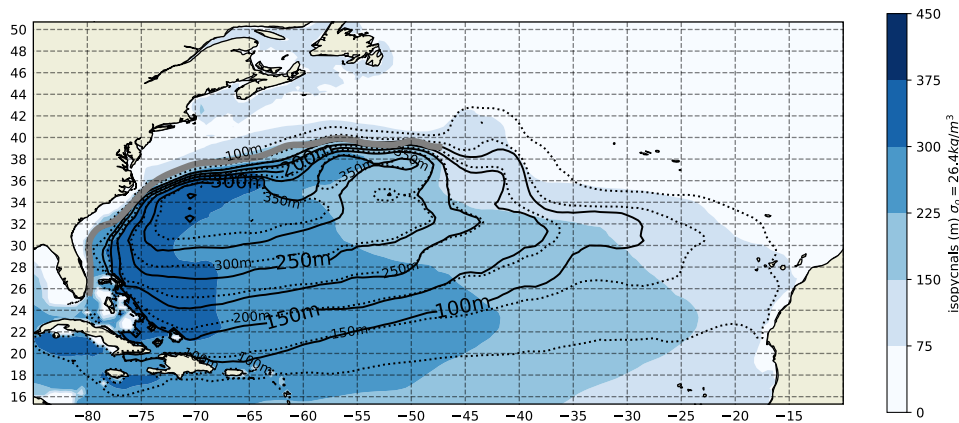


Figure 2.9: 2002-2015 modern EDW layer description based on optimally interpolated Argo data (ISAS product). Blue color shading is the depth of the 26.4 kg m^{-3} isopycnal and black contours are the EDW layer thickness defined as the layer with $\sigma_0 = 26.4 \pm 0.2 \text{ kg m}^{-3}$ and $Q \leq 1.5 \times 10^{-10}$ (dashed contours are thickness without the stratification threshold). Gray thick lines indicate the mean Gulf Stream position determined from altimetry.

produced the following **Figure 2.9** showing the 2002-2015 time mean EDW core layer depth and thickness from the ISAS dataset described above. On this map, the EDW layer is defined using the potential density range and stratification criteria (plain black contours).

Figure 2.9 shows an EDW core layer isopycnal surface deepening from its northern outcropping line (south to 40N to the west of 40W, and south to 35N to the east of 40W) to the southwest. The deepest values of 350m are reached along an arc extending from the Bahamas to 36N and circling around Bermuda all along the U.S. east coast, on the ocean interior flank of the Gulf Stream. This southwestward deepening structure is consistent with the classic wind-driven circulation and the Sverdrup balance.

Figure 2.9 shows a different pattern for the mean EDW layer thickness (black contours). The EDW thickness is maximum in the GS southern recirculation region (about 350m) north of 30N. Thickness decreases southward and eastward, and rapidly vanishes at the GS front. Also in dashed contours is shown the EDW thickness without the stratification threshold. Removing this criteria increases the EDW thickness by about 50m everywhere and extends its coverage eastward and northward (even through the GS). However it does not change significantly the EDW thickness distribution over the Western part of the basin (except that EDW is now found in the Caribbean Sea). This simply highlights that the EDW, as a mode water, is really located in the Western North Atlantic south of the WBC, while the isopycnal layer is obviously covering a larger domain.

Last, it is worth noting here that with the advance of the Argo array and online processing tools, it is now possible to monitor in real time the EDW layer (or any other water mass in fact). Using the Erddap server-side technology, Ifremer offers access to Argo data with unprecedented manipulation service levels. [This is illustrated to the reader if it clicks on this link: \[http://bit.ly/EDW_depth\]\(http://bit.ly/EDW_depth\)](http://bit.ly/EDW_depth), which is going to show the pressure value of data with temperature between 17 and 19°C over the last 6 months. This is a simple and yet very efficient way to retrieve useful informations about the EDW layer depth in real time.

The North Atlantic Mode Water continuum

By definition, the EDW layer shows a relative uniqueness in terms of thermohaline properties. And this is true for other mode waters. However, the ocean stratification is a continuous realm where the different mode water flavors take place. The OAC-P diagnostic can describe this realm and be used to provide a broader context to

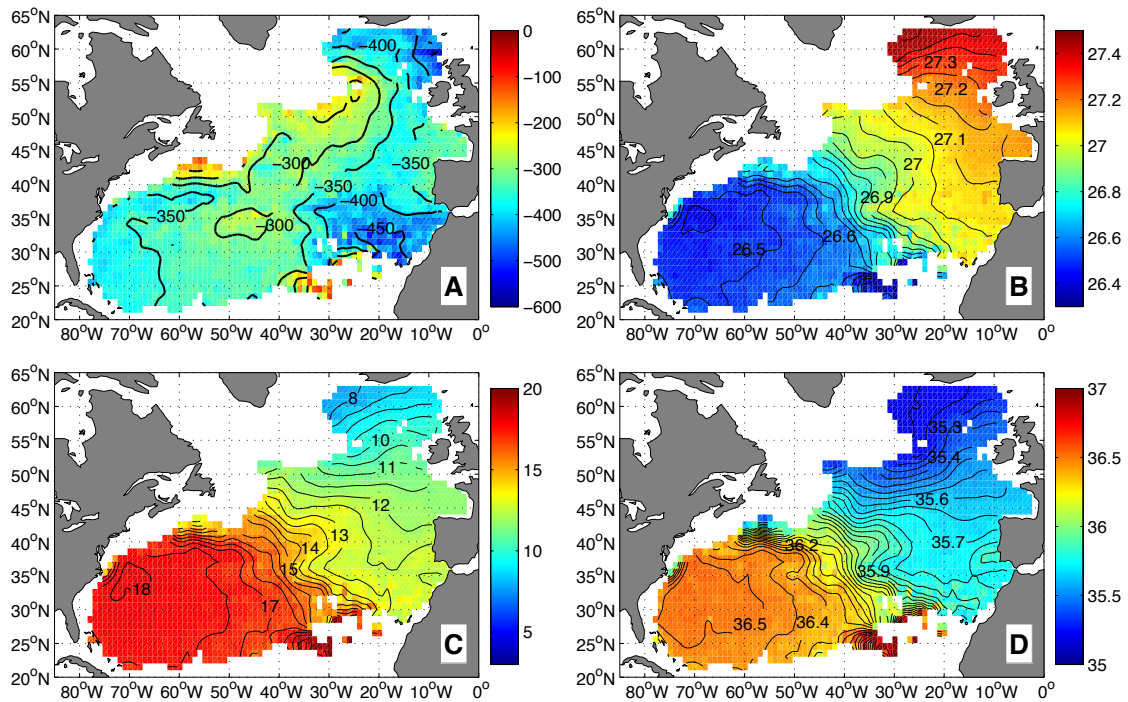


Figure 2.10: Figure reproduced from [Feucher et al. \(2016b\)](#) showing the 2000-2015 climatology of the subtropical mode waters core depth and thermohaline properties. Here the mode water is identified as the stratification minimum above the permanent pycnocline. A: Core depth, B: Potential density (kg/m^3), C: Temperature ($^{\circ}C$) and D: Salinity (psu).

a specific mode water within the warm water sphere.

Contribution highlight In [Feucher et al. \(2016b\)](#) we applied the OAC-P diagnostic to Argo data in the North Atlantic. In this study, we have shown that the EDW is not a water body isolated from the rest of the ocean but is rather a component of a mode water layer that continuously occupies the entire subtropical gyre. This is illustrated [Figure 2.10](#) showing the climatological map of the subtropical mode water layer depth and thermohaline properties.

Here, the most interesting plots are the potential density and temperatures ones (B and C). Let's start from the temperature one. If we focus on the domain where temperature does not vary much, [Figure 2.10-C](#) shows that the EDW spreads from around 40W westward to the U.S. east coast. Its CLT ranges from $17^{\circ}C$ near 40W and warms progressively to reach $18^{\circ}C$, and slightly more, over a small region centered at 70W/35N. This zonal temperature gradient is not entirely compensated in salinity, so that potential density also shows a zonal gradient, from 26.6 near 40W down to 26.45 at 70W/35N. Interestingly the EDW core depth deepens westward as well, from -300m at 40N to nearly -400m along the U.S. east coast. These maps are entirely consistent with previous ones from [Kwon and Riser \(2004\)](#) for instance, but with the key point that here, the EDW component is part of the entire subtropical gyre extending to the eastern part of the basin and up to Iceland. One can also identify the subpolar and central mode waters, as it is discussed at length in [Feucher et al. \(2016b\)](#).

Final remarks

The overall merit of the OAC-P approach based on stratification features rather than isopycnal surfaces, is that it allows for the long-term tracking of the mode water and permanent pycnocline properties. This

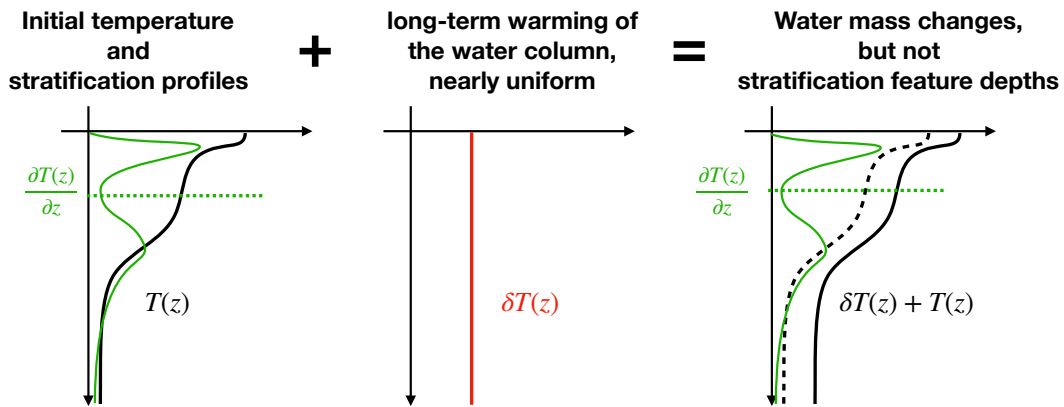


Figure 2.11: Effect on stratification of a naive ocean warming of the water column.

is particularly important in the context of multi-decadal climate changes whereby the ocean heat uptake is affecting the entire water column, and the fast ventilated subtropical one, more than any other regions (Häkkinen et al., 2016; Wang et al., 2017).

Let's illustrate this idea, with the naive scenario where the ocean warms uniformly. See schematic 2.11: the mode water temperature will be shifted to warmer values but not its core layer depth identified as a temperature gradient minimum. Yang and Wang (2009) demonstrated this idea with the Pacific thermocline with future climate simulations of coupled models.

In practice, ocean warming is obviously not uniform with depth but depends on complex 3-dimensional pattern of ocean ventilation schemes.

One key results from Charlène PhD work was to show that we don't have enough observations today to determine accurately decadal stratification changes from vertical temperature and density gradients, the signal is simply beyond the detection level of ocean gridded analysis.

As final remarks to this chapter, I furthermore would like to highlight the following points:

1. No more than 15 years ago, the Argo array reached sufficient synoptic coverage in the Western North Atlantic to allow for an unprecedented 3-dimensional tracking of the EDW layer. This was not such a long time ago !
2. Compared to historical mapping of the EDW, here the EDW estimate is much more reliable in a sense that it is based on more data so that the variance around the mean of the mapping is smaller than ever before. It is not shown here, but one can in fact create ocean climatologies with unprecedented horizontal resolution (e.g. Roemmich and Gilson, 2009, distribute a $1/6 \times 1/6$ climatology).
3. Compared to historical measurements in the region, the deluge of Argo data is primarily a deluge of salinity data that has enabled the EDW layer to be addressed in terms of density instead of temperature only. This has allow for EDW studies to connect with dynamical principals, such as those described at length in chapter 4 and chapter 6.

And moreover:

1. Locally, the mode water layer is not necessarily centered on its mean, or typical, temperature. This comes from the fact that a mode water, although defined as a "mode", is not a "dirac" either and spans a significant range of thermohaline properties because of mixing processes and small variations at the time of formation/subduction. This furthermore highlights the necessity to identify the mode water layer with its signature in the stratification profile, as a minimum.
2. Identifying the mode water layer thickness requires a non-objective choice, using a threshold on some mode water property range for instance. This is very different from the unambiguous identification of the mode water layer core depth using the a local minimum in stratification (PV or N2) profile, or a

pycnostad.

3. Putting back the mode water layer into the more general context of the subtropical stratification has led to a fruitful approach considering the mode-water/permanent-pycnocline tandem as a key structure of the warm water sphere. This idea was further exploited at the global scale and results will be reported [chapter 7](#).



3. Seasonal EDW volume fluctuations

Contribution highlight In this chapter, I will discuss my contribution to the main scientific question: "What is the distribution and amplitude of the EDW seasonal cycle?". To answer this question, my contributions are two folds:

- the synoptic identification of the EDW layer and stratification seasonal fluctuations from observations (Maze et al., 2009; Marshall et al., 2009; Forget et al., 2011),
- the volumetric estimates and reconciliation of the miscellaneous historical values of the EDW seasonal cycle amplitude (Forget et al., 2011).

Since we introduced the EDW layer mean structure in the previous chapter, we can now move on to study its seasonal cycle. In this chapter I will focus on the descriptive part of these fluctuations and in the next two chapters I will address the question of its driving mechanisms.

Content of this chapter:

Data and methods	32
Observation of the seasonal cycle	33
Description	33
Reconciliation of miscellaneous volume estimates	35
Final remarks	37

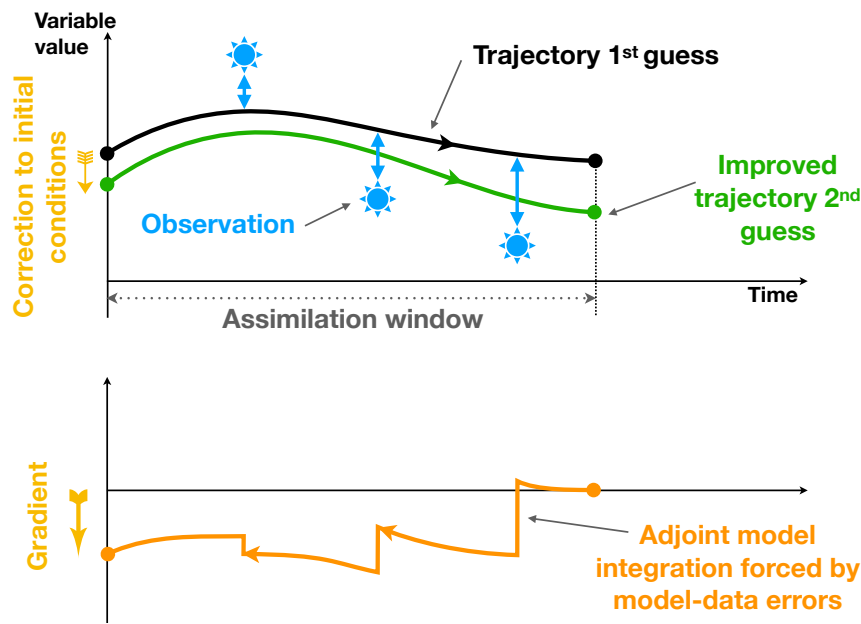


Figure 3.1: Illustration of the 4DVAR assimilation method used to produce the ocean state estimate I used to study the EDW seasonal cycle: OCCA (Forget, 2010). The 4DVAR method can be seen as a method to produce an interpolation of observations (possibly from different platforms, like Argo floats or satellite altimeters) over space and time that is obeying the dynamical constraints of the GFD equations, as provided by a state of the art GCM.

Data and methods

When I arrived at MIT in 2006 and started to study the EDW, the first dataset I looked at was a realistic free forward numerical simulation from the MITgcm. The MITgcm is the core tool of physical oceanographers at MIT. It was initiated during the 90s by Marshall et al. (1997a,b) and, from the beginning was designed to be used for both research and education (<http://mitgcm.org/>). This led to a large versatility and extensive documentation of the code that makes it easy to use. I developed several diagnostic tools for my study of mode waters and I therefore contributed to the MITgcm by sharing and supporting these codes, as well as by providing the necessary documentation for water mass transformation and vorticity diagnostics (e.g. https://mitgcm.readthedocs.io/en/latest/outp_pkgs/outp_pkgs.html#potential-vorticity-matlab-toolbox).

The simulation I used was one of the first global simulation with quite a high resolution, about $1/8^\circ$. It was produced by the ECCO2 group (<http://ecco2.org/>) focusing on "Estimating the circulation and climate of the Ocean, Phase II: High resolution global and sea-ice data synthesis" at JPL. The simulation was interannual and was indeed producing subtropical mode waters South of the Gulf Stream. However, they did not have realistic thermohaline properties: the modeled EDW was too warm, with temperature between 19 and 22°C. We therefore abandoned this dataset (and others from different configurations but still without a good EDW representation) and look for an ocean state estimate that would take into account observations and thus reproduce correctly the EDW. We settled on the OCCA product (Forget et al., 2011).

At MIT, the MITgcm is used for free forward simulations, but also for data assimilation. This later approach was part of the ECCO-GODAE activities supervised by Carl Wunsch at the time of my arrival in early 2006. Data assimilation with the MITgcm is based on the "4DVAR" methodology that is illustrated Figure 3.1.

If M is the prognostic model operator and $\mathbf{x}(t)$ the model state vector at time t , then $\mathbf{x}(t + \delta t) = M(\mathbf{x}(t))$

is the state vector at the next time. The adjoint of the model is the tangent of the prognostic operator, namely M^T , so that it is possible to integrate backward in time the state vector: $\mathbf{x}(t) = M^T(\mathbf{x}(t + \delta t))$. In practice, only the linear part of the prognostic operator is used to determine the tangent model. The adjoint of a GCM with 10s of thousands of lines of code can automatically be computed with specific softwares (see Wunsch and Heimbach, 2007, for more details). The adjoint is used to compute the sensitivity of the initial conditions to the misfit of the model to the observations for a given time/assimilation window (see Figure 3.1). Using a gradient descent algorithm, one can then seek for the best update to the initial conditions that will minimize this misfit. This is an iterative process and the model is run forward and backward multiple times before converging to a trajectory that will minimize the misfit to a satisfactory level. We will keep in mind the key point of the 4DVAR method: the model trajectory remains coherent and consistent (over the assimilation window, which is typically several years for ECCO rather than a couple of days or hours as in operational systems) with the physical conservation principles encoded into the GCM. There are no spurious jumps of the model state between different periods, to the contrary of the widely used 3DVAR methodology. Therefore, an ocean state estimate produced with 4DVAR principles is as close to the observations as a state of the art GCM can be, with the huge advantage compared to other assimilation methods that it allows for budgets to be conducted "properly", i.e. without having to deal with spurious heat source/sink terms added between each assimilation windows.

Gael Forget arrived at MIT the year before me and had the task to work on the assimilation of Argo data, which were starting to pour a lot of data (the global network reached its full target later in 2007, see Figure 2.7). Products developed by the MIT ECCO-GODAE group are running over the satellite altimetry period, starting in 1992. This choice yields the possibility to study the interannual variability of the ocean in a very coherent way. However, in the CLIMODE project we were focusing on the seasonal time scale, and as we pointed out in the last chapter, before the ARGO era not much was known about it. Therefore Gael developed a specific product for the study of the ocean seasonal cycle: the Ocean Comprehensible Atlas (OCCA, Forget, 2010). The term "comprehensible" was added to highlight the fact that the underlying equations of motion were known. The main difference with the regular ECCO-GODAE products is that in OCCA, the assimilation window is of 16 months. This allowed for a more effective control of the initial conditions of the model trajectory, hence a better ocean variability trajectory over a year. Three consecutive years, 2004, 2005 and 2006, were joined together to produce OCCA, which de-facto does not resolve the interannual variations.

Observation of the seasonal cycle

Description

Contribution highlight In Maze et al. (2009) and Marshall et al. (2009) I computed and described the 2003-2006 seasonal cycle from all Argo temperature profiles located within a $10^\circ \times 5^\circ$ box centered on 35N/55W, i.e. just south of the Gulf Stream, in the eastern part of the EDW formation region. It was used to, positively, evaluate the OCCA dataset, and was focusing on the EDW layer defined with a temperature range.

Here I'd like to illustrate the EDW seasonal cycle structure with another method than can furthermore be used to provided an estimate of the EDW volume. From only Argo data, in Forget et al. (2011) we described the EDW seasonal cycle in a very synthetic way by following the fundamental idea that the EDW is a volumetric "mode" in the Western North Atlantic region. From a regular in space and time sampling of the ocean, a mode would simply tends to produce a higher probability for properties within that mode. This is exactly what allows the Argo data set.

Figure 3.2 reproduced from Forget et al. (2011) shows meridional section of *EDW probability*. To produce this figure, we binned Argo data over depth, month and bins of mean March SST outcrops. Then we computed the probability of a measurement to be within the EDW range, i.e. the fraction $R_{EDW} = N_{EDW}/N$ where N_{EDW} is the number of measurements satisfying $\theta = 18 \pm 1^\circ C$ and N the total number of measurements for the

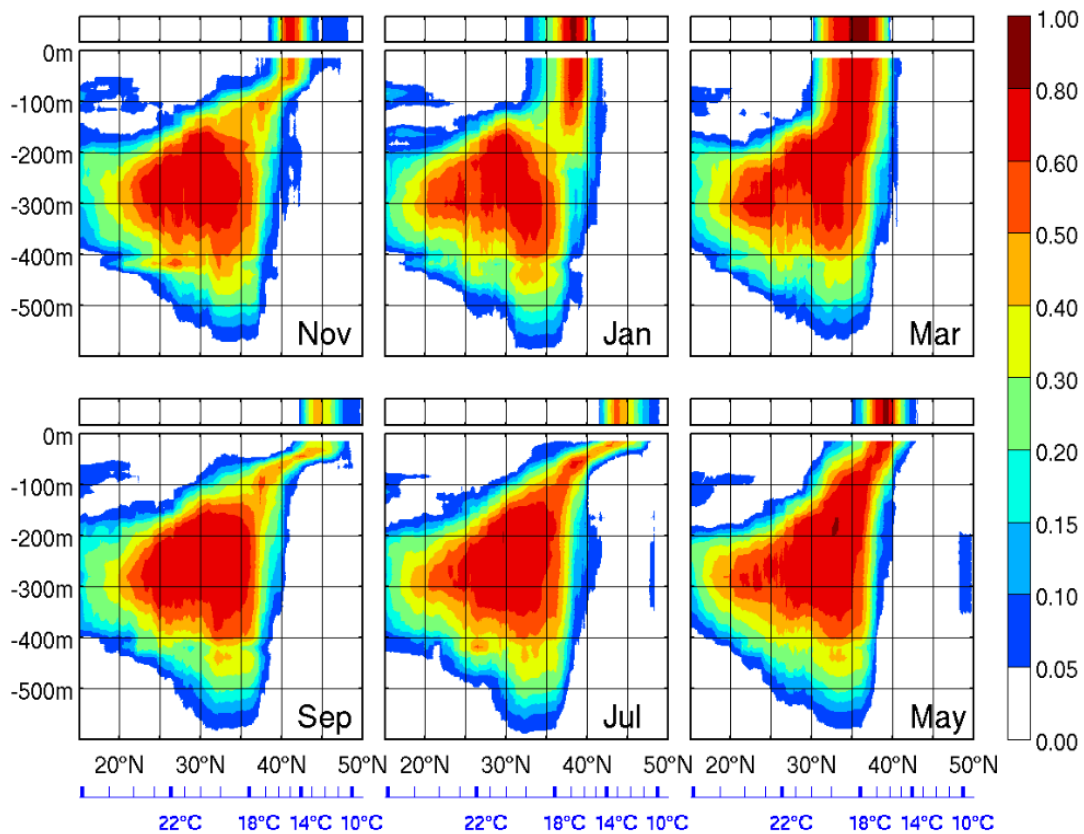


Figure 3.2: Seasonal fluctuations of the EDW layer from Argo data. The colorscale indicates the probability that the temperature at a given depth and latitude band is within the 17 – 19°C EDW range, over the North Atlantic. Reproduced from [Forget et al. \(2011\)](#), figure 4.

given control volume. From the mean March outcrops of SST we furthermore computed an equivalent latitude for easier plotting. See the paper for more details. In the next section, we'll use this probability to compute a EDW volume estimate. We coined this simple method also discussed in [Siedler et al. \(1987\)](#) as Sample Census (SC).

The seasonal fluctuations of the EDW probability reveal a permanent core located between 200m and 300m depths and 25-35N, with a fairly stable meridional and bottom extent. On the other hand, this metric reveals the highly variable near-surface layer above 200m. In that layer, the EDW sweeps back and forth meridionally throughout a seasonal cycle. It reaches its northernmost location in July (near 45N) and its southernmost location in March, which also corresponds to the largest outcropping window near 35S (see the outcrop time series in [Forget et al., 2011](#), figure 1).

Contribution highlight In [Maze and Marshall \(2011\)](#) I extended the EDW description based on the temperature field to a description based on stratification through the analysis of potential vorticity (PV). Results with regard to the EDW seasonal cycle diagnostic are illustrated [Figure 3.3](#). PV was simply defined following [Talley and Raymer \(1982\)](#):

$$Q = -\frac{f}{\rho} \frac{\partial \sigma}{\partial z} \quad (3.1)$$

where the relative vorticity at large scale was neglected, f is the Coriolis parameter, ρ the *in-situ* density

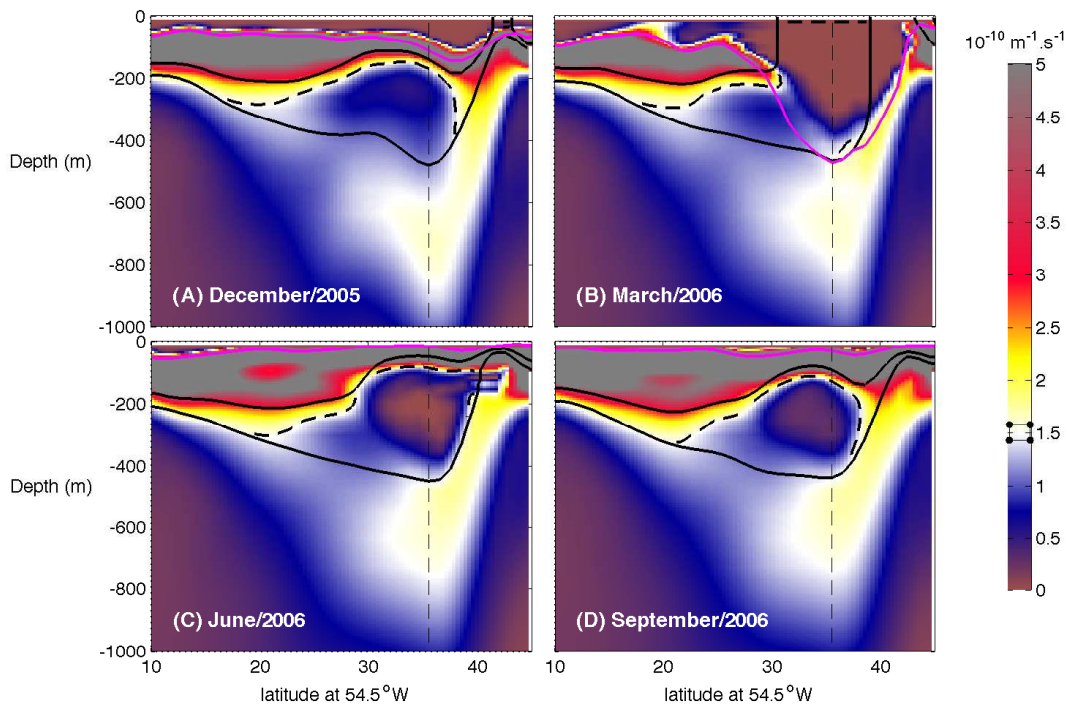


Figure 3.3: Seasonal fluctuations of the EDW layer stratification from OCCA. Meridional section along 54.5°W of: the monthly mean potential vorticity given by Equation 3.1 (color shading), isopycnals defining the EDW $\sigma_{\theta} = 26.4 \pm 0.2 \text{ kg m}^{-3}$ (black) and mixed layer depth (magenta). The STMW subset of EDW with $Q \leq 1.5 \times 10^{-10} \text{ m}^{-1} \text{ s}^{-1}$ is marked by the black dashed contour within the EDW layer (which corresponding to white color shading). Monthly mean fields are shown for (A): December 2005, (B): March 2006, (C): June 2006 and (D): September 2006. Reproduced from [Maze and Marshall \(2011\)](#).

and σ the potential density.

Figure 3.3 shows 4 monthly means of the meridional PV section along 54°W from the OCCA dataset. The EDW isopycnal layer is contoured in black and its low PV subset with dashed black lines. The stratification PV field reveals the EDW layer as the blueish region trapped between the seasonal and the permanent pycnocline south of the GS (reddish stratified regions). March is the month of the year where PV is minimum and the EDW is fully ventilated and penetrated by the mixed layer (magenta contour). Then, from June to December, the seasonal pycnocline develops and seals the EDW from any contact with the atmosphere through the mixed layer. If one look at it carefully, the PV in the EDW layer is steadily increasing over that period. Using Argo data [Billheimer and Talley \(2016\)](#) recently studied this erosion phase of the EDW seasonal cycle and found that the primary source of EDW erosion is by vertical mixing with the seasonal pycnocline. This is further discussed in [section 4](#).

Reconciliation of miscellaneous volume estimates

In CLIMODE, a key issue was to reconcile the several estimates of EDW seasonal variability that was historically determined using miscellaneous datasets and methods and thus, not surprisingly, diverging quite significantly. For instance, the annual mean EDW formation from air-sea fluxes was estimated by [Worthington \(1976\)](#) to 7.3Svy, by [Speer and Tziperman \(1992\)](#) to 14Svy, by [Kwon and Riser \(2004\)](#) to 3.5Svy and by myself in [Maze et al. \(2009\)](#) to 4.6Svy. But thanks to the development of the Argo array, ocean state estimates now allow for a precise characterization of the large scale water mass distribution and seasonal variability. In [Forget et al. \(2011\)](#), I addressed the core, and simple, reasons of historical discrepancies: namely that authors

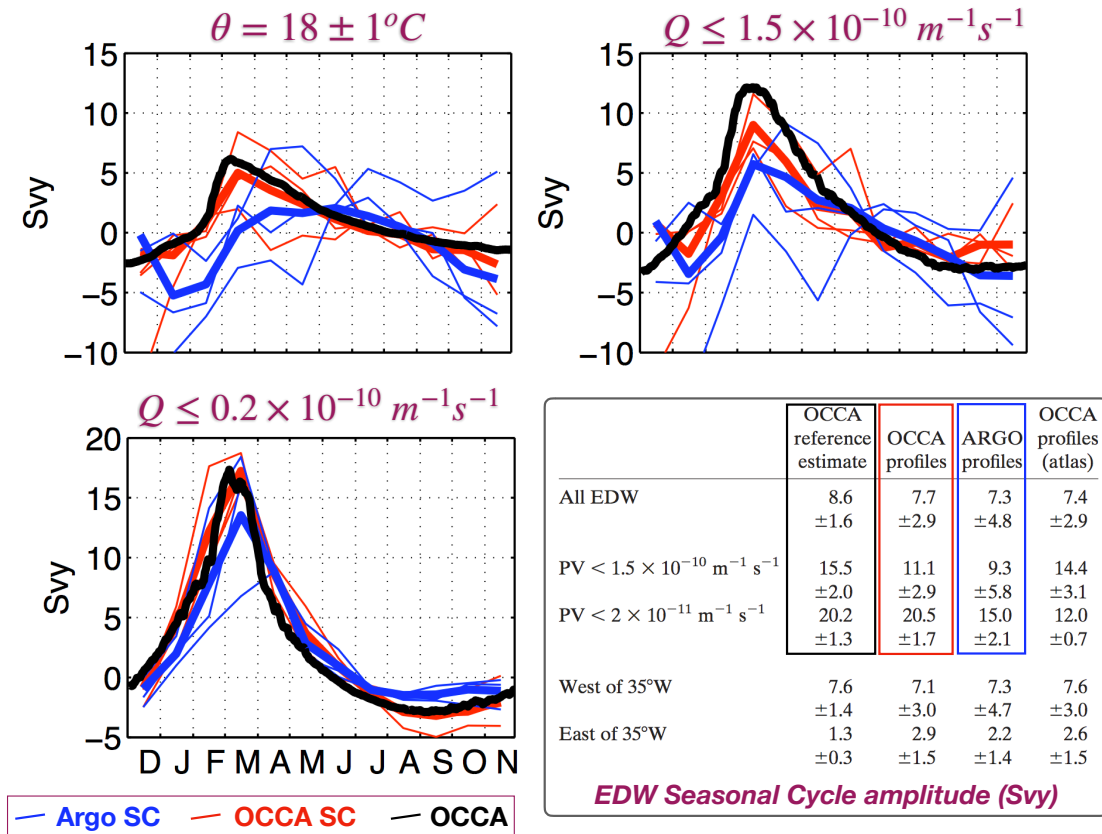


Figure 3.4: EDW layer seasonal fluctuations obtained from several sampling definitions, adapted from Figure 10 and Table 1 of Forget et al. (2011). For each plot: Sample Census (SC) of Argo profiles is in blue, and similar SC of the OCCA dataset in red; thin lines are for the individual years 2004, 2005 and 2006; thick lines are the 3-years time average and the thick black curve is based on the daily gridded OCCA time series. To each subplot corresponds a different EDW definition indicated in sub-titles. The median value has been subtracted from all curves. Units: $Sv_y \simeq 3.15 \times 10^{13} m^3$. The seasonal cycle amplitudes are given in the lower right table.

were not referencing the EDW layer with the same definition, and I provided a quantitative and exhaustive description of the EDW volumetric seasonal cycle.

This is illustrated Figure 3.4 with the EDW seasonal cycle and amplitude estimates that one can get using different EDW layer definitions and datasets. Here we compared 3 datasets: Argo, OCCA sampled as Argo and the full OCCA and 3 definitions: the simple temperature range and 2 additional stratification criteria of different severity. The quantitative estimates are given in the lower right table. We estimated that the volume fluctuation of EDW defined as $\theta = 18 \pm 1^\circ C$ is about $8.6 \pm 1.6 Sv_y$.

Contribution highlight Three key results are to be outlined from this work:

1. For a given method, the difference between each of the datasets, is smaller than the amplitude of the seasonal cycle to be determined. This proves the observability/robustness of the signal.
2. The monthly and interannual spreads are the largest for the Sample Census of Argo profiles (blue curves). This highlights the necessity to *assimilate* observations in order to reduce sampling errors.
3. The stricter the EDW definition in stratification is, the larger the seasonal cycle amplitude. With the stricter threshold, the volume fluctuation amplitude is about $20.2 Sv_y$, compared to $8.6 Sv_y$ without restriction on the stratification.

Final remarks

In reconciling EDW layer seasonal fluctuation estimates found in the literature, we found three sources of divergence and confusion: the first one is the inappropriate comparison of different methods and space/time domains, the second one is the use of imperfect datasets, which leads to large errors in the estimates, and the third one is due to the confusion between the overall layer volume fluctuation and the volume fluctuation attributed to a given process. This later source of divergence will be discussed in the next chapter.

So, now that we have a proper estimate of the seasonal EDW layer volume fluctuation, we can determine and quantify which processes drives such fluctuations.



4. Water-mass transformation processes

Contribution highlight My key contributions to a better understanding of the EDW seasonal cycle through the analysis of water-mass transformation processes can be summarized to:

- a thorough estimate of the surface water mass transformation rate due to air-sea heat fluxes, including daily time series (Maze et al., 2009; Marshall et al., 2009; Forget et al., 2011),
- a precise map of the EDW local formation rates consistent with previous methods and with quantitative assessments from water mass transformation processes (Maze et al., 2009),
- an exhaustive computation of transformation rate errors arising from miscellaneous sources, including poorly constrained bulk formulae (Maze et al., 2009; Forget et al., 2011)

Content of this chapter:

Introduction	40
The kinematic approach	40
The thermodynamic approach: Walin's framework	42
EDW transformation processes	45
Air-sea transformation	46
Mixed-layer entrainment	50
Lateral eddy mixing	51
Interior mixing	54
Synthesis of driving factors	55

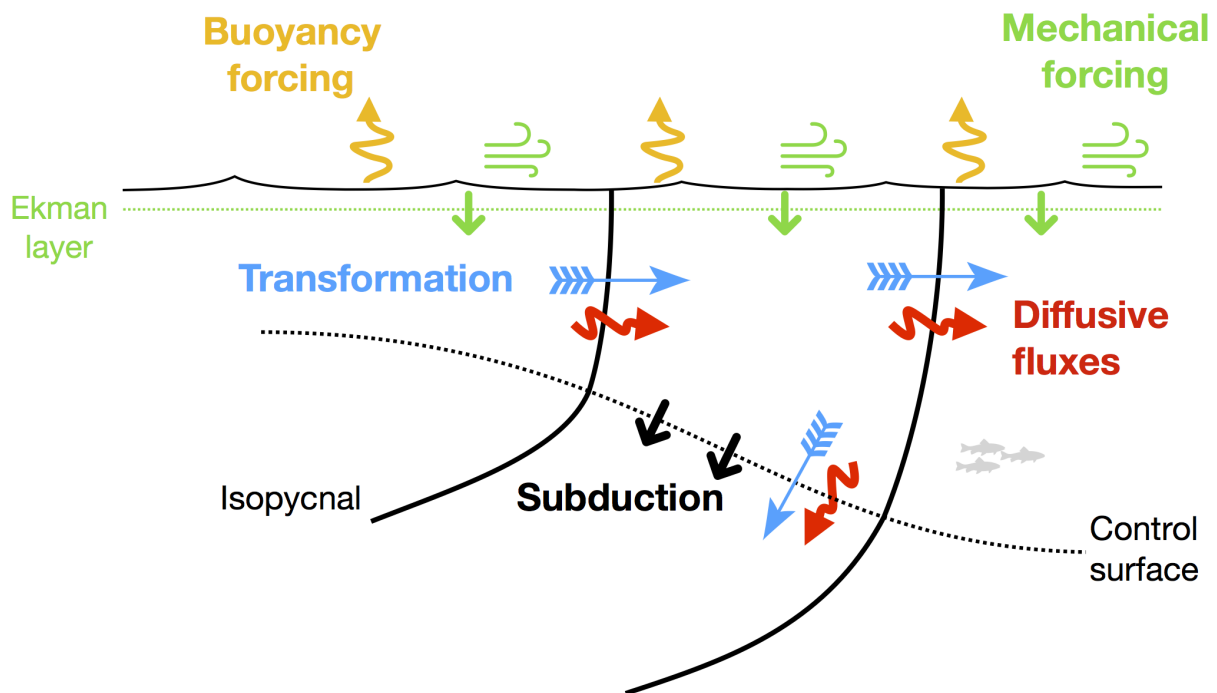


Figure 4.1: A schematic diagram showing two outcropping isopycnal surfaces and a control surface across which subduction is to be monitored. The kinematic approach used the deepest mixed layer depth as a control surface and directly estimate the volume flux through it. The thermodynamic approach diagnoses the water-mass transformation rates through isopycnals from diffusive fluxes.

Introduction

Water masses, and more specifically mode waters, are formed at the ocean surface, in contact with the atmosphere where they acquire the properties they will carry along into the ocean interior. To study the formation of a water mass, two approaches are possible: a kinematic and a thermodynamic one. They are illustrated [Figure 4.1](#). The kinematic method is based on the computation of a volume flux (black arrows) through a control surface that is generally fixed-in-time and set to the mixed layer depth at the end of a given winter. The thermodynamic method is based on the computation of diapycnal volume fluxes (blue arrows) driven by non-advective processes (red and yellow arrows). It is obvious from the schematic that an appropriate choice for isopycnals and the control surface will allow for the two approaches to be connected. This was nicely demonstrated by [Marshall et al. \(1999\)](#) building on earlier work from [Nurser and Marshall \(1991\)](#). They've shown that subduction can be computed from air-sea fluxes and lateral eddy-driven diapycnal volume fluxes.

In the following sub-sections, I briefly develop the kinematic approach because it's a state of the art method, and further introduce the thermodynamic approach.

The kinematic approach

In the classic thermocline ventilation theory ([Luyten et al., 1983](#)), the downward Ekman pumping in the subtropics has been viewed as determining the rate at which water is transferred into the ocean interior, subducted. However, since the seminal work from [Stommel \(1979\)](#) and its "mixed layer demon" that was later supported by tracer analysis (e.g. [Sarmiento, 1983](#); [Jenkins, 1987](#), have shown that the North Atlantic subtropical gyre ventilation rate and time scale are not compatible with Ekman driven subduction alone), it is clear that it is the volume flux through the base of the deepest mixed layers, rather than the Ekman layer, that is effectively transferring permanently water downward and ventilating the *permanent* thermocline. [Williams](#)

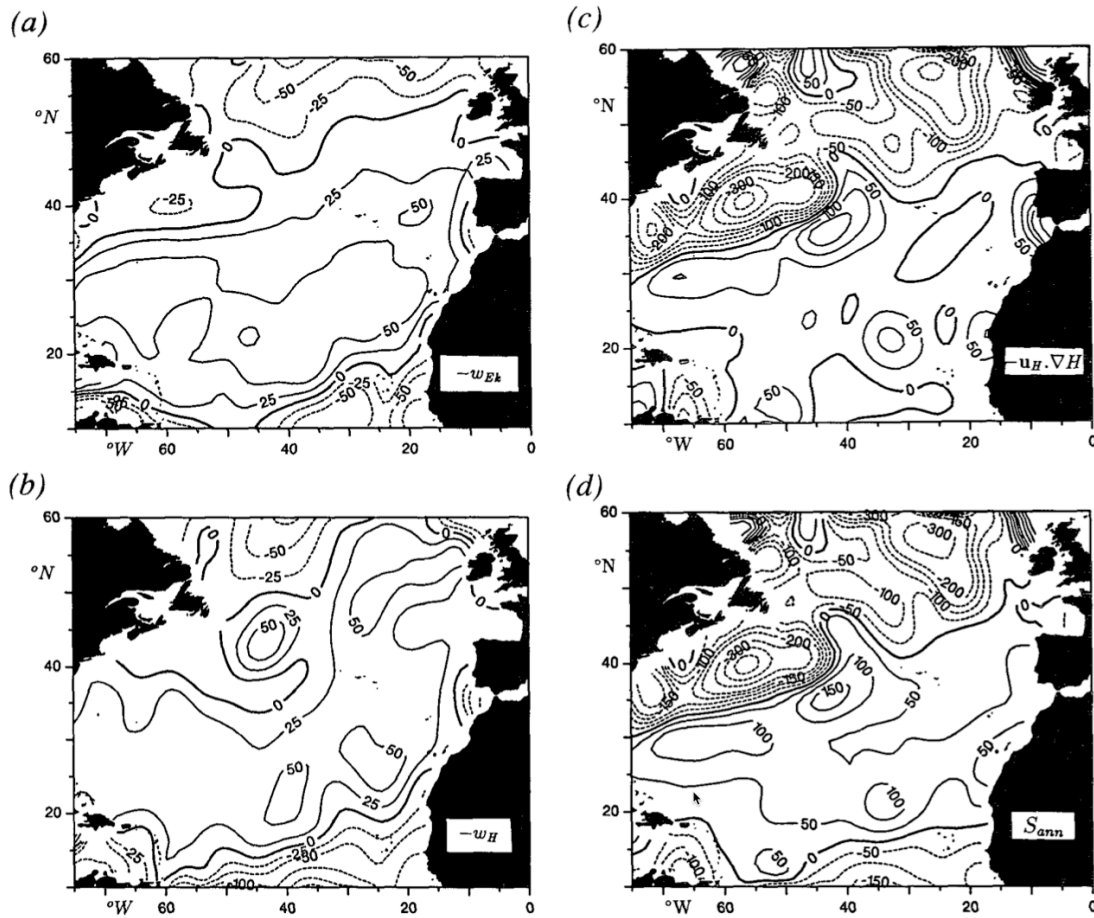


Figure 4.2: Figure 5 from [Marshall et al. \(1993\)](#) showing the different components and the total annual subduction rate from Eq.(4.2) applied to climatological data available in the earlier 90s. We'll note the lateral induction term to be about twice as large as Ekman pumping.

(1989) has introduced the effect of a variable mixed layer to the thermocline ventilation theory to take this effect into account.

The demonstrated importance of subduction to understand ocean ventilation, and basically its stratification, naturally lead to the kinematic approach. This approach requires a very good knowledge of the mixed layer depth structure and variability as well as of the upper surface currents. Therefore, one could think that it is quite complex to adopt. Nonetheless, let's briefly look at the kinematic of subduction. The local and instantaneous subduction rate is given by:

$$S = -\frac{\partial h}{\partial t} - \mathbf{u}_b \cdot \nabla h - w_b \quad (4.1)$$

where h is the mixed layer depth and \mathbf{u}_b and w_b are the horizontal and vertical velocity vectors at the base of the mixed layer. The first r.h.s term is simply the vertical velocity of the mixed layer depth, the second/third r.h.s terms are the lateral and vertical induction terms due to movement of water parcels. If the control surface (Figure 4.1) is fix-in-time and set to the deepest mixed layer over a given winter season, say H , the annual subduction rate from Eq.4.1 is quite simplified to:

$$S_{ann} = -\mathbf{u}_H \cdot \nabla H - w_H \quad (4.2)$$

This was diagnosed from observations for the North Atlantic as soon as the early 90s by [Marshall et al. \(1993\)](#). Results are reproduced Figure 4.2. One can note that the annual subduction rate of water into the permanent

pycnocline (Figure 4.2-d) is about 100 myr^{-1} south of the Gulf Stream in the formation region of the EDW, and typically twice the Ekman pumping over the North Atlantic. We can also note the dominant contribution from the lateral induction term due to the sloping mixed layer depth. This is the primary process explaining why the ventilation of the ocean interior is driven by subduction rather than Ekman pumping.

Last, it is striking to see that the lateral induction term is particularly large in the eddy rich region of the Gulf Stream. This automatically raises the question of the role of mesoscale eddies into the subduction process. This role was investigated by Follows and Marshall (1994); Marshall et al. (1997a) and is still a subject of active research (e.g. Hazeleger and Drijfhout, 2000; Da Costa et al., 2005; Gebbie, 2007; Sallée et al., 2010; Lee and Nurser, 2012; Liu et al., 2016). Furthermore, as the eddy scale decreases, down to the sub-mesoscale, vertical velocities associated with fronts become ever more important (up to 30 m d^{-1}) and large subduction can locally and momentarily occurs. Subduction at these scales are very important for the vertical transfer of organic and inorganic material and thus for the carbon cycle (e.g. Lévy et al., 2001). An increasing amount of observational (Joyce et al., 2009; Thomas and Taylor, 2010; J. et al., 2013) and modeling studies (Karleskind et al., 2011) shows that subduction at the sub-mesoscale may be important for the ventilation of the thermocline and mode water formation. However, observations are sparse and quantifying the impact of such a small scale (1-10km) process onto the large scale ocean stratification remains at the cutting edge of numerical simulations in 2018 (Wenegrat et al., 2018).

The thermodynamic approach: Walin's framework

The thermodynamic approach was introduced by Walin (1982) using temperature and heat fluxes. The idea was briefly illustrated at the end of section 2: as advection can only deform a material surface in an incompressible, inviscid fluid, leaving the volume enclosed by it unchanged, this volume can only be modified by non-advective, diffusive, fluxes (Figure 2.6). The idea was extended to water masses defined in density by Tziperman (1986) and Speer and Tziperman (1992). The principle remains the same though. It provides a theoretical framework to estimate the transformation rate at which a density, or temperature, class of surface water is transformed into another one through density, or heat, exchange with the atmosphere. This thermodynamic approach is much more simple than the dynamic one, to my opinion, as it requires only surface buoyancy fluxes and surface outcrops to determine the formation rate of a given water mass defined by a density range. This air-sea flux driven formation rate is related to the kinematic subduction rate, but depending on non-trivial assumptions like small horizontal mixing in the surface layer (Garrett et al., 1995), that we shall discuss later in this chapter. I'll note that Groeskamp et al. (2019) recently provided an extensive review of the water mass transformation framework for ocean physics but also biogeochemistry.

Let's introduce the Walin's framework in temperature coordinates (Figure 4.3). The volume change rate of a water-body Θ bounded by isothermal surfaces θ_1 and $\theta_2 > \theta_1$ is given by:

$$\frac{\partial \mathcal{V}_\Theta(t)}{\partial t} = A(\theta_2, t) - A(\theta_1, t) - M_\Theta(t) \quad (4.3)$$

where $A(\theta_i, t)$ is the diathermal volume flux across the isothermal surface θ_i and $M_\Theta(t)$ is the volume flux out of the control region defined by $H(x, y)$ for water with temperature $\theta_1 < \theta < \theta_2$ (see schematics from Figure 4.3). Note that by convention, a positive diathermal volume flux corresponds to a flux toward cooler temperatures. Therefore, if $A(\theta_2, t)$ is positive and larger than $A(\theta_1, t)$, the volume $\mathcal{V}_\Theta(t)$ will increase because of a diathermal volume flux convergence between θ_1 and θ_2 (in the absence of export M_Θ). Also, if the control region is limited to the mixed layer, i.e. the domain boundary $H(x, y)$ will come to match the deepest mixed layer depth surface MLD , then the annual mean subduction rate discussed in the previous section can readily be equated to the export term due to the diathermal volume flux convergence in the mixed layer that will be driven by vertical air-sea and lateral eddy fluxes (Marshall et al., 1999).

A diathermal volume flux has a unit of m^3/s . It is the transformation rate at which a water mass with an uniform temperature is transformed into another one. It is positive if it's transformed into a cooler, less buoyant, water mass. The diathermal volume flux is thus intimately related to the velocity of the isothermal

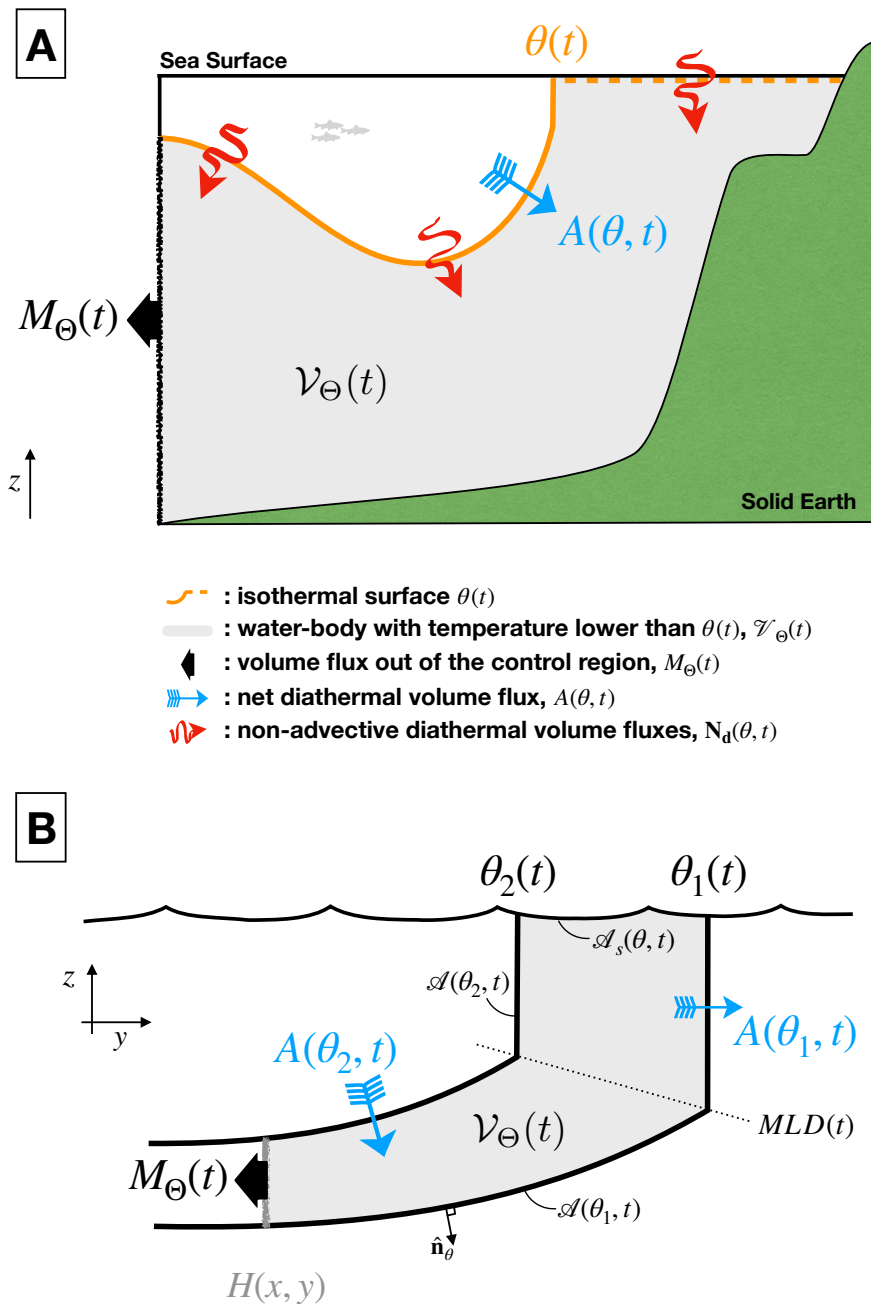


Figure 4.3: Walin (1982) framework illustrated in temperature classes. Schematic A is an adaptation of the idea illustrated Figure 2.6 to an oceanic context: the volume of a water-body with temperature lower than θ can only change by diabatic fluxes acting across the isothermal surface (orange boundary) and possibly export out of the control region. Note how the water-body is closed at the sea surface by an infinitely thin layer with temperature θ (to highlight the fact that non-advective volume fluxes arise from both interior mixing and surface air-sea interactions). Schematic B shows the volume budget elements of a water-body with temperature $\theta_1 < \theta < \theta_2$. It derives from the schematic A applied to two different temperatures. See text or schematic A for variables definition.

surface. Since an isothermal surface may move at a velocity different from the fluid velocity, the diathermal volume flux $A(\theta, t)$ through this isothermal surface θ is given by the integration of the difference between the normal components of the Eulerian fluid velocity \mathbf{v} and the isothermal surface velocity \mathbf{v}_θ . This reads:

$$A(\theta, t) = \iint_{\mathcal{A}(\theta, t)} (\mathbf{v} - \mathbf{v}_\theta) \cdot \hat{\mathbf{n}}_\theta d\mathcal{A} \quad (4.4)$$

with

$$\mathbf{v}_\theta = \frac{\partial_t \theta}{|\nabla \theta|} \hat{\mathbf{n}}_\theta \quad (4.5)$$

where θ is the temperature of the isothermal surface and $\hat{\mathbf{n}}_\theta$ is a unit vector normal to this surface. To maintain consistency in the sign of transformation rates between density and temperature classes, we choose to orient the unit vector down-gradient: $\hat{\mathbf{n}}_\theta = -\frac{\nabla \theta}{|\nabla \theta|}$.

If we now introduce the temperature conservation equation $\partial_t \theta = -\nabla \cdot (\mathbf{N}_d + \mathbf{N}_a)$ where \mathbf{N}_d are the non-advective (diffusive) fluxes of temperature and $\mathbf{N}_a = \mathbf{v}\theta$ the advective fluxes, and assume continuity ($\nabla \cdot \mathbf{v} = 0$), the isothermal surface velocity Eq.(4.5) becomes:

$$\begin{aligned} \mathbf{v}_\theta &= \frac{-\nabla \cdot \mathbf{N}_d - \mathbf{v} \cdot \nabla \theta}{|\nabla \theta|} \hat{\mathbf{n}}_\theta \\ &= -\frac{\nabla \cdot \mathbf{N}_d}{|\nabla \theta|} \hat{\mathbf{n}}_\theta - \mathbf{v} \frac{\nabla \theta \cdot \hat{\mathbf{n}}_\theta}{|\nabla \theta|} \\ &= -\frac{\nabla \cdot \mathbf{N}_d}{|\nabla \theta|} \hat{\mathbf{n}}_\theta + \mathbf{v} \end{aligned} \quad (4.6)$$

where we used $\nabla \theta \cdot \hat{\mathbf{n}}_\theta = -|\nabla \theta|$ because of the down-gradient orientation of the unit vector. The diathermal volume flux Eq.(4.4) is thus entirely and uniquely related to the divergence of non-advective temperature fluxes \mathbf{N}_d scaled by the isothermal spacing:

$$A(\theta, t) = \iint_{\mathcal{A}(\theta, t)} \frac{\nabla \cdot \mathbf{N}_d}{|\nabla \theta|} d\mathcal{A} \quad (4.7)$$

Making use of the Leibniz integral rule for a two dimensional surface moving in three dimensional space (Flanders, 1973), the diathermal volume flux can be written in its derivative formulation:

$$A(\theta, t) = \frac{\partial}{\partial \theta} \iiint_{\mathcal{V}_\theta(t)} \nabla \cdot \mathbf{N}_d d\mathcal{V} \quad (4.8)$$

Or, maybe more conveniently using the Gauss theorem:

$$A(\theta, t) = \frac{\partial}{\partial \theta} \iint_{\mathcal{A}_\theta(t)} \mathbf{N}_d \cdot \hat{\mathbf{n}}_\theta d\mathcal{A} \quad (4.9)$$

Thus, at the heart of the Walin's principle of water mass transformation is this elegant formulation for the diathermal volume flux $A(\theta, t)$ as a function of non-advective temperature fluxes across an isothermal surface.

As an illustration of the Walin's principle, let's take the trivial case of an ocean at rest ($\mathbf{v} = 0$) and where there is no mixing in the interior of the ocean so that the only non-advective flux entering \mathbf{N}_d is from the air-sea heat flux operating across the outcrop surface of the Θ water-mass. This is illustrated Figure 4.4. If the air-sea heat flux cools the ocean over the outcrop, the diathermal volume flux $A(\theta, t)$ is positive¹, transferring volume from the warmer than θ part of the ocean toward the colder region. This furthermore implies that the isothermal surface velocity \mathbf{v}_θ is upgradient, i.e. that the outcrop will migrate southward toward warmer temperatures. This idealized situation leads to the coldest water being formed at the expense of the warmer one. In this case, a steady-state solution over a closed basin cannot be sustained because the formation of cold water either leads to the basin filling up with this cold water or to its export through an open boundary.

¹one can note from Eq.(4.8) that

$$A(\theta, t) = \frac{\partial}{\partial \theta} \iiint_{\mathcal{V}_\theta} -\frac{D\theta}{Dt} d\mathcal{V}$$

so that $A(\theta, t)$ is of the opposite sign of $\frac{D\theta}{Dt}$ over the outcrop, i.e. positive for cooling.

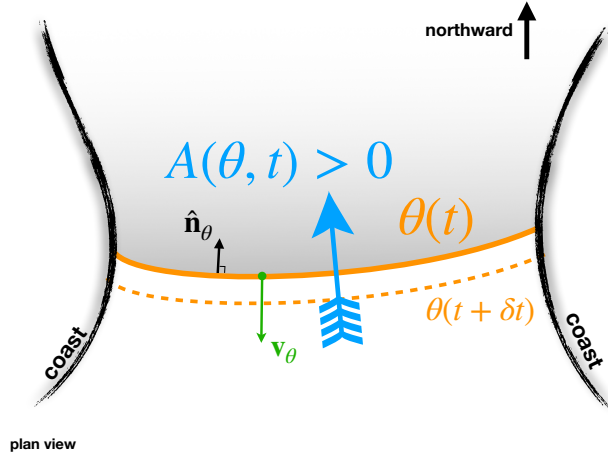


Figure 4.4: Schematic plan view of an idealized basin at rest subject to surface temperature loss and no mixing. The warm water of the basin has temperature warmer than $\theta(t)$, water colder than $\theta(t)$ is shaded. The negative air-sea heat flux implies a positive **diathermal volume flux** $A(\theta, t)$ toward colder waters and a southward migration of the outcrop (dashed orange).

EDW transformation processes

In order to move on to the details of the different processes driving transformation of water-masses and my contributions to their description and understanding with regard to the EDW, let's express the Walin's principle in density coordinates (see [Figure 4.5A](#)).

Following Eq.(4.3), the volume change rate of a water-body Θ bounded by isopycnal surfaces σ_1 and $\sigma_2 < \sigma_1$ is given by:

$$\frac{\partial \mathcal{V}_{\Theta}(t)}{\partial t} = A(\sigma_2, t) - A(\sigma_1, t) - M_{\Theta}(t) \quad (4.10)$$

where $A(\sigma_i, t)$ is the diapycnal volume flux through the isopycnal surface σ_i . Then, following the same line of arguments as for the temperature case, one can show that the diapycnal volume flux is given equivalently by the three expressions:

$$A(\sigma, t) = \frac{\partial}{\partial \sigma} \iint_{\mathcal{A}_{\Theta}(t)} -\mathbf{N}_d \cdot \hat{\mathbf{n}}_{\sigma} d\mathcal{A} = \frac{\partial}{\partial \sigma} \iiint_{\mathcal{V}_{\Theta}(t)} -\nabla \cdot \mathbf{N}_d d\mathcal{V} = \frac{\partial}{\partial \sigma} \iiint_{\mathcal{V}_{\Theta}(t)} \frac{D\sigma}{Dt} d\mathcal{V} \quad (4.11)$$

where the unit vector for the isopycnal surface velocity is now up-gradient $\hat{\mathbf{n}}_{\sigma} = \frac{\nabla \sigma}{|\nabla \sigma|}$.

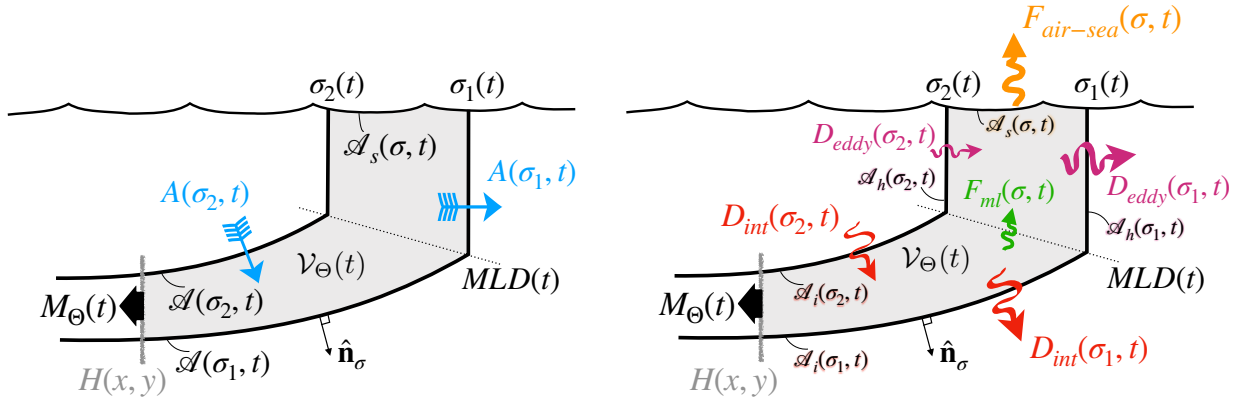
We will now follow the notation introduced by [Garrett et al. \(1995\)](#). Let's make a first distinction between fluxes directly driven by air-sea interactions and all other non-advective fluxes:

$$A(\sigma, t) = F_{air-sea}(\sigma, t) + D(\sigma, t) \quad (4.12)$$

The first r.h.s. term is the diapycnal volume flux driven by air-sea interactions processes and the second r.h.s. term is the flux arising from ocean interior diapycnal processes. [Tandon and Zahariev \(2001\)](#) furthermore decomposed the total diapycnal volume flux as:

$$A(\sigma, t) = F_{air-sea}(\sigma, t) + F_{ml}(\sigma, t) + D_{eddy}(\sigma, t) + D_{int}(\sigma, t) \quad (4.13)$$

that is a decomposition in terms of physical processes and is illustrated [Figure 4.5B](#). It was used in the CLIMODE project ([Marshall and co authors, 2004](#); [Marshall, 2005](#)). The first r.h.s. term is usually referred to as the air-sea transformation rate. The term $F_{ml}(\sigma, t)$ is the contribution due to mixed-layer entrainment, and $D_{eddy}(\sigma, t)$ and $D_{int}(\sigma, t)$ are from the horizontal mixing due to eddies near the surface and from the interior diapycnal mixing, mostly due to internal wave breaking.



(A) Volume budget elements of a water-body with density $\sigma_1 > \sigma > \sigma_2$. Similar to Figure 4.3-B but for a layer defined in density.

(B) Decomposition of the non-advective diapycnal volume flux into: air-sea driven transformation $F_{air-sea}$, entrainment at the base of the mixed layer F_{ml} , lateral eddy fluxes within the mixed layer D_{eddy} and interior thermocline mixing D_{int} .

Figure 4.5: Walin's water mass transformation framework in density classes.

Note that compared to Garrett et al. (1995) and Tandon and Zahariev (2001), here I noted the mixing terms D rather than $\partial_\sigma D$ for consistency with regard to Formation and Destruction processes.

I will now review each of these processes and my contributions to their diagnostic and understanding with regard to the EDW seasonal cycle study.

Air-sea transformation

The air-sea transformation rate term is given by:

$$F_{air-sea}(\sigma, t) = \frac{\partial B_s}{\partial \sigma} \left\{ \frac{\text{m}^3}{\text{s}} \right\} \quad (4.14)$$

where B_s is the surface density flux \mathcal{B}_{in} integrated over the outcrop of σ :

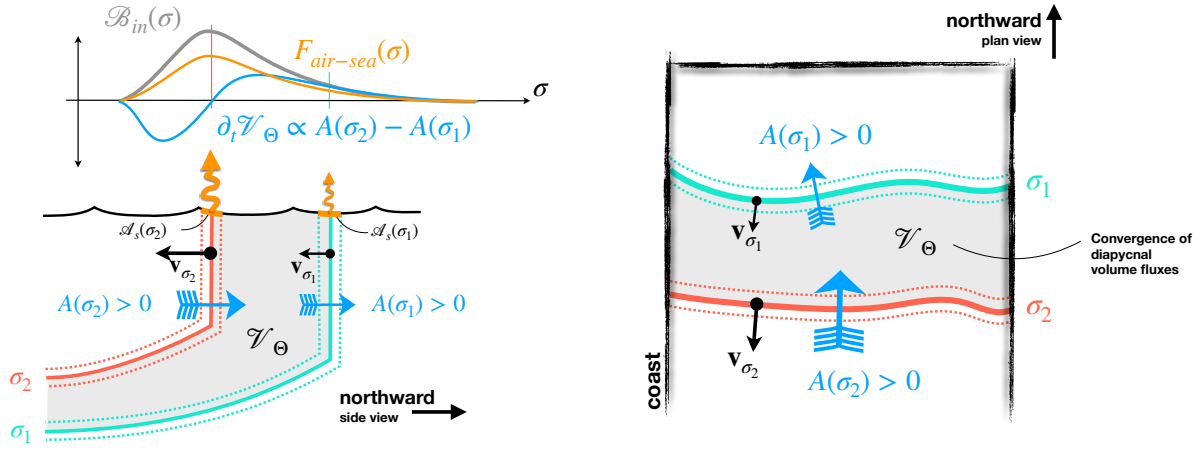
$$B_s(\sigma, t) = \iint_{\mathcal{A}_s(\sigma, t)} \mathcal{B}_{in}(x, y, t) d\mathcal{A} \left\{ \frac{\text{kg}}{\text{s}} \right\} \quad (4.15)$$

$$\mathcal{B}_{in}(x, y, t) = \frac{\alpha Q_{net}}{C_p} + \rho_0 \beta S (E - P) \left\{ \frac{\text{kg}}{\text{m}^2 \text{s}} = \frac{\text{kg m}}{\text{m}^3 \text{s}} \right\} \quad (4.16)$$

with $\alpha \simeq 2.5 \times 10^{-4} K^{-1}$ the thermal expansion coefficient, $C_p = 4187 J kg^{-1} K^{-1}$ the specific heat of seawater, Q_{net} [$\text{W} \cdot \text{m}^{-2}$] the net heat surface flux (positive upward, cooling the ocean), β [PSU^{-1}] the saline contraction coefficient, ρ_0 [kg m^{-3}] a reference density, S [PSU] the surface salinity and $(E - P)$ [$\text{m} \cdot \text{s}^{-1}$] the evaporation minus precipitation fresh water flux. $B_s(\sigma, t)$ corresponds to the density (in)flux into the $\mathcal{V}_\Theta(t)$ layer that is supplied by air-sea density exchange across the horizontal outcropping surface $\mathcal{A}_s(\sigma, t)$, see yellow arrows Figure 4.5B. Convergence or divergence of the air-sea transformation rate lead to the formation or destruction of the volume within a given density range:

$$\partial_t \mathcal{V}_\Theta \propto \Delta F_{air-sea} = F_{air-sea}(\sigma_2) - F_{air-sea}(\sigma_1) \quad (4.17)$$

A difference in outcropping surfaces or density flux experienced by outcrops implies a differential in the transformation rate of water layers at the surface and formation/destruction of water masses. This is



(A) Meridional side view of 2 isopycnal surfaces σ_1, σ_2 experiencing positive (e.g. cooling) but different air-sea buoyancy fluxes across their respective outcrops \mathcal{A}_s .

(B) Surface plan view of the outcrops.

Figure 4.6: Illustration of the transformation rate $F_{air-sea}$ driven by air-sea density fluxes \mathcal{B}_{in} . A positive density flux drives a positive transformation rate $F_{air-sea}$ of light water into denser one. The convergence of this diapycnal volume flux drives an increase in the volume \mathcal{V}_Θ embedded between the isopycnals. Note that this illustrative example cannot sustain a steady state without interior mixing or export out of the control domain.

illustrated Figure 4.6. If an outcrop σ_i is losing buoyancy because of a positive (upward) air-sea heat flux cooling or an excess of evaporation over precipitation, waters lighter than σ_i will be transformed into denser waters and the isopycnal outcrop will migrate equatorward (downgradient). If these transformation rates differ between isopycnal outcrops, volume flux convergence and divergence will appear. In the example Figure 4.6A, the diapycnal volume flux through the southern isopycnal outcrop due to $F_{air-sea}(\sigma_2)$ is larger than the one through the northern one, $F_{air-sea}(\sigma_1)$, the volume of the layer in between, \mathcal{V}_Θ will thus increase (by convergence of the diapycnal volume flux). This can be seen as an increase of the \mathcal{V}_Θ layer outcropping due to a faster southern migration of its warm flank compared to its cold flank ($\mathbf{v}_{\sigma_2} > \mathbf{v}_{\sigma_1}$, Figure 4.6B).

Note that given the distribution of the density flux with density $\mathcal{B}_{in}(\sigma)$ in this example, the air-sea transformation rate $F_{air-sea}(\sigma)$ convergence leads to the destruction of all the water lighter than σ_2 to sustain the formation of water denser than σ_1 . Obviously, without any other processes, this forcing would lead a closed basin to be filled with ever increasing dense waters. To sustain a steady state, this air-sea forcing requires either interior mixing (acting on the density gradient to reverse the air-sea driven transformation, warming up the dense waters) or volume fluxes out/into the domain. In fact, that later case is an elegant constrain to compute a meridional overturning streamfunction (in a basin closed at its northern boundary) since the air-sea driven transformation of warm water into colder one must be sustained by an upper warm water import and a deep export of cold water. This principle was developed by Nurser and Marsh (1998) and Marsh (2000) to diagnose an Atlantic Meridional Overturning Circulation (AMOC) streamfunction at a given latitude as a function of the air-sea density flux integrated over outcrop at the surface (see also Radko et al., 2008; Han et al., 2012).

It is important to note here, that in order to compute water mass transformation rates, one has to discretise Equation 4.14 and Equation 4.15. This leads to the practical formulation:

$$F_{air-sea}(\sigma, t) = \frac{1}{\Delta\sigma} \iint_{\sigma-\Delta\sigma/2}^{\sigma+\Delta\sigma/2} \left(\frac{\alpha Q_{net}}{C_p} + \rho_0 \beta S (E - P) \right) d\mathcal{A} \left\{ \frac{\text{m}^3}{\text{s}} \right\} \quad (4.18)$$

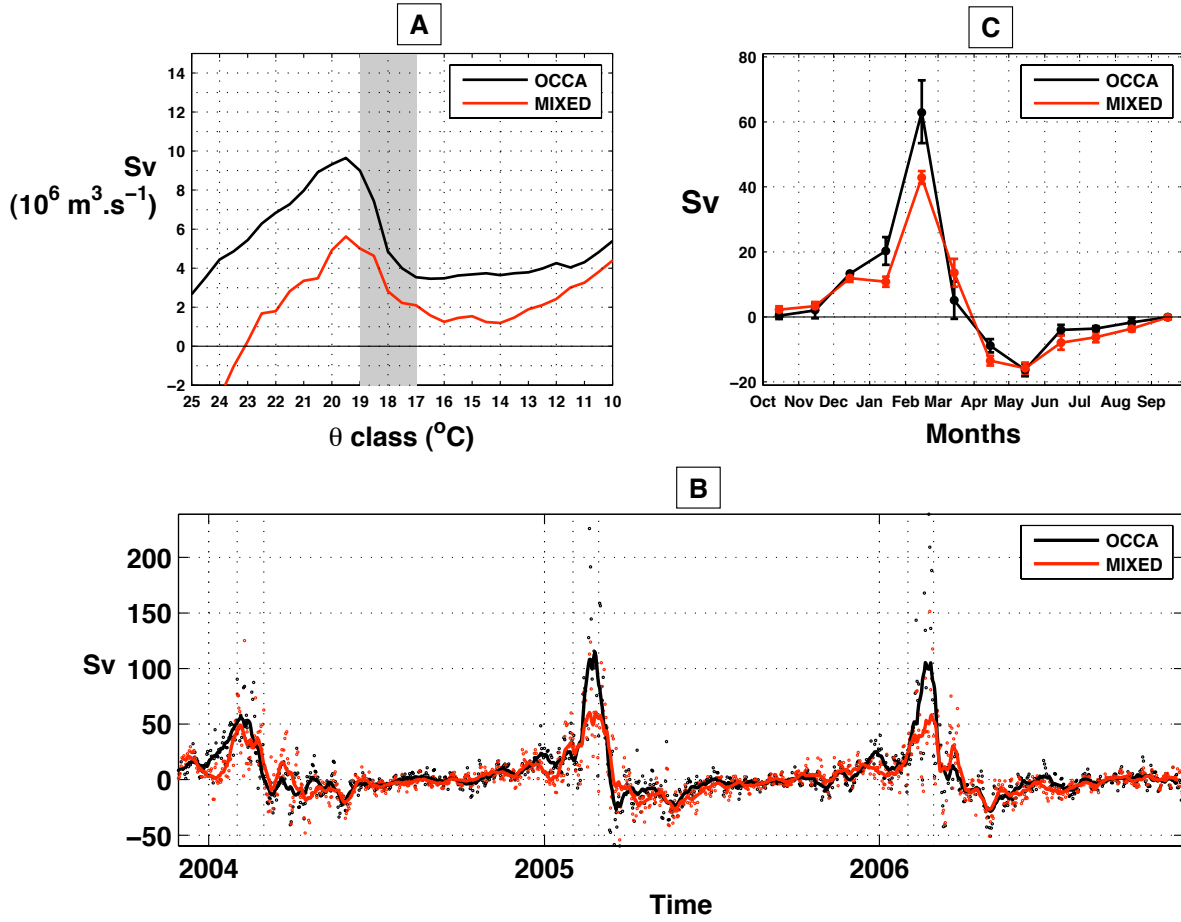


Figure 4.7: Air-sea transformation rates for 2003-2006 over the North Atlantic. Estimate in red is from observations (mix of ECMWF, satellite SST and COARE bulks) and in black from the OCCA dataset. Plot A: 2003-2006 time mean, Plot B and C: daily time series and typical seasonal cycle of $F_{air-sea}(\theta = 18^\circ C)$, the air-sea transformation rate for the EDW layer. Reproduced from [Maze et al. \(2009\)](#) figure 3.

In [Maze et al. \(2009\)](#), I diagnosed the air-sea transformation rate for 2003-2006 over the North Atlantic using a combination of atmospheric re-analysis and satellite data. To be able to work with *observations* I was limited to work in temperature classes. Indeed, only SST satellite data were available at this time, the SMOS mission was not ready and Sea Surface Salinity from satellite not yet available. Using the ECMWF atmospheric state and SST, I computed air-sea heat fluxes with [Fairall et al. \(2003\)](#) COARE bulk formulae. I used the temperature class reformulation of [Equation 4.18](#):

$$F_{air-sea}(\theta, t) = \frac{1}{\Delta\theta} \iint_{\sigma-\Delta\theta/2}^{\sigma+\Delta\theta/2} -\frac{Q_{net}}{\rho C_p} d\mathcal{A} \left\{ \frac{m^3}{s} \right\} \quad (4.19)$$

where the surface density flux integrated over density outcrops B_s is replaced by the surface heat flux integrated over temperature outcrops.

The 2003-2006 time mean of $F_{air-sea}(\theta, t)$ for the $10^\circ C \leq \theta \leq 25^\circ C$ range is shown [Figure 4.7-A](#). One can see the higher transformation rate through the $19^\circ C$ than $17^\circ C$ outcrops ($5Sv$ vs $2Sv$) leading to a volume flux convergence in that temperature range that corresponds to the EDW net formation rate due to air-sea heat fluxes ($3Sv$). Note that the estimate from observations is smaller than the estimate from OCCA.

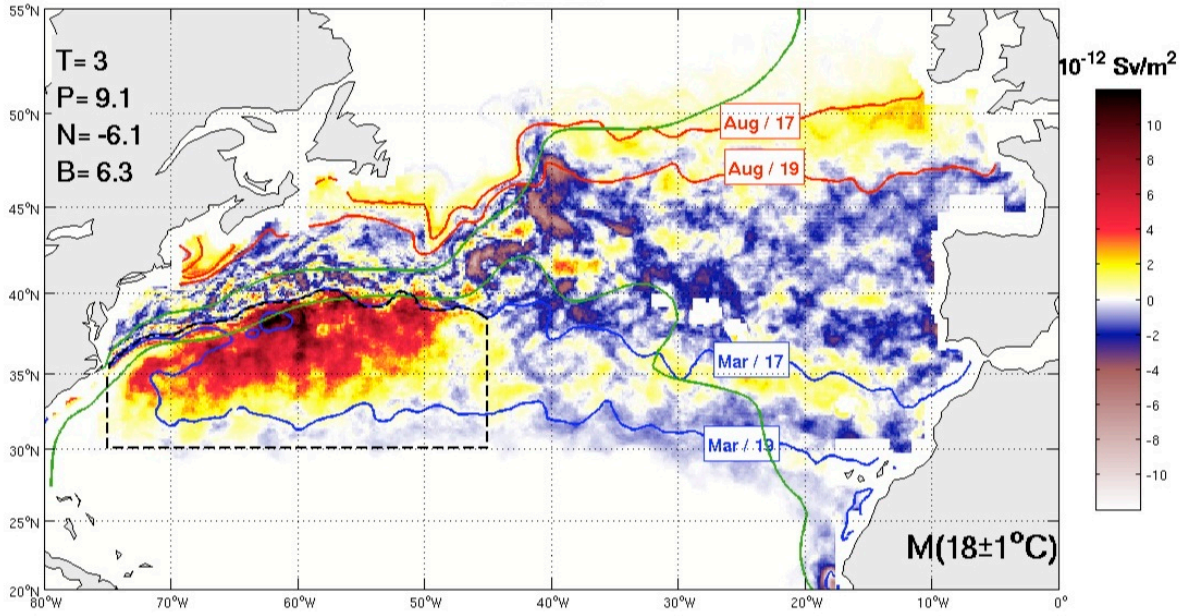


Figure 4.8: 2003-2006 time mean map of EDW local formation rate due to air-sea transformation processes. Red to black regions are where EDW is formed, blue to white where it is destroyed by air-sea heat fluxes. One can readily see emerging the exact location of EDW formation along the southern flank of the Gulf Stream. Reproduced from [Maze et al. \(2009\)](#) figure 6.

Contribution highlight A key result of [Maze et al. \(2009\)](#) was to show the very large amplitude of transformation rates that could be sustained over a few weeks, up to 100Sv from daily time series and 50Sv over a month from the typical seasonal cycle. This result means that the EDW formation through air-sea fluxes is a process taking place over a very short time frame.

In [Maze et al. \(2009\)](#) we furthermore produced for the very first time a spatial distribution of EDW formation rates that is fully consistent with Walin’s framework estimates. Indeed, up to this study, formation rates from Walin’s principals were given as integral statements, by their very definition (see [Equation 4.18](#) for instance) while EDW formation regions were determined using the temperature of the mixed layer as a proxy.

Contribution highlight In [Maze et al. \(2009\)](#) we introduced maps of the Walin’s integrand and provided their complete physical interpretation, thus reconciling quantitative with qualitative approaches in EDW formation studies.

This result arises from a quite simple idea, namely that the accumulated maps of the integrand in [Equation 4.18](#) lead to the time-mean Walin’s estimate of transformation rates. Let’s re-write this equation as:

$$F_{\text{air-sea}}(\sigma, t) = \iint_{x,y} \mathcal{F}(\sigma, t, x, y) d\mathcal{A} \quad (4.20)$$

with:

$$\mathcal{F}(\sigma, t, x, y) = \frac{1}{\Delta\sigma} \mathcal{B}_{in}(x, y, t) \Pi(\sigma, t) \left\{ \frac{\text{m}}{\text{s}} = \frac{\text{Sv}}{\text{m}^2} \right\} \quad (4.21)$$

and where $\Pi(\sigma, t)$ is the outcrop mapping function:

$$\Pi(\sigma, t) = \begin{cases} 1 & \text{if } \sigma - \frac{\delta\sigma}{2} \leq \sigma(x, y, z=0, t) < \sigma + \frac{\delta\sigma}{2} \\ 0 & \text{otherwise} \end{cases} \quad (4.22)$$

Classically we integrate Equation 4.21 over space to yield transformation rates time series. Here, we integrate it over time to yield transformation rate maps. The instantaneous map of \mathcal{F} is zero everywhere except over the EDW outcrop. When averaged in time (over a month or several years), the seasonal migration of surface outcrops sweeps out larger regions and coherent patterns emerge. The 2003-2006 time mean EDW formation rate from observations is given Figure 4.8. The surface integral of this map yields the 3Sv of formation rate determined with a classic formulation of the Walin's principals as shown Figure 4.7-A.

Contribution highlight In Maze et al. (2009) and Forget et al. (2011) we provided, again for the first time, a thorough estimate of errors arising from Walin's principals discretisation of the outcrops over a gridded dataset, from random errors in the outcropping and atmospheric fields and from poorly constrained air-sea heat fluxes.

First, we found that if the outcrop discretisation bin is too small, the outcropping region is too small to be resolved, which leads to considerable noise in both and integral estimates. On the other hand, if the bin is too large, the ability to resolve the temperature class of interest is too bad and useless estimates are produced. We quantitatively estimated the sensitivity of transformation rate estimates to these parameters. Second, using ensembles of random error perturbations, we determined that the random errors in SST and Q_{net} could lead to error of about 1Sv in the EDW transformation and formation rate estimates. Finally, we combined different sets of bulk formulaes with different atmospheric re-analysis to show that uncertainties in air-sea heat fluxes are the primary source of uncertainties in EDW formation rate estimates, with a spread among all possible combination as large as 9Sv for the net annual formation rates.

Mixed-layer entrainment

One will note from Figure 4.5B an additional diathermal volume flux $F_{ml}(\theta, t)$ operating at the base of the mixed layer. Garrett and Tandon (1997) have shown, using simple geometric arguments, that density redistribution in the vertical by turbulent mixing achieves a diapycnal advection across an isopycnal surface. In other words, as mixing occurs whenever a dense interior water is entrained into the lighter mixed layer, there is a water mass transformation, or diapycnal volume flux, through the base of the mixed layer that is due to mixed layer entrainment (Nurser et al., 1999).

This diathermal volume flux due to mixed layer entrainment, per unit of outcrop length, derived by Garrett and Tandon (1997) and Nurser et al. (1999) is given by:

$$F_{ml}(\sigma, t_0) = \frac{1}{t_0} \int_{0, dh>0}^{t_0} \left[\left(\frac{1}{b_{x,i}} - \frac{1}{b_{x,s}} \right) \Delta b - \frac{1}{2} b_{xx} b_x^{-3} (\Delta b)^2 \right] dh \left\{ \frac{\text{m}^2}{\text{s}} = \frac{\text{m}^3}{\text{s}} \frac{1}{\text{m}} \right\} \quad (4.23)$$

where x is the local direction normal to the outcrop in the direction of increasing buoyancy (reverse to $\hat{\mathbf{n}}_\theta$), b_x and b_{xx} is the horizontal buoyancy gradient and its curvature, $b_{x,i}$ and $b_{x,s}$ are the horizontal buoyancy gradients below the mixed layer and at the sea surface, Δb is the change of buoyancy at the base of the mixed layer h before a mixing event, t_0 represents 1 year of integration and dh is the rate of change of mixed layer depth:

$$dh = \left(w_b + \frac{\partial h}{\partial t} \right) dt \quad (4.24)$$

with w_b is the vertical velocity at the base of the mixed layer.

The volume flux F_{ml} is given by the annual integration during mixed layer deepening events ($dh > 0$) of terms depending on the vertical and horizontal (1st and 2nd r.h.s terms in Eq.(4.23), respectively) variations of the horizontal buoyancy gradient b_x . Thus, this term requires relatively high-frequency and high-resolution datasets to be estimated correctly.

Using simple scalings, Garrett and Tandon (1997) and Nurser et al. (1999) estimated a mean F_{ml} to about 3Sv. Using high-frequency 15-mins mooring data from the subpolar North Atlantic region, Tandon and Zahariev (2001) have explored the time-frequency dependence of the entrainment term F_{ml} and found that

resolving the diurnal cycle is important to capture its amplitude, which can peak to about 4Sv. However, this local estimate extrapolated to the entire basin is much larger than another one from [Tandon and Zhao \(2004\)](#) who found values smaller than 1Sv using monthly-mean isopycnals with 6-hourly NCEP fluxes, thus resolving the diurnal cycle. To summarize, [Tandon \(2001\)](#) pointed that F_{ml} estimates are particularly sensitive to the resolution of synoptic events and to the fine-scale frontal structure near the surface. This leads to uncertainty in F_{ml} particularly, and "unacceptably", high from both model based and data based evaluations.

Finally, in the CLIMODE proposal F_{ml} was neglected because estimated to contribute to no more than 10% of the $\Delta F_{air-sea}$ air-sea flux driven EDW formation rate estimated at that time. I have shown that $\Delta F_{air-sea}$ is about $6 \pm 1Sv$ ([Maze et al., 2009](#)). Thus, depending on the F_{ml} estimates, neglecting it may not, *a posteriori* be a valid assumption. Whether F_{ml} is within the relatively large error bars of the air-sea fluxes or not thus remained to be shown.

Lateral eddy mixing

Horizontal stirring by geostrophic eddies entails mixing that contribute to the total diapycnal volume flux $A(\sigma, t)$ in Eq.(4.13). [Marshall et al. \(1999\)](#) have shown that this horizontal, i.e. diapycnal near the surface, mixing by geostrophic eddies must be accounted for in order to reconcile kinematic subduction rates with air-sea flux driven formation rates, i.e. $F_{air-sea}$ is not a good predictor of A in Eq.(4.13).

Even if eddies are assumed to be mostly adiabatic in the ocean interior (see for instance the [Gent and McWilliams, 1990](#), parameterisation) a large number of modelling studies have shown that eddies have strong diabatic effects in near-surface frontal regions (e.g. [Radko and Marshall, 2004a](#)). For instance, using an eddy resolving idealised simulation, [Cerovecki and Marshall \(2008\)](#) have diagnosed eddy temperature fluxes. They are reproduced [Figure 4.9](#). In this simulation, isotherms correspond with isopycnal surfaces. Near the surface, in the upper 100m, the eddy temperature fluxes are not aligned with isotherms, which reveals an eddy-driven diapycnal volume flux component. This contrasts with the ocean interior where eddy temperature fluxes are mostly aligned with isotherms, which is symptomatic of the adiabatic, isopycnal, mixing by eddies.

The lateral eddy transformation rate term is given by:

$$D_{eddy}(\sigma, t) = \frac{\partial B_e}{\partial \sigma} \left\{ \frac{\text{m}^3}{\text{s}} \right\} \quad (4.25)$$

where B_e is the eddy density flux \mathcal{B}_{eddy} integrated over vertical σ isopycnal surfaces:

$$B_e(\sigma, t) = \iint_{\mathcal{A}_h(\sigma, t)} \mathcal{B}_{eddy}(x, y, t) d\mathcal{A} \left\{ \frac{\text{kg}}{\text{s}} \right\} \quad (4.26)$$

$$\mathcal{B}_{eddy}(x, y, t) = -\mathbf{v}'\sigma' \cdot \hat{\mathbf{n}}_\sigma \left\{ \frac{\text{kg}}{\text{m}^2 \text{s}} = \frac{\text{kg m}}{\text{m}^3 \text{s}} \right\} \quad (4.27)$$

where $\mathcal{A}_h(\sigma, t)$ is the lateral surface of constant potential density σ extending from the sea surface down to the bottom of the mixed layer depth h (see [Figure 4.5B](#)).

This eddy flux can be parameterized as a down-gradient Fickian mixing $-\kappa_H \nabla \sigma$ with κ_H [$\text{m}^2 \text{s}^{-1}$] a horizontal eddy diffusivity acting on the density gradient. This diffusivity quantifies the enhancement of small-scale diffusion due to fine-scale tracer gradients created by eddy stirring.

Thus, an estimate of the eddy driven diapycnal volume flux in the mixed layer is:

$$D_{eddy}(\sigma, t) = \frac{1}{\Delta \sigma} \iint_{\sigma-\Delta \sigma/2}^{\sigma+\Delta \sigma/2} -\kappa_H \nabla_H \sigma_m(t) \cdot \hat{\mathbf{n}}_\sigma d\mathcal{A} \left\{ \frac{\text{m}^3}{\text{s}} \right\} \quad (4.28)$$

with ∇_H the horizontal gradient operator and σ_m the mixed layer density.

With such a parameterization, the lateral eddy mixing term accuracy will crucially depend on our knowledge of the horizontal eddy diffusivity coefficient κ_H . Several Eulerian or Lagrangian approaches can be used to estimate it, for instance: in-situ tracer-release experiments (e.g. [Gille et al., 2007](#)), tracer fluctuations combined with mixing length theory (e.g. [Ferrari and Polzin, 2005](#); [Cole et al., 2015](#)), idealised

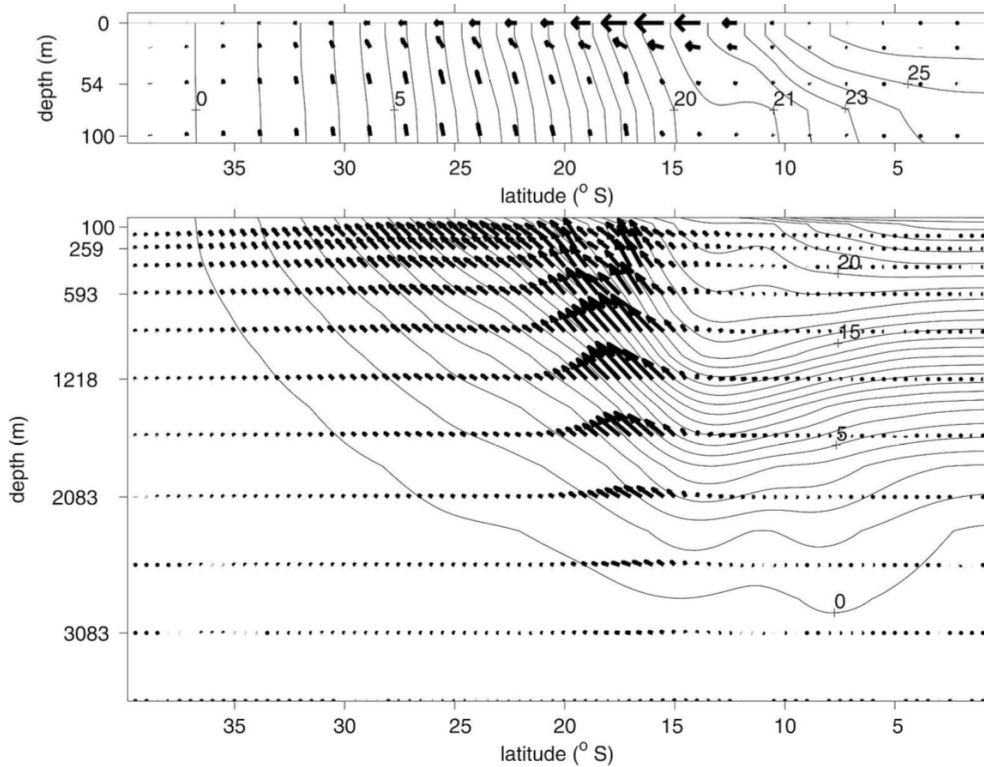


Figure 4.9: Reproduction from [Cerovecki and Marshall \(2008\)](#) showing a meridional section of zonally averaged mean eddy temperature fluxes $\overline{\mathbf{u}'\theta'}$ (arrows) and mean isotherms (solid line; $^{\circ}\text{C}$). See how eddy temperature fluxes crossing isotherms near the surface contrast with the nearly adiabatic interior. In the upper panel, the longest arrow corresponds to $0.15^{\circ}\text{C m s}^{-1}$ and to $0.02^{\circ}\text{C m s}^{-1}$ in the lower panel.

tracers governed by advection/diffusion using surface velocities from altimetry (e.g. [Marshall et al., 2006](#)) or 3-dimensional velocities from an ocean state estimate (e.g. [Abernathey et al., 2010](#)). A canonical value for κ_H is $1000\text{ m}^2\text{ s}^{-1}$ but the studies cited above, and many more (e.g. [Abernathey and Marshall, 2013](#)), have shown that it varies with location and depth, from near zero to $10^4\text{ m}^2\text{ s}^{-1}$.

With regard to CLIMODE and the EDW seasonal cycle, [Nurser et al. \(1999\)](#) and [Marshall and co authors \(2004\)](#) conducted a simple scaling for the eddy driven diapycnal volume flux term. Basically, if we assume lateral mixing to act mainly along the Gulf Stream (1500 km length) and down to a mixed layer of 400 m, a northward cross-stream density gradient of $0.5\text{ kg m}^{-3}/50\text{ km} = 10^{-5}\text{ kg m}^{-4}$ subject to an eddy diffusivity of $1000\text{ m}^2\text{ s}^{-1}$ leads to a positive eddy diapycnal volume flux of 6 Sv. We recall that a positive diapycnal volume flux corresponds to a volume flux from light to dense waters. In this case, the northern EDW isopycnal is thus migrating southward, away from the turbulent Gulf Stream where it usually resides, because of lateral eddy mixing. On the other hand, the southern EDW isopycnal is far from the Gulf Stream and less sensible to this turbulent mixing. With regard to the EDW volume, lateral eddy mixing thus creates a diapycnal volume flux divergence, hence a mode water destruction of about 6 Sv. This is of the same order of magnitude as the air-sea flux driven formation rate and is thus a good candidate to close the EDW volume budget.

More recently, [Billheimer and Talley \(2016\)](#) evaluated the contribution to the EDW destruction from lateral isopycnal stirring of PV that is particularly efficient across a large-scale lateral PV gradient, like the Gulf Stream. They found this term to be maximum near the Gulf Stream because of the enhanced mesoscale activity. However, they found this term to be responsible for only 1/3 of the EDW destruction, the remaining 2/3 being driven by interior vertical mixing (see next section).

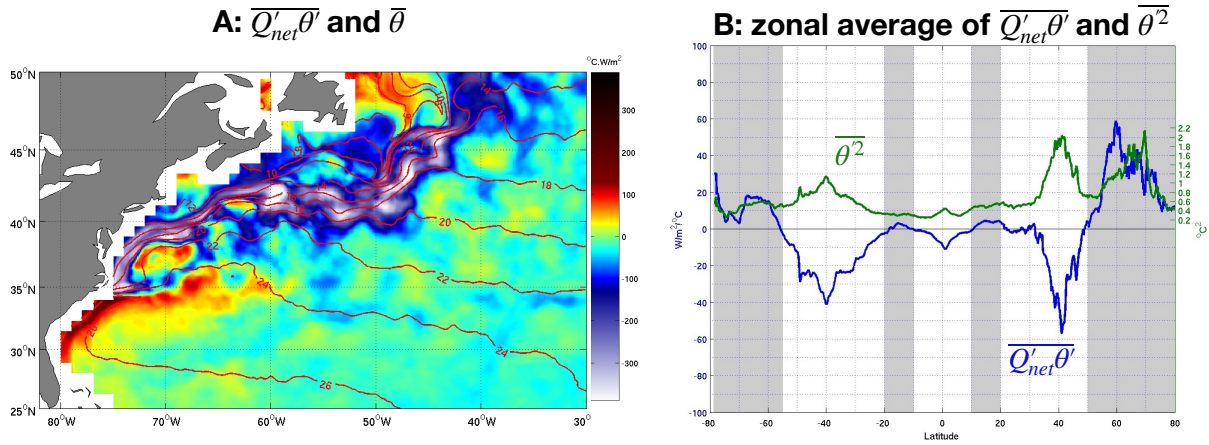


Figure 4.10: Plot A: Eddy correlation of air-sea heat fluxes with sea surface temperatures ($\overline{Q'_{net}\theta'}$, color shading) with mean SST contours (red). Plot B: Zonal mean of $\overline{Q'_{net}\theta'}$ (blue) with temperature eddy variance (green). Data are from 3 years of an $1/8 \times 1/8$ eddy resolving MITgcm simulation. The systematic damping of ocean eddy temperature anomalies by air-sea fluxes increases the surface eddy diffusivity.

Contribution highlight In Shuckburgh et al. (2011), I have contributed to explain a striking feature of κ_H , namely that it is surface intensified because of air-sea interactions. It is that surface intensification that can lead to such high values as $1000\text{m}^2\text{s}^{-1}$, and even more. We've shown that the damping of eddy temperature variance by air-sea fluxes enhances the dissipation of surface temperature fields and thus significantly increases the surface eddy diffusivities over interior values.

We published this result for the Southern Ocean and the Antarctic Circumpolar Current, but it is true in all eddy rich and frontal regions, such as the Gulf Stream. My companion study to Shuckburgh et al. (2011) for the gulf Stream region was, unfortunately, never published out of the CLIMODE group reporting and was presented during seminars I gave at WHOI and LPO in 2007. My result lead to further justify the canonical eddy diffusivity used in the CLIMODE project to estimate the role of lateral eddy mixing in EDW formation.

To briefly illustrate my contribution here, let's apply a standard Reynolds decomposition of the temperature variability, neglecting triple correlation terms. This leads to the temperature variance equation integrated over the mixed layer depth H (Marshall and Shutts, 1981):

$$\frac{D}{Dt} \frac{\overline{\theta'^2}}{2} + \overline{\mathbf{v}'\theta'} \cdot \nabla \overline{\theta} = \frac{\overline{Q'_{net}\theta'}}{\rho C_p H} \quad (4.29)$$

The r.h.s term of eddy correlation of air-sea heat fluxes with SST is shown Figure 4.10 from a MITgcm numerical simulation. Here primes denote fluctuations not including the seasonal cycle and only related to eddy-driven fluctuations. We see that the eddy correlation is negative all along the Gulf Stream region and thus that air-sea fluxes are systematically damping eddies and reducing the eddy temperature variance. This can be explained by the fact that the atmosphere tends to restore SST toward a large scale meridional sea surface atmospheric temperature gradient and thus to damp SST anomalies. This is fundamentally an eddy time scale issue that is different between the ocean and the atmosphere. This point is discussed at length in Shuckburgh et al. (2011).

We have shown for the Southern Ocean and Gulf Stream that if one compute the *true* ocean eddy diffusivity as:

$$\kappa_H = - \frac{\overline{\mathbf{v}'\theta'} \cdot \nabla \overline{\theta}}{\overline{\nabla \theta} \cdot \nabla \overline{\theta}} \left\{ \frac{\text{m}^2}{\text{s}} \right\} \quad (4.30)$$

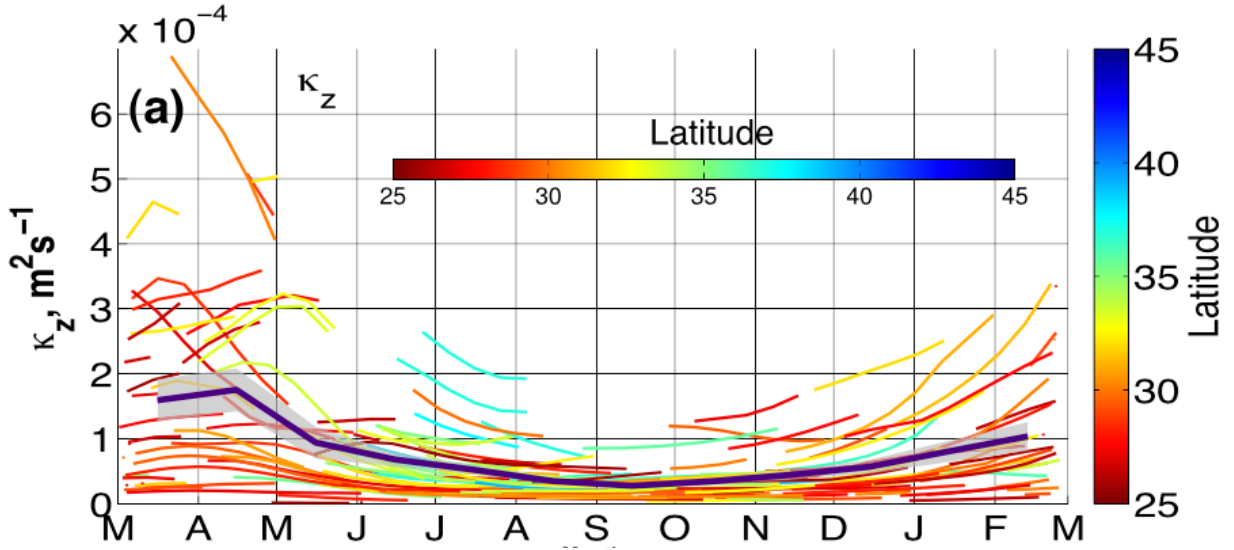


Figure 4.11: Vertical diffusion coefficient at the top of the EDW layer. Estimate based on Argo floats, 2005-2015, reproduced from [Billheimer and Talley \(2016\)](#) figure 5-a. The ensemble average is shown (bold indigo) with a 95% confidence interval (gray shading) obtained from bootstrapping methods.

then, the ocean interior values are enhanced in the mixed layer by the air-sea flux damping contribution that can be estimated as

$$\kappa_{air-sea} = -\frac{1}{\rho C_p H} \frac{\overline{Q'_{net} \theta'}}{\nabla \theta \cdot \nabla \theta} \left\{ \frac{m^2}{s} \right\} \quad (4.31)$$

Interior mixing

The last r.h.s. term in [Equation 4.13](#) is due to interior diapycnal mixing. This term mainly operates vertically, through nearly horizontal isopycnal surfaces \mathcal{A}_i , see [Figure 4.5B](#). Like the lateral eddy term, it can be estimated as:

$$D_{int}(\sigma, t) = \iint_{\mathcal{A}_i(\sigma, t)} -\kappa_z \frac{\partial \sigma(t)}{\partial z} d\mathcal{A} \left\{ \frac{kg}{s} \right\} \quad (4.32)$$

In the CLIMODE proposal, this term was scaled assuming a constant diapycnal diffusivity κ_z of about $10^{-5} m^2 s^{-1}$ (from the tracer release estimate of [Ledwell et al., 1993](#), in the North Atlantic thermocline) acting through a 200m vertical scale for the permanent pycnocline and over the North Atlantic EDW domain ($3 \times 10^{13} m^2$). This leads to an EDW destruction rate of about 1.5Sv.

More recently, [Billheimer and Talley \(2016\)](#) studied seasonal EDW destruction processes from observations. They assumed that EDW erosion from interior mixing is due to vertical diffusion through the upper and lower depths of the EDW. Following observation-based pycnocline or upper pycnocline low estimates of κ_z from [Ledwell et al. \(1993\)](#) and [Whalen et al. \(2012, 2015\)](#), they simply disregarded vertical diffusion at the bottom of the EDW layer to only focus on diffusion through the seasonal pycnocline.

Using Argo float trajectories, [Billheimer and Talley \(2016\)](#) determined the vertical diffusivity at the top of the EDW layer. They used the same methodology as [Qiu et al. \(2006\)](#), which is based on the following simplified potential vorticity budget:

$$\frac{\partial Q}{\partial t} = \frac{\partial}{\partial z} \left(\kappa_z \frac{\partial Q}{\partial z} \right) \left\{ \frac{1}{ms^2} \right\} \quad (4.33)$$

where Q is defined as in [Equation 3.1](#). The vertical diffusivity κ_z is then inferred to reproduce the vorticity seasonal fluctuations determined from time series of EDW *intensity*, which is a mode water characteristic

defined as:

$$I = \int_{z_{bottom}}^{z_{top}} (Q_0 - Q) dz \left\{ \frac{1}{s} \right\} \quad (4.34)$$

Combined with the simplified PV budget, the vertical diffusivity can be computed as:

$$\kappa_z(z_{top}) = \frac{dI/dt}{\partial Q / \partial z(z_{top})} \left\{ \frac{m^2}{s} \right\} \quad (4.35)$$

Using Argo floats data, [Qiu et al. \(2006\)](#) applied this method to the North Pacific Subtropical Mode Water, and [Billheimer and Talley \(2016\)](#) to the North Atlantic EDW. Their κ_z estimate is reproduced here [Figure 4.11](#). One can see that κ_z fluctuates seasonally, with a maximum value of about $2 \times 10^{-4} m^2 s^{-1}$ in March-April, i.e. during the late winter when the vertical PV gradient at the top of the EDW is the weakest.

Unfortunately, [Billheimer and Talley \(2016\)](#) didn't provided an EDW volumetric destruction rate but rather focused on *intensity*. So, if we assume here that a vertical diffusivity of $2 \times 10^{-4} m^2 s^{-1}$ acts upon a 50m vertical scale for the seasonal pycnocline (see [Figure 3.3](#)) and over an $0.3 \times 10^{13} m^2$ outcropping area (see [Figure 1](#) in [Forget et al., 2011](#)): we obtain an EDW destruction rate of about $12 Sv$. Note however, that this rate is only sustained over one month, in April. So, on one hand, this makes it comparable, but much smaller, to air-sea formation rates (see [Figure 4.7-C](#)) and on the other hand, when scaled back to annual rates, interior mixing reduces to about $1 Sv$. It is thus curious to note that the initial CLIMODE estimate was in fact roughly correct but for the wrong reasons.

Synthesis of driving factors

In the previous sections, we described in details the different processes that contribute to the EDW seasonal cycle through their impact on water-mass transformation in the North Atlantic subtropical gyre. In this final part, we'll bring together all these processes within a single robust estimate of the EDW seasonal cycle volume budget.

In [Forget et al. \(2011\)](#), using the OCCA dataset, we computed all terms from (4.13) (except for the mixed-layer entrainment) and integrated them over a typical seasonal cycle. Results are summarised [Figure 4.12](#). It shows the typical seasonal cycle of the air-sea transformation term (red), the mixing terms (black) together with the storage rate (blue) and export terms (green). Note that this later export term is not included in (4.13) because it is not associated with a water transformation but it does slightly contribute to the EDW volume budget (because the domain of analysis was limited to the North Atlantic and thus the $17 - 19^\circ C$ layer was cut through along $5N$).

This synthetic figure shows that:

- the EDW volume rapidly increases by about $8 Sv$ (relative to December 1st) in winter, achieving a maximum at the end of February or early March,
- this EDW volume increase is driven by $9 Sv$ formed because of strong air-sea heat flux cooling from December to early March,
- more surprisingly, air-sea heat flux warming in spring erodes about half of what was formed in winter, $4.5 Sv$, and then remain neutral to the end of the year,
- the mixing term, both horizontal and vertical, constantly erodes the EDW volume all year long with a net destruction of about $2.5 Sv$,
- the EDW volume budget is closed when considering storage ($1 Sv$) and export through the southern open boundary ($1.5 Sv$).

Each term was attributed an error bar from systematic bias due to divergent methods and layer definition criteria. The volume error estimate has already been discussed in [Figure 3.4](#). In [Maze et al. \(2009\)](#) I computed a random error of about $1 Sv$ for air-sea heat flux driven EDW formation rates. In [Forget et al. \(2011\)](#) we complemented this estimate with systematic errors from the choice of the atmospheric state (NCEP vs ECMWF) and bulk formulas to compute fluxes: [Large and Yeager \(2004\)](#) vs [Fairall et al. \(2003\)](#). We have

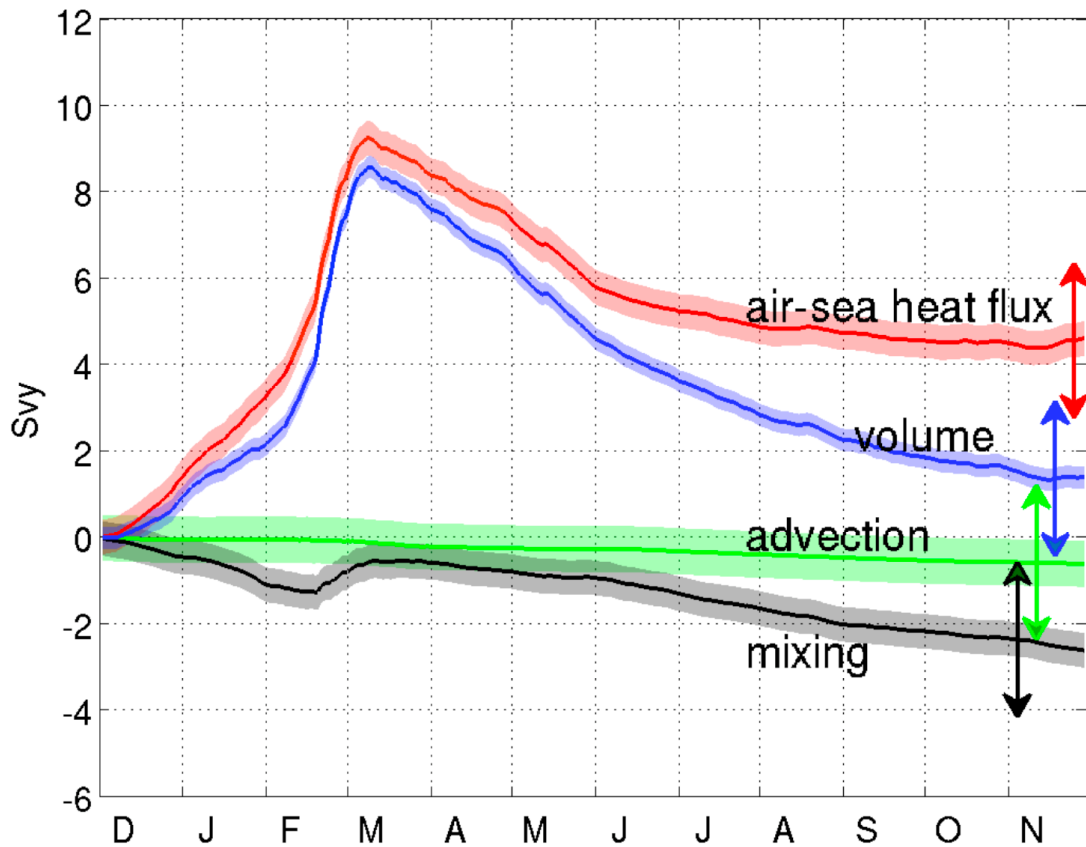


Figure 4.12: Key result from my [Forget et al. \(2011\)](#) study: a robust estimate of the typical seasonal cycle of the main mechanisms driving the EDW layer volume (blue): transformation due to air-sea heat fluxes (red), adiabatic export/import (green) and interior mixing due to vertical diffusion and mixed layer lateral eddy fluxes (black).

shown that the choice of the bulk formulas remains the primary source of divergence in the computation of transformation rates, with values varying by a factor larger than 3. Uncertainties in bulk coefficients for example: we found that a 0.2×10^{-3} (i.e., 15%) change in drag coefficient is sufficient to imply a 1Sv increase in annual EDW formation.



5. Low-frequency variability of the EDW

Contribution highlight My key contributions to a better understanding of the Subtropical North Atlantic low-frequency variability are oriented toward the notion of "extremes" for low-frequency time scales:

- Decadal scale: in [Stevens et al. \(acc., 2020\)](#); [Maze et al. \(2019a,b\)](#) I showed that over the last 5 years (2014-2018), the EDW has experienced changes not seen since 1970 and that EDW properties are reaching extreme values, never seen since 1950.
- Interannual scale: in [Lee \(2020\)](#), we showed that since 2002, the EDW has experienced 3 extreme positive and 3 extreme negative production winters for which we determined that lateral Ekman transport is a key ingredient.

Content of this chapter:

Introduction	58
Data and method	59
Results	59
Unprecedented pentadal recent changes	59
Interannual extremes	61
Final remarks	63

Introduction

Let's start this chapter with a brief overview of the interannual phenomenology of the North Atlantic subtropical gyre.

Bryden et al. (2014) showed that the winter 2009-2010 was marked by a 30% horizontal circulation slow down at 25N. This induced a reduction in the northward meridional heat transport of about 0.4PW which in turn, induced cold temperature anomalies between 25 and 45N. Häkkinen et al. (2013) showed that this abrupt change was visible in SSH variability time series and induced by a gyre spin-down, or weakening. The subtropical and subpolar gyres strength are linked to the "wind stress gyre mode" (the second SSH Empirical Orthogonal Functions, EOFs Häkkinen et al., 2011) which, in turn, is related to the second mode of variability in the North-Atlantic atmospheric circulation: the East-Atlantic Pattern (EAP). When EAP dominates atmospheric variability, the subtropical gyre expands northward and the subpolar gyre shrinks; this facilitates the invasion of warm, salty subtropical water into the eastern subpolar gyre (Desbruyères et al., 2013). The positive phase of the EAP corresponds to the Atlantic-Ridge (AR) weather regime to which most of the Bermuda SSH variability can be attributed (Barrier et al., 2012).

Billheimer and Talley (2013) showed that during the 2011-2012 winter, the EDW was poorly ventilated and that an unusually small amount of this water mass has been formed/renewed (it reached a 8-year period minimum). They showed that this "near cessation of EDW renewal" was not due to a poor local ocean preconditioning (a large sub-surface heat content in 2011 fall) neither to a larger Gulf Stream heat transport, but most likely to a mild late winter inducing unusually weak buoyancy loss at the surface. The mild 2011-2012 winter is characterised by a strong positive phase of the North Atlantic Oscillation (NAO) which is the dominant atmospheric weather regime in the North Atlantic (Visbeck et al., 2001). During this specific winter, deep convection was observed further North in the Irminger Sea (Piron, 2015), highlighting the large scale impact of atmospheric weather regimes on the ocean.

Grist et al. (2015) observed enhanced formation of dense mode waters during the winter 2013-2014 in the northeast corner of the subtropical gyre (a region sometimes placed in the subpolar gyre, but where a subtropical-like permanent pycnocline is observed Feucher et al., 2019). They showed this was due to anomalous turbulent heat fluxes associated with the stormiest winter on record over the western Europe (Matthews et al., 2014) and the largest number of NAO+ regimes assessed from atmospheric reanalyses going back to 1870 (NOA-20CR product). With such a denser mode water, the regional heat content reached its lowest level since 2004 accordingly.

Last, I'll note that since around 2005, there is a growing body of observational evidence that a remarkable reversal of climatic trends is occurring over the North Atlantic ocean. Roemmich et al. (2015) have shown that the positive global heat content trends for the Argo period (2006-2013) is driven by the Southern Hemisphere extratropical ocean warming (67 to 98% of the heat gain) while the North Atlantic is experiencing a cooling trend. This was recently studied by Robson et al. (2016) who analyzed Sea Surface Temperature, 0-700m temperature and salinity trends over the 1990-2004 vs 2005-2014 period. They found that the NA has warmed before 2004, but has clearly experienced a cooling (of about 0.45degC) over the most recent decade. Using specific model simulations, they suggest that this reversal could be driven by changes in the ocean circulation and most notably a slow down of the North Atlantic Current and its associated heat transport. This in fact, corroborates previous findings about a Meridional Overturning Circulation decadal slow down in the North Atlantic (Smeed et al., 2014) which is linked to density anomalies emanating from the Labrador Sea and propagating southward (Jackson et al., 2016).

Overall, the last decade NA cooling trend remains poorly documented in terms of its vertical structure and associated circulation changes over the subtropical gyre (especially along the GSE) while it is not clear if such an "event" has already occurred over the historical record. This lack of diagnostics and historical context impede our understanding of recent changes whereas the NA recent cooling is a prominent change that has implications for the Earth Energy balance and Global Ocean Heat Content estimates. The main goal of my LEFE/SOMOVAR project (2017-2019) was thus to objectively understand the 2000-2015 decadal change in the NATL subtropical gyre structure. Key results are presented in this chapter and published in (Stevens et al.,

Product	Data assimilation method	Period covered
ISAS (15) + NRT	OI (T/S)	2002/01 - 2018/12
CORA (5.2)	OI (T/S)	1990/01 - 2018/12
RGCLIM	OI (T/S)	2004/01 - 2015/12
EN4 (4.2.1.G10)	OI (T/S)	1958/01 - 2019/04
ARMORD3D	OI (SLA/MDT/T/S/SST)	1993/01 - 2014/12
ORAS4	3DVAR (SLA/T/S/SST)	1958/01 - 2017/12
ESTOCv02c	4DVAR (SLA/T/S/SST)	1957/01 - 2011/12
ECCOv4 (r2)	4DVAR (SLA/SSH/T/S/SST)	1992/01 - 2011/12
ORCA025L75GJM189	No DA	1958/01 - 2015/12

Table 5.1: Ocean product analysis and re-analysis used to study the EDW low-frequency variability.

acc., 2020; Maze et al., 2019a,b) and (Lee, 2020). After a brief description of the data and method, I will highlight results showing: unprecedented pentadal recent changes in [section 5](#) and interannual extremes in [section 5](#).

Data and method

I studied the interannual variability of the EDW with observations from the Argo array, the BATS time series, and furthermore using ocean analysis and re-analysis ensembles to capture the robust multi-decadal signal and extreme occurrences. I adopted a multi-definition, multi-product approach to focus on the robustness of the signals found. In results described here after, I used ocean products listed in [Table 5.1](#). For each EDW property to be studied, the time series is diagnosed in all products, and for each products several EDW definitions are tested. Results are presented with all diagnostics super-imposed or as a multi-product average/spread. In [section 2](#) I already discussed the role of the EDW definitions onto its characterization, and in [Forget et al. \(2011\)](#) I described the impact of the EDW definition onto its volume estimate. Using several definitions is a requirement to grab the sensitivity and robustness of the signals possibly observed.

All time series were decomposed using a standard "additive" method, whereby the full time series is split like:

$$C = C^{tr} + C^{sc} + C^{lf} + C^{hf} \quad (5.1)$$

where C^{tr} is a linear trend, C^{sc} the seasonal cycle, C^{lf} a low-frequency and C^{hf} a high frequency signal. We first compute the linear trend (using a linear regression analysis), then we compute a typical seasonal cycle from $C - C^{tr}$. Last, we use a moving average to split $C - C^{tr} - C^{sc}$ into a low and a high frequency signal. For a moving average of size n months, we note the smoothed (low-frequency) component as $C^{lf} = [C - C^{tr} - C^{sc}]_n$ and therefore the remaining higher-frequency component is given by $C^{hf} = C - C^{tr} - C^{sc} - C^{lf}$.

For the decadal signal we used a moving average window of $n = 36$ months, i.e. 3 years size, and to account for the interesting multi-decadal component, the decadal time series will refer to:

$$C_{dc}^{lf} = C^{tr} + [C - C^{tr} - C^{sc}]_{36} \quad (5.2)$$

For the interannual signal we used a band pass filtering approach (still based on a simple moving average). In [Lee \(2020\)](#) we analyzed the 6-30 month interannual signal computed as:

$$C_{ia}^{lf} = [C - [C - C^{tr} - C^{sc}]_{30}]_6 \quad (5.3)$$

Results

Unprecedented pentadal recent changes

Here I describe recent EDW properties changes with regard to the multi-decadal variability record. Basically, one can show that the EDW has warmed, thinned and stratified since 2010, and with unprecedented levels

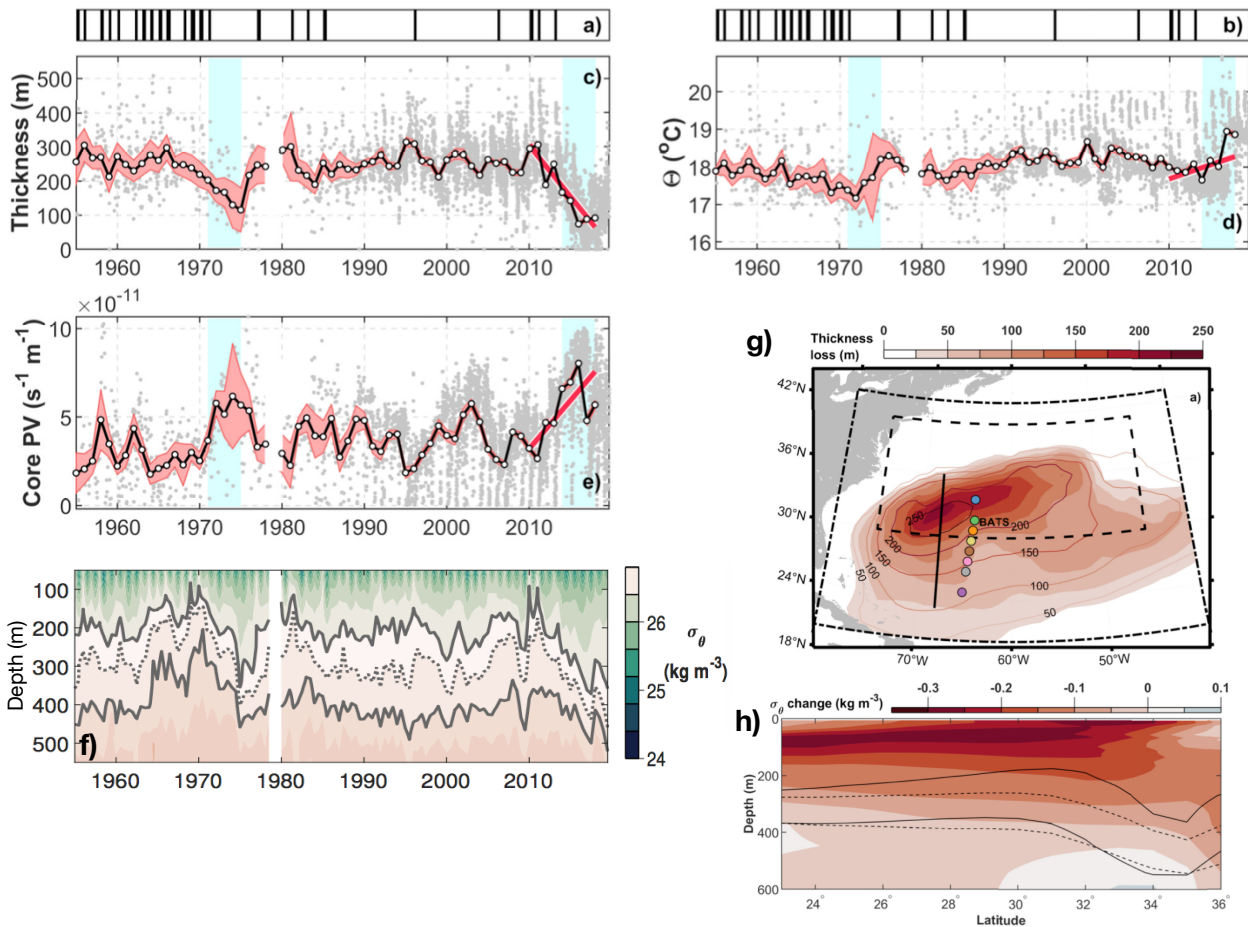


Figure 5.1: Signal of multi-decadal variability of the EDW. Vertical lines in (a and b) indicate periods when EDW outcropping occurred at BATS/Hydrostation S. Time series of EDW thickness (c), temperature (d) and potential vorticity (e) and potential density profiles (f) for the BATS time series. Map (g) and section (h) shows the EDW thickness reduction over 2014-2018 (inclusive) compared to the mean thickness before 2014 and isopycnal migrations (solid: before, dashed: after 2014). Plots (a-b-c-d-e-f) based on BATS data and (g-h) on EN4 dataset. Figures reproduced from [Stevens et al. \(acc., 2020\)](#).

over 2014-2018 compared to the historical records (back to 1950). This extreme pentad, takes place on a significant multi-decadal linear warming trend (for the EDW core) of about $0.84 \pm 0.21^{\circ}\text{C}/\text{century}$. This last estimate is in line with [Sugimoto et al. \(2017\)](#) study who also reported from observations a subtropical mode water warming over the nearly 70 years (1947-2014) in the North Pacific and North Atlantic of $1.31 \pm 0.14^{\circ}\text{C}/\text{century}$.

These results were recently presented in conferences ([Maze et al., 2019a,b](#)) and are part of an article just accepted for publication in *Nature Climate Change* ([Stevens et al., acc., 2020](#)). The 1958-2018 multi-decadal time series of EDW properties are shown in [Figure 5.1](#) for the BATS time series. One can see how the EDW layer thickness has dramatically reduced since 2010 and is currently reaching an historical minimum, with a average thickness smaller than 100m to be compared to an all-time average of about 219m. The core EDW layer has furthermore warmed and stratified (PV increased), reaching extreme values over the 2014-2018 pentad (highlighted with blue strips on figure).

Such a signal is not limited to the BATS time series at Bermuda. When analyzing ocean re-analysis covering this long period (ORAS4 and EN4), and more recent dataset mostly based on Argo analysis, one can note the robustness of the signal. This is illustrated [Figure 4](#) in [Stevens et al. \(acc., 2020\)](#) where the EDW

properties of most ocean dataset are superimposed. I furthermore have shown that the signal is robust to several EDW definitions.

The ocean re-analysis EN4 is used [Figure 5.1](#), plots (g) and (h) to show the spatial extent of the 2014-2018 signal in the horizontal and vertical plans. One can see from map (g) that the EDW has seen its thickness mostly eroded over the western region that hosts the thickest and warmest flavor of EDW ([Feucher et al., 2016b, 2019](#)). But one can note that the EDW erosion is affecting the entire reservoir. [Figure 5.1-h](#) shows changes in potential density (color shading) and isopycnal depths. See how the upper ocean has increased buoyancy and isopycnal deepens. One conclusion of this work was that heaving is a key driver of interannual EDW layer variability and that it is coherent with wind-driven changes of the subtropical gyre. This is true on different time scales, especially interannual as I shall detail in the next section.

It is worth noting that the 2014-2018 most recent period shows EDW changes in temperature that are of opposite sign compared to the earlier 2002-2014 period detailed in [Maze et al. \(2019a,b\)](#) and furthermore analyzed by [Kolodziejczyk et al. \(2019\)](#). Over the 2002-2014 period, the EDW tended to cool, further decreasing the EDW layer heat content along a reduced thickness trend.

Contribution highlight I have shown that recent EDW changes (2014-2018) are multi-decadal extremes in a sense that they only have been seen once since 1950 (over the 1971-1975 period). Our study finds an approximate 90% loss of EDW thickness at BATS over 2010-2018 and a comparable loss all over the western subtropical gyre. This ultimately leads to the weakest EDW pentad on record.

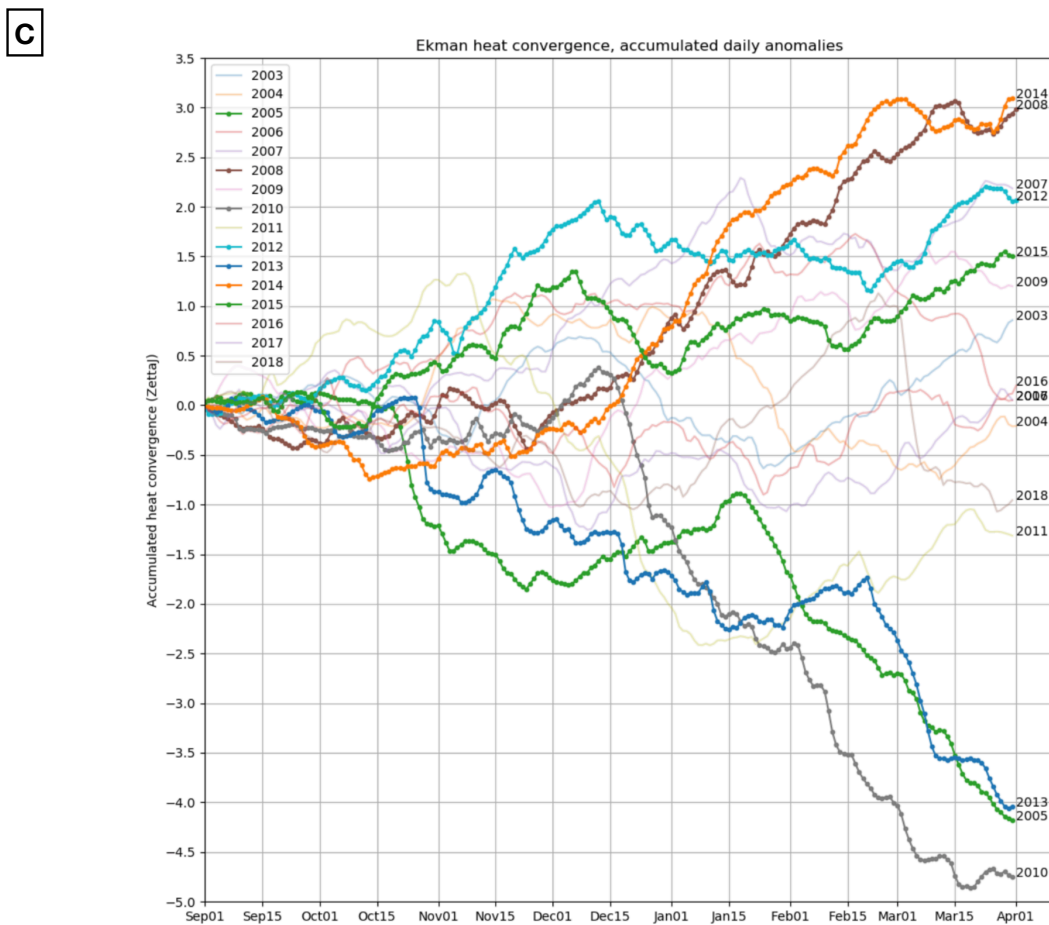
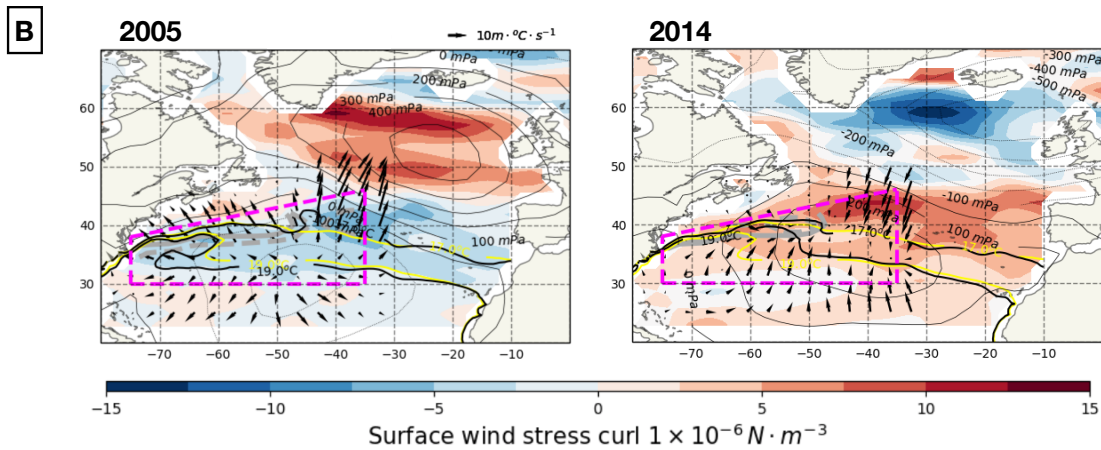
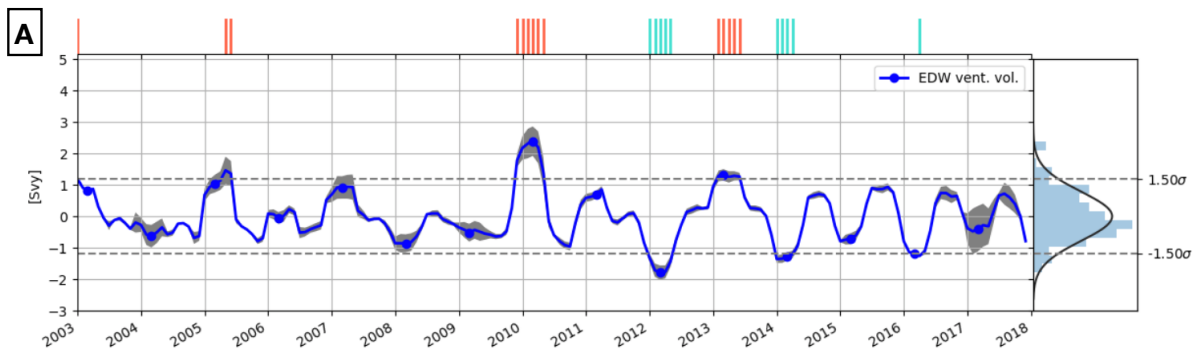
My studies also showed that changes observed at BATS and ocean re-analysis are consistent with changes in the EDW formation area and indicative of a northward migration and warming of the newly formed EDW area and flavor ([Stevens et al., acc., 2020](#); [Maze et al., 2019a,b](#)). However, I haven't yet conducted a surface water mass transformation analysis, using the Walin framework described at length in [chapter 4](#), to further investigate low-frequency changes in surface water-mass transformations. This is left to further studies.

Interannual extremes

My PhD student Kenneth Lee work was about the description and understanding of extreme occurrences in EDW interannual variability signals. Together with Herlé Mercier, I co-supervised this work between February 2017 and 2020. I obviously can't describe here all the work that has been done by Kenneth over these 3 years and articles are still being prepared. The main findings are the following.

[Figure 5.2-A](#) shows the interannual time series of the EDW ventilated volume. In [Lee \(2020\)](#) work, we focused on the EDW volume within the mixed layer, i.e. "ventilated", in order to get a closer look at the EDW fraction in direct contact with the atmospheric forcing. The interannual variability amplitude is typically of

Figure 5.2 (following page): Plot A: Interannual variability of the EDW ventilated volume (ensemble mean and std of ISAS, EN4, IPRC, and Scripps ocean states). To the right is shown the histogram of values and a Gaussian fit used to set a $1.5 \pm 1std$ threshold for extreme detection. The upper green/orange tick marks highlight months when the EDW ventilated volume is below/above the extreme threshold. Plot B: North Atlantic oceanic and atmospheric conditions for the 2005 (left) and 2014 (right) winters. For the atmosphere: color shading is the surface wind-stress curl anomaly, thick grey lines near the Gulf Stream Extension are the zero wind-stress curl line (plain is the climatological mean position, dashed grey for the given winters) and thin black contours are the Sea Level Pressure anomalies. For the ocean: thick black and yellow contours are the 17 and 19°C SST outcrops (black is for the given winters, yellow is the climatological position) and black arrows indicate lateral Ekman heat transports (only for grid points over the analyzed domain denoted by the dashed magenta box). Plot C: September to March daily accumulation of Ekman heat transport convergence over the western North Atlantic gyre, for each winters of 2003-2018. Thick lines highlight extreme EDW ventilation years.



0.8Sv amplitude (i.e. $1std$). From this time series stands out 2 particularly large events: the winter of 2010 and 2012 during which the EDW ventilated volumes were particularly large and small, respectively. If we look at the occurrence of extreme events, defined as months exceeding the $1.5 \pm 1std$ amplitude threshold, we found positive extremes in the winters 2005, 2010 and 2013, and negative extremes in winters 2012, 2014 and 2016. This is a clear new result better characterizing the interannual variability of the EDW, since only the 2010 and 2012 extreme winters were already documented in the bibliography (Bryden et al., 2014; Billheimer and Talley, 2013). Note that the harsh winter 2014 enhanced convection in the eastern subpolar gyre but nothing was yet reported w.r.t. the EDW this particular winter (Grist et al., 2015).

In order to better understand the driving mechanisms of these extreme events, we furthermore derived an observation-based ocean heat content (OHC) budget for the upper 800m of the GSE and northern Sargasso Sea region (magenta dash box Fig. 5.2-B). The OHC rate of change was decomposed into its major driving forces: geostrophic and lateral Ekman heat transports, air-sea heat fluxes and mixing. We determined that the Ekman transport convergence over the domain is a key factor leading to extreme OHC changes over the EDW ventilation season (September-March).

To illustrate the link between Ekman and EDW ventilation, see Figure 5.2-B where the map of wind-stress curl and Ekman transport anomalies for the representative 2005 and 2014 extreme winters are shown. During winter 2005, a negative wind-stress curl anomaly (blue color shading) occupies the domain of analysis, which encompasses the EDW main outcropping area (yellow contours). This negative anomaly is driven by a divergence of lateral Ekman heat transports (black arrows) that promotes a wider EDW outcropping area: see how the 17 and 19°C surface isotherms of 2005 (black contours) define a larger outcrop than the climatological one (yellow contours). On the other hand, during winter 2014 the situation is reversed. A positive wind-stress curl anomaly driven by a convergence of lateral Ekman heat transports ultimately promotes a smaller EDW outcropping area.

Even if the extremely strong ventilation of EDW during the 2005, 2010 and 2013 winters correspond to extreme Ekman transport divergence, it may happen that extreme Ekman convergence (2007 and 2008) do not lead to extremely poor EDW ventilation. This can be seen Figure 5.2-C showing the September to March daily accumulation of Ekman transports. It is also worth noticing that years with extreme winter time OHC changes were not necessarily corresponding to EDW extreme ventilation years, despite Dong and Kelly (2004) statement that OHC and EDW volume are anti-correlated. For instance, 2008 and 2017 are negative extremes for OHC, but not for EDW.

Contribution highlight This work shows that a recipe for EDW extremes, and for OHC, cannot be determined easily and that an event-based comprehension is always necessary. That being said, given the few number of occurrences (by definition of an extreme) in the time series analyzed during Kenneth Lee PhD, it is a remarkable result that we could highlight the role played by Ekman transports, over the last 15 years at least.

Another contribution from Kenneth Lee PhD work was to bridge the amplitude of interannual variability with winter weather events. Figure 5.2-C illustrates how the daily accumulation of weather events over a given winter builds up to an interannual anomaly. This figure shows that both storm duration and amplitude are important to lead an extreme year, with regard to Ekman heat transport convergence over the domain.

Final remarks

From Stevens et al. (acc., 2020); Maze et al. (2019a,b) work, it is clear that EDW multi-decadal trends seat on top of large pentadal to decadal variability. The observed multi-decadal trend of surface warming enhances the surface water stratification and stabilizes the EDW layer. This has 2 consequences: enhanced erosion of the mode water from the top (Billheimer and Talley, 2016, see for instance) and enhanced partitioning of the energy throughout the upper ocean. The former raises the question of the long term existence of the EDW, the later has strong implication with regard to the ocean's heat and CO₂ uptake capacity.

On the higher frequency part of the variability slower than the seasonal cycle, [Lee \(2020\)](#) work has refined the respective role of the geostrophic advection compared to Ekman and air-sea heat fluxes. The Gulf Stream variability dominates around the 18 months period ([Lillibridge III and Mariano, 2012](#)) but Ekman takes over, or at least plays a comparable role, on lower frequencies. This is in line with recent analysis showing that Ekman processes are a key driver in adiabatic changes of the subtropical gyre ([Evans et al., 2017](#), e.g.).

Anomalies observed since 2002, thanks to the Argo array, are due to extreme wintertime weather regimes, either in the strength of each individual events or on average throughout the winter. These anomalies are of paramount importance for climate because of the re-emergence process ([Alexander and Deser, 1995](#)). Re-emergence is the process by which a wintertime temperature anomaly is preserved below the mixed layer in summer and re-appears at the surface in the following fall, possibly modulating the atmosphere. For instance the winter 2010-2011 was marked by a early winter NAO-, which may have been influenced by the re-emergence of the sub-surface temperature anomalies subducted during the harsh precedent 2009-2010 record-low NAO- winter ([Cassou et al, 2007](#), [Taws et al, 2011](#)). [Hanawa and Sugimoto \(2004\)](#) have shown that anomalies re-emergence occur in the sites of subtropical mode water formation. Lagrangian particle analysis confirm that water parcels of subtropical mode waters mostly re-emerge after 1 year in the same area they have been subducted below the mixed layer at the time of their ventilation ([Kwon et al., 2015](#); [Grist et al., 2015](#)). It will be of great interest to keep on studying the interannual extreme events described in this chapter in the light of the their long term impact on the ocean interior.



6. Ventilation of the subtropical Gyre

Contribution highlight My key contributions to a better understanding of the Subtropical North Atlantic gyre ventilation are:

- a time mean oxygen budget for the Northeastern part of the basin ([Maze et al., 2012](#)),
- a better localization of EDW ventilation sites and circulation pathways ([Maze et al., 2009](#); [Maze and Marshall, 2011](#)),
- the determination of the respective role of adiabatic vs diabatic processes in the ventilation process of the EDW ([Maze and Marshall, 2011](#)),
- the quantification of the mesoscales contribution to the EDW ventilation process ([Maze et al., 2013](#)).

Content of this chapter:

Introduction	66
PV fluxes: a dynamical framework to study ocean ventilation	67
Flux form of the PV conservation equation	67
Thermocline structure model	68
EDW ventilation pathways	69
EDW ventilation drivers: partitioning surface PV fluxes	71
Final remarks	73

Introduction

The water mass transformation principles developed at length in the previous [chapter 4](#) allows to determine what are the driving mechanisms of the EDW volume fluctuations when the EDW layer is defined using temperature or density ranges. However, water mass transformation principles cannot easily distinguish the miscellaneous part of the EDW, for instance: the part that is confined to the seasonal thermocline in the northern region of the basin, the part that is freshly formed through convective mixing south of the Gulf Stream or the part that reaches the permanent pycnocline deep in the southwestern region of the subtropical gyre. To distinguish these EDW components, stratification is a key property, and to furthermore understand the dynamic, potential vorticity (PV) is the reference property.

A water mass stratification, and more precisely PV, can be seen as an indicator of its "age", i.e. the time since it was in last contact with the atmosphere. A young water mass (age=0) is not or is poorly stratified because when in contact with the atmosphere it is vertically mixed and loses older properties. It is also saturated with oxygen and acquire other gases like carbon dioxide. Thus in contact with the atmosphere, a water mass simply acquires its initial and defining properties (*birth*). These properties will only be diluted once the water mass is subducted in the ocean interior and will mix with surrounding waters along its circulation pathways (*aging*). When the stratification level cannot be distinguished from other layers, the water mass no longer exists. This does not mean that water parcels that have been part of the water mass cannot be tracked any longer, they can, by use of other tracers such as CFCs, 3H or 3He (e.g. [Jenkins, 1987](#)). I think about this water mass life cycle as the key ocean ventilation process. Note that many subtleties with regard to water mass *age* vs water mass *analysis* exist but are beyond the scope of this manuscript and are left to be discussed by others elsewhere (see for instance [Tomczak, 1999](#); [Haine and Hall, 2002](#)).

Ocean ventilation thus describes how ocean *breathes*, and this concept is naturally associated with the distribution and fluctuation of oxygen concentrations. Since the ocean gains oxygen only at the surface through air-sea fluxes and organic matter respiration/photosynthesis: once a water mass is no longer in contact with the atmosphere and the euphotic layer, oxygen concentrations can only decrease. The rate of decrease (the *oxygen utilization rate*) depends on the oxydation rate of the organic matter (remineralization) and mixing rate with surrounding waters. Even though these rates are local in nature and complex to quantify, maps of oxygen concentration (or utilization rate) at fixed depth or on isopycnal layers have been used qualitatively for decades to infer water mass circulation pathways and their "age" ([Sverdrup et al., 1942](#)).

In this section I will describe how EDW is ventilated, i.e. how the isopycnal layer defining EDW can lose or gain PV (stratification) along its circulation pathways. EDW stratification reduction is associated with EDW formation/creation and stratification increase is associated with EDW destruction. EDW formation is fundamentally associated with convection and the reduction of the stratification at the sea surface. In [Maze and Marshall \(2011\)](#) and [Maze et al. \(2013\)](#) I used an approach more dynamical than the thermodynamic framework of Walin to study this EDW formation process. This approach is naturally based on PV. In the following, I'll explain how to draw a very synthetic and pragmatic derivation of equations and formulas allowing for the computation of PV flux at the ocean's surface and how they can reduce the stratification.

Contribution highlight This is not developed in this chapter but I studied oxygen in [Maze et al. \(2012\)](#). I conducted a surface to bottom northeast Atlantic Ocean budget for mass, nutrients (nitrate and phosphate) and oxygen using an optimization method based on three surveys of the OVIDE transect (from Greenland to Portugal) completed with the World Ocean Atlas 2009. I determined that the region between the OVIDE survey and the Greenland–Scotland Ridge is autotrophic and is a net organic matter production region. I furthermore decomposed the air–sea oxygen flux between its abiotic and biological components. This air–sea oxygen flux partitioning shows that the still poorly studied abiotic mixing flux component can have a very significant impact on air–sea oxygen fluxes in the presence of a strong thermocline oxygen minimum. This latter result may have implications in determining the ocean and land sinks of the atmospheric anthropic carbon with methods based on net air–sea oxygen flux estimates from the thermal

component only.

PV fluxes: a dynamical framework to study ocean ventilation

First I'd like to explain this framework as a "dynamical" one. Stratification, i.e. the local vertical density gradient, is useful to map a water mass but is not a conserved quantity along the propagation of a water parcel. Thus in order to study how EDW is losing stratification at the surface and then how it propagates within the ocean interior, its dynamic, we need a tracer that captures the stratification information and that is conserved along circulation pathways. This is the potential vorticity.

Potential vorticity conservation is usually stated from a Lagrangian perspective like $\frac{DQ}{Dt} = \text{sources} - \text{sinks}$, so that in the absence of sources and sinks a water parcel PV is conserved following that parcel. Here after I will (briefly) present an alternative form of the PV conservation, the so-called "flux-form" because it is particularly suited for mode water studies. This framework is based on work from [Haynes and McIntyre \(1987\)](#), [Marshall and Nurser \(1992\)](#), [Schär \(1993\)](#) and [Marshall et al. \(2001\)](#) who wrote down the theoretical details of the key results and equations presented here.

Flux form of the PV conservation equation

The conservative flux form of the potential vorticity equation is:

$$\frac{\partial \rho Q}{\partial t} = -\nabla \cdot \mathbf{J} \quad (6.1)$$

where the Ertel potential vorticity Q is given by:

$$Q = -\frac{1}{\rho} \omega_a \cdot \nabla \sigma_\theta \left\{ \frac{1}{\text{m.s}} \right\} \quad (6.2)$$

using absolute vorticity $\omega_a = 2\Omega + \nabla \times \mathbf{u}$, and potential density $\sigma_\theta = \sigma(\theta, S, p = 0)$ (later simply noted σ).

Two equivalent formulations for the PV flux vector can be derived.

Formulation A

$$\mathbf{J} = \underbrace{\rho Q \mathbf{u}}_{\text{Advection}} + \underbrace{\omega_a \frac{D\sigma}{Dt}}_{\text{Buoyancy}} + \underbrace{\mathbf{F} \times \nabla \sigma}_{\text{Friction}} \left\{ \frac{\text{kg}}{\text{m}^3 \cdot \text{s}^2} \right\} \quad (6.3)$$

In this first formulation, \mathbf{F} is the viscous body force per unit mass from the Boussinesq momentum equation:

$$\mathbf{F} = \frac{D\mathbf{u}}{Dt} + 2\Omega \times \mathbf{u} + \nabla p \left\{ \frac{\text{m}}{\text{s}^2} \right\} \quad (6.4)$$

where p is the deviation of the pressure from that of a resting, hydrostatically balanced ocean. Note that we omitted one last r.h.s. term in Eq.(6.3) due to pressure-dependent effects in the equation of state, or non-advective thermobaric effects. [Marshall et al. \(2001\)](#) and later [Deremble et al. \(2013\)](#) have shown that it can be neglected in our EDW context, although it plays an important role in setting the PV circulation in the deeper isopycnals of the subtropical gyre.

With this first formulation each of the terms are clearly associated with fundamental processes: advection, buoyancy and frictional fluxes. However, this formulation does not provide an easy way to compute PV fluxes in the interior although it is useful at the surface because observations are available to compute each of the terms. This is the formulation used by [Czaja and Hausmann \(2009\)](#) to precisely map sea surface PV fluxes, globally, from observations.

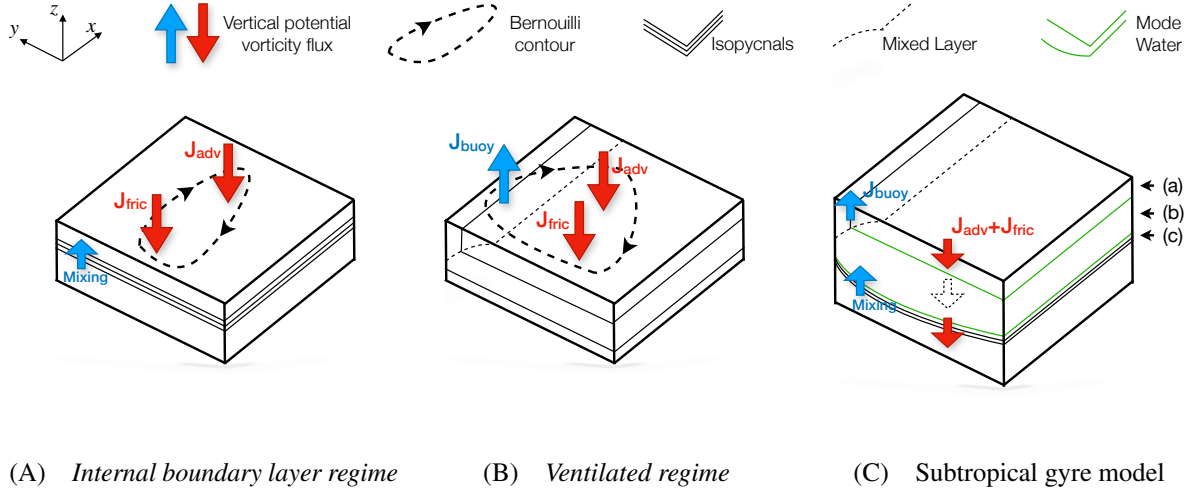


Figure 6.1: Simple model for the subtropical thermocline structure from Marshall (2000) based on the integral PV flux constraint Eq.(6.8)

Formulation B

$$\mathbf{J} = \omega_a \frac{\partial \sigma}{\partial t} + \left(\frac{\partial \mathbf{u}}{\partial t} + \nabla \pi \right) \times \nabla \sigma \quad (6.5)$$

In this second formulation, π is the Bernoulli potential given by:

$$\pi = \frac{|\mathbf{u}|^2}{2} + \frac{p}{\rho_o} + \frac{\rho'}{\rho_o} \Phi \quad (6.6)$$

where Φ is the geopotential.

This formulation is particularly interesting because it reveals the *impermeability* theorem stating that the mass-weighted PV of an isopycnal layer can only be changed through PV fluxes where the layer intersects a boundary. Indeed, since:

- the first r.h.s. term in Eq.(6.5), when projected in the direction normal to the σ surface, is equal to $\rho Q v_\sigma$ with v_σ the isopycnal surface velocity normal to itself (given by $-\left| \nabla \sigma \right|^{-1} \frac{\partial \sigma}{\partial t}$),
- and the second r.h.s. term is always parallel to the σ surface,

the PV flux follows the isopycnal surface but cannot cross it.

This second formulation furthermore layout an interesting information about the steady state: Bernoulli contours on isopycnal surfaces are streamline of PV fluxes. In this case, the PV flux vector nails down to:

$$\mathbf{J} = \nabla \pi \times \nabla \sigma \quad (6.7)$$

In other words, PV flux vector lies on the intersection of surfaces of constant density and surfaces of constant Bernoulli potential. A simple consequence of this formulation is that when integrated over an area \mathcal{A} of enclosed Bernoulli or density contours, it goes to zero:

$$\int_{\mathcal{A}} \mathbf{J} \cdot d\mathcal{A} = 0 \quad (6.8)$$

Thermocline structure model

The integral constraint Eq.(6.8) was used by Marshall (2000) to provide an elegant explanation for the subtropical thermocline structure that is illustrated Figure 6.1. In the ocean interior (Figure 6.1A), both

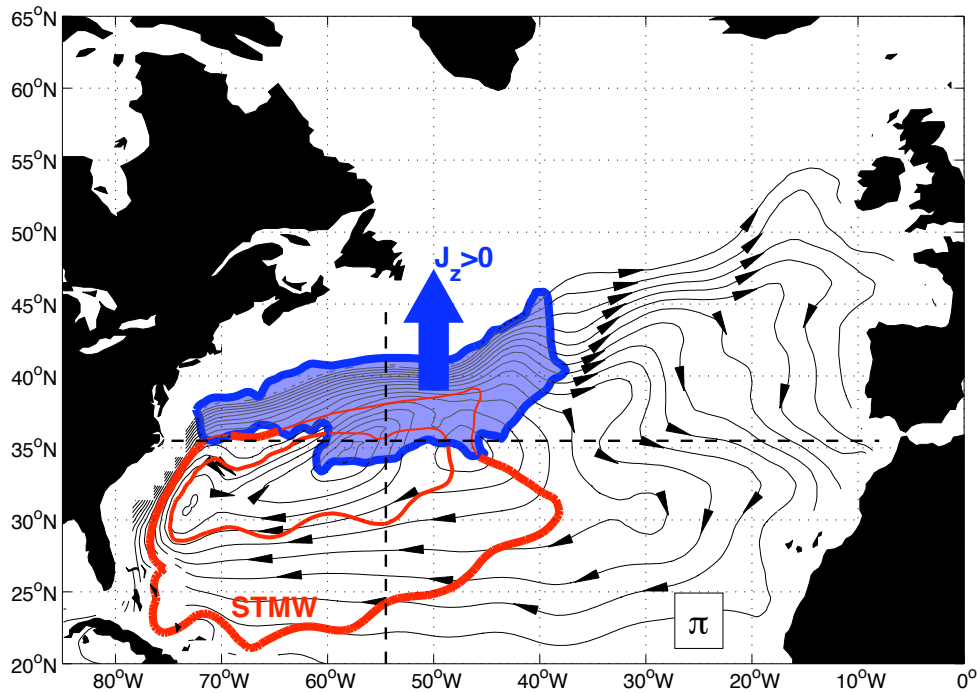


Figure 6.2: Figure 9 from [Maze and Marshall \(2011\)](#). The blue area is the dominant positive vertical PV flux area ($\mathcal{J}_z(x, y, z = 100m) = 0.45 \text{ [kg.m}^{-3} \cdot \text{s}^{-2}]$). Black contours with arrows indicate mean PV flux streamlines (2004-2006 time mean Bernoulli contours on the $\sigma_{EDW} = 26.4 \text{ [kg.m}^{-3}]$ isopycnal). Red contours indicates the poorly stratified subset of EDW (two PV contours of $Q = [0.6; 1.5] \times 10^{-10} \text{ [m}^{-1} \text{s}^{-1}]$ on σ_{EDW}).

advective (driven by negative Ekman pumping) and frictional (friction opposes the anticyclonic circulation and density gradient is outward from the gyre center) PV fluxes are negative. This injects PV downward the base of the subtropical gyre where it accumulates within an internal thermocline. This PV accumulation is limited by diapycnal mixing. This leads to an internal boundary layer reminiscent of the permanent pycnocline ([Luyten et al., 1983](#); [Salmon, 1990](#)). Near the surface ([Figure 6.1B](#)), Bernoulli contours intersect the mixed layer where air-sea buoyancy fluxes trigger convection that leads to PV removal (upward PV flux, see next section). This allows to balance PV injection by advection and friction. Last, one can superimpose the *internal boundary layer regime* with this *ventilated regime* to depict the subtropical gyre structure ([Figure 6.1C](#)). Layers (a) and (c) are the *ventilated* and *internal boundary layer* regimes described above and layer (b) is an intermediate *mode water* regime where all PV fluxes tend to vanish (dashed arrow) and density is constant. This elegant approach is compatible and coherent with the two-thermocline limit found by [Samelson and Vallis \(1997\)](#).

Last, one should note that the contribution of eddies to this simple model is complex to assess, although it was discussed in [Marshall \(2000\)](#) by mean of a bolus velocity term ([Gent et al., 1995](#)). Baroclinic instability found in regions of slumping isopycnals can provide an additional vertical PV flux to be accounted for in [Eq.\(6.3\)](#) and [Eq.\(6.5\)](#). As illustrated in figure 7 in [Marshall \(2000\)](#), on the warm side of the front, eddies will tend to raise isopycnals, thus fluxing PV upward. On the cold side of the front, the opposite goes on. [Radko and Marshall \(2004a,b\)](#) furthermore showed that this cross-layer eddy buoyancy transfer dominate the mixing term that must balance downward frictional and Ekman-driven advective PV fluxes.

EDW ventilation pathways

In [Maze and Marshall \(2011\)](#) I've showed the monthly evolution of the PV distribution on the EDW isopycnal surface together with Bernoulli contours. A simplified view of this analysis is shown [Figure 6.2](#). The EDW

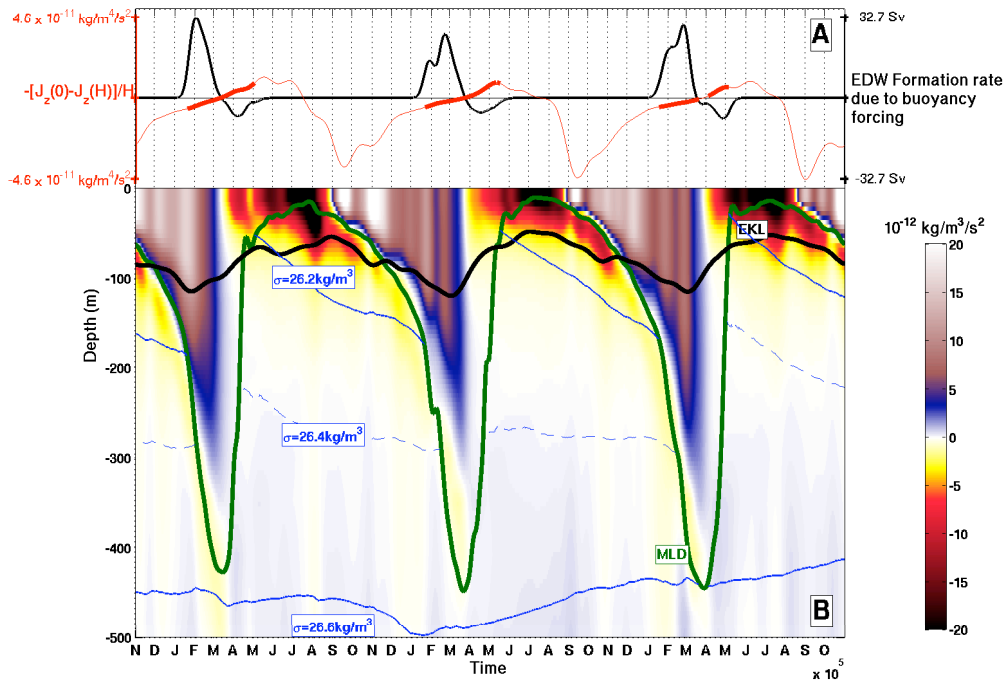


Figure 6.3: Figure 6 from [Maze and Marshall \(2011\)](#). Panel (A): The thick black line is the 2004-2006 daily EDW formation rate due to surface buoyancy forcing for which the maximum amplitude is indicated in Sv on the black scale to the right. The red line is the 2004-2006 daily vertical PV flux divergence over the mixed layer: $-(J_z^0 - J_z^H)H^{-1}$ with H the mixed layer depth and for which the maximum amplitude is indicated in $[\text{kg} \cdot \text{m}^{-4} \cdot \text{s}^{-2}]$ to the right. The thick red portion of the curve highlights days when the mixed layer density is in the range of EDW. Panel (B): The 2004-2006 daily time series of the vertical PV flux: $J_z = f\partial_t\sigma + \mathbf{k} \cdot \nabla\pi \times \nabla\sigma$ between -500m and the sea surface, averaged over the EDW core formation region. The units are $[10^{-12} \text{ kg} \cdot \text{m}^{-3} \cdot \text{s}^{-2}]$ with a color scale located to the right of the panel. The thick green (black) line is the box-averaged mixed (Ekman) layer depth. Blue lines indicate the isopycnal depth averaged over the box: thick lines: $\sigma = [26.2, 26.6] [\text{kg} \cdot \text{m}^{-3}]$ and thin dashed $\sigma = 26.4 [\text{kg} \cdot \text{m}^{-3}]$.

low PV reservoir is indicated by red contours. We see that the Gulf Stream Extension and part of its eastern recirculation gyre is an area of PV removal (blue region). We furthermore see that Bernoulli contours on this isopycnal surface can connect directly to the EDW reservoir (from 45W to 60W) or through a longer journey on the eastern side of the gyre. These contours indicate ventilation pathways of the EDW and part of the subtropical gyre.

One should note however, that this time mean picture hides the key role of the seasonal cycle in the PV extraction process out of the EDW layer. This role is highlighted [Figure 6.3](#) which shows an OCCA-based 2004-2006 daily time series of the time/depth vertical PV flux structure over the EDW formation region, along with the time series of the vertical PV flux divergence over the mixed layer. We can clearly see how the PV divergence from September to the end of March leads to a PV reduction of the mixed layer that come together with its deepening. From April to August PV converges and the mixed layer shoals.

Contribution highlight Using Eq.(6.3), I was able to diagnose and to show a modern perspective of the seasonal ventilation and circulation pathways of the EDW core. In particular, by drawing π contours on σ surfaces, I've shown that the core of the Gulf Stream, its entire warm tongue, is a key region where EDW, and a large part of the upper subtropical gyre, see its PV reduced seasonally.

EDW ventilation drivers: partitioning surface PV fluxes

In the framework of an EDW ventilation study and because EDW is characterized by low PV, we're particularly interested by how PV can be reduced. In [Figure 3.3](#) I already illustrated my contribution to a better description of the EDW seasonal cycle with PV. Note how from December to June (plot [Fig.3.3-A](#) and [Fig.3.3-C](#)), the EDW core sees its PV level dramatically reduced.

An isopycnal layer will see its PV reduced at the surface mainly because of convective mixing. Projecting the full PV flux formulations [Eqs.\(6.3\)-\(6.5\)](#) onto the vertical axis at the surface is not a straightforward computation but details of such derivation are beyond the scope of this study. The vertical PV flux at the sea surface is given by:

$$\mathbf{N}_{Q_z} = J_z^B + J_z^F \quad (6.9)$$

$$J_z^B = \frac{f}{h} \mathcal{B}_{in} = \frac{f}{h} \left(\frac{\alpha Q_{net}}{C_p} + \rho_0 \beta S(E - P) \right) \quad (6.10)$$

$$J_z^F = \frac{1}{\rho \delta_e} \mathbf{k} \times \boldsymbol{\tau} \cdot \nabla \sigma_m \quad (6.11)$$

where \mathbf{N}_{Q_z} is the non-advective component the total PV flux \mathbf{J} , and J_z^B is a buoyancy driven flux and J_z^F a frictional flux. We recall the explicit formulation of the surface density flux \mathcal{B}_{in} already introduced in [Eq.\(4.16\)](#) and scaled here by the mixed layer depth h . δ_e is the Ekman layer depth, $\boldsymbol{\tau}$ the wind stress and σ_m the mixed layer potential density.

Contribution highlight In [Maze and Marshall \(2011\)](#) I introduced a procedure to map surface vertical PV fluxes influencing a given water mass. This is possible if terms from [Eqs.\(6.10\)-\(6.11\)](#), or any other 2-dimensional projection of [Eqs.\(6.3\)-\(6.5\)](#), are masked and then accumulated for a specific isopycnal layer.

I then furthermore define:

$$\mathcal{J}_z(X_i, z) = \int_{X_j} J_z(t, x, y, z) \mathcal{H}_h^z(t, x, y) dX_j \quad (6.12)$$

where (t, x, y, z) are the time, zonal, meridional and vertical axes. A spatial average is obtained by setting $X_i = t$ and $X_j = (x, y)$; a temporal average by setting $X_i = (x, y)$ and $X_j = t$. The outcrop mapping function \mathcal{H}_h^z is given by:

$$\mathcal{H}_h^z(t, x, y) = \begin{cases} 1 & \text{if } \begin{cases} \sigma_{EDW} - \frac{\delta\sigma}{2} < \sigma(z) \\ \sigma(z=h) \leq \sigma_{EDW} + \frac{\delta\sigma}{2} \\ h \leq z \end{cases} \\ 0 & \text{otherwise} \end{cases} \quad (6.13)$$

where h stands for mixed layer depth. This is a binary function which has a value of unity when the potential density at depth z is in the EDW outcrop range $\sigma_{EDW} \pm \delta\sigma$ (and has thus been penetrated by the mixed layer) and zero otherwise. The mixed layer depth criterion ensures that the mapping is restricted to times when the outcrop at depth z is in direct contact with the atmosphere and thus remains a surface outcropping region. At the surface ($z = 0$), the function \mathcal{H}_h^0 reduces to the EDW surface outcrop region.

Let's now see how EDW PV can be reduced at the sea surface.

Diabatic processes

In order to better understand how surface diabatic fluxes can drive EDW ventilation, let's take the PV flux due to the surface buoyancy forcing from [Eq.\(6.10\)](#) and simplify it as:

$$J_z^B \simeq \frac{\alpha f}{h C_p} Q_{net} \quad (6.14)$$

When the net surface heat flux Q_{net} is upward i.e. positive and cooling the ocean (buoyancy loss), surface density increases and convective mixing is triggered. This corresponds to a positive/upward PV flux at the surface, hence a PV flux divergence over the mixed layer and thus a PV reduction (see Eq.(6.1)). This is consistent with a reduction of stratification due to mixing:

$$\begin{aligned}
 Q_{net} &> 0 \text{ (upward, cooling)} \\
 J_z^B &> 0 \text{ (upward)} \\
 -\rho^{-1}\nabla \cdot J_z^B &< 0 \text{ (PV flux divergence)} \\
 PV &\searrow \text{ where } Q_{net} > 0
 \end{aligned} \tag{6.15}$$

Contribution highlight Using this PV diagnostic framework I was able in [Maze and Marshall \(2011\)](#) and [Maze et al. \(2013\)](#) to quantify, map and attribute the seasonal PV reduction process to air-sea buoyancy fluxes, dominated by air-sea heat fluxes, with unprecedented details and accuracy.

Frictional processes

Now let's take the PV flux due to the "wind-driven buoyancy flux" from Eq.(6.11) and simplify it as:

$$J_z^F \simeq \frac{1}{\rho\delta_e} \tau_x \frac{\partial \sigma}{\partial y} \tag{6.16}$$

to illustrate this process in the simple case of a zonal wind blowing over a meridional density gradient. If the wind is blowing eastward ($\tau_x > 0$) on a positive density gradient ($\partial_y \sigma > 0$), a "down-front" wind, then the PV flux is positive because the southward Ekman advection of water from the northern side of the front onto the southern side will trigger convective mixing and a PV reduction:

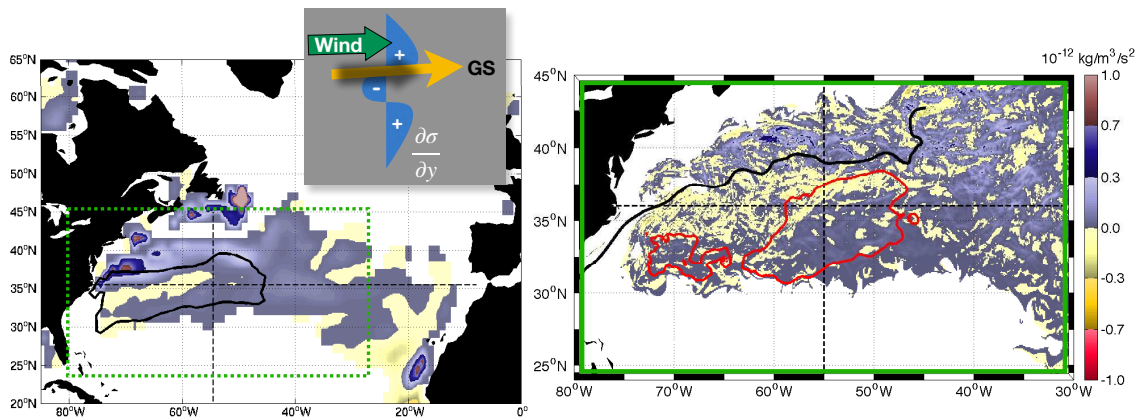
$$\begin{aligned}
 \mathbf{k} \times \boldsymbol{\tau} \cdot \nabla \sigma &> 0 \text{ ("Down-front" wind)} \\
 J_z^F &> 0 \text{ (upward)} \\
 -\rho^{-1}\nabla \cdot J_z^F &< 0 \text{ (PV flux divergence)} \\
 PV &\searrow \text{ where winds are down-front: } \mathbf{k} \times \boldsymbol{\tau} \cdot \nabla \sigma > 0
 \end{aligned} \tag{6.17}$$

[Thomas \(2005\)](#) and [Thomas and Ferrari \(2008\)](#) studied this process at length and suggested that it could be a significant PV sink.

In the case of the EDW, this PV extraction structure is slightly more complicated because, if the wind is indeed blowing eastward above the Gulf Stream, the latter is not an uniform positive density gradient region, it is a warm tongue of water that is warmer than the subtropical gyre center located further south. This creates a small region on the southern flank of the GS where the meridional density gradient is negative. This is illustrated [Figure 6.4](#) where the wind-driven frictional PV flux over EDW outcropping regions is plotted for two datasets of different horizontal resolution.

The Ekman driven advection of dense water from the northern side of the GS doesn't reach the southern flank of the GS but is rather triggering convection along the northern flank of the GS warm core. To the opposite, that same wind drives Ekman advection of GS warm core layer southward that restratifies the southern flank of the GS. This is clearly seen in [Figure 6.4A](#) for the OCCA dataset which has a 1° horizontal resolution.

Contribution highlight Obviously this process is crucially dependent on the intensity of horizontal density gradients. That's why in [Maze et al. \(2013\)](#) I proposed the first diagnostic of this term with a realistic meso-scale eddy resolving simulation. Instantaneous fields show much larger frictional PV fluxes than in the coarse resolution dataset. However, and perhaps more surprisingly, seasonal accumulation of frictional PV fluxes show large scale patterns, with very similar amplitudes, whatever the resolution of the



(A) OCCA dataset with horizontal resolution: 1° (B) NATL12 simulation with horizontal resolution: $1/12^\circ$

Figure 6.4: Figures reproduced from [Maze and Marshall \(2011\)](#) and [Maze et al. \(2013\)](#). Seasonal time averaged vertical PV flux due to surface frictional forces induced by winds over the EDW outcrop. This was computed using the mapping method Eq.(6.12) and flux formulation Eq.(6.11). Maps are for two datasets with different resolution, coarse to the left, eddy-resolving to the right. In the left plot, a schematic inset shows how westerlies blowing over the warm tongue of the Gulf Stream can explain the large scale PV flux structure observed in both maps.

dataset, see [Figure 6.4B](#).

Diabatic versus frictional processes

To better understand the EDW ventilation, an important point is to determine which one of the processes described above is the dominant one. Indeed, following [Thomas \(2005\)](#) at the time of the CLIMODE project, see [section 2](#), a question was whether frictional fluxes due to down-front winds could substantially contribute to the formation and ventilation of the EDW.

Contribution highlight I've shown that surface diabatic PV fluxes are the dominant sink of PV for the EDW, with the frictional PV flux component driven by winds contributing no more than 15% to the total seasonal PV out-flux. I've shown this to be true from meso to large scales ([Maze and Marshall, 2011](#); [Maze et al., 2013](#)).

Final remarks

It is important to note here that my contributions and focus to analyze the EDW PV dynamic has been from a meso-to-large scale point of view. Submeso-to-meso scales processes have been less studied at this point, simply because of a lack of observations and realistic numerical simulations. However, recent works from [Thomas and Joyce \(2010\)](#) and [Wenegrat et al. \(2018\)](#) for instance, suggest that sub-mesoscale processes can have a large impact on surface PV fluxes and hence on the EDW, and more generally the subtropical gyre circulation. Sub-mesoscale turbulence in the surface boundary layer can indeed generate a source of PV in the presence of sharp horizontal buoyancy gradients. Studying and determining the role of these processes onto the large scale ocean circulation and structure is clearly a challenge for the community that will be tackled over the coming years thanks to the availability of very high resolution realistic numerical simulations of ever increasing domain and temporal sizes ([Gula, 2020](#), e.g.).



7. Coherence of the gyre stratification

Contribution highlight My key contributions to the overall subtropical gyre stratification understanding are:

- A modern and objective description of the subtropical gyre vertical structure, from the surface mode water to the underlying permanent pycnocline (Feucher et al., 2015, 2016a,b; Feucher, 2016; Feucher et al., 2019),
- A description of the 3D structure of the eddy potential energy in subtropical gyres (Roulet et al., 2014).
- A new perspective on the horizontal coherence of stratification structures, showing:
 - the bi-modality of the subtropical gyre permanent pycnocline (Feucher et al., 2019),
 - the continuum of superimposed mode water and permanent pycnocline in the subtropical realm (Feucher et al., 2019),
 - the uniqueness of the 3-dimensional and Lagrangian redistribution of heat in the ocean (Maze et al., 2016a; Maze, 2017; Maze et al., 2017c).
- Observational evidences for the southern subtropical gyre stratification role in surface intensified sub-mesoscale turbulence in link with the mode water (Capet et al., 2016).

Content of this chapter:

Introduction	76
Methods	76
OACP	76
PCM: Profile Classification Model	76
Results	79
A modern and objective description of the warm water sphere	79
Class of stratification structures	81
Uniqueness of the Lagrangian redistribution of heat	81
Final remarks	83

Introduction

All my contributions to the understanding of the EDW life cycle described throughout previous chapters lead me to investigate the more fundamental question of the ocean, and specifically subtropical gyres, stratification and its overall coherence.

This is the topic I mostly investigated at Ifremer since 2012: on one hand with my first PhD student Charlène Feucher who I co-supervised with Herlé Mercier from 2013 to 2016 and on the other hand, with collaborators from IMT Pierre Tandéo and Ronan Fablet. The collaboration with IMT data scientists allowed me to discover new analysis technics and to investigate with IMT student internships (about 7 in total) their applications in physical oceanography problems.

Contribution highlight A deep dive into the data mining literature and practical use for my research lead me to construct and teach a new class for the UBO/IUEM Master 2 students entitle "Ocean's Big Data Mining". I thought this class in 2018 and 2019, and in 2020 it was integrated to a new "oceanographic data science" curriculum for the IMT-A, ENSTA and IUEM students.

Methods

OACP

I already introduced the "Objective Algorithm for the Characterisation of the Pycnocline" (OACP) method in [section 2](#). So I will simply note here that OACP was initially applied to the North Atlantic by [Feucher et al. \(2016b\)](#) and later extended to the global ocean in [Feucher et al. \(2019\)](#). All the technical details can be found in these papers. In this chapter I'll be highlighting results from this later global analysis.

PCM: Profile Classification Model

PCM or a "Profile Classification Model" is a method I developed and introduced in [Maze et al. \(2017c\)](#). It allows to automatically assemble ocean profiles in clusters according to similarities in their stack of vertical structures. The geospatial properties of these clusters can be used to address a large variety of oceanographic problems: front detection, water mass identification, natural region contouring (gyres, eddies), reference profile selection for QC validation [Maze et al. \(2017b\)](#). The vertical structure of these clusters furthermore provides a highly synthetic representation of large ocean areas that can be used for dimensionality reduction and coherent inter-comparisons of ocean data (re)-analysis or simulations.

Data preprocessing

In order to be able to clusterize a collection of vertical profiles (of temperature, or salinity, or both, or any other ocean property), each of the variables must go through a preprocessing "pipeline" described [Figure 7.1](#):

- **Ravel:** From any dataset, extract a collection of vertical profiles for a given variable (eg: temperature) and ravel it to a 2-dimensional format while ensuring plain data values, i.e. data must be defined on standard depth levels and not NaNs. Interpolation may be required (for raw Argo profiles for instance), but this is not necessary when working with profiles from a gridded product (such as ISAS15 or any numerical simulation output). This step includes handling of missing values, either with interpolation or simple removal of the profile from the collection. When processing more than one variable, one need to ensure that all variables will be defined and adapt the mask accordingly. For multi-dimensional variables (defined on a latitude, longitude, time grid for instance) this is also the step where all dimensions but the vertical one are stacked along a "sampling" dimension.
- **Scale:** Variables must then be normalized by removing the mean and scaling to unit variance for each vertical levels:

$$\mathbf{x}(z) \rightarrow \frac{\mathbf{x}(z) - \boldsymbol{\mu}(z)}{\boldsymbol{\sigma}^2(z)} \quad (7.1)$$

This step ensures that patterns located at depth in the profile, will be considered similarly to those close to the surface by the classifier.

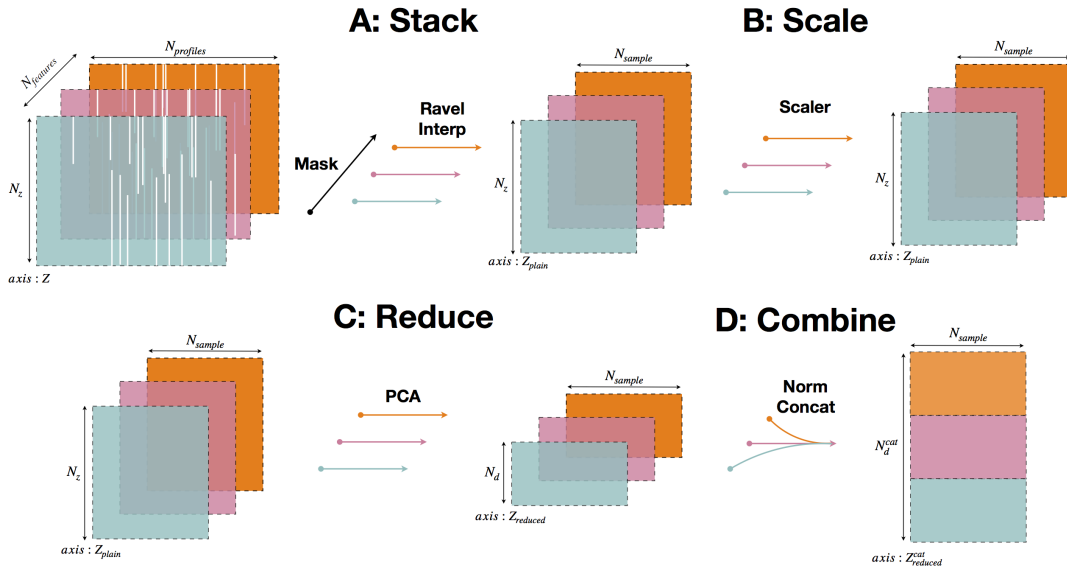


Figure 7.1: Pre-processing steps of the Profile Classification Model method. A collection of profiles is given as input (with possibly more than one variable such as temperature and salinity, these are represented by colors, and possibly with missing values, represented by white stripes) and preprocessed to output a plain 2-dimensional array. This array is in turn used as input for an unsupervised-classifier, a Gaussian Mixture Model in [Maze et al. \(2017c\)](#). Details of each steps are given in the text.

- **Reduce:** The vertical dimension should be *reduced*. In this problem, the statistical dimensions of features are the vertical depth levels, and more often than not, profiles have a significant number of vertical levels (from 50 to 1000 for Argo profiles, for instances, or from 50 to about 100 for a GCM output). For the classifier to identify structures in a 100-dimensional space is very complex, if not impossible. We therefore need to compress the information and to reduce the number of vertical levels. Many methods exists to reduce dimensionality, by default we use a Principal Component Analysis (e.g. [Thomson and Emery, 2014](#), p 335) on which spatio/temporal EOFs are based ([Bjornsson and Venegas, 1997](#)). With PCA, we can decompose a dataset $\mathbf{x}(z)$ as:

$$\mathbf{x}(z) = \sum_{j=1}^d \mathbf{P}(z, j) \mathbf{y}(j) \quad (7.2)$$

where $\mathbf{P} \in \mathbb{R}^{D \times d}$ and $\mathbf{y} \in \mathbb{R}^{d \times N}$ with $d \leq D$. The first rows of \mathbf{P} contain profiles maximizing the structural variance throughout the collection of profiles. Thus if we choose $d \ll D$, we can reduce the number of dimensions of the dataset \mathbf{x} while preserving most of its structure.

- **Combine:** This last step is necessary when a PCM is using more than 1 feature variable (e.g.: temperature and salinity). Each reduced array is normalized (with all population mean and std) and are then concatenated along the reduced dimensions. The normalization ensures that all feature variables have the same *weight* in the clustering analysis.

Clustering

Clustering, or unsupervised classification, is a classic and powerful data mining analysis. In fact, "Organizing data into sensible groupings is one of the most fundamental modes of understanding and learning." as pointed out by [Jain \(2010\)](#). Clustering find groups of related data so that data that belong to the same cluster are more similar to each other than data that belong to other clusters. Clustering is already widely used in atmospheric dynamic, in particular it lead to the Weather Regimes paradigm that allows to describe non-gaussian asymmetric atmospheric states more efficiently than EOFs (e.g. asymmetric NAO states in the North

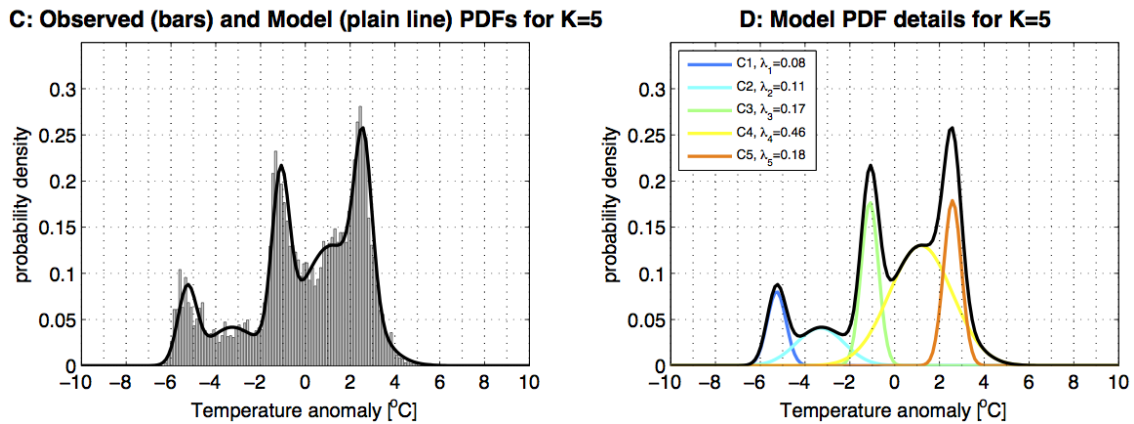


Figure 7.2: Illustration of the Gaussian Mixture Models method on 1-dimension data of vertically average temperature of Argo profiles in the North Atlantic. Left plot: gray bars are the observed PDF and thick black lines are the GMM PDFs for $K = 5$ mixture components. Right plot: Decomposition of the GMM PDF into its 5 components. Colored PDFs are the weighted Gaussians of each component that together sum up to the GMM one (black). Three distinct modes are clearly visible in the dataset (at the extreme and center of the complete PDF) and are nicely captured by GMM. Reproduced from [Maze et al. \(2017c\)](#).

Atlantic [Cassou, 2004](#)). However, in oceanography clustering is not yet part of the classic toolkit of analysis. One of the first usage is the identification of trophic regimes from clustering of satellite data time series from [D'Ortenzio and Ribera d'Alcalà \(2009\)](#). My [Maze et al. \(2017c\)](#) study is the first of its kind and the technic was re-used by [Jones et al. \(2019\)](#) in the Southern Ocean and by [Rosso et al. \(acc, 2020\)](#) in the Indian Ocean. [Sonnewald et al. \(submitted\)](#) also used clustering to reveals geography of global ocean dynamical region, i.e. they seek for clusters in the PV balance of the ECCOv4 re-analysis [Forget et al. \(2015\)](#).

Among the statistical methods that can be used to perform clustering, the most widely used is the K-means (see the extensive review from [Jain, 2010](#)). K-means is popular because it is simple to implement and scale well with large datasets. However it has some limitations: it's a "hard" classifier, i.e. it provides a binary classification (probability is reduced to either 0 or 1, [Lloyd, 1982](#)) and it handles poorly clusters that are of very different size.

In [Maze et al. \(2017c\)](#) I used another method that doesn't suffer from these limitations and is yet still very popular in the machine learning community: Gaussian Mixture Models (GMM). The simple principle of a GMM is that any probability density function (PDF) can be described as closely as desired with a model of weighted sum of Gaussian PDF, each of these K Gaussian functions creating a prototype of the clusters ([Anderson and Moore, 1979](#)). Clustering with GMM thus consists in fitting a GMM to the observed PDF of a dataset. Each of K GMM modes, or Gaussian functions, describe a cluster through its mean and co-variance. [Figure 7.2](#) shows a trivial illustration of the technic for a one-dimensional dataset.

All the technical details and subtleties can be found in [Maze et al. \(2017c\)](#). In the classic use case scenario, clusters are defined by GMM by a mean vertical profile and its square co-variance matrix describing the stack of vertical patterns correlations. As GMM is a "fuzzy" classifier, the method output is a series of probabilities for each profile that provide the probability of that profile to have been drawn out of each mode. If the GMM is fitted with K modes, we thus have K probabilities for each profile, their sum being 1. The mode with the maximum probability is the one can be used to "label" this profile.

Contribution highlight As described above, a significant pre-processing procedure is required to perform this analysis. I therefore developed a software to easily implement the Profile Classification Modeling technic. The software is fully documented here <https://pyxpcm.readthedocs.io> and is implemented in python, as an open source code (<https://github.com/obidam/pyxpcm>).

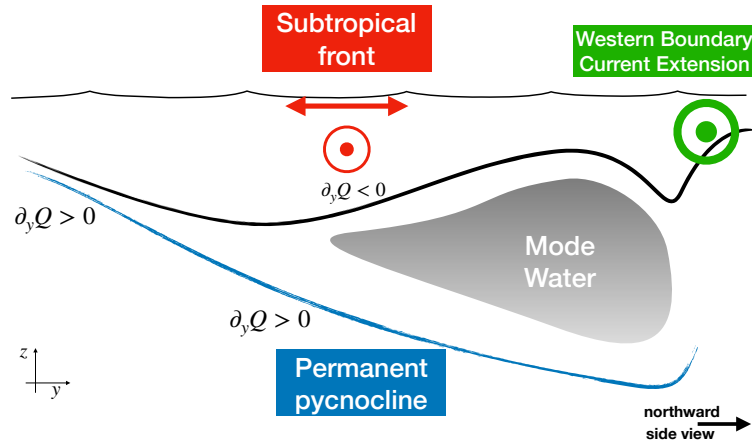


Figure 7.3: Schematic showing a meridional section through the mode water and permanent pycnocline and highlighting the location of positive and negative meridional PV gradients that could sustain the existence of a surface intensified subtropical counter current (red). This STCC is the equatorward limit of the mode water extension.

Results

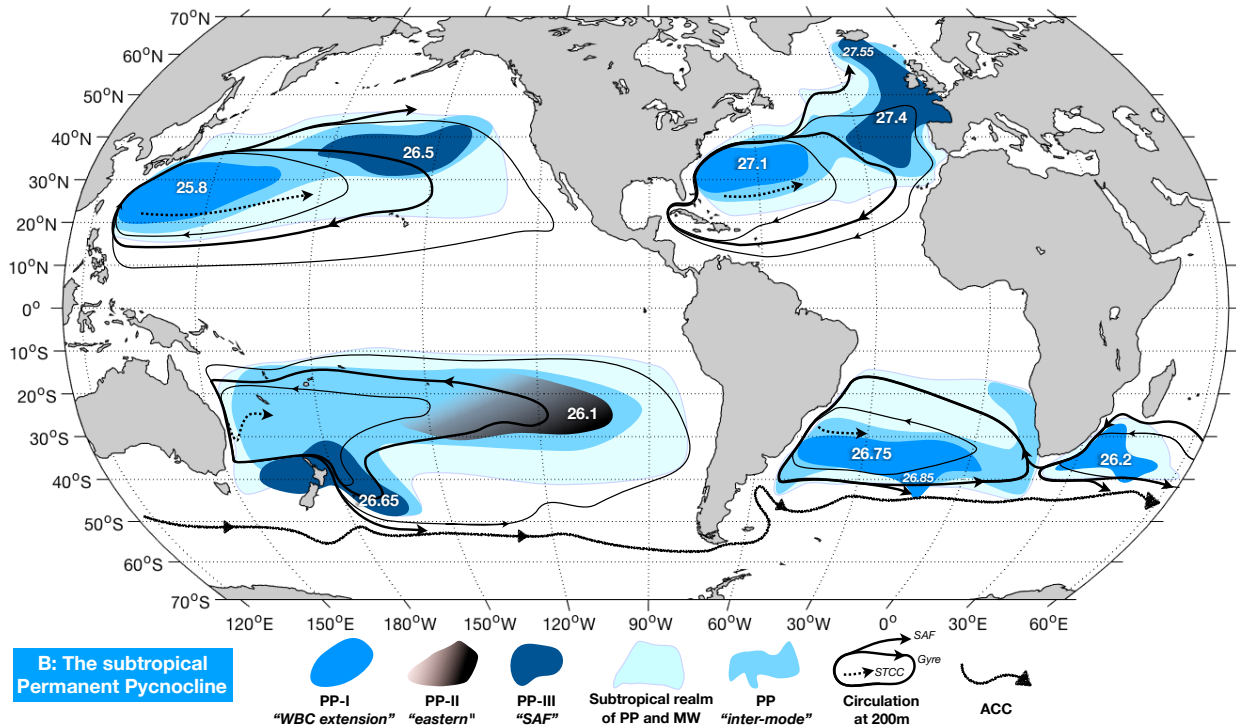
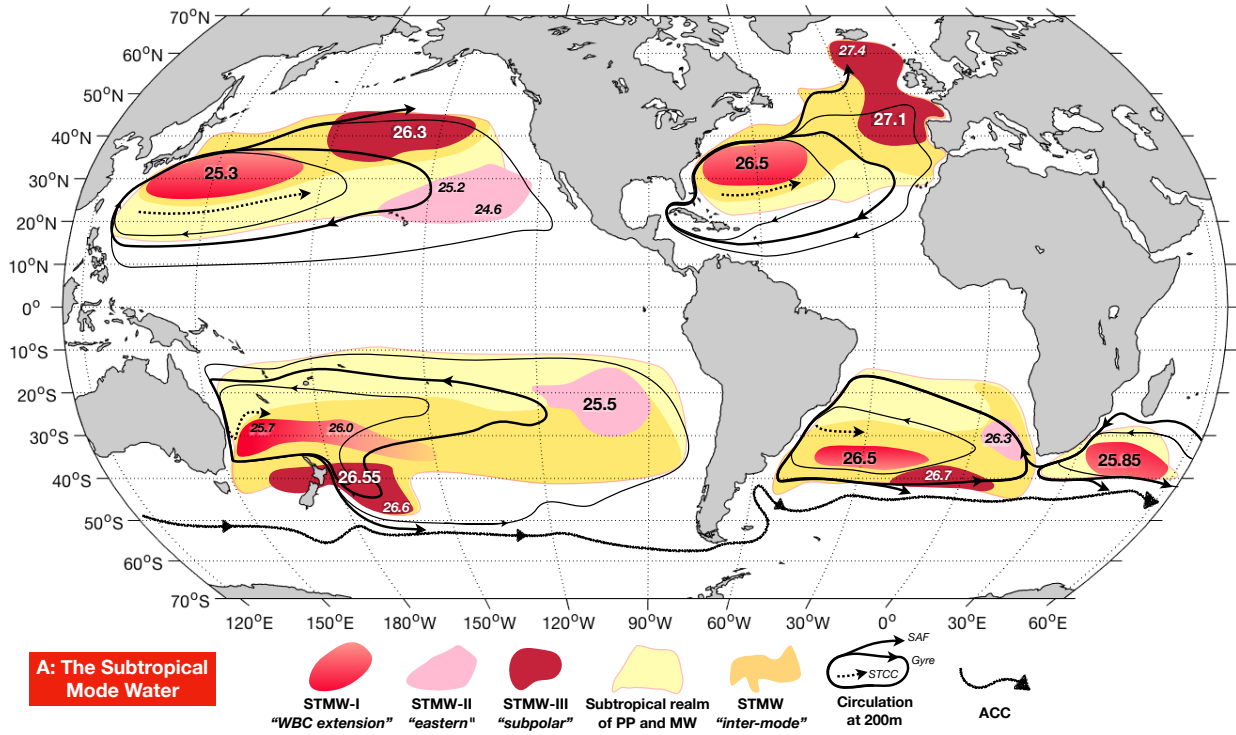
A modern and objective description of the warm water sphere

Since [Hanawa and Talley \(2001\)](#), the description of subtropical mode waters has not been synthesized and updated using the wealth of new Argo observations. [Tsubouchi et al. \(2016\)](#) provided a first attempt in that direction, but they limited their analysis to temperature and Type-I mode waters.

In [Feucher et al. \(2019\)](#), we derived a full updated view based on the objective description of the mode waters from OACP and we furthermore added an unprecedented description of the underlying permanent pycnoclines. Detailed maps and properties can be found in [Feucher et al. \(2019\)](#). Here I will simply show in [Figure 7.4](#) the final schematic we produced that can be seen as an augmented and updated schematic of the standard reference [Figure 2.3](#).

This figure shows the mode water and permanent pycnocline key properties and distribution. One of the main key point of this figure and our work is that the STMW "inter-mode" flavors are explicitly found and represented. This "inter-mode" water mass connects the more standard modes clearly identified in σ_0/N^2 diagrams (see figure 5 in [Feucher et al., 2019](#)). This is a key point because, for the first time, it shows a continuously defined vertical stack of mode-water/pycnocline throughout the subtropical gyre. Hence, we are able here to present here the entire realm of the subtropical gyre. That being said, the main result of [Feucher et al. \(2019\)](#) is probably the bi-modality of the subtropical gyre permanent pycnocline. We indeed showed that the permanent pycnocline couldn't be represented by a single isopycnal surface.

Figure 7.4 (*following page*): Schematic representation of Subtropical Mode Waters (A) and Permanent Pycnocline (B) distributions, with typical potential densities and subtropical gyre and ACC circulation at 200m depth. The MW and PP color codes are given in the legends of each schematics (for MWs I used the same color code as [Hanawa and Talley, 2001](#)). The subtropical circulation is from the Argo-based Geopotential height at 200m derived from [Ollitrault and Colin de Verdière \(2014\)](#). Dash arrows indicate the main surface-trapped subtropical counter-currents ([Memery et al., 2000](#); [Ullman et al., 2007](#); [Kobashi and Kubokawa, 2012](#); [Ganachaud et al., 2014](#)).



Another update was the more detailed description of the circulation patterns associated with the subtropical dynamic. In particular, there is an explicit representation of subtropical counter currents (STCC, dashed arrows). As reviewed by [Kobashi and Xie \(2012\)](#) in the North Pacific and more recently suggested by [Capet et al. \(2016\)](#) in the North Atlantic, the meridional potential vorticity gradient associated with the equatorward edge of the mode water of type I plays a crucial role in the STCC formation. The STCC can thus be seen as the equatorward limit of the mode water of type I extent.

Contribution highlight I think that one of the key new point raised by the work conducted during the C. Feucher PhD and presented in [Feucher et al. \(2019\)](#) is the crucial role of Subtropical Counter Currents (STCC) into the dynamic and structure of Type-I Subtropical Mode Waters. As highlighted in [Figure 7.4](#), the equatorward meridional extent of STMW-I coincides with STCC.

A possible mechanism explaining this result was introduced by [Kobashi et al. \(2006\)](#) and is illustrated here [Figure 7.3](#). Since STMW-I are a low PV reservoir and the underlying permanent pycnocline is a high PV layer (as was leveraged by [Feucher \(2016\)](#) to develop OACP), and since the wind-driven wind-stress curl is pulling the permanent pycnocline toward the surface at low latitudes, there exists a change of sign in the vertical direction of the meridional PV gradient. Integrating this PV gradient upward induces a large meridional isopycnal slope that could sustain a surface intensified eastward current. Since the Sverdrup balance drives an overall westward circulation in this region (the Equatorial Currents closing subtropical gyres), this surface current is coined counter-current.

Contribution highlight I furthermore contributed to show that this mode water-induced subsurface frontogenesis could be associated with intensified sub-mesoscale turbulence through a Charney baroclinic instability triggered in spring on the dawn of the mode water formation, when the meridional PV gradient is at its largest seasonal amplitude ([Capet et al., 2016](#)).

Class of stratification structures

When the PCM analysis is performed on all Argo temperature profiles of the North Atlantic, one obtain an optimal decomposition into 8 clusters of different profile patterns. The vertical structure of these clusters is shown [Figure 7.5](#) as the percentile of profiles attributed to each clusters. Unit is anomalous temperature, i.e. the difference with the full sample mean (all North Atlantic profiles). One can note that:

- Class 1 is homogeneously cold,
- Class 2 is cold at mid-depth cold and warm near the surface,
- Class 3 is nearly neutral throughout the profile but is marked by a large spread,
- Class 4 is cold and with a surface spread,
- Class 5 is nearly neutral at the surface and warm at depth,
- Class 6 is neutral at depth and warm in the sub-surface,
- Class 7 is homogeneously warm,
- Class 8 is nearly neutral at surface and depth but warm at mid-depth.

One important point to note here is that the description of a class, or cluster, of profiles is with both the core profile (the 50% percentile in this case) and the spread around that profile (the 5-95% percentile here). This means that the description of a class with PCM can capture both mode waters (small spread throughout the class population) and pycnoclines (large spread), at it is evident in class 8. This furthermore highlights that PCM provides a model for a given stack of vertical structures (see below).

Uniqueness of the Lagrangian redistribution of heat

Remark

The PCM method was developed with colleagues and a student from IMT-A in 2014 (Pierre Tandéo, Ronan Fablet and Manuel Lopez-Radcenco). I still remember the first time we saw the map of geographic distribution of classes. This came to me as an amazing result that motivated a large chunk of my research

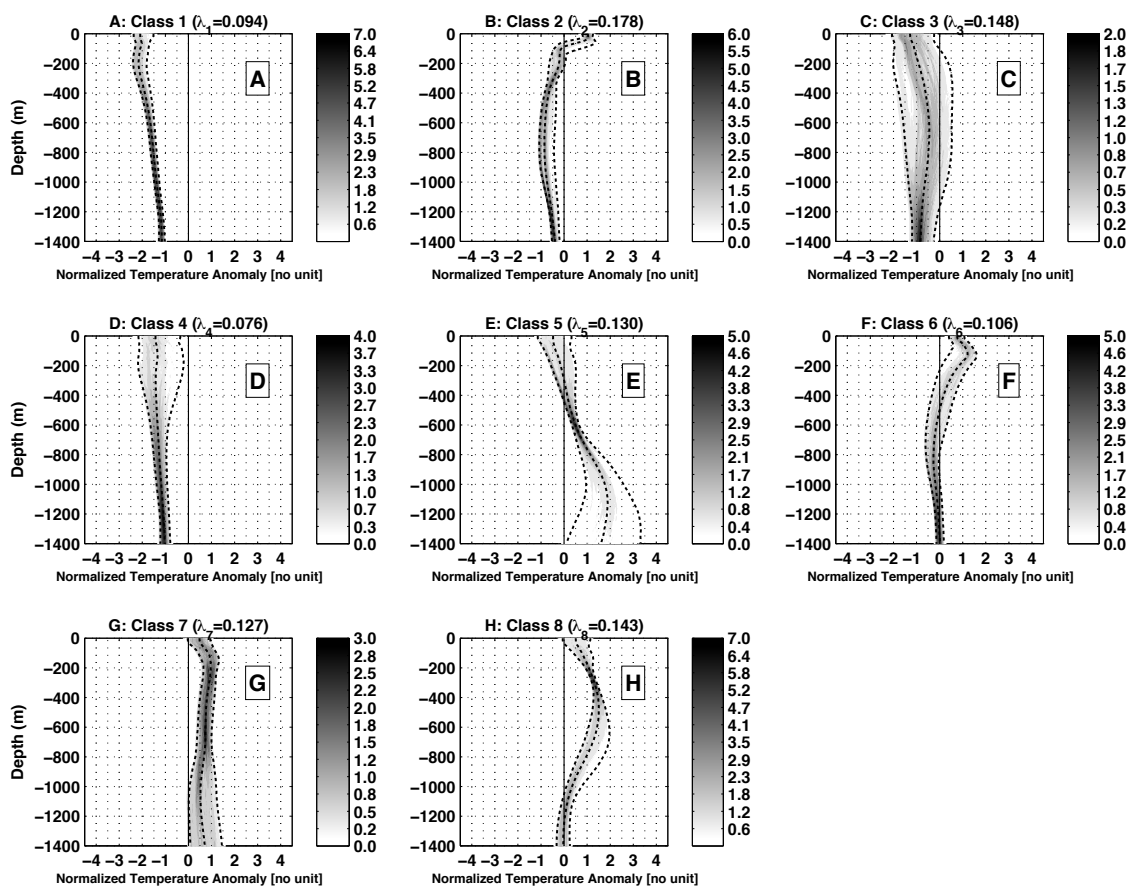


Figure 7.5: Normalized temperature anomaly for each class as a function of depth: black dashed lines are the 5, 50 and 95% percentiles of the class. Grey shading is the corresponding PDF for each depth and each class temperature anomalies. Figure 10 from [Maze et al. \(2017c\)](#).

since then.

One key point of the PCM method is that it doesn't use profile coordinates to classify profiles, clustering only operates on similarities of vertical patterns. In other words, PCM provides a model for a given stack of vertical structures. Therefore, the geographic distribution of profiles attributed to each classes is a consequence of the analysis that has no *a priori*. And this is where PCM shows its main outcome.

Figure 7.6 represents the geographic distribution of PCM classes obtained from Argo temperature data and 8 classes. It is now fruitful to link the vertical structure of classes to well-known ocean features. For instance class 8 showed homogeneity near 300m and a large spread at 700m. Figure 7.6 shows that class 8 is located in the western subtropical gyre, where the EDW and permanent pycnocline are found. One can also note how class 2 captures the equatorial band structure: cold at depth, a shallow pycnocline and then warm at the surface. And so on. It could even be taken as an exercise for students to take Figure 7.5 and to guess to which region of the ocean they correspond.

Contribution highlight The fact that the geographic distribution of classes is coherent, in a sense that it naturally defines regions that are nearly not overlapping, shows the Eulerian uniqueness of the 3-dimensional Lagrangian redistribution of heat in the ocean. Indeed, the Lagrangian circulation of a water mass, once subducted, is nearly following isopycnals and more importantly operates in 3-dimensions. This circulation is usually studied for a single water mass as it dives or shoals. With the PCM method, in [Maze](#)

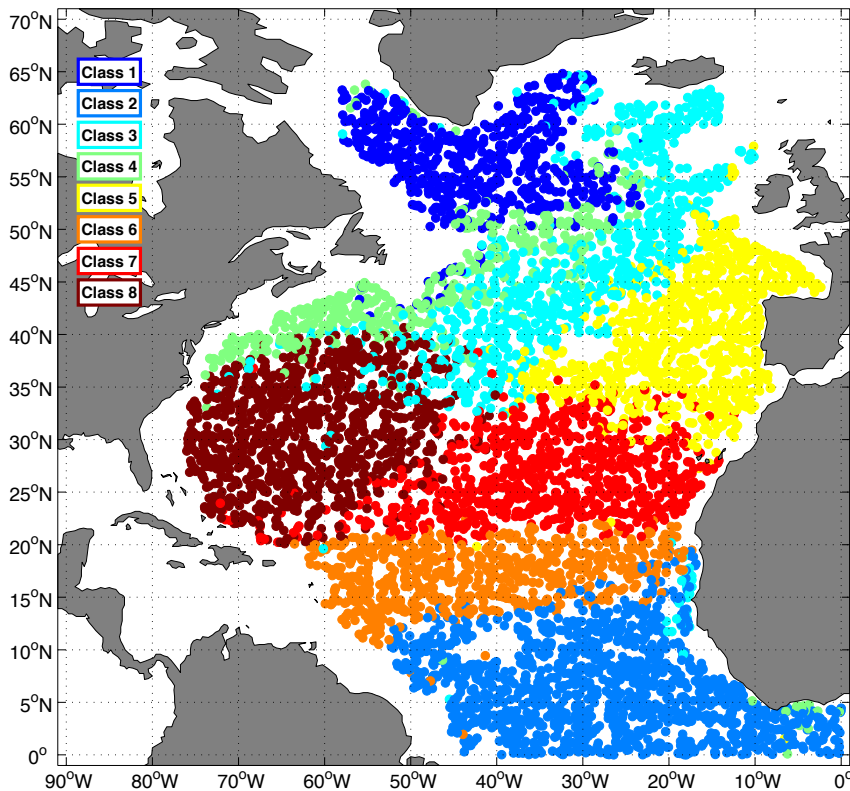


Figure 7.6: Geographic distribution of PCM classes obtained with PCM(K=8, Temperature) in the North Atlantic and with Argo data. This figure shows the Eulerian uniqueness of the 3-dimensional Lagrangian redistribution of heat in the ocean. Reproduction of Figure 11 from [Maze et al. \(2017c\)](#).

(2017) I showed that, locally speaking, from a Eulerian point of view, this 3-dimensional redistribution of water masses gives rise to a unique stack of water masses.

Final remarks

Using Argo data and the OACP method, I presented a 2000-2015 climatology of the warm water sphere stratification at mid-latitudes. This climatology, schematically represented in a more dynamical context Figure 7.4 highlighted the following key results:

1. in each basins, the subtropical stratification pattern of a mode water pycnostad overlying a permanent pycnocline exists continuously throughout the gyre,
2. the subtropical permanent pycnocline shows two deep centers colocated with thick mode waters (either subtropical and/or subpolar mode waters) in the NATL, NPAC and SPAC,
3. the pycnocline is shallower in the center of the subtropical gyres, which creates a double-bowl pattern at the basin scale,
4. the approximation of the permanent pycnocline depth by an isopycnal surface is only possible in limited regions, i.e. in the western boundary current recirculation and eastern flow regions on the equatorward flank of SAF,
5. the singularity of the North Atlantic subtropical gyre stratification is shown, with the deepest/thickest mode water and permanent pycnocline observed.

Using Argo data, I introduced a new analysis (coined PCM for Profile Classification Modeling) that provides a synthetic and coherent description of the vertical stack of stratification features. I furthermore showed that these stacks are geographically unique. There exists many applications to such results, as I laid

out in [Maze et al. \(2017b\)](#): front detection, water mass identification, natural region contouring (gyres, eddies), reference profile selection for QC validation. I currently work on these applications with colleagues from Grenoble (T. Penduff), IMT-A (P. Tandéo), Scripps (I. Rosso, L. Talley) and the Argo community.



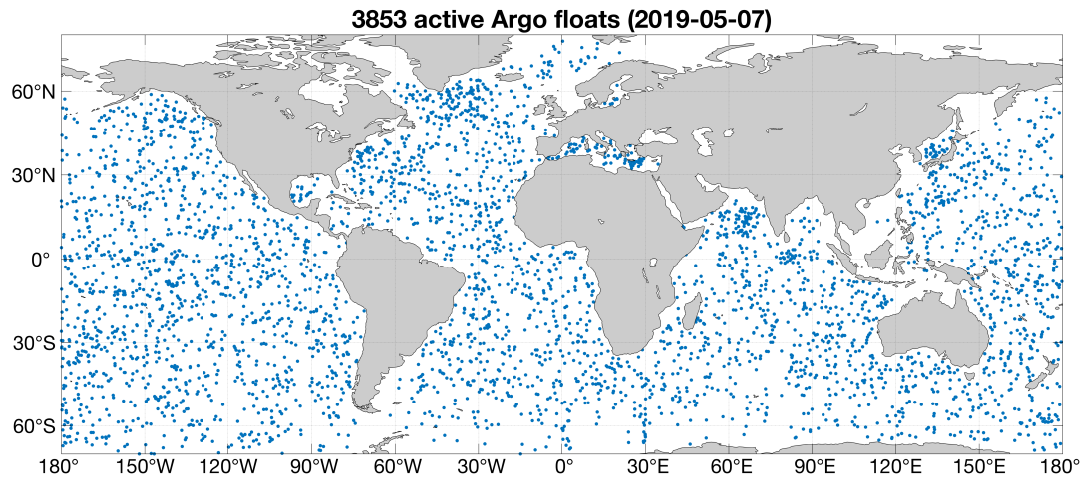
8. Observing the ocean with Argo

Contribution highlight My key contributions to a better observation of the ocean through a sustained Argo network are:

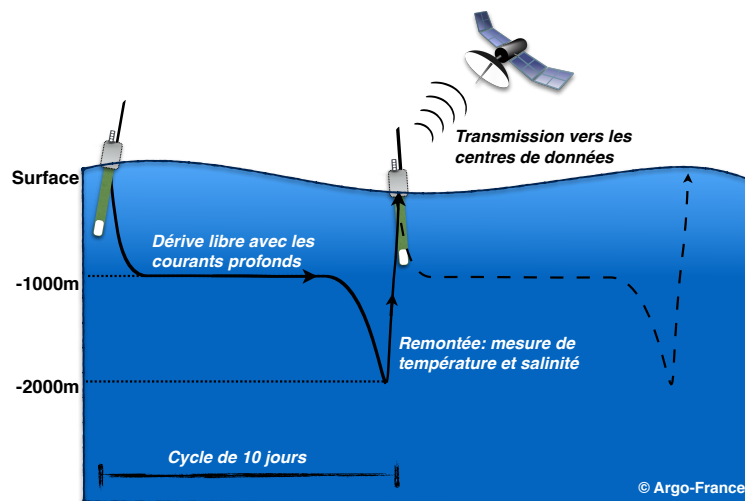
- a strong involvement in the management of the ocean observing system:
 - the coordination of national contributions to the global network ([Maze et al., 2015a](#)),
 - the representation of France activities in Argo international governance bodies (AST, ADMT and Euro-Argo: [Maze et al., 2014c, 2015b, 2016b, 2017d, 2018d, 2019c](#)),
 - the valorisation of the network in the name of Argo-France activities ([Riser et al., 2016](#); [Roemmich et al., 2019](#))
- a contribution to the Argo extension toward measuring deeper layers of the ocean ([Maze and Thierry, 2014](#); [Zilberman and Maze, 2015](#); [Le Reste et al., 2016](#); [de Lavergne et al., 2016](#)),
- the evaluation of a new CTD sensor for the core and deep mission ([Maze et al., 2018e](#)),
- the improvement of the Argo database quality through assessment of existing, and development of new, quality control procedures based on machine learning ([Maze et al., 2017a, 2018a,b,c](#); [Tokunaga and Maze, 2019a](#)),
- the deployment of floats in the North Atlantic Subtropical Gyre.

Content of this chapter:

Introduction: what is Argo ?	86
Managing an ocean observing system	87
Improving Argo	90
Quality control procedures	90
Technology readiness	91
Western Boundary Currents	93
Extending Argo toward the deeper ocean	94
Final Remarks	95



(A) Current status of the global Argo network: 3853 active floats reported 13 268 profiles in April 2019



(B) Typical 10 days cycle of an Argo float

Figure 8.1: The Argo real-time global ocean observing system at a glance.

Introduction: what is Argo ?

Argo is a real-time global ocean observing system. It is a global network of nearly 4000 probes measuring pressure, temperature and salinity from the surface to 2000m depth every 10 days. The localisation of these probes is nearly random between the 60° parallels (Figure 8.1A).

Each Argo probe is a free drifting profiling float, i.e. an autonomous probe that can't control its trajectory but is able to control its buoyancy and thus to move up and down the water column as it wishes. Argo floats continuously operate the same program, or cycle, illustrated Figure 8.1B. After 9 days of free drift at a parking depth of about 1000m, an Argo float dives down to 2000m and then shoals back to the surface while measuring pressure, temperature and salinity. Once it reaches the surface, the float sends by satellite its measurements to a data center where they are processed in real time and made freely available on the web in less than 24h00.

The Argo international observation array was initiated in 1999 (Roemmich et al., 1998) and soon revolutionized our perspective on the large scale structure and variability of the ocean by providing seasonally and regionally unbiased in situ temperature/salinity measurements of the ocean interior, key information that satellites can provide (Riser et al., 2016).

The Argo array reached its full global coverage (of 1 profile per month and per 3x3 horizontal cell) in 2007, right at the beginning of the CLIMODE project. [Figure 8.1A](#) shows the current coverage of the network. It now extends to higher latitudes than the original $\pm 60^\circ$ and some of the floats are now able to profile down to 4000m and 6000m (see later). New floats can also be equipped with biogeochemical sensors, measuring oxygen and chlorophyll for instance. All these evolutions of the network rises the total number of floats to nearly 4000. Argo is thus providing a deluge of in situ data: more than 400 profiles per day (I produced [this animation](#) to illustrate this).

Managing an ocean observing system

Argo is integrated in the international Global Climate Observing System (GCOS) and Global Ocean Observing System (GOOS). The global network is operated by more than 30 countries and need strong coordination at the international level. The technical coordination is conducted through the Join IOC-WMO technical Commission for Marine Meteorology and Oceanography (JCOMMOPS) while the scientific coordination is managed by the Argo Steering Team (AST) since 1999. The AST provides scientific leadership and oversees the development and implementation of the global array of profiling floats operated by national and regional Argo projects. The AST relies on the international Argo Data Management Team (ADMT) to implement and organize the monumental task of collecting, aggregating and distributing data from dozens of different float and sensor models that continuously evolve over time.

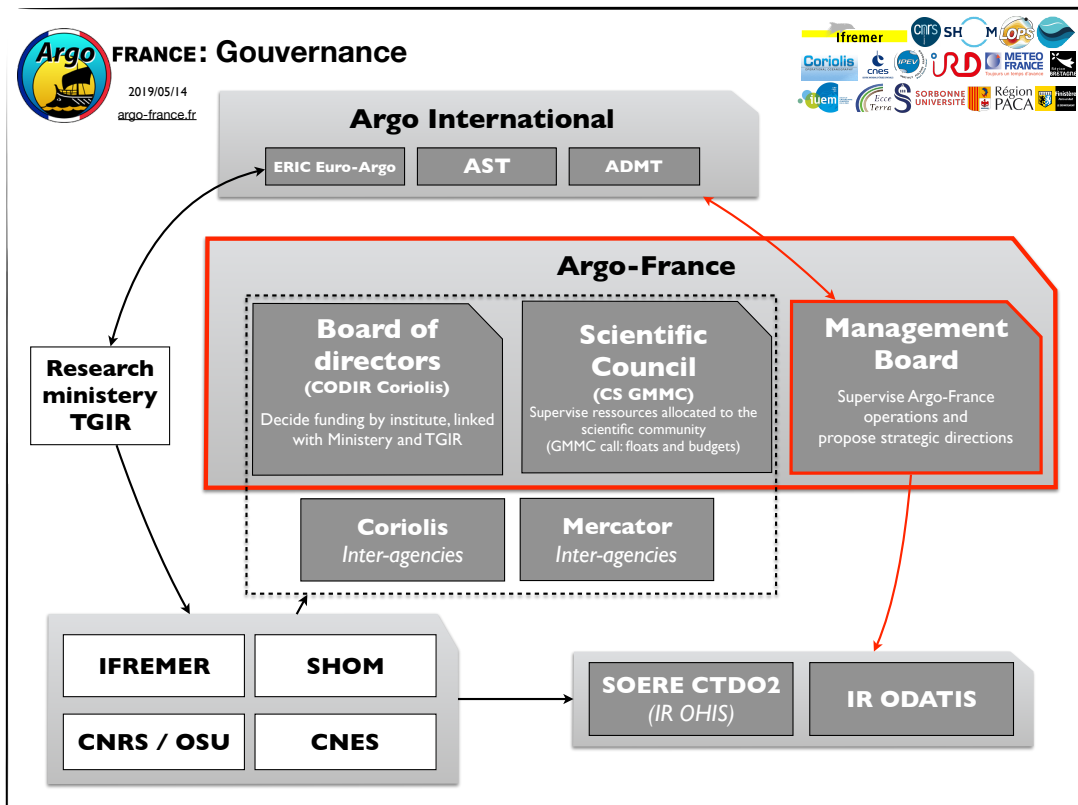
At the European level, an European Research Infrastructure Consortium (ERIC) dedicated to Argo has been created in 2014. The objective of the Euro-Argo ERIC consortium of 12 countries is to organize and consolidate the European contribution to the Argo program.

Contribution highlight France has been an active member of the AST, ADMT and Euro-Argo ERIC from their very creation to today's operations. I'm France representative to the AST since 2013. Over the last 7 years I've been responsible for reporting and valorizing all France activities related to the Argo array: floats procurements and deployments, floats technological developments, data management and scientific analysis. I also tried to provide leadership in items such as the extension toward deeper measurements, new sensors integration and data management through new machine learning technics.

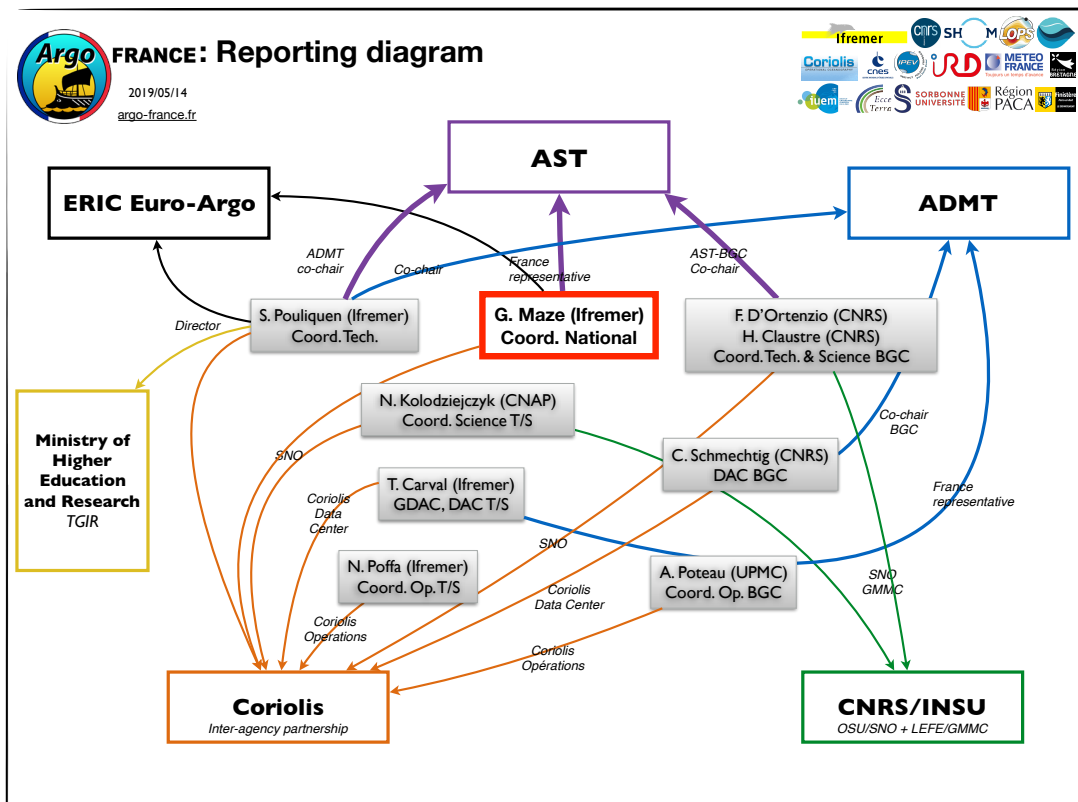
Since 2017, I am furthermore assuming the role of France representative to the Euro-Argo ERIC management board where I contribute to the development of the European contribution to the Argo array. France is a key and historical player in Argo and my responsibility has been both challenging and rewarding.

The Argo-France national program is the French contribution to the international Argo program. Argo-France gathers all the French activities related to Argo and its extension toward deep and biogeochemical measurements. [Figure 8.2](#) represents all these activities, how they are organized and where are my contributions. To implement these activities Argo-France relies on scientific projects (eg: equipex NAOS, ERC RemoOcean, H2020 E-ARISE, CPERs) as well as on long-term partnership through consortium like the "Service National d'Observation" (SNO) Argo-France and Coriolis.

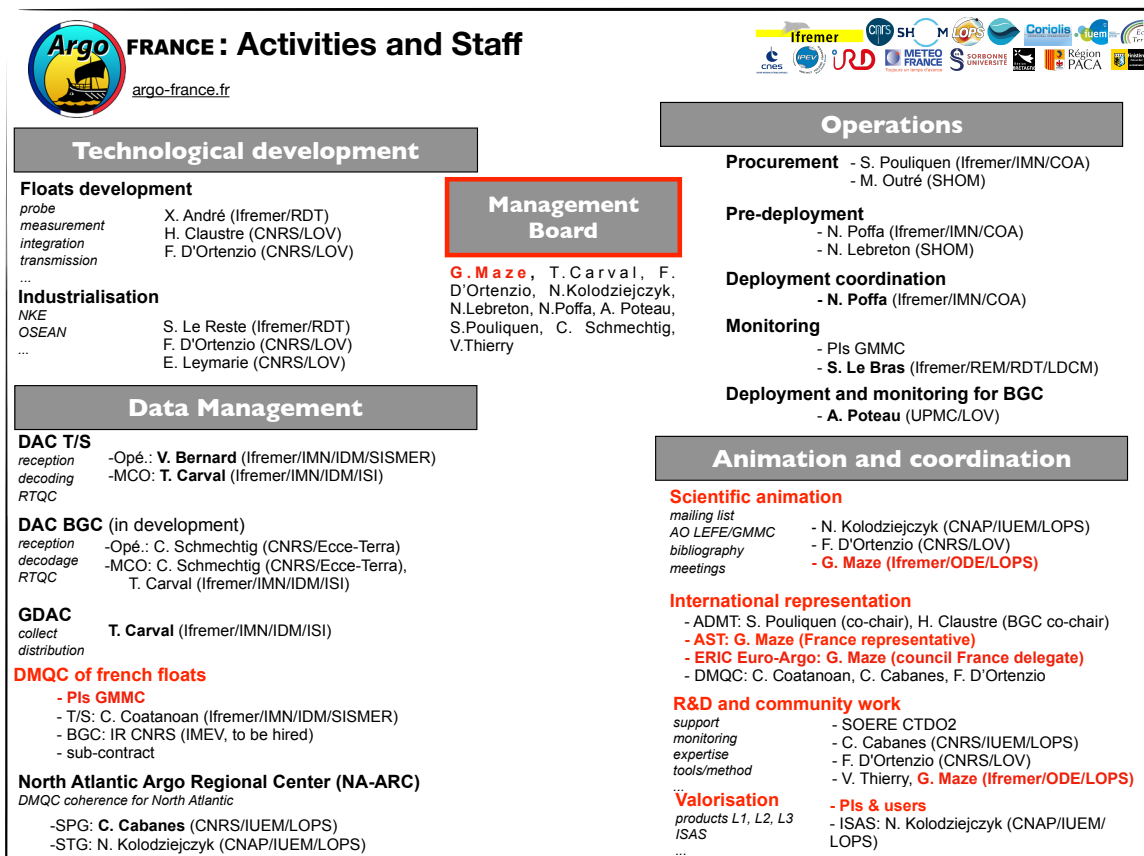
The SNO Argo-France organizes scientific activities. The SNO, which is affiliated to the OSU IUEM (Institut Universitaire Europeen de la Mer) is a partnership of two research laboratories: the "Laboratoire d'Océanographie Physique et Spatiale" (LOPS, Brest, France) and the "Laboratoire d'Océanographie de Villefranche – Institut Marin de l'environnement de Villefranche" (LOV-IMEV, Villefranche, France). Argo-France operational activities are organized through the Coriolis partnership (IFREMER, SHOM, INSU, IRD, Météo France, CNES and IPEV) and its governance bodies. The Euro-Argo TGIR and Argo-France are part of the Ministry of Research national roadmap on research infrastructure.



(A) Argo-France national scheme of governance. I am head of the National Management Board since 2014.



(B) Reporting diagram of the National Management Board members. I report to AST, Euro-Argo and Coriolis.



(C) Exhaustive view of Argo-France activities and staff involved (my contributions highlighted in red).

Figure 8.2: Organisation of Argo-France and my contributions therein.

Contribution highlight Argo-France recurrent activities are funded through the TGIR and by research institutes through the SNO and Coriolis partnership. These long-term fundings are crucial to sustain the Argo array and to build a very long time series of observations to monitor the state of the ocean. My contribution to these activities has been to secure funding for the SNO since 2015 (Maze et al., 2015a).

France hosts a lot of activities related to Argo, in many different domains. Another of my contributions to the management of these activities has been to create in 2014 the Argo-France management board and to lead its activities (Figure 8.2). The board's role is to ensure the scientific coordination of all activities taking place in many different groups and to elaborate and implement annual activity plans to operate the France contribution to the global Argo network.

In 2020, I will hand over the Argo-France management board coordination and assume the role of chairman for the scientific council of the joined Coriolis / Mercator Ocean International Group (CNRS LEFE/GMMC).

The Argo-France management board coordinates national efforts and provide a formal body to discuss a long-term strategy for the national contribution to the Argo program, independently from short-term projects constraints. The committee has worked to produce a program strategy to face three challenges over the next 10 years: (i) sustain the core program at its current state of excellence, (ii) sustain the BGC-Argo global network build up and propagation of the core standard of data quality and (iii) sustain the contribution to the Deep-Argo extension towards the achievement of full-depth multidisciplinary network. Since its creation in 2014, I organized 3 to 4 board meeting a year. In 2018, a Memorandum Of Understanding has been elaborated

by Ifremer, CNES and SHOM in order to organize their contributions to the TGIR Argo France and to enforce the governance scheme shown [Figure 8.2A](#).

Improving Argo

Contribution highlight Currently, one of the main challenges of the international Argo program is to ensure its long-term sustainability. In 2018, I participated in the elaboration of a H2020 project gathering 18 partners in Europe. The 4 millions euros project EA-RISE (Euro-Argo Research Infrastructure Sustainability and Enhancement) was accepted and started in January 2019. I coordinate Ifremer participation in 4 Work Packages and lead one work package focusing on the core Argo mission and its improvement. Within this H2020 project I will coordinate and lead activities dedicated to: diversify sensors available to the core mission, improve Argo observation of boundary currents, improve floats lifetime and improve the



quality control procedure.

Quality control procedures

Data qualification is one of the main challenge of the observational network. The Argo dataset, which is freely distributed to the scientific community, needs the required precision for climate change studies. To guarantee this precision, data are qualified in delayed mode to detect and correct possible biases or drift of the sensors. These detections are conducted by human operators with the required scientific expertise and is based on a suite of automatic quality control procedures. To date, about 1.1 millions of Argo profiles (64% of the dataset) have been quality controlled in delayed mode, i.e. for research purposes. This historical work provides an unique, and large, training dataset that should allows for the development of new supervised algorithms to predict the research quality flag of new data.

In 2017 I co-supervised with Pierre Tandéo from IMT-A an internship student who worked on the use of machine learning to predict the human decision of alarm status raised by an automatic QC test. Working with the ISAS group, I assembled a training dataset with the list of all alarms raised by the objective comparison of Argo data with the climatology and the status of these alarms that were all determined by human experts (who decided wether the alarm was true, and the data bad, or the alarms was false, and the data good). The idea was to reduce the time spent by operators at un-validating false alarms raised by the test, a significant fraction of their workload. We used a machine learning technic called random forest of decision trees for which a simple illustration is given [Figure 8.3A](#). For a given feature space (the decision making domain) the decision tree is a set of tests to determine in which category, or part of the domain, a set of features correspond. A forest of such decision trees is used to make predictions robust. Our preliminary results where very encouraging and help us moved further.

As part of the H2020 MOCCA (Monitoring the Oceans and Climate Change with Argo) and E-ARISE (Euro-Argo Research Infrastructure Sustainability and Enhancement) projects, I hired for 18 months (2018-2020) and supervised Sean Tokunaga, a research engineer in data science. As control procedures do not evolve significantly and mostly rely on comparisons with a climatology, our activities have been centered around the use of machine learning methods to (i) develop prediction models of the quality flag of Argo data, in real time and delayed mode and (ii) to develop disruptive quality control procedures.

Contribution highlight This work is still ongoing and not published yet. At this time, our main conclusions with regard to machine learning applied to QC are:

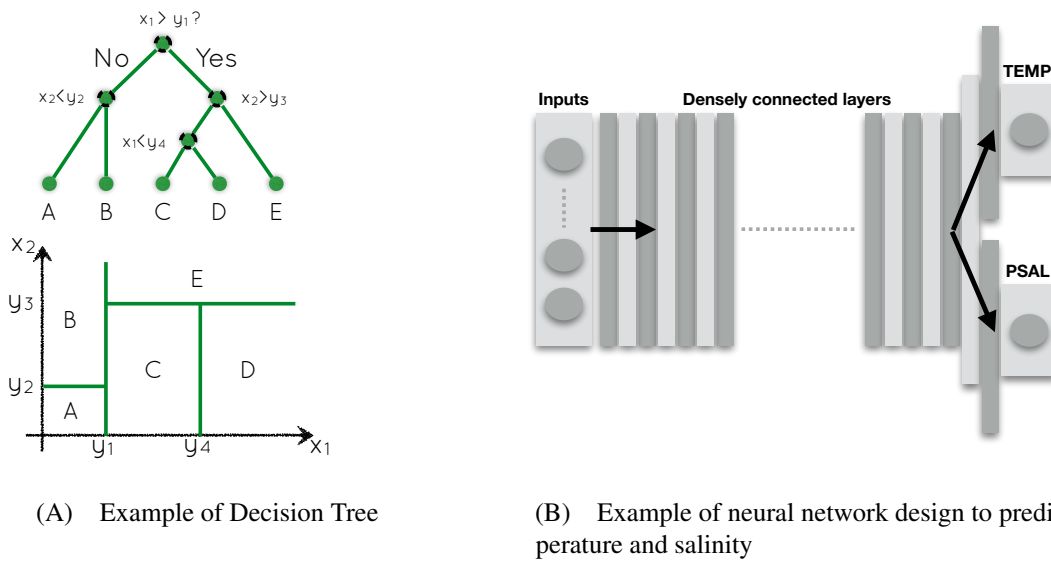


Figure 8.3: Machine learning techniques used to improve the Argo quality control procedure.

- to reduce workload after an automatic test, improving the test is a more effective solution than plugging a supervised classifier afterward (like a recommendation engine),
- instead of improving each tests, optimizing the sequence of tests could lead to much better true/false alarms,
- QC tests fall into 2 categories: those fixing technical issues and those comparing measurements to a reference climatology. To improve tests in the 1st category simply means improving decoders, to improve tests in the 2nd category requires a probabilistic approach whereby the test outcome is not binary (data good or bad) but a probability that the ocean water parcel could have, indeed, of that property value.
- Comparison to the climatology nails down to looking for "ghost" sensors in past measurements that could be considered like additional sensors embarked on the float. These comparisons struggle when the "ghost" sensor approximation is bad. Therefore improving what is called a "reference" climatology is a new area of research to improve QC.

The 1st conclusion above is not a trivial one and it is built upon a thorough quantitative analysis of the existing dataset and procedures. It is primarily due to the fact that human operators never look a single measurement to validate it, they look at full water columns and all float profiles. Therefore, even for the best ever new QC test made on a single measurement basis, the operator work load cannot significantly be reduced.

A promising and perhaps most stimulating conclusion is the last point made above. This is the item we're working on actively. Our first approach is to develop a new predictor for the reference state against which measurements could be compared. This approach has been successful for biogeochemical variables (Sauzède et al., 2015, e.g.). To do so, we are developing an ensemble of moderately deep neural networks, Figure 8.3B, to predict temperature and salinity anywhere in the ocean. The model is trained using all Argo data and AVISO surface altimetry. Preliminary results are again very encouraging and were reported for the 1st time during the 7th Euro-Argo Science Workshop in Athens in October 22-23rd, 2019 (Tokunaga and Maze, 2019b).

Technology readiness

The Argo array largely depends on a single CTD manufacturer: SeaBird. This monopoly position has benefited the Argo array during its development phase because it needed a reliable manufacturer willing to invest into a network that was not yet a success. This phase is over and Argo is now trying to sustain its historical, or

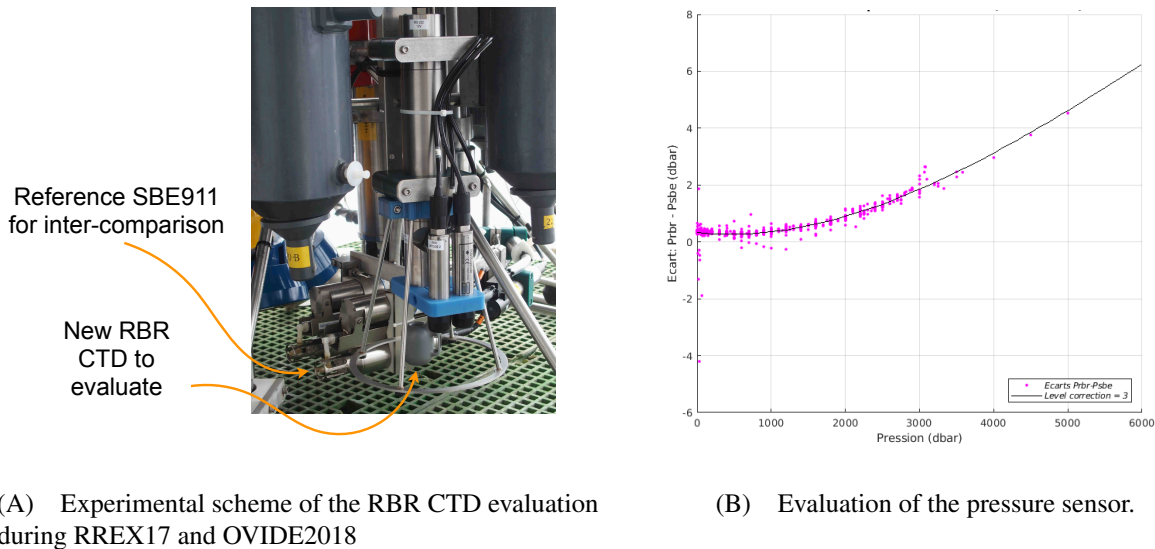


Figure 8.4: Evaluating a new CTD for the long-term sustainability of the Argo array.

"core" mission over a very long run. Breaking the SeaBird monopoly is now a key ingredient to the long term sustainability of the Argo network; recent and several issues found on the SeaBird CTDs furthermore stretching this point. However, the diversification of CTD models is conditioned by the ability of new suppliers to provide reliable and accurate sensors, up to Argo scientific standards. RBR, a Canadian company is the most serious candidate today.

Contribution highlight Since 2017, I work on the diversification of CTD sensors available to the Argo network for its long term sustainability. I deployed a new CTD manufactured by RBR, both for the core and deep Argo mission, during 2 oceanographic campaigns (RREX17 and OVIDE18) and evaluated its performances using comparison with a reference SBE911 mounted on the rosette. My contribution is to perform these evaluations and to communicate results with the manufacturer who improve its CTD quality through revised models of its sensor.

During the RREX17 cruise that took place in the North Atlantic in summer 2017 (Thierry, 2017), I supervised the LOPS technical group who managed to mount the RBRargol6000 CTD on the rosette near the SBE911 for 125 stations. The design of the experiment is shown Figure 8.4A. The RBRargol6000 CTD is a candidate for the Deep-Argo extension in test phase. The RBRargol6000 CTD performed well and reported data for all casts.

Due to specific preparation of the CTD for this experiment (addition of two oxygen sensors on the same logger as the CTD), some un-expected issues came to complicate the analysis of the data: spiking in the pressure and temperature channels and irregular sampling frequencies. A significant work was thus necessary to clean up and correct the data time series before evaluation. Once corrected, the data were compared against the SBE911 (pressure, temperature, conductivity) and bottle chemical measurements (salinity, oxygen) during the upcast and downcast. We found the RBR pressure to be within the initial accuracy of 3db but having a systematic bias dependent on time as shown Figure 8.4B.

The RBR temperature bias shows an unexpected large scatter that is probably due to the pre-processing of the data, more work has to be done to clarify this. Note however that the downcast RBR temperature bias against the SBE911 is nearly within the initial accuracy of 0.002°C with a very small pressure dependence. The RBR conductivity, once corrected for static pressure and temperature and dynamic temperature effects is almost within 0.01mS/cm accuracy. But the RBR conductivity and salinity, present a systematic non-linear

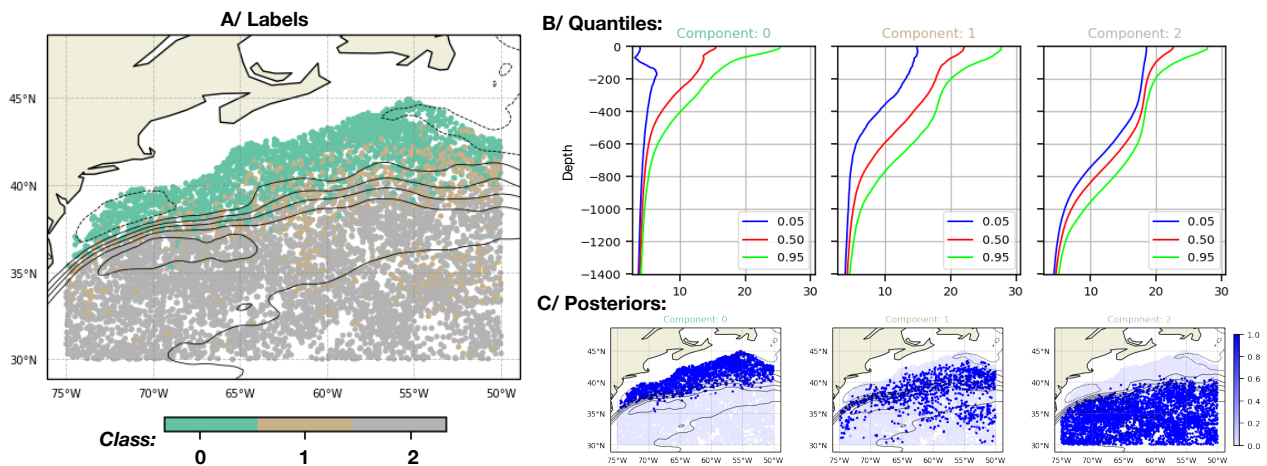


Figure 8.5: Using new machine learning technics to improve information retrieval from the Argo array. Example of a PCM analysis of Argo data in the Gulf Stream Extension Region (see [section 7](#) for more details on PCM). A PCM with $K=3$ classes is fitted on temperature and salinity profiles from the surface down to 1400m depth. Resulting labels are shown in plot A (contours are mean SSH from AVISO) and their vertical structure in plot B. Plot C shows the probability of each profile to belong to a given class. Note how a PCM is able to distinguish profiles located in the warm vs cold flank of the GS, *without using SSH data*.

pressure dependent bias. It can be corrected for this particular sensor. More technical corrections due to the specific electronics of this CTD should be done. In summer 2018 another RBRargol6000 CTD, along with a SBE61 were mounted on a rosette for a couple of CTD casts during the OVIDE18 cruise deepest stations (>4000db). These new data allowed us to determine if the bias observed during the RREX17 experiment were truly systematic, and hence correctable. That was indeed the case for the pressure and salinity data. Analysis was reported to the manufacturer who is still working on improving its sensor. Also in 2018, a triple CTD Deep-Arvor float was tested (RBRargol6000, SBE41CP/7000 and SBE61) but only the electronic of the float was evaluated. Full deployment of the float should take place in 2020. In 2019, we also started the design of a Deep-Arvor and an Arvor equipped with the RBRargo OEM model on the tap, as part of the EA-RISE project. Early deployments of prototypes are expected in 2020 or 2021.

Western Boundary Currents

Western Boundary Currents extensions are turbulent regions where the core Argo sampling of 1 profile per 3×3 every 10 days is not sufficient to resolve the dominant mesoscale dynamic. This simply means that there won't be enough Argo observations to interpolate a 3D thermohaline structure with mesoscales (50 to 200km). The main consequence of this lack of data, is that ocean analysis and re-analysis are poorly constrained in these regions, which gives rise to large (representativity) errors. The recommended strategy of the Argo network to try to tackle this problem is to double the density of profiles in WBC. This has been done by Japan for the Kuroshio region. Although mapping errors were reduced, the amplitude of the reduction was not very large. So, the additional cost of doubling the observation density in these regions may not necessarily be worth it scientifically. Or to put differently, the return on investment is poor.

Therefore, it is of primary importance to try to improve the use of existing Argo observations in WBC, by improving information extracted from existing Argo and by developing multi-observing systems synergy.

Using the PCM method ([Maze, 2017](#)), it is possible to assess the representativeness of Argo profiles within the turbulent context of WBC regions (e.g. if the float is within a cold/warm eddy, the WBC front, a meander). Indeed, if a PCM is asked to identify 3 clusters in a WBC, it will naturally capture the vertical structures of the warm and cold flank of the WB, but also the "fuzzy" profiles in the frontal region. This is illustrated [Figure 8.5](#). The component 0 class captures the cold flank structure (see how the spread is limited to



Figure 8.6: Promotion of the Argo new mission toward the deep ocean in front of the G7 parliament's presidents, during their annual meeting held in Brest in September 2019. [See Euro-Argo news brief.](#)

the surface and capturing the local seasonality of the mixed layer). The component 2 class captures the warm flank structure (see the small spread near the EDW mode water around 300m/18°C, and larger spread at the permanent pycnocline depth around 700m). And component 1 class captures all the other possible profiles in the region, which, in this case, account for all the "fuzzy" profiles in frontal regions associated with meanders.

This classification can then be used to derive new metrics of the WBC variability, for instance one can determine the heat content for the warm flank reservoir only, and it won't be biased by an eulerian approach that can't account for a change in the Gulf Stream position for instance.

Last, I will note that these new information can be combined with complementary data from other observing platforms (e.g. altimetry, XBT, satellite sea surface temperature) using mapping methods (e.g.: optimal interpolation) in order to develop a new ocean dataset describing the WBC state and its variability with better accuracy and resolution than existing products. I develop this methodology for the Gulf Stream and it will be distributed to the other participants of the EA-RISE project to be applied in other BC regions and create a complete new dataset dedicated to the monitoring of BC. Analysis has started with the co-supervision of 3 internships at IMT-A, among which one has already produced a conference paper ([Cosne et al., 2019](#)).

Extending Argo toward the deeper ocean

Deep-ocean (> 2000 m) hydrographic observations are limited to sparse shipboard hydrographic sections repeated every decade and short-lived moored arrays of confined spatial coverage. Upper-ocean (< 2000 m) sampling, largely carried out by the Argo array, has much higher resolution in space and time. The need for more intensive sampling in the deep ocean has been widely recognized by the scientific community ([de Lavergne et al., 2016](#); [Roemmich et al., 2019](#)). The development of deep profiling Argo floats, a new generation of autonomous instruments capable of diving and recording temperature and salinity down to 4000 to 6000 m depth, has been achieved over the last 10 years ([Le Reste et al., 2016](#)). The Argo community is now looking to secure fundings in order to ramp up toward a global coverage of deep floats.

In 2015, I co-organized the first Deep Argo Workshop ([Zilberman and Maze, 2015](#)) to initiate science and implementation planning for a global Deep Argo array, to satisfy broad-scale requirements for measurement of temperature, salinity, and ocean circulation and for combination with other observing system technologies that will complement the float array's large-scale attributes. The workshop allowed for the development of arguments to:



Figure 8.7: The VAIMOS drone: a basis for an un-manned surface vehicle aiming to autonomously deploy and recover Argo floats.

1. articulate key scientific issues for Deep Argo: (i) closing the heat, freshwater, and sea level budgets, (ii) characterizing decadal variability in deep ocean water masses, (iii) estimating the mean and decadal variability in deep ocean circulation including meridional overturning circulations;
2. determine sampling requirements to achieve Deep Argo objectives;
3. refine plans for the deployments of Deep Argo pilot arrays;
4. promote international collaboration within the Deep Argo community.

Since then, I promoted the deployment of deep floats at the highest political level, see [Figure 8.6](#) but also through H2020 project funding search (EA-RISE/WP3) and my involvement into the evaluation of the CTD sensors for the deep array (see [8](#)).

Final Remarks

I had the amazing opportunity to enter the Argo-France community in 2012, at a time when key projects were already underway (Equipex/NAOS and ERC/REMOCEAN) to develop the new generation of Argo floats. In 2014, the ERIC Euro-Argo was started and a motivated group was being built. Evolving with responsibilities within this community, at the national, European and global level has been amazing and a great learning experience. Year after year, I progressively identified what I wanted to be my added value to a system legacy that was nearly 20 years old:

- an easier end user access to Argo data (eg: the NAARC web API and Standard Depth Levels products)
- a fresh look at the QC organization (eg: machine learning, online collaborative tools)
- and a repeated concern with regard to the environmental impact and constantly increasing societal demand for a responsible approach of ocean observations (eg: can we trash Argo floats for ever to the bottom of the ocean ?)

With regard to this later point, I want to mention that in 2019 I have initiated what will probably be a long-term project aiming at using un-manned surface vehicles to deploy and recover Argo floats. Recovering Argo floats will allow our community to address the issue of the long-term sustainability of ocean observations. This possibility has furthermore scientific and economic motivations: recovering floats will allow for the post-calibration of sensors (thus improving the dataset quality) and allow for the possible re-fitting of very expensive biogeochemical sensors. Several un-manned surface vehicles design are possible. At this time, we

are experiencing ideas with the VAIMOS sailing drone that was developed at Ifremer a few years ago (see Fig. 8.7).



9. Future work

I am in the early years of a large H2020 project (EA-RISE), so my plan over the next 2 to 3 years is first of all, to fully manage and contribute to the ambitious working plan of this project focusing on improving the core Argo mission. Scientifically, this project will take me to a much deeper analysis of the Western Boundary Currents variability (a postdoc will arrive to work me with in 2021), so below I develop a little bit more this item. However, I obviously don't want to stop the constant flow of ideas and opportunities, so I will also develop two projects for the short and medium term that I'd like to push along.

Content of this chapter:

A new perspective on Western Boundary Currents variability	98
Projected EDW variability	99
Optimal Control of Ocean Observing Systems	100

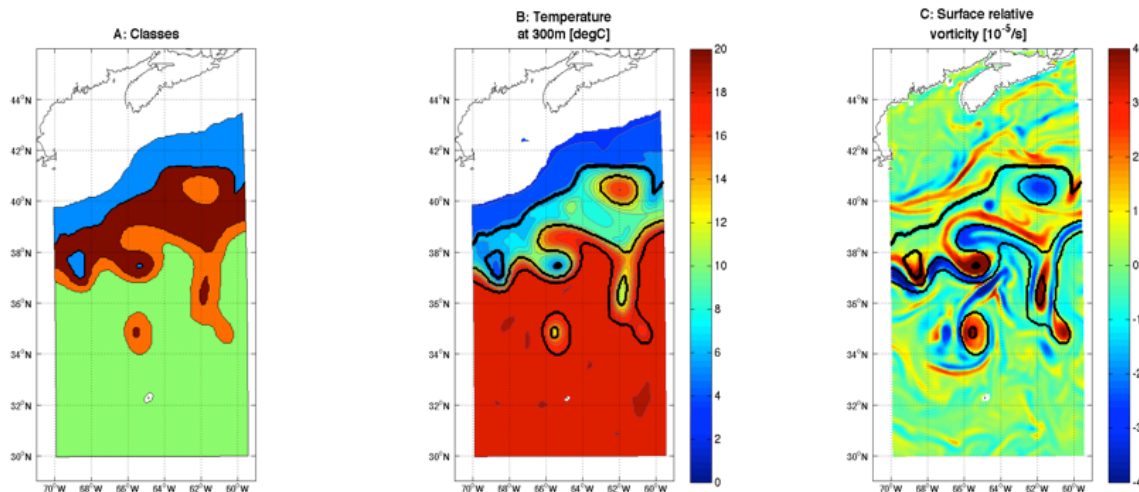


Figure 9.1: Demonstration with a 5-day averaged model output (1/12o resolution) that un-supervised classification of profiles can distinguish the Gulf Stream front from flank waters and mesoscale eddies. A: 4 different classes of profiles obtained with the [Maze et al. \(2017c\)](#) PCM method, B-C: temperature and surface relative vorticity superimposed with class contours (black). We will investigate how this innovative method applied to historical in-situ profiles can help our detection of low-frequency changes in turbulent WBC regions.

A new perspective on Western Boundary Currents variability

Assessing the robustness and reliability of ocean changes is a key challenge that is classically tackled using inter-comparison of ocean re-analysis products. But this approach cannot overcome the limitation arising from the coarse resolution, both horizontal and vertical, of all existing re-analysis products ([Balmaseda et al., 2015](#), e.g. usually 1x1 degree, 1/4 at best, see). This is particularly an obstacle for frontal systems where such horizontal resolution does not allow a proper representation of fine thermohaline ocean structures.

A preeminent frontal system found in all subtropical gyres is the Western Boundary Current (WBC, the Gulf Stream for the NASTG). WBC are thought to be "hot spots" of the low frequency climate signal and some studies suggest their poleward shift and increased intensity over 1900-2008 ([Wu et al., 2012](#); [Yang and San Liang, 2016](#)). However, these secular trends remain uncertain because of the above-mentioned dataset limitations that impede their robust detection and understanding. For instance, it is particularly difficult to distinguish a local warming trend driven by a northward meridional shift or increased transport of the WBC that steepens the isopycnal slopes from a water mass warming. One objective of this project would be to develop a novel approach to extract information about WBC systems variability from direct in situ observations to specifically tackle this issue.

This approach will be based on the PCM ([Maze et al., 2017c](#)) methodology whereby profiles are clustered according to their similarities in temperature, salinity or density. [Figure 9.1](#) illustrates the method for the Gulf Stream Extension region. It shows from an eddy resolving simulation how the classification technique can make the distinction possible between profiles located within eddies from those within the front or located on either equatorward or poleward flanks of the Gulf Stream. Compared to classic methods relying on coarse resolution gridded dataset, this method has the strong advantage to make direct use of observed profiles and to not rely on objective mapping.

Time series of ocean properties for each classes (e.g. heat content, volume, surface, temperature/density profile statistics - mean/std profile of a class at a given time) can be derived to determine the WBC variability from a completely new and totally objective perspective. This should allow us to discriminate diabatic water mass changes (e.g. from typical profiles of class located on the WBC flanks) from adiabatic advective changes (e.g. from the volume and typical profiles of the class associated with the frontal region) and to determine eddy statistic property changes (e.g. from surface of class associated with eddies), all together leading to

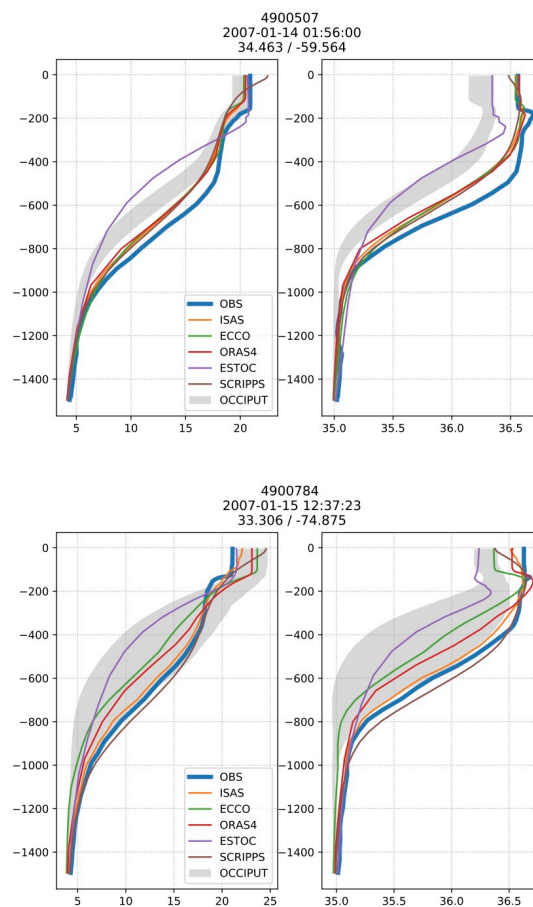


Figure 9.2: Illustration of the OCCIPUT ensemble spread (grey shading) interpolated onto the location of two Argo profiles (blue curve) in the Northern Sargasso Sea. Other ocean state products interpolation at these location are shown (colored curves).

expected major steps in our understanding of WBC systems.

Moreover, it is known that the Gulf Stream is a source of variability for its southern recirculation region and most notably the low-PV EDW water mass (Dong and Kelly, 2004; Lee, 2020). But some studies have shown in idealized configurations that EDW may generate its own low frequency variability from instabilities of the mean flow (Hazeleger and Drijfhout, 2000). To better determine the chaotic variability of the EDW is thus key to a better understanding of the GSE. To do so, we will use data from the OCCIPUT (OceanIC Chaos – ImPacts, strUcture, predicTability) project that performed a long (1960–2015), large ensemble (50 members) of global ocean/sea ice $1/4^\circ$ simulations driven by the same atmospheric reanalysis, but with perturbed initial conditions. Figure 9.2 gives an illustration of the OCCIPUT ensemble spread interpolated onto the location of two Argo profiles in the Northern Sargasso Sea. We will complement the WBC system description given above with a PCM analysis of the OCCIPUT ensemble spread that will lead to a better characterization of the chaotic component of the EDW variability. The primary goal here is to better distinguish the chaotic from the directly forced variability of the EDW, and more generally GSE system.

Projected EDW variability

In the LEFE/SOMOVAR project I addressed the question of the historical interannual-to-decadal variability of the North Atlantic subtropical gyre (NATSG). My first short-term project will be to analyze the newly

available CMIP6 simulations in order to study from RCP projections the expected fate of the EDW in the future.

Future climate scenarios show an increase in global ocean stratification that is mainly driven by the pronounced warming at the surface ocean (Levitus et al., 2012; Wang et al., 2015). Stratification is a natural "stressor" for the ocean life activity, mostly because it impacts the nutrient supply in the euphotic layer, both through seasonal and permanent pycnoclines (Jenkins and Doney, 2003; Bopp et al., 2013). Stratification changes in climate models are determined using density differences between a surface and a given level at depth (Matear and Hirst, 2003, e.g.) and specific stratification features, such as the pycnocline, are approximated by isopycnal or isothermal surfaces (Wang et al., 2015). As illustrated earlier Figure 2.11, such an approach has serious limitations and uncertainties: the complexity of the processes involved in the evolution of stratification may be different if the local density derivative is considered, compared to iso-tracer surfaces (Wang et al., 2009). Vertical resolution in climate models is generally very coarse and could preclude a good representation of the stratification processes; for instance, in the CNRM-CM and IPSL-CM suite of models, their CMIP5 version had only 42 and 31 vertical levels respectively. Dong and Kelly (2013) have shown how the EDW variability is poorly represented in CMIP5 models because of the low vertical (and horizontal) resolution. In their new version developed for CMIP6, 75 levels are used instead, allowing for a better representation of the vertical structure and processes.

In this short-term project, I will for instance use OACP to diagnose the NATSG stratification and to answer the following questions:

- How the STMW and permanent pycnocline mean and variability are represented in CNRM-CM5 vs CM6 configuration in historical simulations ?
- How the stratification and associated processes are projected to change under different climate scenarios?

Optimal Control of Ocean Observing Systems

As evoked in section 8, I started in 2019 a reflection around the opportunity to develop a surface drone that would be able to deploy and recover Argo floats. In fact, before this technological application of a drone, I was thinking about the different possible ways to optimize observations information retrieval. That first lead to the WBC/EDW new perspective developed above section 9 and later to the idea that I will now layout.

Systematically observing the ocean has been a technological challenge that is on the verge of being tackled, thanks to the ground breaking successful development of autonomous platforms like Argo floats, gliders and other surface drones. However, the size of Observing Systems based on operational fleets of these platforms is limited, both by resources (direct funding and man power) and by societal risks (security and environmental impact).

Since we won't be able to fund and manage fleets of such platforms with an ever increasing size (and this would not be justifiable to the society in terms of environmental impact), the technological challenge has now become a statistical one: **how to make the most out of a limited set of observations ?**

This question is tightly linked to two statistical problems:

1. how to assimilate more efficiently a limited set of observations ?
2. how to control in real time an observing system ?

These problems are strongly tied to each others because solving one does make sense only if the other is solved as well. Controlling an observing system is useful only if we know the target, and determining this target makes sense only if we can indeed control the observing system.

The overarching goal of this project would be to reduce uncertainties in ocean state estimates in the most turbulent regions of the ocean, a requirement for EOY delivery.

Up to now, data assimilation has been used to determine the impact of a given observing system, and for "random" systems, like Argo, this was limited to the random space/time density of possibly available observations. The question this project aim to answer is fundamentally different, it reads: the quantity of observations is limited (eg: 10 profiles per week in this region, or one glider transect), where these observations must be acquired to maximize their impact on the analysis quality ?

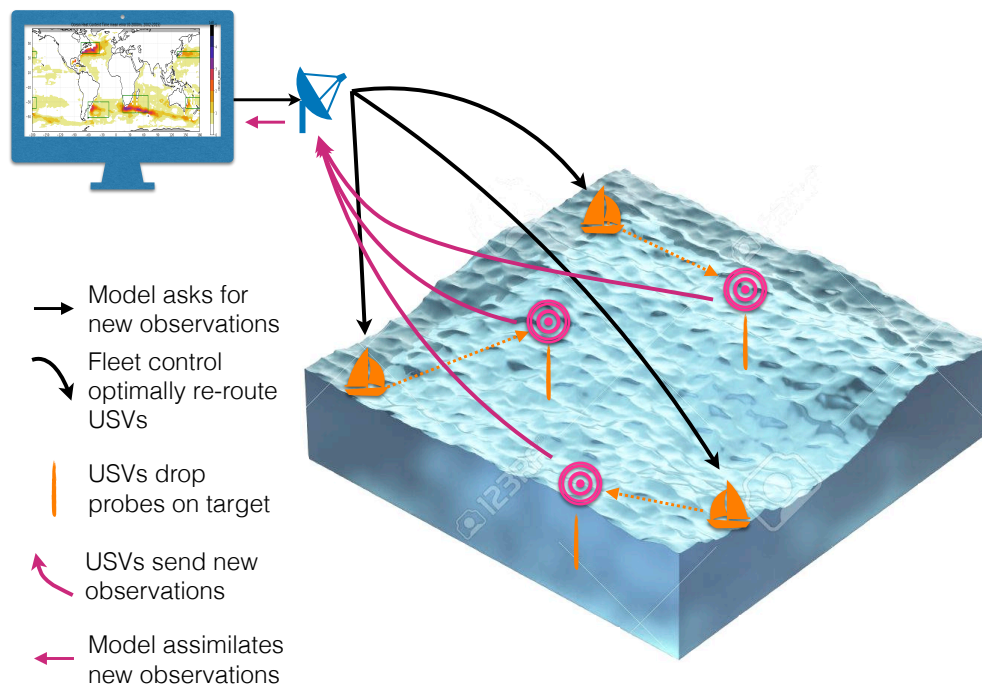


Figure 9.3: Schematic representation of a use-case scenario whereby a fleet of USV is remotely controlled by a data assimilation model and forecasting system. It is the model that is able to determine automatically where observations are needed to reduce forecast errors. The typical USV speed is about $3/4kt$, i.e. $6km/h$, meaning that the half/day covered distance is around 70 km.

In this project, we would aim to answer these problems through an innovative combination of statistical approaches and technological developments.

We will create observing systems simulators and use dynamical systems approach with artificial intelligence (eg: deep reinforcement learning) to determine:

- where a limited amount of observations should be localized to minimize the analysis misfit
- how to control from the ground, a fleet of autonomous platforms

It is important to note that the potential of existing observing platforms to be controlled in real-time depends on our ability to predict the trajectory of passive tracers transported by turbulent and chaotic ocean currents. Although ground breaking advances fostered by artificial intelligence will be made during the project with regard to this issue, it is sound to conduct parallel technological developments to complement the existing sets of autonomous observing platforms with fully controllable platforms.

In this project, we will thus develop an observing platform from a surface sailing drone (unmanned surface vehicle, USV) that will carry a collection of sensors for surface observations and more importantly have the ability to deploy profiling devices on demand (Eg: XBT, XCTD, Argo floats). It is important to note that the baseline for such a USV has already been developed at LOPS (VAIMOS project, see Fig.8.7) and that in this project we would take it to another level by making it suited for the open ocean and by adding the ability to deploy profiling devices on demand (eg: increase payload of the USV). A longer-term objective would be for the USV to recover Argo floats when and if necessary.

A typical use-case scenario, illustrated Figure 9.3 of this project would be:

- an assimilating system determines where in situ informations are required in order to best resolve the 3-dimensional structure of the ocean in a given region,
- the ground control system of autonomous platforms determines how USVs can be re-routed to optimal

sampling locations, and order them to do so,

- once USVs are on site, they collect required variables: surface measurements and/or interior data obtained by automatic release of a profiling probe (e.g. XBT or XCTD).



10. Appendix

Here after:

- my CV
- a nearly exhaustive list of my scientific production.

CV Guillaume Maze

Laboratoire d'Océanographie
Physique et Spatiale
IFREMER, Bât. 611
B.P. 70, 29280 Plouzané
FRANCE

gmaze@ifremer.fr
Tél: +33 2 98 22 43 39

<http://annuaire.ifremer.fr/cv/17182/>

ORCID: 0000-0001-7231-2095

Resarcher-ID: B-5247-2008

Expériences professionnelles

Chercheur, Ifremer; Brest – 2012-présent

Laboratoire d'Océanographie Physique et Spatiale, équipe Océan et Climat.

Dynamique océanique subtropicale et systèmes d'observations globaux.

Mots-clés: Subtropicale, climat, analyse de données, Argo

Postdoctorant, Ifremer; Brest – 2011-2012

Mots-clés: Analyse de données in situ, Argo

Postdoctorant, GIS Europôle Mer – 2009-2010

Mots-clés: Analyse de données in situ, méthodes inverses d'optimisations non linéaires

Postdoctorant, Massachusetts Institute of Technology – 2006-2008

Mots-clés: Analyse de simulations numériques réalistes, assimilation de données

Responsabilités

Niveau Internationale

Membre du comité de pilotage de l'ERIC Euro-Argo (>2017)

Membre du Conseil Exécutif de l'équipe de direction internationale Argo (>2013)

Niveau Nationale

Président du Conseil Scientifique CNRS LEFE/GMMC (>2020)

Coordinateur national du programme Argo-France (>2014)

Membre du Conseil Scientifique et du bureau CNRS LEFE/IMAGO (2017-2019)

Niveau Local

Membre du Conseil d'Administration de l'IUEM (>2013)

Membre du Groupe de Travail "Données" de Datarmor (>2016)

Responsable de l'axe transverse "Données" LOPS (2016-2019)

Membre du Conseil Scientifique du LOPS (2016-2019)

Diplômes

Habilitation à Diriger des Recherches : Université Bretagne Occidentale, Brest, 2020

Titre: Structure et variabilité du gyre subtropical

Doctorat : Université Pierre et Marie-Curie, Paris, 2006

Directeurs de thèse: Alain Colin de Verdière (Professeur, UBO) et Fabio D'Andrea (CNRS)

Titre: Interactions basses fréquences océan-atmosphère dans l'océan Austral

DEA : Université de Bretagne Occidentale, Brest, 2002

Océanographie, Météorologie et Environnement

Maîtrise : Université de Toulon et du Var, Toulon, 2001

Physique et Applications, mention Océan-Atmosphère

Licence : Université de Toulon et du Var, Toulon, 2000

Physique et Applications, mention Océan-Atmosphère

DEUG : Université Bordeaux I, Bordeaux, 1999

Sciences de la matière

Researcher ID: <http://www.researcherid.com/rid/B-5247-2008>

Orcid ID: <https://orcid.org/0000-0001-7231-2095>

Page web personnelle: <https://annuaire.ifremer.fr/cv/17182>

Articles type ACL

ACL: *Articles dans des revues internationales ou nationales avec comité de lecture répertoriées par l'HCERES ou dans les bases de données internationales*

1. Stevens Samuel W. and R. J. Jonhson and Guillaume Maze and Nicholas R. Bates (2020). **A recent decline in North Atlantic Subtropical Mode Water Formation**. *Nature Climate Change*. ACCEPTED.
2. Rosso, Isabella and Mazloff, Matt and Lynne D. Talley and Purkey, Sarah and Freeman, Nathalie and Maze, Guillaume (2020). **Water Mass and Biogeochemical Variability in the Kerguelen Sector of the Southern Ocean: A Machine Learning Approach for a Mixing Hotspot**. *Journal of Geophysical Research: Ocean*. IN PRESS. <https://doi.org/10.1029/2019JC015877>
3. Feucher Charlene, Maze Guillaume, Mercier Herle (2019). **Subtropical Mode Waters and Permanent Pycnocline properties in the World Ocean**. *Journal of Geophysical Research: Ocean*, 142(2), 1139-1154. Publisher's official version : <https://doi.org/10.1029/2018JC014526> , Open Access version : <https://archimer.ifremer.fr/doc/00480/59176/>
4. Desbroyères, D. G. and Mercier, H. and Maze, G. and Daniault, N. (2019). **Surface predictor of overturning circulation and heat content change in the subpolar North Atlantic**. *Ocean Sci.*, 15, 809–817, <https://doi.org/10.5194/os-15-809-2019>
5. Roemmich Dean, Alford Matthew H., Claustre Hervé, Johnson Kenneth, King Brian, Moum James, Oke Peter, Owens W. Brechner, Pouliquen Sylvie, Purkey Sarah, Scanderbeg Megan, Suga Toshio, Wijffels Susan, Zilberman Nathalie, Bakker Dorothee, Baringer Molly, Belbeoch Mathieu, Bittig Henry C., Boss Emmanuel, Calil Paulo, Carse Fiona, Carval Thierry, Chai Fei, Conchubhair Diarmuid Ó., D'ortenzio Fabrizio, Dall'olmo Giorgio, Desbroyeres Damien, Fennel Katja, Fer Ilker, Ferrari Raffaele, Forget Gael, Freeland Howard, Fujiki Tetsuichi, Gehlen Marion, Greenan Blair, Hallberg Robert, Hibiya Toshiyuki, Hosoda Shigeki, Jayne Steven, Jochum Markus, Johnson Gregory C., Kang Kiryong, Kolodziejczyk Nicolas, Körtzinger Arne, Traon Pierre-Yves Le, Lenn Yueng-Djern, Maze Guillaume, Mork Kjell Arne, Morris Tamaryn, Nagai Takeyoshi, Nash Jonathan, Garabato Alberto Naveira, Olsen Are, Pattabhi Rama Rao, Prakash Satya, Riser Stephen, Schmechtig Catherine, Schmid Claudia, Shroyer Emily, Sterl Andreas, Sutton Philip, Talley Lynne, Tanhua Toste, Thierry Virginie, Thomalla Sandy, Toole John, Troisi Ariel, Trull Thomas W., Turton Jon, Velez-Belchi Pedro Joaquin, Walczowski Waldemar, Wang Haili, Wanninkhof Rik, Waterhouse Amy F., Waterman Stephanie, Watson Andrew, Wilson Cara, Wong Annie P. S., Xu Jianping, Yasuda Ichiro (2019). **On the Future of Argo: A Global, Full-Depth, Multi-Disciplinary Array** . *Frontiers In Marine Science* , 6(439), 28p. Publisher's official version : <https://doi.org/10.3389/fmars.2019.00439> , Open Access version : <https://archimer.ifremer.fr/doc/00509/62043/>
6. Penduff Thierry, Serazin Guillaume, Leroux Stephanie, Close Sally, Molines Jean-Marc, Barnier Bernard, Bessieres Laurent, Terray Laurent, Maze Guillaume (2018). **Chaotic Variability of Ocean: Heat Content Climate-Relevant Features and Observational Implications**. *Oceanography*, 31(2), 63-71. Publisher's official version : <https://doi.org/10.5670/oceanog.2018.210> , Open Access version : <https://archimer.ifremer.fr/doc/00448/55959/>
7. Maze Guillaume, Mercier Herle, Fablet Ronan, Tandeo Pierre, Radcenco Manuel Lopez, Lenca Philippe, Feucher Charlene, Le Goff Clement (2017a). **Coherent heat patterns revealed by unsupervised classification of Argo temperature profiles in the North Atlantic Ocean**. *Progress In Oceanography*, 151, 275-292. Publisher's official version : <https://doi.org/10.1016/j.pocean.2016.12.008> , Open Access version : <https://archimer.ifremer.fr/doc/00363/47431/>
8. Feucher Charlene, Maze Guillaume, Mercier Herle (2016). **Mean structure of the North Atlantic subtropical permanent pycnocline from in-situ observations**. *Journal Of Atmospheric And Oceanic Technology*, 33(6), 1285-1308. Publisher's official version : <https://doi.org/10.1175/JTECH-D-15-0192.1> , Open Access version : <https://archimer.ifremer.fr/doc/00326/43710/>
9. De Lavergne Casimir, Madec Gervan, Capet Xavier, Maze Guillaume, Roquet Fabien (2016). **Getting to the bottom of the ocean**. *Nature Geoscience*, 9(12), 857-858. Publisher's official version : <https://doi.org/10.1038/ngeo2850> , Open Access version : <https://archimer.ifremer.fr/doc/00359/46988/>
10. Capet Xavier, Rouillet Guillaume, Klein Patrice, Maze Guillaume (2016). **Intensification of upper ocean submesoscale turbulence through Charney baroclinic instability**. *Journal Of Physical Oceanography*, 46(11), 3365-3384. Publisher's official version : <https://doi.org/10.1175/JPO-D-16-0050.1> , Open Access version : <https://archimer.ifremer.fr/doc/00347/45785/>
11. Le Reste Serge, Dutreuil Vincent, Andre Xavier, Thierry Virginie, Renaut Corentin, Le Traon Pierre-Yves, Maze Guillaume (2016). **“Deep-Arvor”: A new profiling float to extend the Argo observations down to 4000m depth**. *Journal Of Atmospheric And Oceanic Technology*, 33(5), 1039-1055. Publisher's official version : <https://doi.org/10.1175/JTECH-D-15-0214.1> , Open Access version : <https://archimer.ifremer.fr/doc/00318/42969/>

12. Riser Stephen C., Freeland Howard J., Roemmich Dean, Wijffels Susan, Troisi Ariel, Belbeoch Mathieu, Gilbert Denis, Xu Jianping, Pouliquen Sylvie, Ann Thresher, Le Traon Pierre-Yves, Maze Guillaume, Klein Birgit, Ravichandran M., Grant Fiona, Poulain Pierre-Marie, Suga Toshio, Lim Byunghwan, Sterl Andreas, Sutton Philip, Mork Kjell-Arne, Joaquin Velez-Belch Pedro, Ansorge Isabelle, King Brian, Turton Jon, Baringer Molly, Jayne Steven R. (2016). **Fifteen years of ocean observations with the global Argo array.** *Nature Climate Change*, 6(2), 145-153. Publisher's official version : <https://doi.org/10.1038/NCLIMATE2872>, Open Access version : <https://archimer.ifremer.fr/doc/00310/42106/>
13. Rouillet Guillaume, Capet Xavier, Maze Guillaume (2014). **Global Interior Eddy Available Potential Energy Diagnosed from Argo Floats.** *Geophysical Research Letters*, 41(5), 1651-1656. Publisher's official version : <https://doi.org/10.1002/2013GL059004>, Open Access version : <https://archimer.ifremer.fr/doc/00175/28579/>
14. Cerovecki Ivana, Talley Lynne D., Mazloff Matthew R., Maze Guillaume (2013). **Subantarctic Mode Water Formation, Destruction, and Export in the Eddy-Permitting Southern Ocean State Estimate.** *Journal Of Physical Oceanography*, 43(7), 1485-1511. Publisher's official version : <https://doi.org/10.1175/JPO-D-12-0121.1>, Open Access version : <https://archimer.ifremer.fr/doc/00154/26487/>
15. Maze Guillaume, Deshayes Julie, Marshall John, Treguier Anne-Marie, Chronis Alexandros, Vollmer Lukas (2013). **Surface vertical PV fluxes and subtropical mode water formation in an eddy-resolving numerical simulation.** *Deep-sea Research Part ii-topical Studies In Oceanography*, 91, 128-138. <https://doi.org/10.1016/j.dsr2.2013.02.026>
16. Maze Guillaume, Mercier Herle, Thierry Virginie, Memery Laurent, Morin P., Perez F.F. (2012). **Mass, nutrient and oxygen budgets for the northeastern Atlantic Ocean.** *Biogeosciences*, 9(10), 4099-4113. Publisher's official version : <https://doi.org/10.5194/bg-9-4099-2012>, Open Access version : <https://archimer.ifremer.fr/doc/00100/21101/>
17. Shuckburgh Emily, Maze Guillaume, Ferreira David, Marshall John, Jones Helen, Hill Chris (2011). **Mixed Layer Lateral Eddy Fluxes Mediated by Air-Sea Interaction.** *Journal Of Physical Oceanography*, 41(1), 130-144. <https://doi.org/10.1175/2010JPO4429.1>
18. Forget Gael, Maze Guillaume, Buckley Martha, Marshall John (2011). **Estimated seasonal cycle of North Atlantic Eighteen Degree Water Volume.** *Journal Of Physical Oceanography*, 41(2), 269-286. <https://doi.org/10.1175/2010JPO4257.1>
19. Maze Guillaume, Marshall John (2011). **Diagnosing the Observed Seasonal Cycle of Atlantic Subtropical Mode Water Using Potential Vorticity and Its Attendant Theorems.** *Journal Of Physical Oceanography*, 41(10), 1986-1999. <https://doi.org/10.1175/2011JPO4576.1>
20. Maze Guillaume, D'Andrea Fabio, Colin De Verdiere Alain, Klein Patrice (2011). **Stationary Atmospheric Responses to an Idealized Sea Surface Temperature Anomaly in the Southern Ocean.** *Journal Of Climate*, 24(14), 3686-3704. <https://doi.org/10.1175/2011JCLI3737.1>
21. Marshall J., Andersson A., Bates N., Dewar W., Doney S., Edson J., Ferrari R., Forget G., Fratantoni D., Gregg M., Joyce T., Kelly K., Lozier S., Lumpkin R., Maze Guillaume, Palter J., Samelson R., Silverthorne K., Skillingstad E., Straneo F., Talley L., Thomas L., Toole J., Weller R. (2009). **The CLIMODE field campaign. Observing the cycle of convection and restratification over the Gulf Stream system and the subtropical gyre of the North Atlantic Ocean.** *Bulletin - American Meteorological Society*, 90, 1337-1350. <https://doi.org/10.1175/2009BAMS2706.1>
22. Maze Guillaume, Forget Gael, Buckley Martha, Marshall John, Cerovecki Ivana (2009). **Using transformation and formation maps to study the role of air-sea heat fluxes in North Atlantic Eighteen Degree Water formation.** *Journal of Physical Oceanography*, 39, 1818-1835. Publisher's official version : <https://doi.org/10.1175/2009JPO3985.1>, Open Access version : <https://archimer.ifremer.fr/doc/00115/22647/>
23. Maze Guillaume, D'Andrea Fabio, Colin De Verdiere Alain (2008). **Correction to "Low-frequency variability in the Southern Ocean region in a simplified coupled model".** *Journal of Geophysical Research (JGR) - Oceans*, 113(C07008), 1-4. <https://doi.org/10.1029/2008JC004802>
24. Maze Guillaume, D'Andrea Fabio, Colin De Verdiere Alain (2006). **Low-frequency variability in the Southern Ocean region in a simplified coupled model.** *Journal of Geophysical Research (JGR) - Oceans*, 111(C05010), 1-14. <https://doi.org/10.1029/2005JC003181>
25. Maze Guillaume, Carton Xavier, Lapeyre Guillaume (2004). **Dynamics of a 2D vortex doublet under external deformation.** *Regular And Chaotic Dynamics*, 9(4), 477-497. <https://doi.org/10.1070/RD2004v009n04A-BEH000291>
26. Carton Xavier, Maze Guillaume, Legras B (2002). **A two-dimensional vortex merger in an external strain field.** *Journal Of Turbulence*, 3(45), 1-7. <https://doi.org/10.1088/1468-5248/3/1/045>

Articles type ASCL

ASCL: *Articles dans des revues sans comité de lecture*

1. Maze Guillaume, Mercier Herle, Cabanes Cecile (2017b). **Profile Classification Models.** *Mercator Ocean Journal*, (55), 48-56. Open Access version : <https://archimer.ifremer.fr/doc/00387/49816/>

2. Barnier B., Blaker A.T., Biatosch A., Böning C.W., Coward A., Deshayes Julie, Hirshi J., Le Sommer J., Madec G., Maze Guillaume, Molines J.M., New A., Penduff T., Scheinert M., Talandier Claude, Treguier Anne-Marie (2014). **DRAKKAR: developing high resolution ocean components for European Earth system models**. *CLIVAR Exchange*, 65 - 19(2), 18-21. Open Access version : <https://archimer.ifremer.fr/doc/00326/43698/>
3. Maze Guillaume (2012). **A new information and data mining tool for North Atlantic Argo Data**. *Mercator Ocean - CORIOLIS Quarterly Newsletter*, (45), 38-40. Open Access version : <https://archimer.ifremer.fr/doc/00114/22551/>

Communications sans actes (selection)

C-COM: Communications orales sans actes dans un congrès international ou national

1. Maze Guillaume and Kevin Balem and Thierry Penduff (2020). **North-Atlantic Ocean Subtropical Gyre: New perspective and mechanisms of low-frequency Variability**. Ocean Sciences Meeting, 16-21 Feb. 2020, San Diego, CA, USA.
2. G. Cosne and G. Maze and P. Tandéo (2019). **Coupling Oceanic Observation Systems to Study Mesoscale Ocean Dynamics**. NeurIPS 2019 Workshop « Tackling Climate Change with Machine Learning ». <https://arxiv.org/abs/1910.08573>
3. Odaka Tina, Banihirwe Anderson, Eynard-Bontemps Guillaume, Ponte Aurelien, Maze Guillaume, Paul Kevin, Baker Jared, Abernathy Ryan (2019). **The Pangeo Ecosystem: Interactive Computing Tools for the Geosciences: Benchmarking on HPC**. Proceedings of the SC'19 workshops - The International Conference for High Performance Computing, Networking, Storage, and Analysis. 17-22 Nov. 2019, Denver. pp.1-14.
4. Tokunaga Sean, Maze Guillaume (2019). **A brief update on Machine Learning of Argo (DM)QC**. 15th Euro-Argo Management Board. February 21-22, 2019, Hamburg.
5. Maze Guillaume, Balem Kevin, Odaka Tina, Queric Antoine (2018). **What was tried as data mining with spark on Datarmor**. 17th PCIM meeting. 2018/05/17.
6. Maze Guillaume (2018). **Ocean's (Big) Data Mining**. Séminaire SHOM. 2018/04/24, Brest.
7. Maze Guillaume, Thierry Virginie, Le Reste Serge, Hamon Michel, Branellec Pierre, Halverson Mark, Johnson Greg, Leconte Jean Michel, Taylor Jon, Zhang Rui (2018). **Preliminary evaluation of the deep RBRconcerto during the RREX17 cruise**. AST 1- 19th Argo Steering Team Meeting. March 12-15, 2018, Sidney, B.C., Canada.
8. Maze Guillaume, Cabanes Cecile, Lagadec Catherine, Tandéo Pierre, Perez Florent, Szekely Tanguy (2018). **Machine Learning of Argo QC**.
 1. ASW6 - 6th Argo Science Workshop "The Argo program in 2020 and beyond : Challenges and opportunities". October 22-24, 2018, Tokyo, Japan.
 2. 1st European Argo Delayed-Mode QC Workshop . 17-18 April 2018, Brest, France.
 3. AST-19 Meeting - 19th meeting of the International Argo Steering Team. 12 - 16 March 2018, Sydney-Victoria, Canada.
 4. ADMT-18 - eighteenth Argo Data Management Team meeting. 27 November - 1 December 2017, Hamburg, Germany.
9. Maze Guillaume (2017). **Profile Class Modelling. Introduction and Applications**. Data Science and Environment Workshop + Summer School. July 3-7th, Brest, France.
10. Maze Guillaume (2017). **In-situ ocean observations. An introduction. An example: the Argo network**. 1st Ocean Observers Workshop. 13-14 June 2017, Brest.
11. Le Bot Philippe, Maze Guillaume (2017). **Les APIs d'échange et mining de données**. Workshop NOUMEA. 31 Mai 2017, Brest, France.
12. Maze Guillaume, Mercier Herle, Feucher Charlene (2017). **ORCA025 representation of large-scale stratification features in the North-Atlantic**. DRAKKAR 2017 Annual Workshop. 16-18 January 2017, Grenoble.
13. Maze Guillaume, Cabanes Cecile (2016). **Un-supervised classification of in-situ T/S profiles to select appropriate reference in Delayed Mode validation procedure**. Argo-France workshop. 10th June 2016, Toulon, France.
14. Maze Guillaume, Kolodziejczyk Nicolas, Kermabon Catherine, Le Bot Philippe, Paul Frederic (2016). **Data analysis tools and data mining in ensemble of ocean re-analysis and climate models**. 16th PCIM meeting - Journée de rencontre des utilisateurs du PCIM "De CAPARMOR vers DATARMOR ". 30 septembre 2016, Ifremer.
15. Maze Guillaume, Mercier Herle, Feucher Charlene, Paul Frederic, Kermabon Catherine, Tandéo P, Fablet Ronan, Lenca P, Radcenco M., Le Goff C (2016). **Profile Class Modelling: Applications to Argo data**. 5ème reunion annuelle Projet NAOS. 21/09/2016, Villefranche sur Mer.
16. Maze Guillaume, Mercier Herlé, Feucher Charlène, Fablet Ronan, Lenca Philippe, Radcenco Manuel, Le Goff Clément (2016). **Ocean heat content structure revealed by un-supervised classification of hydrographic profiles**. 2016 Ocean Sciences Meeting. 21-26 Feb. 2016, New Orleans, Louisiana, USA.
17. Maze Guillaume, Mercier Herlé, Feucher Charlène, Fablet Ronan, Lenca Philippe, Radcenco Manuel, Tandéo Pierre, Le Goff Clément (2015). **Using Gaussian Mixture Model to characterize the North Atlantic climatology and variability or Ocean heat content structure revealed by un-supervised classification of hydrographic profiles**. 5th Euro-Argo User Meeting. 16-17 March 2015, Brest, France.

18. Maze Guillaume, Thierry Virginie (2014). **International Strategy: Argo-Deep**. 3rd NAOS annual meeting. 16-17 June 2014, Brest, France.
19. Cabanes Cecile, Maze Guillaume, Thierry Virginie, Lagadec Catherine (2013). **NA-ARC Activities**. ADMT14 - 14th Argo Data Management Meeting. Southampton, UK.
20. Maze Guillaume (2013). **Analyse de la structure verticale océanique à partir des données Argo**. Conférence "TIC et mer: nouveaux défis et solutions. Les technologies de l'information au service de la recherche marine". 26 Nov. 2013, Brest, France.
21. Maze Guillaume, Mercier Herle, Thierry Virginie (2013). **The main pycnocline of the Atlantic Ocean**. 4th Euro-Argo Science Meeting and Workshop on the Arctic and sub-Polar North Atlantic. June 18-20th, 2013, National Oceanographic Center, Southampton, U.K.
22. Maze Guillaume (2012). **Information & Data Mining Tool for North Atlantic Argo Data**. Séminaire technique LOPS. 20 janvier 2012, Brest, France.
23. Maze Guillaume, Marshall John (2012). **Diagnosing the Observed Seasonal Cycle of Atlantic Subtropical Mode Water Using Potential Vorticity and Its Attendant Theorems**. 2012 Ocean Sciences Meeting. 20-24 Feb. 2012, Salt Lake City, Utah, USA.
24. Maze Guillaume, Marshall John, Deshayes Julie (2012). **Using potential vorticity and its attendant theorems to study the subtropical thermocline water mass**. Séminaire scientifique LOPS. 16 Mars 2012, Brest, France.
25. Maze Guillaume, Thierry Virginie, Mercier Herlé (2011). **Oxygen budget in the North-East Atlantic Ocean**. Annual OVIDE Meeting. January 10-11 2011, Brest, France.
26. Maze Guillaume, Thierry Virginie, Mercier Herlé, Perez Fiz, Memery Laurent, Morin Pascal (2011). **Mass, nutrients and oxygen budgets in the North-East Atlantic**. OVIDE/CATARINA meeting. 19-21 Dec. 2011, Vigo, Spain.
27. Maze Guillaume (2010). **Using Argo-O2 profiles to study/document interactions between the oxygen minimum layer and the thermocline**. 6th Argo-France Meeting. 21/05/2010, Villefranche sur Mer, France.

Chapitre d'ouvrage

1. Maze Guillaume, Morrow Rosemary (2017). **Océan et Big Data**. In Les Big Data à découvert. 2017. Bouzeghoub, M, Mosseri, R (Dir.). ISBN : 978-2-271-11464-8 . Collection : À découvert . Chap.4, pp.180-181 (CNRS Editions).

Base de données

OR: *Outils de recherche (bases de données,...)*

1. Feucher Charlene, Maze Guillaume, Mercier Herle (2018). **2000-2015 climatology of the Subtropical Mode Waters and Permanent Pycnocline properties in the World Ocean**. SEANOE. <https://doi.org/10.17882/56503>
2. Feucher Charlene, Maze Guillaume, Mercier Herle (2016). **2000-2014 climatology of the North Atlantic permanent pycnocline properties**. SEANOE. <https://doi.org/10.17882/42386>
3. Maze Guillaume (2017). **A Profile Classification Model from North-Atlantic Argo temperature data**. SEANOE. <https://doi.org/10.17882/47106>

Posters

AFF: *Communications par affiche dans un congrès international ou national*

1. Desbrières, D. G. and Mercier, H. and Maze, G. and Daniault, N. (2020). **Surface predictor of overturning circulation and heat content change in the subpolar North Atlantic**. 2020 Ocean Sciences Meeting. 16-21 Feb. 2020, San Diego, California
2. Isabella Rosso, Matthew R Mazloff, Lynne D Talley, Sarah G Purkey, Natalie M Freeman and Guillaume Maze (2020). **Characterization of Physical and Biogeochemical Variability around the Kerguelen Plateau and across the Southern Ocean Frontal Zones: A Machine Learning Approach**. 2020 Ocean Sciences Meeting. 16-21 Feb. 2020, San Diego, California
3. Elodie Claire Martinez, Anwar Brini, Thomas Gorgues, Ronan Fablet, Lucas Drumetz, Pierre Tandeo and Guillaume Maze (2020). **Deep learning applied to ocean color to reconstruct long time-series of phytoplankton biomass in the global ocean**. 2020 Ocean Sciences Meeting. 16-21 Feb. 2020, San Diego, California.
4. Maze Guillaume, Feucher Charlene, Mercier Herle, Dewar William (2018). **Large-scale structure of the pycnocline stratification in subtropical gyres**. 2018 Ocean Sciences Meeting. 11–16 February 2018, Portland, Oregon. <https://archimer.ifremer.fr/doc/00435/54641/>
5. Feucher Charlene, Maze Guillaume, Mercier Herle (2016). **Mean structure of the North Atlantic subtropical permanent pycnocline from in-situ observations**. Ocean Sciences Meeting 2016, 21-26 February, New Orleans, Louisiana, USA. <https://archimer.ifremer.fr/doc/00318/42870/>
6. Thierry Virginie, Mercier Herle, Maze Guillaume, Le Reste Serge, Dutreuil Vincent, Andre Xavier, Lenault Yannick (2015). **Deep-Arvor floats (4000m) : first results and future plans**. GAIC2015 - "Sustained ocean observing for the next decade" A combined GO-SHIP/Argo/ IOCCP conference on physical and biogeochemical measurements of the water column. 14 – 18 September 2015, Galway, Ireland. <https://archimer.ifremer.fr/doc/00281/39195/>

7. Feucher Charlene, Maze Guillaume, Mercier Herle (2015). **A complex North Atlantic permanent pycnocline revealed by Argo data**. EGU 2015 - European Geosciences Union General Assembly, 12-17 avril 2015, Vienne, Autriche. <https://archimer.ifremer.fr/doc/00257/36818/>
8. Feucher Charlene, Maze Guillaume, Mercier Herle (2014). **The main pycnocline in the North Atlantic subtropical gyre from Argo Data**. OBIDAM 14 - Ocean's Big Data Mining Summer School 2014 : Data mining in large sets of complex oceanic data: new challenges and solutions. 8-9 Sep 2014, Brest, France. <https://archimer.ifremer.fr/doc/00242/35315/>
9. Maze Guillaume, Thierry Virginie, Mercier Herle (2013). **The Atlantic Ocean main pycnocline from Argo data**. EGU 2013 - European Geosciences Union General Assembly, 7-12 avril 2013, Vienne, Autriche. <https://archimer.ifremer.fr/doc/00133/24435/>
10. Maze Guillaume, Thierry Virginie, Mercier Herle, Perez Fiz F., Memery Laurent, Morin Pascal (2012). **Mass, nutrients and oxygen budgets in the North Eastern Atlantic Ocean**. 2012 Ocean Sciences Meeting, 20-24 February 2012, Salt Lake City, Utah, USA.
11. Maze Guillaume, Thierry Virginie, Mercier Herle (2012). **The North Atlantic main pycnocline from Argo data**. 4th Argo Science workshop, 27-29 September 2012, Venice, Italy.
12. Cerovecki Ivana, Talley Lynne D., Mazloff Matthew R., Maze Guillaume (2008). **Subantarctic mode water formation estimates from data assimilating model**. AGU Fall meeting, 15-19 December 2008, San Francisco, USA.
13. Maze Guillaume, Marshall John (2006). **Analysis of the North Atlantic subtropical mode water formation in an eddy resolving model**. AGU Fall meeting, 11-15 December 2006, San Francisco, USA.
14. Maze Guillaume, D'Andrea Fabio, Colin De Verdiere Alain (2005). **Antarctic Circumpolar Wave dynamics in a simplified ocean-atmosphere coupled model**. EGU 2005. EGU 2005, 24 - 29 April 2005, Vienne.
15. Maze Guillaume, D'Andrea Fabio, Colin De Verdiere Alain (2004). **Antarctic Circumpolar Wave dynamics in a simplified ocean-atmosphere coupled model**. EGU 2004. AGU Fall meeting, 13-17 December 2004, San Francisco, USA.

Rapports et Comptes Rendus (selection)

AP : Autres productions. Bases de données, logiciels enregistrés, comptes rendus d'ouvrages, rapports de fouilles, guides techniques, catalogues d'exposition, rapports intermédiaires de grands projets internationaux, etc.

1. Kolodziejczyk Nicolas, Carval Thierry, Claustre Hervé, D'Ortenzio Fabrizio, Lebreton Nathanaele, Le Traon Pierre-Yves, Maze Guillaume, Poffa Noe, Pouliquen Sylvie, Poteau Antoine, Schmechtig Catherine, Thierry Virginie (2019). **Stratégie nationale pour les déploiements d'opportunité des profileurs du réseau global Argo / National Strategy for Argo Global Network Profiling floats Deployments of Opportunity**. Comité de pilotage Argo-France/Argo-France Steering Committee. AF-2019-DEP-STRAT. <https://doi.org/10.13155/59297>
2. Maze Guillaume, Cabanes Cecile, Carval Thierry, Claustre Hervé, Coatanoan Christine, D'Ortenzio Fabrizio, Kolodziejczyk Nicolas, Lebreton Nathanaele, Poteau Antoine, Le Reste Serge, Schmechtig Catherine, Le Traon Pierre-Yves, Pouliquen Sylvie, Thierry Virginie (2018). **French National Report on Argo - 2017**. <https://archimer.ifremer.fr/doc/00435/54642/>
3. Maze Guillaume, Cabanes Cecile, Carval Thierry, Claustre Hervé, Coatanoan Christine, D'Ortenzio Fabrizio, Kolodziejczyk Nicolas, Lebreton Nathanaele, Poteau Antoine, Le Reste Serge, Schmechtig Catherine, Le Traon Pierre-Yves, Poffa Noe, Pouliquen Sylvie, Thierry Virginie (2017). **French National Report on Argo - 2016. Present status and future plans**. <https://archimer.ifremer.fr/doc/00397/50844/>
4. Pouliquen Sylvie, Maze Guillaume, Lebreton Nathanaele, D'Ortenzio Fabrizio, Alory Gaël, Delcroix Thierry, Bourles Bernard, Blouch Pierre, Guinet Christophe, Gouriou Yves, Gaillard Fabienne, Heyndrickx Céline, Le Menn Marc, Testor Pierre, Donato Vincent, Charria Guillaume, Carval Thierry, Reverdin Gilles, Emzivat Gilbert (2017). **CORIOLIS. Rapport d'activités 2016**. <https://doi.org/10.13155/49970>
5. Zilberman Nathalie, Maze Guillaume (2015). **Report on the Deep Argo Implementation Workshop**. Hobart, May 5-7th 2015. Ifremer/LPO/15-04. <https://archimer.ifremer.fr/doc/00281/39238/>
6. Maze Guillaume, Cabanes Cecile, Carval Thierry, Coatanoan Christine, D'Ortenzio Fabrizio, Kolodziejczyk Nicolas, Lebreton Nathanaele, Le Traon Pierre-Yves, Poffa Noe, Pouliquen Sylvie, Thierry Virginie (2016). **French National Report on Argo - 2015. Present status and future plans**. LPO/16-01. <https://archimer.ifremer.fr/doc/00318/42967/>
7. Maze Guillaume, Cabanes Cécile, Carval Thierry, Coatanoan Christine, D'Ortenzio Fabrizio, Lebreton Nathanaele, Le Reste Serge, Le Traon Pierre-Yves, Pouliquen Sylvie, Thierry Virginie (2015). **French National Report on Argo - 2014. Present status and future plans**. LPO-15-01. <https://archimer.ifremer.fr/doc/00254/36504/>
8. Maze Guillaume, Cabanes Cecile, Coatanoan Christine, D'Ortenzio Fabrizio, Lebreton Nathanaele, Le Reste Serge, Le Traon Pierre-Yves, Mamaca Emina, Pouliquen Sylvie, Thierry Virginie (2014). **French National Report on Argo - 2013. Present status and future plans**. LPO/14-02. <https://archimer.ifremer.fr/doc/00180/29100/>
9. Maze Guillaume, Mercier Herle, Fablet Ronan, Lenca Philippe, Piolle Jean-Francois (2014). **Brève introduction à la fouille de grandes bases de données océaniques**. ODE/LPO-14-101. <https://doi.org/10.13155/32710>

10. Maze Guillaume, Mercier Herle, Fablet Ronan, Lenca Philippe, Piolle Jean-Francois (2014). **Fouille de grandes bases de données océaniques: nouveaux défis et solutions. Compte-rendu factuel de l'école d'été OBI-DAM14** organisée par l'Ifremer, le CNRS et Telecom Bretagne, 8-9 septembre 2014, Brest. ODE/LPO/14-100. <https://doi.org/10.13155/32413>

Autres interventions orales (selection):

1. Maze Guillaume, Mercier Herlé, Feucher Charlene, Fablet Ronan, Lenca Philippe, Radcenco Manuel, Le Goff Clement. **Ocean heat content structure revealed by un-supervised classification of hydrographic profiles.**
 - 1.1. Seminar University of Reading. 19/11/2015, Reading, UK.
 - 1.2. Seminar National Oceanographic Center. 18/11/2015, Southampton, UK.
 - 1.3. Seminar Atmospheric, Oceanic and Planetary Physics. Department of Physics, University of Oxford. 17/11/2015, UK.
2. Maze Guillaume. **Argo: système d'observation du climat des océans. Histoire d'une révolution.**
 - 2.1. Conférence Lycée Le Likès. 2017/10/17, Quimper, France.
 - 2.2. Conférence Collège de Keranroux. 10/05/2016, Brest, France.
 - 2.3. Conférence Lycée Vauban. 03/03/2016, Brest, France.
 - 2.4. Conférence Grand Public Ifremer. 20/01/2016, Brest, France.
3. Maze Guillaume, Mercier Herle, Feucher Charlene, Paul Frederic, Kermabon Catherine, Tandeo Pierre, Fablet Ronan, Radcenco Manuel, Le Goff Clement (2016). **Analyse de la structure verticale des océans: nouvelles approches basées sur les méthodes de fouille.** Journée de restitution / Direction Scientifique Ifremer. 16/09/2016, Brest.



Bibliography

- Abernathy, R., J. Marshall, M. Mazloff, and E. Shuckburgh, 2010: Enhancement of mesoscale eddy stirring at steering levels in the southern ocean. *Journal of Physical Oceanography*, **40** (1), 170–184, doi:10.1175/2009JPO4201.1, URL <https://doi.org/10.1175/2009JP04201.1>.
- Abernathy, R. P. and J. Marshall, 2013: Global surface eddy diffusivities derived from satellite altimetry. *Journal of Geophysical Research: Oceans*, **118** (2), 901–916, doi:10.1002/jgrc.20066, URL <https://doi.org/10.1002/jgrc.20066>.
- Alexander, M. A. and C. Deser, 1995: A mechanism for the recurrence of wintertime midlatitude sst anomalies. *J. Phys. Oceanogr.*, **25** (1), 122–137, URL <http://dx.doi.org/10.1175%2F1520-0485%281995%29025%3C0122%3AAMFTRO%3E2.0.CO%3B2>.
- Anderson, B. D. and J. B. Moore, 1979: Optimal filtering. 1979. Prentice-Hall, Englewood Cliffs, NJ.
- Atlas of World Maps, 1943: *Ocean Currents and Sea Ice*. United States Army Service Forces, Army Specialized Training Division. Army Service Forces Manual M-101.
- Balmaseda, M. A., et al., 2015: The ocean reanalyses intercomparison project (ora-ip). *Journal of Operational Oceanography*, **8** (sup1), s80–s97, doi:10.1080/1755876X.2015.1022329, URL <http://dx.doi.org/10.1080/1755876X.2015.1022329>.
- Barrier, N., A.-M. Treguier, C. Cassou, and J. Deshayes, 2012: Impact of the winter north-atlantic weather regimes on subtropical sea-surface height variability. 1–13, doi:10.1007/s00382-012-1578-7, URL <http://dx.doi.org/10.1007/s00382-012-1578-7>.
- Bates, N., A. Pequignet, R. Johnson, and N. Gruber, 2002: A short-term sink for atmospheric co₂ in subtropical mode water of the North Atlantic ocean. *Nature*, **420** (6915), 489–493.
- Billheimer, S. and L. D. Talley, 2013: Near cessation of eighteen degree water renewal in the western north atlantic in the warm winter of 2011–2012. *Journal of Geophysical Research: Oceans*, **118** (12), 6838–6853, doi:10.1002/2013JC009024, URL <http://dx.doi.org/10.1002/2013JC009024>.
- Billheimer, S. and L. D. Talley, 2016: Annual cycle and destruction of eighteen degree water. *Journal of Geophysical Research: Oceans*, doi:10.1002/2016JC011799, URL <http://dx.doi.org/10.1002/2016JC011799>.

- Bjornsson, H. and S. A. Venegas, 1997: *A Manual for EOF and SVD Analyses of Climatic Data*. Center for Climate and Global Change Research.
- Bopp, L., et al., 2013: Multiple stressors of ocean ecosystems in the 21st century: projections with cmip5 models. *Biogeosciences*, **10** (10), 6225–6245, doi:10.5194/bg-10-6225-2013, URL <http://www.biogeosciences.net/10/6225/2013/>.
- Bretherton, F. P., R. E. Davis, and C. B. Fandry, 1976: A technique for objective analysis and design of oceanographic experiments applied to mode-73. *Deep Sea Research and Oceanographic Abstracts*, **23** (7), 559–582, doi:[http://dx.doi.org/10.1016/0011-7471\(76\)90001-2](http://dx.doi.org/10.1016/0011-7471(76)90001-2), URL <http://www.sciencedirect.com/science/article/pii/0011747176900012>.
- Bryden, H. L., B. A. King, G. D. McCarthy, and E. L. McDonagh, 2014: Impact of a 30% reduction in atlantic meridional overturning during 2009–2010. *Ocean Science Discussions*, **11** (2), 789–810, doi:10.5194/osd-11-789-2014, URL <http://www.ocean-sci-discuss.net/11/789/2014/>.
- Capet, X., G. Roullet, P. Klein, and G. Maze, 2016: Intensification of upper-ocean submesoscale turbulence through charney baroclinic instability. *Journal of Physical Oceanography*, **46** (11), 3365–3384, doi:10.1175/JPO-D-16-0050.1, URL <https://doi.org/10.1175/JPO-D-16-0050.1>.
- Cassou, C., 2004: Du changement climatique aux régimes de temps: l'oscillation nord-atlantique. *La Meteorologie*.
- Cerovecki, I. and J. Marshall, 2008: Eddy modulation of air-sea interaction and convection. *J. Phys. Oceanogr.*, **38** (1), 65–83, URL <http://dx.doi.org/10.1175%2F2007JP03545.1>.
- Cerovečki, I., L. D. Talley, M. R. Mazloff, and G. Maze, 2013: Subantarctic mode water formation, destruction, and export in the eddy-permitting southern ocean state estimate. *Journal of Physical Oceanography*, **43** (7), 1485–1511, doi:10.1175/JPO-D-12-0121.1, URL <http://dx.doi.org/10.1175/JPO-D-12-0121.1>.
- Cessi, P., 2007: Regimes of thermocline scaling: The interaction of wind stress and surface buoyancy. *J. Phys. Oceanogr.*, **37** (8), 2009–2021, URL <http://dx.doi.org/10.1175%2FJP03103.1>.
- Church, J. A. and N. J. White, 2006: A 20th century acceleration in global sea-level rise. *Geophys. Res. Lett.*, **33** (1), L01 602, doi:10.1029/2005GL024826, URL <http://dx.doi.org/10.1029/2005GL024826>.
- Cole, S. T., C. Wortham, E. Kunze, and W. B. Owens, 2015: Eddy stirring and horizontal diffusivity from argo float observations: Geographic and depth variability. *Geophysical Research Letters*, **42** (10), 3989–3997, doi:10.1002/2015GL063827, URL <https://doi.org/10.1002/2015GL063827>.
- Cosne, G., G. Maze, and P. Tandéo, 2019: Coupling oceanic observation systems to study mesoscale ocean dynamics. *CCAI-NeurIPS conference*, URL <https://arxiv.org/abs/1910.08573>.
- Czaja, A. and U. Hausmann, 2009: Observations of entry and exit of potential vorticity at the sea surface. *Journal of Physical Oceanography*, **39** (9), 2280–2294, URL <http://dx.doi.org/10.1175%2F2009JP04024.1>.
- Da Costa, M., H. Mercier, and A. Treguier, 2005: Effects of the mixed layer time variability on kinematic subduction rate diagnostics. *J. Phys. Oceanogr.*, **35** (4), 427–443.
- de Lavergne, C., G. Madec, X. Capet, G. Maze, and F. Roquet, 2016: Getting to the bottom of the ocean. *Nature Geosci.*, **9** (12), 857–858, doi:10.1038/ngeo2850, URL <http://dx.doi.org/10.1038/ngeo2850>.
- Deremble, B., N. Wienders, and W. K. Dewar, 2013: Potential vorticity budgets in the north atlantic ocean. *Journal of Physical Oceanography*, doi:10.1175/JPO-D-13-087.1, URL <http://dx.doi.org/10.1175/JPO-D-13-087.1>.

- Desbruyères, D., V. Thierry, and H. Mercier, 2013: Simulated decadal variability of the meridional overturning circulation across the a25-ovide section. *Journal of Geophysical Research: Oceans*, **118** (1), 462–475, doi:10.1029/2012JC008342, URL <http://dx.doi.org/10.1029/2012JC008342>.
- Dong, S. and K. A. Kelly, 2004: Heat budget in the gulf stream region: The importance of heat storage and advection. *J. Phys. Oceanogr.*, **34** (5), 1214–1231, URL <http://dx.doi.org/10.1175%2F1520-0485%282004%29034%3C1214%3AHBITGS%3E2.0.CO%3B2>.
- Dong, S. and K. A. Kelly, 2013: How well do climate models reproduce north atlantic subtropical mode water? *Journal of Physical Oceanography*, **43** (10), 2230–2244, doi:10.1175/JPO-D-12-0215.1, URL <http://dx.doi.org/10.1175/JPO-D-12-0215.1>.
- D’Ortenzio, F. and M. Ribera d’Alcalà, 2009: On the trophic regimes of the mediterranean sea: a satellite analysis. *Biogeosciences*, **6** (2), 139–148, doi:10.5194/bg-6-139-2009, URL <https://www.biogeosciences.net/6/139/2009/>.
- Ebbesmeyer, C. and E. Lindstrom, 1986: Structure and origin of 18° c water observed during the polymode local dynamics experiment. *J. Phys. Oceanogr.*, **16** (3), 443–453.
- Evans, D. G., J. Toole, G. Forget, J. D. Zika, A. C. Naveira Garabato, A. J. G. Nurser, and L. Yu, 2017: Recent wind-driven variability in atlantic water mass distribution and meridional overturning circulation. *Journal of Physical Oceanography*, **47** (3), 633–647, doi:10.1175/JPO-D-16-0089.1, URL <https://doi.org/10.1175/JPO-D-16-0089.1>.
- Fairall, C., E. Bradley, J. Hare, A. Grachev, and J. Edson, 2003: Bulk parameterization of air–sea fluxes: Updates and verification for the COARE algorithm. *J. Climate*, **16** (4), 571–591.
- Ferrari, R. and K. L. Polzin, 2005: Finescale structure of the t–s relation in the eastern north atlantic. *Journal of Physical Oceanography*, **35** (8), 1437–1454, doi:10.1175/JPO2763.1, URL <https://doi.org/10.1175/JPO2763.1>.
- Feucher, C., 2016: Stratification structure in subtropical gyres and its decadal variability in the north atlantic ocean. Ph.D. thesis, Université de Bretagne Occidentale.
- Feucher, C., G. Maze, and H. Mercier, 2015: A complex north atlantic permanent pycnocline revealed by argo data. *EGU 2015 - European Geosciences Union General Assembly, 12-17 avril 2015, Vienne, Autriche*, URL <http://archimer.ifremer.fr/doc/00257/36818/>.
- Feucher, C., G. Maze, and H. Mercier, 2016a: 2000-2014 climatology of the north atlantic permanent pycnocline properties. Seanoë, Ifremer, France, URL <http://dx.doi.org/10.17882/42386>, doi:10.17882/42386, URL <http://dx.doi.org/10.17882/42386>.
- Feucher, C., G. Maze, and H. Mercier, 2016b: Mean structure of the north atlantic subtropical permanent pycnocline from in-situ observations. *Journal of Atmospheric and Oceanic Technology*, doi:10.1175/JTECH-D-15-0192.1, URL <http://dx.doi.org/10.1175/JTECH-D-15-0192.1>.
- Feucher, C., G. Maze, and H. Mercier, 2019: Subtropical mode water and permanent pycnocline properties in the world ocean. *Journal of Geophysical Research: Oceans*, **124** (2), 1139–1154, doi:10.1029/2018JC014526, URL <https://doi.org/10.1029/2018JC014526>.
- Flanders, H., 1973: Differentiation under the integral sign. *The American Mathematical Monthly*, **80** (6), 615–627, doi:10.2307/2319163, URL <http://www.jstor.org/stable/2319163>.
- Follows, M. and J. Marshall, 1994: Eddy driven subduction at fronts. *Ocean Modelling*, **102**, 5–9.

- Forget, G., 2010: Mapping ocean observations in a dynamical framework: A 2004-06 ocean atlas. *Journal of Physical Oceanography*, **40** (6), 1201–1221, doi:10.1175/2009JPO4043.1.
- Forget, G., J. M. Campin, P. Heimbach, C. N. Hill, R. M. Ponte, and C. Wunsch, 2015: Ecco version 4: an integrated framework for non-linear inverse modeling and global ocean state estimation. *Geosci. Model Dev.*, **8** (10), 3071–3104, doi:10.5194/gmd-8-3071-2015, URL <http://www.geosci-model-dev.net/8/3071/2015/>.
- Forget, G., G. Maze, M. Buckley, and J. Marshall, 2011: Estimated seasonal cycle of north atlantic eighteen degree water volume. *Journal of Physical Oceanography*, **41** (2), 269–286, doi:10.1175/2010JPO4257.1, URL <http://journals.ametsoc.org/doi/abs/10.1175/2010JP04257.1>, <http://journals.ametsoc.org/doi/pdf/10.1175/2010JP04257.1>.
- Gaillard, F., 2015: Isas-13 temperature and salinity gridded fields. SEANOE, Ifremer, LPO â“UMR 6523 CNRS, Ifremer, IRD, UBO, URL <http://doi.org/10.17882/45945>, doi:10.17882/45945, URL <http://doi.org/10.17882/45945>.
- Gaillard, F., E. Autret, V. Thierry, P. Galaup, C. Coatanoan, and T. Loubrieu, 2009: Quality control of large argo datasets. *Journal of Atmospheric and Oceanic Technology*, **26** (2), 337–351, doi:10.1175/2008JTECHO552.1, URL <http://dx.doi.org/10.1175/2008JTECHO552.1>.
- Gaillard, F., T. Reynaud, V. Thierry, N. Kolodziejczyk, and K. Von Schuckmann, 2016: In-situ based reanalysis of the global ocean temperature and salinity with isas: variability of the heat content and steric height. *Journal of Climate*, **in press**.
- Ganachaud, A., et al., 2014: The southwest pacific ocean circulation and climate experiment (spice). *Journal of Geophysical Research: Oceans*, **119** (11), 7660–7686, doi:10.1002/2013JC009678, URL <https://agupubs.onlinelibrary.wiley.com/doi/abs/10.1002/2013JC009678>, <https://agupubs.onlinelibrary.wiley.com/doi/pdf/10.1002/2013JC009678>.
- Garrett, C., K. G. Speer, and E. Tragou, 1995: The relationship between water mass formation and the surface buoyancy flux with application to Phillip’s Read Sea model. *J. Phys. Oceanogr.*, **25**, 1696–1705.
- Garrett, C. and A. Tandon, 1997: The effects on water mass formation of surface mixed layer time-dependence and entrainment fluxes. *Deep Sea Research Part I: Oceanographic Research Papers*, **44** (12), 1991–2006, doi:https://doi.org/10.1016/S0967-0637(97)00055-1, URL <http://www.sciencedirect.com/science/article/pii/S0967063797000551>.
- Gebbie, G., 2007: Does eddy subduction matter in the NorthEast Atlantic ocean? *J. Geophys. Res.*, **112**.
- Gent, P. R. and J. C. McWilliams, 1990: Isopycnal mixing in ocean circulation model. *J. Phys. Oceanogr.*, **20** (1), 150–155, doi:10.1175/1520-0485(1990)020<0150:IMIOCM>2.0.CO;2, URL [http://ams.allenpress.com/perlserv/?request=get-abstract&doi=10.1175%2F1520-0485\(1990\)020%3C0150:IMIOCM%3E2.0.CO%3B2](http://ams.allenpress.com/perlserv/?request=get-abstract&doi=10.1175%2F1520-0485(1990)020%3C0150:IMIOCM%3E2.0.CO%3B2).
- Gent, P. R., J. Willebrand, T. J. McDougall, and J. C. McWilliams, 1995: Parameterizing eddy-induced tracer transports in ocean circulation models. *Journal of Physical Oceanography*, **25** (4), 463–474, doi:10.1175/1520-0485(1995)025<0463:PEITTI>2.0.CO;2, URL [https://doi.org/10.1175/1520-0485\(1995\)025<0463:PEITTI>2.0.CO;2](https://doi.org/10.1175/1520-0485(1995)025<0463:PEITTI>2.0.CO;2).
- Gille, S. T., K. Speer, J. R. Ledwell, and A. C. Naveira Garabato, 2007: Mixing and stirring in the southern ocean. *Eos, Transactions American Geophysical Union*, **88** (39), 382–383, doi:10.1029/2007EO390002, URL <https://doi.org/10.1029/2007EO390002>.

- Grist, J., S. Josey, Z. Jacobs, R. Marsh, B. Sinha, and E. Van Sebille, 2015: Extreme air–sea interaction over the north atlantic subpolar gyre during the winter of 2013–2014 and its sub-surface legacy. *Climate Dynamics*, 1–19, doi:10.1007/s00382-015-2819-3, URL <http://dx.doi.org/10.1007/s00382-015-2819-3>.
- Groeskamp, S., S. M. Griffies, D. Iudicone, R. Marsh, A. J. G. Nurser, and J. D. Zika, 2019: The water mass transformation framework for ocean physics and biogeochemistry. *Annual Review of Marine Science*, **11** (1), 271–305, doi:10.1146/annurev-marine-010318-095421, URL <https://doi.org/10.1146/annurev-marine-010318-095421>.
- Gula, J., 2020: Mesoscale and submesoscale turbulence in the presence of topography. Ph.D. thesis, Université de Bretagne Occidentale.
- Haine, T. W. N. and T. M. Hall, 2002: A generalized transport theory: Water-mass composition and age. *Journal of Physical Oceanography*, **32** (6), 1932–1946, URL <http://dx.doi.org/10.1175%2F1520-0485%282002%29032%3C1932%3AAGTTWM%3E2.0.CO%3B2>.
- Häkkinen, S., P. B. Rhines, and D. L. Worthen, 2011: Warm and saline events embedded in the meridional circulation of the northern north atlantic. *Journal of Geophysical Research: Oceans*, **116** (C3), n/a–n/a, doi:10.1029/2010JC006275, URL <http://dx.doi.org/10.1029/2010JC006275>.
- Häkkinen, S., P. B. Rhines, and D. L. Worthen, 2013: Northern north atlantic sea-surface height and ocean heat content variability. *Journal of Geophysical Research: Oceans*, n/a–n/a, doi:10.1002/jgrc.20268, URL <http://dx.doi.org/10.1002/jgrc.20268>.
- Häkkinen, S., P. B. Rhines, and D. L. Worthen, 2015: Heat content variability in the north atlantic ocean in ocean reanalyses. *Geophysical Research Letters*, 2015GL063299, doi:10.1002/2015GL063299, URL <http://dx.doi.org/10.1002/2015GL063299>.
- Häkkinen, S., P. B. Rhines, and D. L. Worthen, 2016: Warming of the global ocean: Spatial structure and water-mass trends. *Journal of Climate*, **29** (13), 4949–4963, doi:10.1175/JCLI-D-15-0607.1, URL <https://doi.org/10.1175/JCLI-D-15-0607.1>.
- Han, M., I. Kamenkovich, T. Radko, and W. E. Johns, 2012: Relationship between air-sea density flux and isopycnal meridional overturning circulation in a warming climate. *Journal of Climate*, doi:10.1175/JCLI-D-11-00682.1, URL <http://dx.doi.org/10.1175/JCLI-D-11-00682.1>.
- Hanawa, K. and S. Sugimoto, 2004: ‘reemergence’ areas of winter sea surface temperature anomalies in the world’s oceans. *Geophysical Research Letters*, **31** (10), n/a–n/a, doi:10.1029/2004GL019904, URL <http://dx.doi.org/10.1029/2004GL019904>.
- Hanawa, K. and L. Talley, 2001: *Ocean Circulation and Climate: Observing and Modelling the Global Ocean*, chap. Mode waters, 373–386. Academic Press.
- Haynes, P. and M. McIntyre, 1987: On the evolution of vorticity and potential vorticity in the presence of diabatic heating and frictional or other forces. *Journal of the Atmospheric Sciences*, **44** (5).
- Hazeleger, W. and S. S. Drijfhout, 2000: Eddy subduction in a model of the subtropical gyre. *Journal of Physical Oceanography*, **30** (4), 677–695, doi:10.1175/1520-0485(2000)030<0677:ESIAMO>2.0.CO;2, URL [http://dx.doi.org/10.1175/1520-0485\(2000\)030<0677:ESIAMO>2.0.CO;2](http://dx.doi.org/10.1175/1520-0485(2000)030<0677:ESIAMO>2.0.CO;2).
- Henning, C. C. and G. K. Vallis, 2004: The effects of mesoscale eddies on the main subtropical thermocline. *Journal of Physical Oceanography*, **34** (11), 2428–2443, URL <http://dx.doi.org/10.1175%2FJP02639.1>.

- Hurrell, J. W., 1995: Decadal trends in the North Atlantic oscillation region temperatures and precipitation. *Science*, **269**, 676–679.
- IPCC, 2007: The physical science basis. *Climate Change 2007*, S. Solomon, D. Qin, M. Manning, M. Marquis, K. Averyt, M. Tignor, and H. L. Miller, Eds., Cambridge University Press, Working Group I Contribution to the Fourth Assessment Report of the IPCC.
- Iselin, C. O., 1936: A study of the circulation of the western north atlantic. Massachusetts Institute of Technology and Woods Hole Oceanographic Institution, URL <http://dx.doi.org/10.1575/1912/1087>, Published by MIT and WHOI, doi:10.1575/1912/1087, URL <http://dx.doi.org/10.1575/1912/1087>.
- J., H. P., G. M. C., and A. M. H., 2013: Wind-driven submesoscale subduction at the north pacific subtropical front. *Journal of Geophysical Research: Oceans*, **118** (10), 5333–5352, doi:doi:10.1002/jgrc.20385, URL <https://doi.org/10.1002/jgrc.20385>.
- Jackson, L. C., K. A. Peterson, C. D. Roberts, and R. A. Wood, 2016: Recent slowing of atlantic overturning circulation as a recovery from earlier strengthening. *Nature Geosci*, **9** (7), 518–522, URL <http://dx.doi.org/10.1038/ngeo2715>.
- Jain, A. K., 2010: Data clustering: 50 years beyond k-means. *Pattern Recognition Letters*, **31** (8), 651 – 666, doi:http://dx.doi.org/10.1016/j.patrec.2009.09.011, URL <http://www.sciencedirect.com/science/article/pii/S0167865509002323>, award winning papers from the 19th International Conference on Pattern Recognition (ICPR) 19th International Conference in Pattern Recognition (ICPR).
- Jenkins, W. and S. Doney, 2003: The subtropical nutrient spiral. *Global Biogeochemical Cycles*, **17** (4), 1110.
- Jenkins, W. J., 1982: Oxygen utilization rates in north atlantic subtropical gyre and primary production in oligotrophic systems. *Nature*, **300**, URL <http://dx.doi.org/10.1038/300246a0>.
- Jenkins, W. J., 1987: 3h and 3he in the beta triangle: Observations of gyre ventilation and oxygen utilization rates. *Journal of Physical Oceanography*, **17** (6), 763–783, URL <http://dx.doi.org/10.1175%2F1520-0485%281987%29017%3C0763%3AAITBT0%3E2.0.CO%3B2>.
- Jones, D. C., H. J. Holt, A. J. S. Meijers, and E. Shuckburgh, 2019: Unsupervised clustering of southern ocean argo float temperature profiles. *Journal of Geophysical Research: Oceans*, doi:10.1029/2018jc014629, URL <http://dx.doi.org/10.1029/2018JC014629>.
- Joyce, T. M. and P. Robbins, 1996: The long-term hydrographic record at bermuda. *J. Climate*, **9** (12), 3121–3131, URL <http://dx.doi.org/10.1175%2F1520-0442%281996%29009%3C3121%3ATLTHRA%3E2.0.CO%3B2>.
- Joyce, T. M., L. N. Thomas, and F. Bahr, 2009: Wintertime observations of subtropical mode water formation within the gulf stream. *Geophys. Res. Lett.*, **36**, URL <http://dx.doi.org/10.1029/2008GL035918>.
- Karleskind, P., M. Lévy, and L. Mémerly, 2011: Modifications of mode water properties by sub-mesoscales in a bio-physical model of the northeast atlantic. *Ocean Modelling*, **39** (1), 47–60, doi:https://doi.org/10.1016/j.ocemod.2010.12.003, URL <http://www.sciencedirect.com/science/article/pii/S1463500310001794>.
- Kelly, K. A., R. J. Small, R. M. Samelson, B. Qiu, T. M. Joyce, Y.-O. Kwon, and M. F. Cronin, 2010: Western boundary currents and frontal air–sea interaction: Gulf stream and kuroshio extension. *Journal of Climate*, **23** (21), 5644–5667, doi:10.1175/2010JCLI3346.1, URL <http://dx.doi.org/10.1175/2010JCLI3346.1>.

- Kobashi, F. and A. Kubokawa, 2012: Review on north pacific subtropical countercurrents and subtropical fronts: role of mode waters in ocean circulation and climate. *Journal of Oceanography*, **68** (1), 21–43, doi:10.1007/s10872-011-0083-7, URL <https://doi.org/10.1007/s10872-011-0083-7>.
- Kobashi, F., H. Mitsudera, and S.-P. Xie, 2006: Three subtropical fronts in the north pacific: Observational evidence for mode water-induced subsurface frontogenesis. *Journal of Geophysical Research*, **111** (C9), doi:10.1029/2006jc003479, URL <http://dx.doi.org/10.1029/2006JC003479>.
- Kobashi, F. and S.-P. Xie, 2012: Interannual variability of the north pacific subtropical countercurrent: role of local ocean–atmosphere interaction. *Journal of Oceanography*, **68** (1), 113–126, doi:10.1007/s10872-011-0048-x, URL <http://dx.doi.org/10.1007/s10872-011-0048-x>.
- Kolodziejczyk, N., W. Llovel, and E. Portela, 2019: Interannual variability of upper ocean water masses as inferred from argo array. *Journal of Geophysical Research: Oceans*, **124** (8), 6067–6085, doi:10.1029/2018JC014866, URL <https://doi.org/10.1029/2018JC014866>.
- Kolodziejczyk, N., A. Prigenet, and F. Gaillard, 2017: Isas-15 temperature and salinity gridded fields. SEANOE, URL <http://doi.org/10.17882/52367>, doi:10.17882/52367, URL <http://doi.org/10.17882/52367>.
- Kwon, Y., 2003: Observation of general circulation and water mass variability in the north atlantic subtropical mode water region. Ph.D. thesis, Univ. of Washington, Seattle.
- Kwon, Y. and S. Riser, 2004: North Atlantic subtropical mode water: A history of ocean-atmosphere interaction 1961–2000. *Geophys. Res. Lett.*, **31**, doi:10.1029/2004GL021116, URL <http://dx.doi.org/10.1029/2004GL021116>.
- Kwon, Y.-O., J.-J. Park, S. F. Gary, and M. S. Lozier, 2015: Year-to-year reoutcropping of eighteen degree water in an eddy-resolving ocean simulation. *Journal of Physical Oceanography*, **45** (4), 1189–1204, doi:10.1175/JPO-D-14-0122.1, URL <http://dx.doi.org/10.1175/JPO-D-14-0122.1>.
- Kwon, Y.-O. and S. C. Riser, 2005: General circulation of the western subtropical north atlantic observed using profiling floats. *J. Geophys. Res.*, **110** (C10), doi:10.1029/2005JC002909, URL <http://dx.doi.org/10.1029/2005JC002909>.
- Large, W. and S. Yeager, 2004: Diurnal to decadal global forcing for ocean and sea-ice models: The data sets and flux climatologies. near tech. note. Tech. rep., NCAR/TN-460+STR, 111 pp. URL <http://www.cgd.ucar.edu/oce/pubs/04pubs.html>.
- Le Reste, S., V. Dutreuil, X. André, V. Thierry, C. Renault, P.-Y. Le Traon, and G. Maze, 2016: “deep-arvor”: A new profiling float to extend the argo observations down to 4000m depth. *Journal of Atmospheric and Oceanic Technology*, doi:10.1175/JTECH-D-15-0214.1, URL <http://dx.doi.org/10.1175/JTECH-D-15-0214.1>.
- Ledwell, J. R., A. J. Watson, and C. S. Law, 1993: Evidence for slow mixing across the pycnocline from an open-ocean tracer-release experiment. *Nature*, **364** (6439), 701–703, doi:10.1038/364701a0, URL <https://doi.org/10.1038/364701a0>.
- Lee, K., 2018: Interannual-to-decadal impact of extreme wintertime weather regimes onto the north atlantic subtropical stratification, PhD annual report.
- Lee, K., 2020: Interannual extreme variability of the subtropical north-western atlantic ocean. Ph.D. thesis, Université de Bretagne Occidentale.

- Lee, M.-M. and A. J. G. Nurser, 2012: Eddy subduction and the vertical transport streamfunction. *Journal of Physical Oceanography*, **42** (11), 1762–1780, doi:10.1175/JPO-D-11-0219.1, URL <https://doi.org/10.1175/JPO-D-11-0219.1>.
- Levitus, S., 1982: Climatological atlas of the world ocean. Prof. Paper 13 173pp, NOAA, U.S. Department of Commerce, Washington, D.C.
- Levitus, S., J. Antonov, and T. Boyer, 2005: Warming of the world ocean, 1955–2003. *Geophys. Res. Lett.*, doi:10.1029/2004GL021592.
- Levitus, S., et al., 2012: World ocean heat content and thermosteric sea level change (0–2000 m), 1955–2010. *Geophysical Research Letters*, **39** (10), n/a–n/a, doi:10.1029/2012GL051106, URL <http://dx.doi.org/10.1029/2012GL051106>.
- Lévy, M., P. Klein, and A.-M. Treguier, 2001: Impact of sub-mesoscale physics on production and subduction of phytoplankton in an oligotrophic regime. *Journal of Marine Research*, **59** (4), 535–565, doi:10.1357/002224001762842181, URL <http://dx.doi.org/10.1357/002224001762842181>.
- Lillibridge III, J. L. and A. J. Mariano, 2012: A statistical analysis of gulf stream variability from 18+ years of altimetry data. *Deep Sea Research Part II: Topical Studies in Oceanography*, doi:10.1016/j.dsr2.2012.07.034, URL <http://www.sciencedirect.com/science/article/pii/S0967064512001208>.
- Liu, L., R. Huang, and F. Wang, 2016: Subduction/obduction rate in the north pacific diagnosed by an eddy-resolving model. *Chinese Journal of Oceanology and Limnology*, **34** (4), 835–846, doi:10.1007/s00343-016-5036-y, URL <https://doi.org/10.1007/s00343-016-5036-y>.
- Lloyd, S., 1982: Least squares quantization in pcm. *IEEE Transactions on Information Theory*, **28** (2), 129–137, doi:10.1109/TIT.1982.1056489.
- Luyten, J., J. Pedlosky, and H. Stommel, 1983: The Ventilated Thermocline. *J. Phys. Oceanogr.*, **13** (2), 292–309.
- Marsh, R., 2000: Recent variability of the north atlantic thermohaline circulation inferred from surface heat and freshwater fluxes. *Journal of Climate*, **13** (18), 3239–3260, doi:10.1175/1520-0442(2000)013<3239:RVOTNA>2.0.CO;2, URL [https://doi.org/10.1175/1520-0442\(2000\)013<3239:RVOTNA>2.0.CO;2](https://doi.org/10.1175/1520-0442(2000)013<3239:RVOTNA>2.0.CO;2).
- Marshall, D. P., 2000: Vertical fluxes of potential vorticity and the structure of the thermocline. *J. Phys. Oceanogr.*, **30** (12), 3102–3112, URL <http://dx.doi.org/10.1175%2F1520-0485%282000%29030%3C3102%3AVFOPVA%3E2.0.CO%3B2>.
- Marshall, J., 2005: Climode: a mode water dynamics experiment in support of clivar. *Clivar Variations*, **3** (2), 8–14.
- Marshall, J., A. Adcroft, C. Hill, L. Perelman, and C. Heisey, 1997a: A finite-volume, incompressible Navier Stokes model for studies of the ocean on parallel computers. *J. Geophys. Res.*, **102** (C3), 5753–5766.
- Marshall, J. and co authors, 2004: Climode: the clivar mode water dynamics experiment. Massachusetts Institute of Technology, MA, USA, NSF-Proposal.
- Marshall, J., C. Hill, L. Perelman, and A. Adcroft, 1997b: Hydrostatic, quasi-hydrostatic, and nonhydrostatic ocean modeling. *J. Geophys. Res.*, **102** (C3), 5733–5752.
- Marshall, J., D. Jamous, and J. Nilsson, 1999: Reconciling thermodynamic and dynamic methods of computation of water-mass transformation rates. *Deep-Sea Res.*, **46**, 545–572.

- Marshall, J., D. Jamous, and J. Nilsson, 2001: Entry, flux and exit of potential vorticity in ocean circulation. *J. Phys. Oceanogr.*, **31** (3), 777–789, doi:10.1175/1520-0485(2001)031<0777:EFAEOP>2.0.CO;2, URL [http://dx.doi.org/10.1175/1520-0485\(2001\)031<0777:EFAEOP>2.0.CO;2](http://dx.doi.org/10.1175/1520-0485(2001)031<0777:EFAEOP>2.0.CO;2).
- Marshall, J., H. Jones, R. Karsten, and R. Wardle, 2002: Can eddies set ocean stratification? *J. Phys. Oceanogr.*, **32** (1), 26–38, URL <http://dx.doi.org/10.1175%2F1520-0485%282002%29032%3C0026%3ACESOS%3E2.0.CO%3B2>.
- Marshall, J., A. Nurser, and R. Williams, 1993: Inferring the subduction rate and period over the North Atlantic. *J. Phys. Oceanogr.*, **23** (7), 1315–1329.
- Marshall, J. and J. G. Nurser, 1992: Fluid dynamics of oceanic thermocline ventilation. *J. Phys. Oceanogr.*, **22**, 583–595.
- Marshall, J., E. Shuckburgh, H. Jones, and C. Hill, 2006: Estimates and implications of surface eddy diffusivity in the Southern ocean derived from a tracer transport. *J. Phys. Oceanogr.*, **36**, 1806–1821.
- Marshall, J. and G. Shutts, 1981: A note on rotational and divergent eddy fluxes. *J. Phys. Oceanogr.*, **11**, 1677–1680.
- Marshall, J., et al., 2009: The climode field campaign: Observing the cycle of convection and restratification over the gulf stream. *Bulletin of the American Meteorological Society*, **90** (9), 1337–1350, doi:10.1175/2009BAMS2706.1, URL <http://dx.doi.org/10.1175%2F2009BAMS2706.1>.
- Masuzawa, J., 1969: Subtropical mode water. *Deep Sea Research and Oceanographic Abstracts*, **16** (5), 463–472, doi:http://dx.doi.org/10.1016/0011-7471(69)90034-5, URL <http://www.sciencedirect.com/science/article/pii/0011747169900345>.
- Matear, R. J. and A. C. Hirst, 2003: Long-term changes in dissolved oxygen concentrations in the ocean caused by protracted global warming. *Global Biogeochem. Cycles*, **17**, URL <http://dx.doi.org/10.1029/2002GB001997>.
- Matthews, T., C. Murphy, R. L. Wilby, and S. Harrigan, 2014: Stormiest winter on record for ireland and uk. *Nature Clim. Change*, **4** (9), 738–740, URL <http://dx.doi.org/10.1038/nclimate2336>.
- Maze, G., 2006: Ocean-atmosphere low-frequency interactions in the southern ocean. Ph.D. thesis, Université Paris VI, 130 pp.
- Maze, G., 2017: A profile classification model from north-atlantic argo temperature data. Seanoë, URL <http://doi.org/10.17882/47106>, doi:10.17882/47106, URL <http://doi.org/10.17882/47106>.
- Maze, G., C. CABANES, C. LAGADEC, P. TANDEO, F. PEREZ, and T. SZEKELY, 2017a: Can machine learning help for argo (dm)qc ? *ADMT-18 - eighteenth Argo Data Management Team meeting. 27 November - 1 December 2017, Hamburg, Germany*, URL <https://w3.ifremer.fr/archimer/doc/00435/54640/56059.pdf>.
- Maze, G., C. CABANES, C. LAGADEC, P. TANDEO, F. PEREZ, and T. SZEKELY, 2018a: Can machine learning help for argo (dm) qc ? *AST-19 Meeting - 19th meeting of the International Argo Steering Team. 12 - 16 March 2018, Sydney-Victoria, Canada*, URL <https://w3.ifremer.fr/archimer/doc/00482/59406/62199.pdf>.
- Maze, G., C. CABANES, C. LAGADEC, P. TANDEO, F. PEREZ, and T. SZEKELY, 2018b: Can machine learning help for argo (dm) qc ? *1st European Argo Delayed-Mode QC Workshop . 17-18 April 2018, Brest, France*, URL <https://w3.ifremer.fr/archimer/doc/00482/59408/62205.pdf>.

- Maze, G., C. CABANES, C. LAGADEC, P. TANDEO, F. PEREZ, and T. SZEKELY, 2018c: Machine learning of argo qc. *ASW6 - 6th Argo Science Workshop "The Argo program in 2020 and beyond : Challenges and opportunities"*. October 22-24, 2018, Tokyo, Japan, URL <https://w3.ifremer.fr/archimer/doc/00468/58000/60394.pdf>.
- Maze, G., F. D'Andrea, and A. Colin de Verdière, 2006: Low-frequency variability in the Southern ocean region in a simplified coupled model. *J. Geophys. Res.*, **111** (C05010), doi:10.1029/2005JC003181.
- Maze, G., F. D'Andrea, A. Colin de Verdière, and P. Klein, 2011: Stationary atmospheric responses to an idealised sst anomaly in the Southern ocean. *J. Climate*, **24**, 3686–3704, doi:10.1175/2011JCLI3737.1, URL <http://journals.ametsoc.org/doi/abs/10.1175/2011JCLI3737.1>.
- Maze, G., J. Deshayes, J. Marshall, A.-M. Tréguier, A. Chronis, and L. Vollmer, 2013: Surface vertical pv fluxes and subtropical mode water formation in an eddy-resolving numerical simulation. *Deep Sea Research Part II: Topical Studies in Oceanography*, **91** (0), 128–138, doi:10.1016/j.dsr2.2013.02.026, URL <http://www.sciencedirect.com/science/article/pii/S0967064513000830>.
- Maze, G., F. D'ORTENZIO, V. THIERRY, C. CABANES, C. SCHMECHTIG, and M. B. Argo-France, 2015a: Sno argo-france. 2010-2014 report and 2015-2019 evolution. Tech. rep. doi:10.13155/60435, URL <https://archimer.ifremer.fr/doc/00493/60435/>.
- Maze, G., G. Forget, M. Buckley, J. Marshall, and I. Cerovecki, 2009: Using transformation and formation maps to study the role of air-sea heat fluxes in north atlantic eighteen degree water formation. *Journal of Physical Oceanography*, **39** (8), 1818–1835, doi:10.1175/2009JPO3985.1, URL <http://dx.doi.org/10.1175%2F2009JPO3985.1>.
- Maze, G., K. Lee, and H. Mercier, 2019a: North-atlantic ocean subtropical gyre: Mechanisms of observed low-frequency variability. Conference poster for the 7th Euro-Argo Science Meeting, Athens, Greece.
- Maze, G., K. Lee, and H. Mercier, 2019b: North-atlantic ocean subtropical gyre: Mechanisms of observed low-frequency variability. Conference poster for the 2019 GMMC Meeting, Toulon, France.
- Maze, G. and J. Marshall, 2011: Diagnosing the observed seasonal cycle of atlantic subtropical mode water using potential vorticity and its attendant theorems. *Journal of Physical Oceanography*, **41**, 1986–1999, doi:10.1175/2011JPO4576.1.
- Maze, G., H. Mercier, and C. Cabanes, 2017b: 55. Profile classification models. URL <https://archimer.ifremer.fr/doc/00387/49816/>, 48–56 pp., URL <https://archimer.ifremer.fr/doc/00387/49816/>.
- Maze, G., H. Mercier, R. Fablet, P. Lenca, and J.-F. Piollé, 2014a: Brève introduction à la fouille de grandes bases de données océaniques. Scientific report, Ifremer. doi:10.13155/32710.
- Maze, G., H. Mercier, R. Fablet, P. Lenca, and J.-F. Piolle, 2014b: Fouille de grandes bases de données océaniques: nouveaux défis et solutions. compte-rendu factuel de l'école d'été obidam14 organisée par l'ifremer, le cnrs et telecom bretagne, 8-9 septembre 2014, brest. Scientific report, Ifremer. doi:10.13155/32413.
- Maze, G., H. Mercier, R. Fablet, P. Lenca, M. L. Radcenco, P. Tandeo, C. Le Goff, and C. FEUCHER, 2016a: Ocean heat content structure revealed by un-supervised classification of hydrographic profiles. *2016 Ocean Sciences Meeting: Toward a Subsurface Ocean Climate Record and Applications that Improve Understanding of Climate Variability and Change*.

- Maze, G., H. Mercier, R. Fablet, P. Tandeo, M. Lopez Radcenco, P. Lenca, C. Feucher, and C. Le Goff, 2017c: Coherent heat patterns revealed by unsupervised classification of argo temperature profiles in the north atlantic ocean. *Progress in Oceanography*, **151**, 275–292, doi:10.1016/j.pocean.2016.12.008, URL <http://www.sciencedirect.com/science/article/pii/S0079661116300714>.
- Maze, G., H. Mercier, V. Thierry, L. Memery, P. Morin, and F. F. Perez, 2012: Mass, nutrient and oxygen budgets for the northeastern atlantic ocean. *Biogeosciences*, **9** (10), 4099–4113, doi:10.5194/bg-9-4099-2012, URL <http://www.biogeosciences.net/9/4099/2012/>.
- Maze, G. and V. Thierry, 2014: International strategy: Argo-deep. *3rd NAOS annual meeting. 16-17 June 2014, Brest, France.*, URL <https://w3.ifremer.fr/archimer/doc/00483/59437/62275.pdf>.
- Maze, G., et al., 2014c: French national report on argo - 2013. present status and future plans. Tech. rep., COPIL Argo-France. URL <http://archimer.ifremer.fr/doc/00180/29100/>.
- Maze, G., et al., 2015b: French national report on argo - 2014. present status and future plans. Tech. rep., COPIL Argo-France. URL <http://archimer.ifremer.fr/doc/00180/29100/>.
- Maze, G., et al., 2016b: French national report on argo - 2015. present status and future plans. Tech. rep., COPIL Argo-France, Ifremer, France. URL <http://archimer.ifremer.fr/doc/00318/42967/>.
- Maze, G., et al., 2017d: French national report on argo - 2016. present status and future plans. Tech. rep., COPIL Argo-France. URL <http://archimer.ifremer.fr/doc/00397/50844/>.
- Maze, G., et al., 2018d: French national report on argo - 2017. Tech. rep., COPIL Argo-France. URL <http://archimer.ifremer.fr/doc/00435/54642/>.
- Maze, G., et al., 2018e: Preliminary evaluation of the deep rbrconcerto during the rrex17 cruise. *AST 19- 19th Argo Steering Team Meeting. March 12-15, 2018, Sidney, B.C., Canada*, URL <https://w3.ifremer.fr/archimer/Visu?id=58354>.
- Maze, G., et al., 2019c: French national report on argo - 2018. Tech. rep. URL <https://archimer.ifremer.fr/doc/00484/59523/>.
- McCartney, M., 1982: The subtropical recirculation of mode waters. *Journal of Marine Research*, **40**, 427–464.
- Memery, L., M. Arhan, X. A. Alvarez-Salgado, M. J. Messias, H. Mercier, C. G. Castro, and A. F. Rios, 2000: The water masses along the Western boundary of the South and equatorial Atlantic. *Progress In Oceanography*, **47** (1), 69–98, URL <http://www.sciencedirect.com/science/article/B6V7B-419BG95-2/2/175731ece4305d49aa12b41ed5079398>.
- Nurser, A. and R. Marsh, 1998: Water mass transformation theory and the meridional overturning streamfunction. *International WOCE newsletter*, **31**, 36–39.
- Nurser, A. J. G., R. Marsh, and R. G. Williams, 1999: Diagnosing water mass formation from air-sea fluxes and surface mixing. *J. Phys. Oceanogr.*, **29** (7), 1468–1487, URL <http://dx.doi.org/10.1175/2F1520-0485%281999%29029%3C1468%3ADWMFFA%3E2.0.CO%3B2>.
- Nurser, A. J. G. and J. C. Marshall, 1991: On the relationship between subduction rates and diabatic forcing of the mixed layer. *Journal of Physical Oceanography*, **21** (12), 1793–1802, doi:10.1175/1520-0485(1991)021<1793:OTRBSR>2.0.CO;2, URL [https://doi.org/10.1175/1520-0485\(1991\)021<1793:OTRBSR>2.0.CO;2](https://doi.org/10.1175/1520-0485(1991)021<1793:OTRBSR>2.0.CO;2).
- Ollitault, M. and A. Colin de Verdière, 2014: The ocean general circulation near 1000-m depth. *Journal of Physical Oceanography*, **44** (1), 384–409, doi:10.1175/JPO-D-13-030.1, URL <http://dx.doi.org/10.1175/JPO-D-13-030.1>.

- Paiva, A. M. and E. P. Chassignet, 2002: North Atlantic modeling of low-frequency variability in mode water formation. *J. Phys. Oceanogr.*, **32** (9), 2666–2680, doi:10.1175/1520-0485(2002)032<2666:NAMOLF>2.0.CO;2.
- Perez, F., 2017: Machine learning pour l’océanographie opérationnelle. M.S. thesis, SC, Telecom Bretagne.
- Piron, A., 2015: Observation of irmingier sea deep convection by argo floats during the 2002–2015 period. Ph.D. thesis, Université de Bretagne Occidentale.
- POULIQUEN, S., et al., 2017: Coriolis. rapport d’activités 2016. Tech. rep., CNES, CNRS, Ifremer, IPEV, IRD, Meteo France, SHOM, CEREMA. doi:10.13155/49970, URL <http://archimer.ifremer.fr/doc/00388/49970/>.
- Qiu, B., P. Hacker, S. Chen, K. A. Donohue, D. R. Watts, H. Mitsudera, N. G. Hogg, and S. R. Jayne, 2006: Observations of the subtropical mode water evolution from the kuroshio extension system study. *J. Phys. Oceanogr.*, **36** (3), 457–473, URL <http://dx.doi.org/10.1175%2FJP02849.1>.
- Radko, T., I. Kamenkovich, and P.-Y. Dare, 2008: Inferring the pattern of the oceanic meridional transport from the air–sea density flux. *Journal of Physical Oceanography*, **38** (12), 2722–2738, URL <http://dx.doi.org/10.1175%2F2008JP03748.1>.
- Radko, T. and J. Marshall, 2004a: Eddy-induced diapycnal fluxes and their role in the maintenance of the thermocline. *J. Phys. Oceanogr.*, **34** (2), 372–383, URL <http://dx.doi.org/10.1175%2F1520-0485%282004%29034%3C0372%3AEDFATR%3E2.0.CO%3B2>.
- Radko, T. and J. Marshall, 2004b: The leaky thermocline. *Journal of Physical Oceanography*, **34** (7), 1648–1662, URL <http://dx.doi.org/10.1175%2F1520-0485%282004%29034%3C1648%3ATLT%3E2.0.CO%3B2>.
- Riser, S. C., et al., 2016: Fifteen years of ocean observations with the global argo array. *Nature Clim. Change*, **6** (2), 145–153, doi:10.1038/nclimate2872, URL <http://dx.doi.org/10.1038/nclimate2872>.
- Robson, J., P. Ortega, and R. Sutton, 2016: A reversal of climatic trends in the north atlantic since 2005. *Nature Geosci.*, **advance online publication**, –, doi:10.1038/ngeo2727, URL <http://dx.doi.org/10.1038/ngeo2727>.
- Roemmich, D., J. Church, J. Gilson, D. Monselesan, P. Sutton, and S. Wijffels, 2015: Unabated planetary warming and its ocean structure since 2006. *Nature Clim. Change*, **advance online publication**, –, URL <http://dx.doi.org/10.1038/nclimate2513>.
- Roemmich, D. and J. Gilson, 2009: The 2004–2008 mean and annual cycle of temperature, salinity, and steric height in the global ocean from the argo program. *Progress in Oceanography*, **82** (2), 81–100, doi:10.1016/j.pocean.2009.03.004, URL <http://dx.doi.org/10.1016/j.pocean.2009.03.004>.
- Roemmich, D., et al., 1998: On the design and implementation of argo: A global array of profiling floats. Tech. rep., The Argo Science Team.
- Roemmich, D., et al., 2019: On the future of argo: A global, full-depth, multi-disciplinary array. *Frontiers in Marine Science*, **6**, 439, doi:10.3389/fmars.2019.00439, URL <https://www.frontiersin.org/article/10.3389/fmars.2019.00439>.
- Rosso, I., M. Mazloff, L. D. Talley, S. Purkey, N. Freeman, and G. Maze, acc, 2020: Water mass and biogeochemical variability in the kerguelen sector of the southern ocean: A machine learning approach for a mixing hotspot. *Journal of Geophysical Research: Oceans*.

- Roulet, G., X. Capet, and G. Maze, 2014: Global interior eddy available potential energy diagnosed from argo floats. *Geophysical Research Letters*, n/a–n/a, doi:10.1002/2013GL059004, URL <http://dx.doi.org/10.1002/2013GL059004>.
- Sallée, J.-B., K. Speer, S. Rintoul, and S. Wijffels, 2010: Southern ocean thermocline ventilation. *Journal of Physical Oceanography*, **40** (3), 509–529, doi:10.1175/2009JPO4291.1, URL <http://dx.doi.org/10.1175/2009JPO4291.1>.
- Salmon, R., 1990: The thermocline as an " internal boundary layer". *Journal of Marine Research*, **48** (3), 437–469.
- Samelson, R. and G. K. Vallis, 1997: Large-scale circulation with small diapycnal diffusion: The two-thermocline limit. *Journal of Marine Research*, **55** (53), 223–275, doi:doi:10.1357/0022240973224382, URL <http://www.ingentaconnect.com/content/jmr/jmr/1997/00000055/00000002/art00003>.
- Sarmiento, J. L., 1983: A tritium box model of the north atlantic thermocline. *Journal of Physical Oceanography*, **13** (7), 1269–1274, doi:10.1175/1520-0485(1983)013<1269:ATBMOT>2.0.CO;2, URL [https://doi.org/10.1175/1520-0485\(1983\)013<1269:ATBMOT>2.0.CO;2](https://doi.org/10.1175/1520-0485(1983)013<1269:ATBMOT>2.0.CO;2).
- Sauzède, R., H. Claustre, C. Jamet, J. Uitz, J. Ras, A. Mignot, and F. D’Ortenzio, 2015: Retrieving the vertical distribution of chlorophyll a concentration and phytoplankton community composition from in situ fluorescence profiles: A method based on a neural network with potential for global-scale applications. *Journal of Geophysical Research: Oceans*, **120** (1), 451–470, doi:10.1002/2014JC010355, URL <http://dx.doi.org/10.1002/2014JC010355>.
- Schär, C., 1993: A generalization of bernoulli’s theorem. *Journal of the Atmospheric Sciences*, **50** (10), 1437–1443, URL <http://dx.doi.org/10.1175%2F1520-0469%281993%29050%3C1437%3AAAGOB%3E2.0.CO%3B2>.
- Schroeder, E., H. Stommel, D. Menzel, and W. Sutcliffe, 1959: Climatic stability of eighteen degree water at bermuda. *Journal of Geophysical Research*, **64** (3), 363–366, doi:10.1029/JZ064i003p00363, URL <http://dx.doi.org/10.1029/JZ064i003p00363>.
- Shuckburgh, E., G. Maze, D. Ferreira, J. Marshall, H. Jones, and C. Hill, 2011: Mixed layer lateral eddy fluxes mediated by air–sea interaction. *Journal of Physical Oceanography*, **41** (1), 130–144, doi:10.1175/2010JPO4429.1, URL <http://journals.ametsoc.org/doi/abs/10.1175/2010JPO4429.1>, <http://journals.ametsoc.org/doi/pdf/10.1175/2010JPO4429.1>.
- Siedler, G., A. Kuhl, and W. Zenk, 1987: The madeira mode water. *J. Phys. Oceanogr.*, **17** (10), 1561–1570, URL <http://dx.doi.org/10.1175%2F1520-0485%281987%29017%3C1561%3ATMMW%3E2.0.CO%3B2>.
- Smeed, D. A., et al., 2014: Observed decline of the atlantic meridional overturning circulation 2004–2012. *Ocean Science*, **10** (1), 29–38, doi:10.5194/os-10-29-2014, URL <http://www.ocean-sci.net/10/29/2014/>.
- Sonnewald, M., C. Wunsch, and P. Heimbach, submitted: Unsupervised learning reveals geography of global ocean dynamical regions. *Journal of Geophysical Research: Oceans*.
- Speer, K. G. and E. Tziperman, 1992: Rates of water mass formation in the North Atlantic ocean. *J. Phys. Oceanogr.*, **22**, 93–104, doi:10.1175/1520-0485(1992)022<0093:ROWMFI>2.0.CO;2.
- Stevens, S. W., R. J. Jonhson, G. Maze, and N. R. Bates, acc., 2020: A recent decline in north atlantic subtropical mode water formation. *Nature Clim. Change*.

- Stocker, T., et al., 2013: The physical science basis. *Climate Change 2013*, Cambridge University Press, Working Group I Contribution to the Fifth Assessment Report of the IPCC.
- Stommel, H., 1979: Determination of water mass properties of water pumped down from the ekman layer to the geostrophic flow below. *Proceedings of the National Academy of Sciences*, **76** (7), 3051–3055, doi:10.1073/pnas.76.7.3051, URL <http://dx.doi.org/10.1073/pnas.76.7.3051>.
- Sugimoto, S. and K. Hanawa, 2007: Impact of remote reemergence of the subtropical mode water on winter sst variation in the central North Pacific. *J. Climate*, **20** (2), 173–186, URL <http://dx.doi.org/10.1175%2FJCLI4004.1>.
- Sugimoto, S., K. Hanawa, T. Watanabe, T. Suga, and S.-P. Xie, 2017: Enhanced warming of the subtropical mode water in the north pacific and north atlantic. *Nature Climate Change*, **7**, 656 EP –, URL <http://dx.doi.org/10.1038/nclimate3371>.
- Sverdrup, H. U., M. W. Johnson, and R. H. Fleming, 1942: *The Oceans: Their physics, chemistry, and general biology*, Vol. 7. New York: Prentice-Hall, URL <http://ark.cdlib.org/ark:/13030/kt167nb66r/>.
- Talley, L. and M. Raymer, 1982: Eighteen degree water variability. *Journal of Marine Research*, **40**, 757–775.
- Talley, L. D., 1999: *Some aspects of ocean heat transport by the shallow, intermediate and deep overturning Circulations*, 1–22. American Geophysical Union (AGU), doi:10.1029/GM112p0001, URL <https://agupubs.onlinelibrary.wiley.com/doi/abs/10.1029/GM112p0001>, <https://agupubs.onlinelibrary.wiley.com/doi/pdf/10.1029/GM112p0001>.
- Tandon, A., 2001: Water mass transformation due to mixed layer entrainment and mesoscale stirring: In series or parallel? University of Massachusetts, MA 02747, USA, URL <citeseer.ist.psu.edu/473745.html>, URL <citeseer.ist.psu.edu/473745.html>.
- Tandon, A. and K. Zahariev, 2001: Quantifying the role of mixed layer entrainment for water mass transformation in the north atlantic. *Journal of Physical Oceanography*, **31** (4), 1120–1131, doi:10.1175/1520-0485(2001)031<1120:QTROML>2.0.CO;2, URL [https://doi.org/10.1175/1520-0485\(2001\)031<1120:QTROML>2.0.CO;2](https://doi.org/10.1175/1520-0485(2001)031<1120:QTROML>2.0.CO;2).
- Tandon, A. and L. Zhao, 2004: Mixed layer transformation for the North Atlantic for 1990–2000. *J. Geophys. Res.*, **109**.
- Thierry, V., 2017: Rrex 2017. Archimer, doi:10.17600/17001400.
- Thomas, L., 2005: Destruction of Potential Vorticity by Winds. *J. Phys. Oceanogr.*, **35** (12), 2457–2466.
- Thomas, L. and R. Ferrari, 2008: Friction, frontogenesis and the stratification of the surface mixed layer. *J. Phys. Oceanogr.*, **preprint** (2008), 0000–0000, URL <http://dx.doi.org/10.1175%2F2008JP03797.1>.
- Thomas, L. N. and T. M. Joyce, 2010: Subduction on the northern and southern flanks of the gulf stream. *Journal of Physical Oceanography*, **40** (2), 429–438, doi:10.1175/2009JPO4187.1, URL <http://journals.ametsoc.org/doi/abs/10.1175/2009JP04187.1>, <http://journals.ametsoc.org/doi/pdf/10.1175/2009JP04187.1>.
- Thomas, L. N. and J. R. Taylor, 2010: Reduction of the usable wind-work on the general ciruclation by forced symmetric instability. *Geophysical Research Letters*.
- Thomson, R. E. and W. Emery, 2014: *Data analysis methods in physical oceanography*. Newnes.

- Tokunaga, S. and G. Maze, 2019a: A brief update on machine learning of argo (dm)qc. Tech. rep., Ifremer, FRANCE. URL <https://w3.ifremer.fr/archimer/Visu?id=62169>, 15th Euro-Argo Management Board. February 21-22, 2019, Hamburg.
- Tokunaga, S. and G. Maze, 2019b: Osnet: a neural network to predict ocean temperature and salinity. Conference poster for 7th Euro-Argo Science Workshop, Athens, Greece.
- Tomczak, M., 1999: Some historical, theoretical and applied aspects of quantitative water mass analysis. *J. Mar. Res.*, **57** (2), 275–303, doi:10.1357/002224099321618227, URL <http://dx.doi.org/10.1357/002224099321618227>.
- Tsubouchi, T., T. Suga, and K. Hanawa, 2016: Comparison study of subtropical mode waters in the world ocean. *Frontiers in Marine Science*, **3**, doi:10.3389/fmars.2016.00270, URL <http://dx.doi.org/10.3389/fmars.2016.00270>.
- Tziperman, E., 1986: On the role of interior mixing and air-sea fluxes in determining the stratification and circulation of the oceans. *J. Phys. Oceanogr.*, **16** (4), 680–693, doi:10.1175/1520-0485(1986)016<0680:OTROIM>2.0.CO;2.
- Ullman, D. S., P. C. Cornillon, and Z. Shan, 2007: On the characteristics of subtropical fronts in the north atlantic. *Journal of Geophysical Research: Oceans*, **112** (C1), n/a–n/a, doi:10.1029/2006JC003601, URL <http://dx.doi.org/10.1029/2006JC003601>.
- Visbeck, M. H., J. W. Hurrell, L. Polvani, and H. M. Cullen, 2001: The north atlantic oscillation: Past, present, and future. *Proceedings of the National Academy of Sciences*, **98** (23), 12 876–12 877, doi:10.1073/pnas.231391598, URL <http://www.pnas.org/content/98/23/12876.abstract>, <http://www.pnas.org/content/98/23/12876.full.pdf>.
- Walín, G., 1982: On the relation between sea-surface heat flow and thermal circulation in the ocean. *Tellus*, **34**, 187–195, doi:10.1111/j.2153-3490.1982.tb01806.x.
- Wang, C., S. Dong, and E. Muñoz, 2009: Seawater density variations in the north atlantic and the atlantic meridional overturning circulation. *Climate Dynamics*, URL <http://dx.doi.org/10.1007/s00382-009-0560-5>.
- Wang, G., L. Cheng, J. Abraham, and C. Li, 2017: Consensuses and discrepancies of basin-scale ocean heat content changes in different ocean analyses. *Climate Dynamics*, doi:10.1007/s00382-017-3751-5, URL <http://dx.doi.org/10.1007/s00382-017-3751-5>.
- Wang, G., S.-P. Xie, R. X. Huang, and C. Chen, 2015: Robust warming pattern of global subtropical oceans and its mechanism. *Journal of Climate*, doi:10.1175/JCLI-D-14-00809.1, URL <http://dx.doi.org/10.1175/JCLI-D-14-00809.1>.
- Wenegrat, J. O., L. N. Thomas, J. Gula, and J. C. McWilliams, 2018: Effects of the submesoscale on the potential vorticity budget of ocean mode waters. *Journal of Physical Oceanography*, doi:10.1175/JPO-D-17-0219.1, URL <https://doi.org/10.1175/JPO-D-17-0219.1>.
- Whalen, C. B., J. A. MacKinnon, L. D. Talley, and A. F. Waterhouse, 2015: Estimating the mean diapycnal mixing using a finescale strain parameterization. *Journal of Physical Oceanography*, **45** (4), 1174–1188, doi:10.1175/JPO-D-14-0167.1, URL <https://doi.org/10.1175/JPO-D-14-0167.1>.
- Whalen, C. B., L. D. Talley, and J. A. MacKinnon, 2012: Spatial and temporal variability of global ocean mixing inferred from argo profiles. *Geophysical Research Letters*, **39** (18), n/a–n/a, doi:10.1029/2012GL053196, URL <http://dx.doi.org/10.1029/2012GL053196>.

- Williams, R. G., 1989: The influence of air–sea interaction on the ventilated thermocline. *Journal of Physical Oceanography*, **19** (9), 1255–1267, doi:10.1175/1520-0485(1989)019<1255:TIOAIO>2.0.CO;2, URL [https://doi.org/10.1175/1520-0485\(1989\)019<1255:TIOAIO>2.0.CO;2](https://doi.org/10.1175/1520-0485(1989)019<1255:TIOAIO>2.0.CO;2).
- Williams, R. G., J. C. Marshall, and M. A. Spall, 1995: Does stommel’s mixed layer “demon” work? *Journal of Physical Oceanography*, **25** (12), 3089–3102, doi:10.1175/1520-0485(1995)025<3089:DSMLW>2.0.CO;2, URL [https://doi.org/10.1175/1520-0485\(1995\)025<3089:DSMLW>2.0.CO;2](https://doi.org/10.1175/1520-0485(1995)025<3089:DSMLW>2.0.CO;2).
- Worthington, L., 1959: The 18 water in the sargasso sea. *Deep-Sea Res.*, **5**, 297–305.
- Worthington, L., 1976: *On the North Atlantic Circulation*. Johns Hopkins University Press, 110 pp.
- Worthington, L. V., 1972: Negative oceanic heat flux as a cause of water-mass formation. *J. Phys. Oceanogr.*, **2** (3), 205–211, URL <http://dx.doi.org/10.1175%2F1520-0485%281972%29002%3C0205%3A%28NOHFAA%3E2.0.CO%3B2>.
- Wu, L., et al., 2012: Enhanced warming over the global subtropical western boundary currents. *Nature Clim. Change*, **2** (3), 161–166, URL <http://dx.doi.org/10.1038/nclimate1353>.
- Wunsch, C. and P. Heimbach, 2007: Practical global oceanic state estimation. *Physica D: Nonlinear Phenomena*, **230** (1-2), 197–208, URL <http://www.sciencedirect.com/science/article/B6TVK-4MD9FYG-1/2/f1f064bd9a6ee7bd1f729a51531f40b8>.
- Wyville Thomson, C., 1877: *The voyage of the “Challenger”: the Atlantic: a preliminary account of the general results of the exploring voyage of H.M.S. “Challenger” during the year 1873 and the early part of the year 1876 / by Sir C. Wyville Thomson*. Harper, doi:10.5962/bhl.title.11338, URL <http://dx.doi.org/10.5962/bhl.title.11338>.
- Xue, Y., et al., 2017: A real-time ocean reanalyses intercomparison project in the context of tropical pacific observing system and enso monitoring. *Climate Dynamics*, doi:10.1007/s00382-017-3535-y, URL <http://dx.doi.org/10.1007/s00382-017-3535-y>.
- Yang, H. and F. Wang, 2009: Revisiting the thermocline depth in the equatorial pacific. *Journal of Climate*, **22** (13), 3856–3863, doi:10.1175/2009JCLI2836.1, URL <http://dx.doi.org/10.1175/2009JCLI2836.1>.
- Yang, Y. and X. San Liang, 2016: The instabilities and multiscale energetics underlying the mean–interannual–eddy interactions in the kuroshio extension region. *Journal of Physical Oceanography*, **46** (5), 1477–1494, doi:10.1175/JPO-D-15-0226.1, URL <http://dx.doi.org/10.1175/JPO-D-15-0226.1>.
- Zilberman, N. and G. Maze, 2015: Report on the deep argo implementation workshop. hobart, may 5-7th 2015. Tech. rep., University of California San Diego and Ifremer, Scripps Institution of Oceanography UC San Diego 9500 Gilman Drive # 0230 La Jolla CA, 92093-0230, USA. URL <http://archimer.ifremer.fr/doc/00281/39238/>.

A final word

I choose to illustrate this document chapters with science fiction classics of Isaac Asimov: a personal touch to this professional work.

Maybe in another life I would have been astrophysicist to watch space. Maybe someday, on some remote planet, we'll be able to scan the 3 dimensional structure of some ocean from the deck of a spaceship. But in this life, at this time, imagination and science fiction books are the only way to travel even further away.

The most exciting phrase to hear in science, the one that heralds new discoveries, is not 'Eureka!' (I've found it!), but 'That's funny...'

- Isaac Asimov

Un dernier mot

J'ai choisi d'illustrer les chapitres de ce document avec des classiques de la science fiction d'Isaac Asimov: une touche personnelle à ce document professionnel.

Peut-être que dans une autre vie j'aurais été astrophysicien pour observer l'espace. Peut-être qu'un jour, sur une planète éloignée, nous pourrions scanner la structure tridimensionnelle d'un océan depuis le pont d'un vaisseau spatial. Mais dans cette vie, à cette époque, l'imagination et les livres de science fiction sont le seul moyen de voyager encore plus loin.

La phrase la plus excitante à entendre en science, celle qui annonce de nouvelles découvertes, n'est pas "Eureka !" (je l'ai trouvée !), mais "C'est drôle..."

- Isaac Asimov



"Foundation's Edge"
Denoël, 2006



"Runaround",
Folio Society, 2016, illustration by Alex Wells



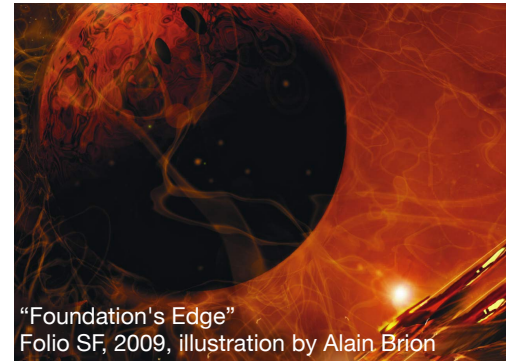
"Foundation"
Folio SF, 2009, illustration by Alain Brion



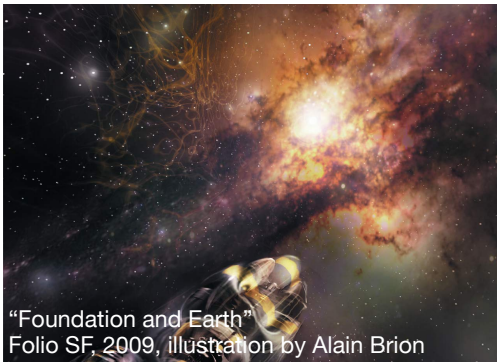
"Foundation and Empire"
Folio SF, 2009, illustration by Alain Brion



"Second Foundation"
Folio SF, 2009, illustration by Alain Brion



"Foundation's Edge"
Folio SF, 2009, illustration by Alain Brion



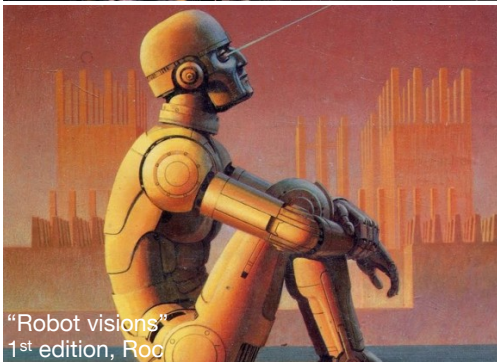
"Foundation and Earth"
Folio SF, 2009, illustration by Alain Brion



"Robby"
Folio Society, 2016, illustration by Alex Wells



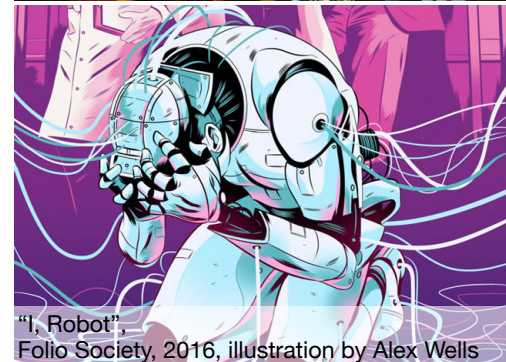
"The naked sun"
Bantam Books, 1991, illustration by Stephen Youll



"Robot visions"
1st edition, Roc



"I, Robot"
Folio Society, 2016, illustration by Alex Wells



"I, Robot"
Folio Society, 2016, illustration by Alex Wells



Titre : Structure et variabilité du gyre subtropical

Mots clés : Dynamique océanique aux moyennes latitudes, cycle de vie des masses d'eau, processus océaniques et d'interactions océan-atmosphère de méso à grande échelle, variabilité saisonnière à interannuelle.

Résumé : Le gyre subtropical est un grand système de courants océaniques et de masses d'eau qui s'étendent sur chacun des océans aux moyennes latitudes. Principalement entraînée par les vents, la circulation océanique proche de la surface a tendance à accumuler des masses d'eau au centre du gyre. Cette accumulation entraîne : une stratification spécifique, une circulation de grande échelle dirigée vers l'équateur dans la partie supérieure de l'océan et un courant compensateur très étroit dirigé vers le pôle, circulant le long du bord ouest de l'océan. La circulation du gyre est responsable du transfert de la chaleur absorbée par l'océan aux basses latitudes vers les hautes latitudes et l'atmosphère, ainsi que d'un stockage important de chaleur et de carbone anthropique dans les masses d'eau aux moyennes latitudes. La dynamique du gyre entraîne également une ventilation peu profonde de l'océan (1000m) sur des échelles de temps allant de 1 à 20 ans, ce qui joue un rôle dans le climat en modérant les flux océan-atmosphère à ces échelles de temps intermédiaires.

Pendant 14 ans, mes travaux se sont concentrés sur ces gyres subtropicaux, en particulier celui de l'océan Atlantique Nord et ses masses d'eau. Je décris mes contributions de recherche aux problématiques de caractérisation et de compréhension de la stratification océanique dans le gyre: vis à vis de sa structure méso-grande échelle et de sa variabilité saisonnière à décennale. Je réponds à ces problématiques appliquées à la plus importante masse d'eau du gyre subtropical de l'océan Atlantique Nord, l'eau dite "à dix-huit degrés". Pour ce faire, je montre comment j'ai utilisé les principes de dynamique des fluides géophysiques liés à la ventilation de l'océan. L'accent est clairement mis sur le processus de transformation de masse d'eau. Je présente en outre de nouvelles techniques d'analyse et de diagnostic que j'ai développées pour étudier objectivement la stratification de l'océan à partir de simulations numériques de la circulation océanique, d'estimations de l'état de l'océan basées sur l'assimilation de données et de mesures directes de l'océan. Enfin, je conclus par les principaux axes de recherche que je me propose d'étudier dans les années à venir : la variabilité passée et future des courants de bord ouest.

Title : Structure and variability of the subtropical gyre

Keywords : Mid-latitude ocean dynamic, water mass life cycle, oceanic processes and air-sea interactions from meso to large scale, seasonal to interannual variability.

Abstract : The subtropical gyre is a large system of ocean currents and water masses stretching across each of the oceans at mid-latitudes. Primarily driven by winds, the upper ocean circulation tends to accumulate water masses in the center of the gyre. This accumulation drives: a specific stratification, a large scale equatorward circulation in the upper ocean and a compensating intense and narrow current flowing poleward along the western boundary of the ocean (eg: the Gulf Stream in the North Atlantic or the Kuroshio in the North Pacific). The gyre circulation is responsible for redistributing heat taken up by the ocean at low-latitudes to the higher latitudes and to the atmosphere, as well as for storing heat and anthropogenic carbon in its water masses at mid-latitudes. The gyre dynamic furthermore leads to a shallow (1000m) ventilation of the ocean on time scale ranging from 1 to 20 years that plays a role in climate by moderating ocean-atmosphere fluxes on these intermediate timescales.

Over 14 years, my work has been centered on subtropical gyres with a focus on the North Atlantic gyre and its water masses. I provide a description of my research contributions to key physical oceanographic questions: what is, and what controls, the ocean stratification structure and variability on seasonal to decadal time-scales ? I answer these questions applied to the most important subtropical gyre water mass of the North Atlantic, the "Eighteen Degree water". I show how I used geophysical fluid dynamic principles of the ocean ventilation. A clear emphasis is made on the water-mass transformation process. I will furthermore present new analysis and diagnostic techniques I developed to objectively study the ocean stratification from ocean circulation numerical simulations, ocean state estimates based on data assimilation and direct ocean measurements. Last, I conclude with the main research axes I propose to investigate in the upcoming years: the past and future variability of western boundary currents.